UNIVERSITY OF SOUTHAMPTON

Faculty of Engineering and the Environment

Institute of Sound and Vibration Research

Vibration analysis using approximate methods for heavily damped systems with variability

by

Lluís Cortés Mochales

Thesis for the degree of Doctor of Philosophy

April 2016

Vibration analysis using approximate methods for heavily damped systems with variability,

This thesis was prepared by
Lluís Cortés Mochales

Supervisors
Dr. Neil Stuart Ferguson
Prof. Atul Bhaskar

Release date:	April 2016
Category:	1 (public)
Edition:	First
Comments:	This report is part of the requirements to achieve the Ph.D. in Sound and Vibration at the University of Southampton.

Institute of Sound and Vibration Research (ISVR)
Faculty of Engineering and the Environment
University of Southampton
Highfield Campus building 13
SO17 1BJ Southampton
Hampshire, United Kingdom

www.isvr.soton.ac.uk
Tel: (+44) (0)23 8059 2291
E-mail: sjb@isvr.soton.ac.uk

UNIVERSITY OF SOUTHAMPTON

ABSTRACT

Faculty of Engineering and the Environment

Institute of Sound and Vibration Research

Thesis for the degree of Doctor of Philosophy

Vibration analysis using approximate methods for heavily damped systems with variability

by Lluís Cortés Mochales

In many engineering fields, vibration analysis is required for a safe design of mechanical structures. At an early stage, the design process relies on computer models for assessing the performance of the structure. Computational methods, such as the Finite Element Method (FEM), are typically used in order to predict the vibration behaviour of the modelled structure. These methods, however, involve a high computational cost for obtaining the dynamic response of a system model, specially when the analyses are targeted at vibrations in the mid-frequency range. Furthermore, repeated vibration analyses are often required in structural design since the model parameters may be variable, e.g. in model updating from vibration measurements, in model optimisation algorithms, or in vibration analysis of systems subject to uncertainty. Therefore, in applications where repeated analyses need to be conducted intensively, the vibration analyses cost may add up, so that the overall computation time becomes unbearable for the engineering needs. For this reason, there already exist efficient methods for the approximate vibration *reanalysis* of systems with varying properties. However, these approximate methods most often neglect the energy dissipation mechanisms in the structure, and just address the system dynamics through undamped modal analysis. This produces sufficiently fair approximations for lightly damped structures, but it may not be the case for locally/heavily damped structures.

This thesis presents novel approximate vibration analysis methods for heavily damped structures, which are based on the state-space formulation for the modal analysis of generally damped systems. It is shown how, whereas the modal solution of

the state-space equations of motion presents some added computational difficulties, linear approximations on state-space models present equivalent computational complexity to those on undamped models, while providing better estimates of the variation in the damped dynamics. In particular, the variations in (state-space) damped modes due to variations in the system model parameters are efficiently estimated through perturbation and interpolation methods. Moreover, a recently defined Rayleigh quotient for damped systems is proposed for improving the accuracy of the linear approximate methods. In order to enhance the efficiency of the approximate reanalyses, it is further proposed to reduce the state-space models through Component Mode Synthesis (CMS). Existing CMS methods based on state-space formulation are investigated for the reduction of large built-up systems which are locally and/or heavily damped. A perturbation propagation scheme on state-space CMS models is then introduced. By simplifying this general scheme for a given CMS method much efficient perturbation methods for damped systems are attained. Finally, these latter methods are used in a numerical case study in application to uncertainty analysis.

Acknowledgements

Ars longa, vita brevis. The completion of this thesis would not had been possible without the support of many people at the University of Southampton. I would like to start by very specially expressing my gratitude to Dr. Neil Ferguson who guided me through this long journey and made me see the forest when I could just see the trees. Also for his human facet, for his encouragement in the hard times, for being always willing to help, without exception. It has been a pleasure working with you. I am also grateful to Prof. Atul Bhaskar and Prof. Brian Mace whose advises have been very helpful and have always pointed towards the relevant research horizons. Thank you to all the staff and post-graduate students at the ISVR Dynamics Group for forming part of a very pleasant working environment, to Dr. Jamil Renno and Prof. David Thompson for their punctual feedback, and to Adriano, Jacques, Michał, Giacomo and Andrea for those sparse discussions on common research issues. I will not miss the opportunity to show my gratitude also to all the people in the Mid-frequency network from which I have learned so much and with whom I travelled around Europe. Thank you as well to all the staff at La Salle that hosted me during the thesis writing period and made those stressful months a bit more bearable.

Mens sana in corpore sano. Not everything has been about work, but about life. I would like to thank those who have shared much more than just a very-ultra-spicy Lai's noodle soup at the Brewed Awakening with me, specially the recurrent attendants: Adriano, Toni, Jou-Yi and Sonia. Also to Jordan and Luca that made my home, and Toni, Txell, Gisela and Ariadna who made me feel like home. Just as much important, I also would like to thank all who formed part many times of the Sports & Stag's combined experience, Ken, Olivier, Edu, Marcos, Richard and Fernando. And to Aristea, Jordi, Sophie, Kioko, Teo, Patrick, Sonia, Ana Luisa, Daniela, Maria, Anthony, Fiona and surely many more with whom I have shared

laughs and problems. I will keep the very good memories for long time.

Semper fidelis. Per acabar, agraïments a tots els incondicionals, perquè sí, perquè per poc que us vegi sou *la* referència. Perquè en aquest temps heu seguit compartint les coses importants, casaments, naixements, aniversaris. Xavi, Raúl, Toni, Pau, Tam, Sandra, Ramon, Jana, Marc, Jorge. I als més incondicionals de tots, la família, que hi han sigut sempre i sempre hi seran. Que sé que sempre tenen un pensament per mi encara que no truquin per si estic enfeinat. Gràcies Albert i Sandra. Gràcies Pepet i Carme. I a l'Àngels, que de tan important com ha sigut, hauria de posar el seu nom a la portada de la tesi. Perquè m'ha ajudat a aixecarme mil i una vegades, perquè m'ha fet posar les piles quan calia i perquè m'ha fet la vida bonica.

DECLARATION OF AUTHORSHIP

I, Lluís Cortés Mochales, declare that this thesis and the work presented in it are my own and has been generated by me as the result of my own original research.

I confirm that:

1. This work was done wholly or mainly while in candidature for a research degree at this University;

2. Where any part of this thesis has previously been submitted for a degree or any other qualification at this University or any other institution, this has been clearly stated;

3. Where I have consulted the published work of others, this is always clearly attributed;

4. Where I have quoted from the work of others, the source is always given. With the exception of such quotations, this thesis is entirely my own work;

5. I have acknowledged all main sources of help;

6. Where the thesis is based on work done by myself jointly with others, I have made clear exactly what was done by others and what I have contributed myself;

7. Either none of this work has been published before submission, or parts of this work have been published as:

   - L. Cortés, N. S. Ferguson, A. Bhaskar, A perturbation method for locally damped dynamic systems, 19th International Congress on Sound and Vibration (ICSV 19), Vilnius (Lithuania), 8-12 July 2012.

   - L. Cortés, N. S. Ferguson, A. Bhaskar, Uncertainty propagation in locally damped dynamic systems, Conference on Noise and Vibration Engineering (ISMA 2012), Leuven (Belgium), 17-19 September 2012.

   - L. Cortés, N. S. Ferguson, A. Bhaskar, Uncertainty propagation in complex modes based Component Mode Synthesis, International Conference on Recent Advances in Structural Dynamics (RASD 2013), Pisa (Italy), 1-3 July 2013.

Contents

List of Figures

List of Tables

Nomenclature

Acronyms

CAE Computer-Aided Engineering

CB Craig-Bampton

CCH Craig-Chang

CMP Component Modal-Propagation

CMS Component Mode Synthesis

CN Craig-Ni

DOF Degree Of Freedom

EVP Eigenvalue Problem

FE Finite Element

FEA Finite Element Analysis

FEM Finite Element Method

FRF Frequency Response Function

GEVP Generalised Eigenvalue Problem

GHEVP Generalised Hermitian Eigenvalue Problem

IRA Implicit Restarted Arnoldi

IRS Improved Reduction System

KL Karhunen-Loève

LMP Local Modal Perturbation

MAC Modal Assurance Criterion

MAM Modal Acceleration Method

MC Monte Carlo

MCB Morgan-Craig-Bampton

MSILM Modified Symmetric Indefinite Lanczos Method

ODE Ordinary Differential Eqution

PC Polynomial Chaos

PDE Partial Differential Equation

PPF Perturbation Propagation Function

QEVP Quadratic Eigenvalue Problem

SCMS Stochastic Component Mode Synthesis

SEA Statistical Energy Analysis

SEREP System Equivalent Reduction-Expansion Process

SFEM Stochastic Finite Elements

SILM Symmetric Indefinite Lanczos Method

SRBM Stochasic Reduced Basis Methods

UEVP Undamped Eigenvalue Problem

VWP Virtual Work Principle

WFE Wave Finite Elements

Greek Symbols

α Proportional damping constant

$\boldsymbol{\theta}$ Set of varying parameters / random field

$\boldsymbol{\xi}$ Set of independent varying parameters

λ Eigenvalue

μ mean / covariance eigenvalue

ω Circular frequency / natural frequency

ω_d Damped modal frequency

σ Decay rate / standard deviation

θ Generic varying parameter

ε Normalised varying parameter

ϑ Generic correlated random variable

ξ Generic uncorrelated random variable

ζ Damping ratio

Matrices

$\boldsymbol{\mathcal{C}}$ Coupling matrix

$\mathbf{\Lambda}$ Eigenvalues matrix

$\mathbf{\Omega}$ Natural frequencies matrix

$\mathbf{\Phi}$ Damped eigenvectors matrix

$\mathbf{\Psi}$ Component modes matrix

$\mathbf{\Upsilon}$ State-space component modes matrix

$\mathbf{A}$ State-space 'mass' matrix

$\mathbf{B}$ State-space 'stiffness' matrix

$\mathbf{C}$ Damping matrix

$\mathbf{D}$ Dynamic stiffness matrix

$\mathbf{G}$ Flexibility matrix

$\mathbf{H}$ Receptance matrix

$\mathbf{I}$ Identity matrix

J	Single-entry matrix
K	Stiffness matrix
M	Mass matrix
P	Projection matrix
S	Condensation matrix
T	Coordinates transformation matrix
U	Undamped eigenvectors matrix
X	State-space eigenvectors matrix
Cov	Covariance matrix

Roman Symbols

z	Set of output quantities
d	Distance
E	Young's elastic modulus
L_c	Correlation length
M	Number of modes
N	Number of DOFs
P_z	Perturbation propagation function for z
Q	Rayleigh Quotient for damped equations of motion
R	Rayleigh Quotient
S_z	Sensitivity function for z
t	Time
z	Generic output quantity
CV	Coefficient of Variation

Superscripts

$*$	Conjugate
A	Attachment
C	Constraint
CC	Characteristic constraint
F	Fixed-interface
H	Conjugate transpose
R	Residual attachment
s	Generalised displacement coordinates
T	Transpose
u	Physical displacement coordinates
v	Undamped component-modal coordinates
w	Undamped coupled-modal coordinates
x	State-space coordinates
y	Damped component-modal coordinates
z	Damped coupled-modal coordinates

Subscripts

a	Attachment DOFs
c	Coupling DOFs
D	Displacement partition
d	Dependent DOFs
e	Element index
f	Interval end
h	Higher order modes

i	Interior DOFs
k	Kept modes
l	Linearly independent DOFs
M	Master DOFs
m	Global mode index
n	Physical parameter index
NZ	Non-zero
o	Interval origin
r	Rigid body DOFs
S	Slave DOFs
s	Component index
V	Velocity partition

Vectors

$\boldsymbol{\phi}$	Damped eigenvector / mode shape vector
$\boldsymbol{\psi}$	Component mode /Covariance eigenvector
$\boldsymbol{u}$	Undamped eigenvector / mode shape vector
$\boldsymbol{x}$	State-space eigenvector
$\boldsymbol{z}$	State-space coupled-modal eigenvector
$\ddot{\mathbf{u}}$	Acceleration vector
$\dot{\mathbf{u}}$	Velocity vector
$\mathbf{f}$	Force vector
$\mathbf{p}$	Undamped modal displacement vector
$\mathbf{Q}$	Modal force vector
$\mathbf{q}$	Damped modal displacement vector

$\mathbf{r}$ Residual vector

$\mathbf{s}$ State-space residual vector / Generalised displacement vector

$\mathbf{u}$ Displacement vector

$\mathbf{v}$ Undamped component-modal displacement vector

$\mathbf{w}$ Undamped coupled-modal displacement vector

$\mathbf{x}$ State-space displacement vector

$\mathbf{y}$ Damped component-modal displacement vector

$\mathbf{z}$ State-space coupled-modal displacement vector

Other Symbols

$\bar{}$ Mean value / Modal matrix

Δ Perturbation

δ Functional variation

$\Delta(\ )$ Perturbation matrices product

$\mathcal{K}$ Krylov subspace

$\mathcal{V}$ Vector space

$\tilde{\Delta}$ Approximate perturbation

$\tilde{}$ Approximate value

Chapter 1

Introduction

In many industrial fields, control of vibrations is an issue of significant importance when designing engineering structures. Structures such as bridges, buildings, machinery, cars, trains, airplanes or spacecrafts might vibrate excessively in operating conditions if they are not properly designed. Excess vibration might cause mechanical structures to fail and it may also produce noise and vibration annoyance to human beings. For instance, structural vibrations are a common cause of material fatigue due to the local stress loadings induced by the vibration. An excess of vibration will increase the level of vibration-fatigue and, consequently, the risk of fracture in parts of the structure. In time, this will worsen the performance of the overall structure, failing to execute its task, or jeopardising human safety. Likewise, excess vibration in a structure may cause instability. For example, a bridge or a building may go into resonance due to external loading, so that the vibration response grows increasingly leading to structural collapse. It is therefore important to take into account the vibration response behaviour in the design of mechanical (and civil) structures.

In the design stage, an engineer needs to analyse the vibration behaviour of the structure so that the vibration response, the internal forces and stresses, the sound radiation, etc. of the structure in operating conditions can be estimated. Based on these estimates one has to make a judgement whether the design needs to be improved with respect to its dynamics. The influence that vibrations have on mechanical structures can be predicted as long as the dynamic characteristics of the structure are known. The dynamic characteristics of a structure depend on the physical properties of the structure. That is, the material properties (e.g. mass

density, elastic modulus, shear modulus, Poisson ratio, etc.), the geometry and dimensions of the structure, the connections between the parts that form the structure and the boundary conditions of the structure (e.g. grounding, supports, etc.). All of these properties determine how the structure responds to any given dynamic loading. Therefore, the design process is a cyclic process in which the physical properties of the structure are being adjusted to meet certain requirements, in this case through vibration analysis and control.

1.1 The design process

The adequacy of a structural design needs to be assessed repeatedly in order to improve its performance through design modifications. In the early stages, the structure is modelled using Computer-Aided Engineering (CAE) tools and its performance is estimated using numerical methods such as the Finite Element Method (FEM). The model is refined iteratively according to the design requirements, either based on the engineer judgement and experience, using *model optimisation* algorithms, or a combination of both. In the later stages, structure mockups are built physically according to the computer model. These are then evaluated through measurements.

In most cases, the measured performance does not match with that of the structural model. This means that the structural model is not an exact representation of the real structure. At first, the numerical model is built under certain assumptions regarding the physical properties of the structure. It may happen that the physical models assumed for each of the structure parts (e.g. beams, plates, block solids, porous materials, composites, junctions, etc...) do not match with their actual physical nature, or are incomplete models. Eventually, this would lead to completely erroneous estimates of the vibration response. On the other hand, even if the physical model assumed is correct (or sufficiently approximated), it is possible that the numerical estimates diverge significantly from the measured ones. This is the case when the physical properties of the real structure materials and the physical model parameters have been wrongly assumed or are *uncertain*, i.e. they are not known with sufficient accuracy. In all these situations the initial model predictions will be very much imprecise.

Given that the original numerical simulations may be inaccurate, it is likely that the prototype-structure does not meet the design requirements adequately. This implies that more modifications need to be introduced in the design. Introducing

modifications and estimating the updated model performance is a relatively cost-effective task both in terms of time and economic cost. On the contrary, introducing modifications in prototypes is much more expensive because additional materials need to be paid for and, possibly, a new mockup needs to be built from the ground up. Furthermore, the manufacturing-time cost is larger than the time needed for updating a computer model. On top of that, the measurement tests also increase significantly the time and economic budget for the performance estimation in comparison to computer simulations. Thence, it is desirable to spend some extra efforts to devise a model closer to reality rather than to carry on with the design process through modification and testing of prototypes. In this way, the structural design can be further improved using a much more accurate model, taking advantage of the numerical method's capabilities.

A physical model may be corrected in view of structure measurements. On one hand, there is the need to verify that the physical model corresponds to the physical nature of the materials and parts that form the structure. On the other hand, the values assigned to the physical model parameters have to be validated so that the numerical simulations match with the real structure performance. However, it is impractical to perform model *verification* and *validation* of a built up structure directly. Instead, the physical model of each of the parts and materials may be identified through separate measurements. This is known generically as *model identification*. Having identified the models for the different physical elements of the structure, an enhanced model of the full structure can be formulated. This new model should be a closer representation of the real structure. Nevertheless, the connections that assemble together the built up structure have not been identified. Also, the assembled parts may have significantly different boundary conditions than when measured separately. These aspects remain assumed in the full model so that its performance may still well deviate from that of the actual structure. At this point, measurements of the full structure can be conducted in order to perform the full model validation. This is typically referred to as *model updating*. The updating process consists in adjusting those model parameters that are still to be determined in order for the model to produce numerical results in accordance to the measurements.

Although it has just been stated that a model may be verified and validated through model identification and updating, it is not always possible to determine the true values for the model parameters. Sometimes it is just unattainable to measure physical quantities with sufficient precision. There are material properties which are easy to measure, like the mass density or the elasticity of a beam or plate, but

some other properties are not trivial to obtain. For example, properties of composite materials or non homogeneous materials are usually approximated to simpler material models. Also, energy dissipation mechanisms in structures are usually diverse and not fully understood so that the physical model will be an average representation of the dissipation in the structure. Moreover, the physical properties of a real structure may vary during its life time due to material degradation, temperature and weather conditions variability and other causes. It must also be taken into account that the industrial manufacturing process is never exact, and the material, geometries, junctions and other properties of a structure will inevitably be in a tolerance range around the nominal design values. All in all, this means that there is always a degree of *uncertainty* that impedes us to know the true physical properties of a structure.

Nowadays, uncertainty is increasingly being taken into account in the modelling of structures. Including uncertainty in the physical model parameters implies that the estimated performance of the structure consists of a range of possible operating responses. That is, the structure is not a deterministic system, and therefore its performance may vary within a range. There is the need for a designed structure to be robust and reliable to the variability in the modelled operating structure that the uncertainty in the physical parameters induces. Hence, analysis of the response uncertainty is needed to determine the variation range. Therefore, the modelling and numerical methods used in engineering design must provide uncertainty analysis on the estimated performance.

1.2 Analysis of vibrations

In the beginning of this chapter, the reasons for taking vibrations into account in the design of structures have been highlighted. Therefore, design modifications are to be selected in accordance with the vibration control targets. In order to effectively decide which modifications are needed, analysis of vibrations must be considered.

Vibration analysis involves the evaluation of the dynamic displacement throughout the structure or, alternatively, its time derivatives, i.e. velocity and acceleration. Typically, the analysis of vibrations is conducted in the frequency domain. Time domain analyses may be of interest when transient responses are to be evaluated, but they will not be considered here, and the consideration throughout is that the structure is linear in its behaviour. Therefore, one usually evaluates displacement, velocity and/or acceleration frequency responses in a frequency range of interest.

The frequency responses of a structure depend on the properties of the structure and the dynamic loading applied to the structure. The dynamic forces applied to the structure may be also expressed in the frequency domain. Then, one can determine the frequency response functions that establish the relation between the frequency responses and the input forces in the frequency domain. The *frequency response functions* (FRFs) are characterized by the structure's physical properties only. Thus, obtaining the frequency response functions makes it possible to understand the dynamic characteristics of the structure in a target frequency range, and it also allows one to study the steady state vibration response.

Generally, the study of the dynamic properties of vibrating structures is done through *modal analysis*. In modal analysis the dynamic behaviour of a structure is represented by means of a mathematical model that expresses the vibration response as a linear combination of vibration *modes*. Hence, the structure is regarded as a linear time-invariant dynamic system. This model is called the *modal model* and it is fully determined by the *modal parameters* of the system, i.e. the modal frequency, modal damping and scaled mode shape of each mode of vibration. In time, the FRFs of a dynamic system can be worked out from the modal parameters. Hence, knowing the modal parameters makes it possible to characterize the linear dynamics of a vibrating structure. Thus, the key point for the analysis of vibration through modal analysis is to have good estimates of the modal parameters of the system, which is in general an arduous task. Nevertheless, the effort in obtaining such estimates is worth its cost because the representation in terms of vibration modes greatly facilitates the subsequent analysis of vibrations.

The advantage of using modal analysis is that the vibration of a structure in a target frequency range is sufficiently described with a rather reduced number of modes. This means that the number of modal parameters needed to characterise the system is far below the number of parameters in the physical model. Moreover, under certain assumptions, each mode of vibration behaves as a single harmonic oscillator uncoupled from the other modes. Thence, in modal analysis each mode of vibration can be evaluated independently, with the benefit that not too many modes are to be analysed. Actually, the number of modes required to analyse a dynamic system depends on the width of the frequency range considered with respect to the dimensions of the structure. Each mode of vibration generally contributes mainly to the frequency response around its modal frequency. Hence, in the frequency response functions a resonance peak emerges for each mode. The frequency width of the resonance peak is proportional to its modal damping. In consequence, only the modes that contribute significantly to the response in the target frequency range

are required.

1.2.1 Estimation of modal parameters

The modal parameters can be calculated from the physical properties of the structure. The dynamics of a system are governed by the partial differential equations (PDEs) that describe its physical behaviour, that is, the system's physical model. The modes of vibration may be derived analytically from the governing equations. However, defining the PDEs and obtaining the analytical modes is only possible for simple geometries and materials such as a single homogeneous beam or plate. For more general systems a finite element (FE) model may be used.

An FE model is a discretisation of the physical model where the governing PDEs are defined for each of the *elements* in which the system is discretised. A number of *nodes* are defined usually at the boundary of the element. The element nodal positions are chosen to coincide with the nodes of the adjacent elements. Then, based on the virtual work principle (VWP) [1], the element PDE is approximated at the element nodes with a set of Ordinary Differential Equations (ODEs). For a dynamic FE model these nodal ODEs are the so called *equations of motion* of the element. The element set of equations of motion is posed in matrix equation form in terms of the element mass, stiffness and damping matrices. Eventually, the equations of motion of all elements are coupled together by assembling the element matrices at the corresponding nodes, leading to the system equations of motion. Thus, the equations of motion are a discretisation of the system governing equations at the nodal positions.

The modes of the structure can be computed numerically as the solutions of the eigenvalue problem (EVP) corresponding to the system equations of motion. The number of modes that can be estimated accurately through FE modelling depends on the refinement in the discretisation. At the same time, the finer the discretisation the larger the size of the system matrices and, consequently, the computational cost for finding the modes. Therefore, there is a trade-off between the number of modes that can be estimated, the accuracy of the estimates and the computation time required.

Considering that the modal parameters can be estimated from an FE model and that, at the same time, the response functions may be calculated in terms of the system modes, the vibration analysis of a structure may be fully modelled using an FE model. In other words, Finite Element Analysis (FEA) of dynamic structures

can be done based on modal analysis. Figure 1.1 shows a schematic of the stages for the FE-modelling of dynamic systems. From the physical properties of a system a finite element model is defined. Then the corresponding modal model is computed through the EVP-solution of the FE equations of motion. Finally, the frequency responses of the dynamic system are calculated using modal superposition. When designing large structures, the solution of EVPs is by far the most computationally expensive process in FEA of dynamic systems. On the contrary, the construction of the system matrices and the computation of response functions take a minor part of the computation time.

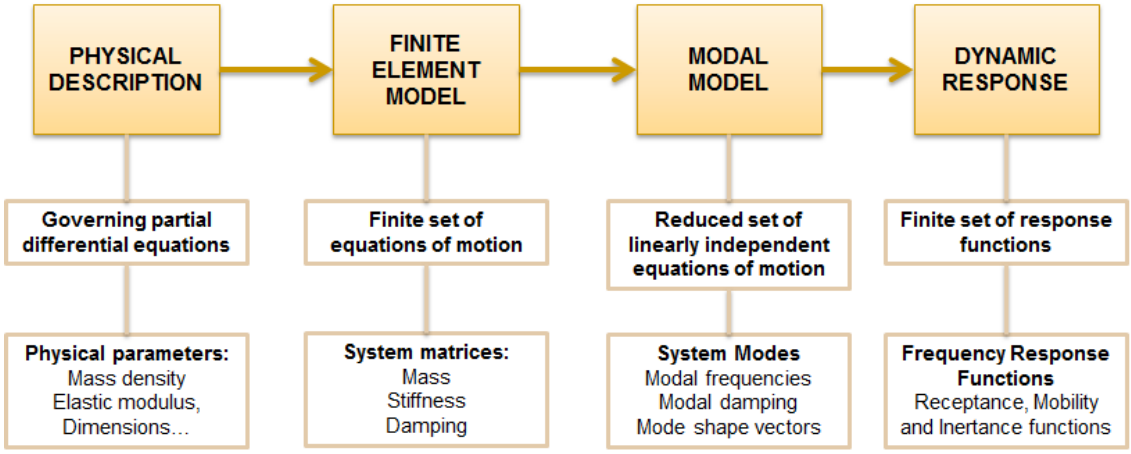

Figure 1.1: Dynamic systems FE-modelling block diagram.

Alternatively, the modal parameters of a structure can be estimated from frequency responses measurements, i.e. modal parameter identification. This is generally known as *modal testing*. Modal testing involves, first, the measurement of the frequency response functions of the structure at a set of locations and, second, the fitting of a modal model to the measured FRFs. The measurement phase is usually done through an *impact hammer test* or a *shaker test*. In such tests, the FRFs between the measurement points are obtained from the measured input force and responses spectra at those locations.

Once the frequency response functions are measured the next step is to estimate the modal parameters. The way to do so is to fit a mathematical model to the measured functions. The fitting process is a linear inverse problem which is referred to as *linear regression* [2]. Several mathematical models can be used for the linear regression, e.g. state-space models, polynomial models, time-series models, etc. These models are linear models of response functions. Therefore, they are equivalent to the modal model and, therefore, the modal parameters can be straightforwardly obtained from these identified models. For example, the modal frequencies and damping are found

by finding the roots of the polynomials in an FRF polynomial model. Thus, there exist a wide range of algorithms that perform modal parameter identification from measurements.

Modal testing is the inverse process to the computation of frequency responses from the modal model. In principle, the number of modes that can be estimated accurately through modal testing depends on the number of measured positions and the quality of the measurements. Notice that there will always be a physical (and time) limitation on the number of positions that can be measured in a real structure. Furthermore, inverse problems are computationally complex and typically need to employ iterative methods to be solved. This is also a limitation in the number of modes estimated, because the time needed to solve the inverse problem may be unattainable. Moreover, an inverse problem becomes ill-conditioned as the size of the model increases. This means that the identified modal parameters become very sensitive to any error, e.g. noise in the measured data when a large number of modes are attempted to be identified. For all these reasons, modal testing is in practice restricted to the identification of a reduced number of modes of the structure.

1.2.2 Low, high and mid-frequency analysis

The specific vibration features that need to be analysed depend on the frequency range for which the analysis is aimed. Typically, the first modes of vibration of a structure, i.e. the modes with lower modal frequency, show up frequency-spaced from one another. On the contrary, for higher frequency modes, the FRF resonance peaks overlap in frequency since the width of the frequency band in which a mode resonates become of similar order to the frequency spacing between consecutive modes. The frequency at which the modes start overlapping depends on the modal density of the system, i.e. on the average number of modes per frequency band.

Furthermore, if the system under study is subject to uncertainty, e.g. manufacturing process variability, the modes of vibration may vary accordingly. In general, low frequency modes are only slightly modified in the presence of uncertainty. Their dynamic characteristics keep steady since uncertainty caused by local variations have little influence in the low frequency modes with smooth mode shape patterns. On the other hand, high frequency modes have short wavelength variations in the shape so that they are very unsteady with respect to uncertainty. This means that their modal parameters, and specially their modal frequency, may get shifted significantly for a small amount of uncertainty.

The combination of these factors, i.e. modal density, modal overlap and uncertainty, motivates the definition of three frequency ranges for vibration analysis. There exists a *low-frequency* range in which the system dynamics may be regarded to be deterministic. In the low-frequency range the FRFs are characterised by the low modal density and overlap so that different separate resonant peaks can be identified. These peaks remain constant regardless of system uncertainty. The analysis of vibration in this frequency range focuses on the individual analysis of each mode in the frequency response throughout the system spatial extent.

Thus, in the low-frequency range it is very convenient to perform modal analysis. It is suitable to use Finite Element Analysis for this purpose since the number of modes is small in this range and consequently, the computational cost for the FE solution is bearable. Additionally, uncertainty does not need to be taken into account due to the deterministic nature of the low frequency modes. The FEA may be further complemented by posterior modal testing.

On the other hand, there is a *high-frequency* range characterised by a high modal density and modal overlap. In addition, the variability of the modal frequency with uncertainty is considerable. This implies that the system frequency responses in this frequency range may be regarded as a random mixture of modal contributions. Therefore, in the high-frequency range it is not relevant to study the one by one contribution of each mode. To start with, there is a high number of modes in this region so that the amount of modal information is overwhelming to the analyst. Moreover, the system frequency and spatial responses are very sensitive to any uncertain system property.

For these reasons, the analysis of vibrations at high frequencies is expressed in terms of averaged quantities. It is not important to study the exact value of an FRF peak because of the high variability of modes. Instead, the statistical average value of the frequency responses is of interest. Likewise, the spatial distribution of the response is not constant. Hence, it is only meaningful to the analyst to consider spatial averages of the energy of the responses in a given frequency. In short, the analysis of vibration in the high-frequency range is generally performed through the analysis of spatial and ensemble averages of the response energies.

The most common method for high-frequency vibration analysis is the *Statistical Energy Analysis* (SEA). In SEA the system is divided into several subsystems. An SEA model characterises the average energy in each subsystem and the energy transmission between subsystems. SEA takes advantage of the high modal overlap and randomness in the high frequency modes to simplify the (sub)system's modal model

based on statistical considerations. SEA assumes average values for the modal density and overlapping so that all modes in a subsystem carry the same amount of energy, i.e. there is modal energy equipartition. It also assumes that the high frequency modes are local to the subsystem and that, in consequence, there is weak coupling between the subsystems. This implies that the energy transfer between two subsystems is independent of the rest of the subsystems. These simplifications make it possible to calculate the averaged energies and energy transfers in the subsystems without the need of a detailed estimation of the modal parameters of the subsystems. If the analysis at high frequency was to be made through FEA, the computational cost would be prohibitive.

In between the low and high frequency ranges there is a transition region that has combined characteristics. This is the so-called *mid-frequency* range. The modal density in the mid-frequencies is usually higher than in the low-frequencies and the modal contributions to the FRFs start overlapping. However, the modal overlap is low and the different modal resonances can be still identified in the frequency response functions. Furthermore, the modes in the mid-frequency region are sensitive to uncertainty, although to a lesser extent than for the high-frequency region. This means that, in the mid-frequencies, the frequency responses of several structures with identical nominal values show variations in the position and magnitude of the resonances. Yet, the modal variations keep in a limited range around the nominal values. Thus, the mid-frequency dynamics of a system cannot be regarded to as deterministic nor as a random mixture of modes.

These combined characteristics make the analysis of vibration in the mid-frequency range rather complicated. The FEA of a nominal system is not sufficient to characterise the mid-frequency dynamics. Instead one needs to determine the statistics of the system response due to model parameter variability. On the other hand, the information about the frequency content and the spatial distribution of the responses is of interest. The average frequency responses of the structure's ensemble retain a smooth shape with resonances. Similarly, the ensemble average of the responses' spatial distribution presents different areas with regard to response amplitude. Therefore, frequency and spatial averaged quantities - such as the energies in SEA - may lack the required detail for the analysis.

Mid-frequency analysis presents several issues either if finite element analysis or statistical energy analysis is attempted. To start with, for an accurate FEA in the mid-frequencies the physical model has to be finely discretised. This implies a large size of the FE model matrices, so that the FE solution becomes very computation-

ally expensive. Additionally, the uncertainty in the model requires to evaluate the variability in the system responses, which multiplies the computational cost of the solution of an already large FE model. On the contrary, the SEA assumptions - high modal density, modal energy equipartition and weak coupling - do not hold in the mid-frequencies. This means that the simplifications in the SEA formulation lead to erroneous results when applied to the mid-frequency range. For these reasons, there is still on-going research for developing new mid-frequency analysis methods [3], either by using alternative deterministic methods to FEA, or through the development of statistical methods with relaxed assumptions with respect to SEA, or by hybrid methods coupling deterministic and statistic methods. Nevertheless, finite element analysis remains the conventional mid-frequency analysis approach.

1.3 Motivation

In many design situations, it is necessary to perform repeated analyses of a structure due to variation of the design parameters. The dynamic analysis of a vibrating system to be designed is usually modelled using the Finite Element Analysis (FEA). This is certainly the case when the analysis is targeted at the low and mid-frequency ranges. The modal parameters of a system, that is the modal frequencies, the modal damping and the mode shape vectors, are obtained from its finite element model. In order to compute the modal parameters, the eigenvalue problem corresponding to the model equations of motion has to be solved. The solution of an eigenvalue problem (EVP) is typically the most costly computational task in the dynamic modelling and analysis of the system. Therefore, for systems whose design parameters may vary, eigensolution reanalysis must be conducted over and over again.

Situations in which the model parameters may be indeterminate include design processes such as *model updating*, *model identification* and *model optimization* - which are essentially inverse problems - and also include the analysis of systems subject to *uncertainty*. In all these situations the dynamics of the system are re-evaluated iteratively. The exact reanalysis of the finite element model would involve the EVP (or inverse problem) solutions to be computed at each iteration. However, the computational cost for calculating such solutions is prohibitive for the large models needed in industrial design.

It is common practice to use approximate methods for solution reanalysis which are significantly more time efficient than solving EVPs; that is, to perform the reanalysis without actually solving EVPs. These methods approximate the dynamics

of a system whose parameters have changed from the solution prior to the variation. This may be done through *sensitivity* analysis or *interpolation* of previous FEA solutions. The gain in efficiency comes from the fact that the full FE model has to be solved once (or a few times) only, and the reanalysis solutions are obtained through computationally time-saving linear approximations. However, the approximate variations in the solution have to be evaluated independently for each indeterminate model parameter. Therefore, the number of varying model parameters affects the efficiency of the approximate methods.

What's more, the total number of FE model *degrees of freedom* (DOFs) also limit the efficiency of the approximate methods. The solution approximate reanalyses involve a number of arithmetic operations proportional to the order of the system FE matrices. This is even exacerbated for inverse problems where, typically, the matrices have to be inverted. Therefore, the use of approximate methods does in principle reduce the computational cost of the reanalysis, but the computational time may still be excessive for the needs of the designer.

For this reason, it is very convenient to use model order reduction methods in conjunction with approximate reanalysis methods. The order of the FE model - i.e. the number of degrees of freedom - can be reduced through transformation of the physical DOFs into a reduced coordinate space. Hence, if the FE model is reduced, the solution reanalyses can be conducted on the reduced model which supposes a significative gain in efficiency. Eventually, the reduced model solutions can be transformed back into full system solutions.

Engineering structures are usually large structures built up of several subsystems. When one applies design modifications, these are likely to involve only a few subsystems at a time. Similarly, when analysing uncertainty, not all subsystems need to be considered uncertain, and the degree of uncertainty may be different on different subsystems. On the other hand, the full finite element model order of such structures is remarkably large, specially if one desires to analyse the dynamic behaviour at the mid-frequencies. The FE model may contain thousands or millions of DOFs. These facts make it suitable to use *Component Mode Synthesis* for the solution and reduction of the FE model.

Component Mode Synthesis (CMS) is a well established method that efficiently computes the vibration modes of a system by substructuring the FE model into several components (i.e. subsystems), and reducing the order of the component models by means of the component modes. As reviewed later in this chapter, it has so far been widely used together with uncertainty analysis, model optimisation

and model updating. In the literature, the applications to these fields invariably use CMS methods based on the undamped component modes. Therefore, all these applications make the simple assumption that the damping in the structure is of the Rayleigh kind, i.e. the damping in the structure is distributed proportionally to the mass and stiffness properties.

However, damping in built-up structures has by no means this spatial distribution. Typically, the damping in structures is very localised. Most of the damping may come initially from the dissipation phenomena that occur at the structural junctions. Apart from that, additional damping treatments are employed for the control of vibrations by placing on the structure viscoelastic materials such as rubbers, polymers, etc. Damping materials are generally expensive materials and they add unwanted mass to the system. Therefore, it is convenient to use the least possible amount of damping materials necessary to control vibration. Hence, damping materials are placed in the structure only at the locations where they are most effective. Thus, the modelling of damping in FEA should be trustworthy enough so that the damping treatments in the design are effective but not oversized.

This rises some questions on the suitability of undamped modes based CMS methods for the reanalysis of systems with localised damping. On one hand, these CMS methods compute the undamped modal solution of the full system model. The modal damping is calculated a posteriori by transforming the damping matrix into the undamped modal coordinates. This way of computing the modal damping is just an approximation which is valid for lightly damped systems. Therefore, it may present some inaccuracies when applied to locally damped systems.

Nevertheless, it is not just the error in the estimation of modal damping what puts in question the use of the undamped CMS methods in the reanalysis of damped systems. The approximate solution reanalysis methods rely on the CMS model to find the variation in the modal parameters and responses of the system. Since the CMS model consists of undamped modes it contains no information on damping. Therefore, when the undamped CMS model is used, it is not possible to know the rate of change in modal damping when there are variations in the model parameters. In consequence, applications such as damping optimisation or model damping updating produce no benefit with the introduction of CMS. In contrast, damping modifications become a blind search if undamped CMS is used for the reanalysis.

Alternatively, there exist CMS methods based on damped component modes. These later methods directly obtain the exact damped modes of the full model regardless of the damping being small or not proportional. Although accurate estimates of

the modal damping are an asset, the damped modes based CMS methods have not been extensively used because of their higher computational cost. However, it might be beneficial to use them in the context of solution reanalysis of locally damped systems. Therefore, the motivation for this thesis is the efficient reanalysis of damped systems using approximate methods in conjunction with damped modes based Component Mode Synthesis.

1.4 Literature review

Component Mode Synthesis for undamped systems was introduced in the late 1960's by Hurty [4] and Craig and Bampton [5]. Numerous variations of the CMS method were developed over time depending on the basis functions used for the component model reduction and how the coupling of components is specified. Nevertheless, the Craig-Bampton method, which is based on fixed-interface component modes together with so called constraint modes, is the one that has earned greater success due to its ease of component coupling.

Also, CMS methods using free-interface modes are widely used in applications involving measurements. This is because free-interface normal modes can be validated with modes estimated from free vibration measurements of the physically uncoupled substructure.

Free-interface modes CMS was introduced by Goldman [6]. However, it wasn't until the appearance of the CMS method developed by Craig and Chang [7] that free-interface methods became accurate enough. This method included residual-flexibility attachment modes for a better modelling of the components coupling. However, the coupling of components in the Craig and Chang method is system-specific. Later, Craig [8] developed a systematic method for coupling components regardless of the type of modes used.

Component Mode Synthesis methods based on complex-valued damped modes in state-space coordinates were explored once the undamped CMS methods had been well-established in the late 1970's. A method with fixed-interface complex modes was proposed first by Hasselman and Kaplan [9]. Similarly, Craig and Chung [10] extended Goldman's method using free-interface complex modes. Other complex mode methods based on state-space formulation followed, such as those by Wu and Grief [11] and by Martin and Ghlaim [12]. Nonetheless, these methods did not obtain the required accuracy to be competitive against classic CMS methods based

on undamped modes.

It was much later that Craig and Ni [13] devised a damped modes CMS method that was significantly precise for non-proportional viscous damped systems. They formulated the residual attachment modes in state-space form to be used with free-interface damped modes, analogous to the Craig-Chang undamped CMS method. More recently, Morgan et al. [14] proposed two new methods where the constraint modes and the residual attachment modes in state-space form were formed from the classic CMS constraint and attachment modes respectively. In this way the extension from undamped modes CMS to damped modes CMS is direct with the addition of the damped normal modes computed from the state-space EVP. These latter methods were compared together with the Craig-Ni method by Craig and Morgan [15] presenting similar accuracy.

The classic (undamped) CMS methods have been widely used in conjunction with solution reanalysis methods for uncertainty analysis and for solution of inverse problems. In the following, the use of CMS in these applications is briefly summarized with a focus on their use in association with approximate reanalysis methods.

1.4.1 Component Mode Synthesis and Uncertainty

During the 1980s the research community started introducing uncertainty into finite element modelling. The initial approaches consisted of introducing probabilistic uncertainties into the parameters in order to compute system response statistics through the Monte Carlo method [16]. Subsequently, perturbation methods were proposed by Liu et al. [17], where the stochastic finite element matrices were expanded using first and second order Taylor expansions, so that response variability (i.e. the response covariance matrix) are approximated efficiently. In the early 1990s, Ghanem and Spanos presented a spectral approach for the uncertainty in FE models based on the homogeneous chaos [18]. They introduced the use of matrix expansions which efficiently model random fields with a minimum number of parameters. Namely, the Karhunen-Loéve (KL) expansion for Gaussian distributed fields, and the Polynomial Chaos (PC) expansion for non-Gaussian fields. These expansions may be used with the perturbation method or with the spectral approach.

All of these uncertainty propagation methods are based on the probabilistic description of the uncertainties in the finite element model parameters. This is generically known as the Stochastic Finite Element Method (SFEM). A review of probabilistic methods and their applications can be found in reference [19]. Later, uncertainties

for which a probabilistic description could not be given (i.e. epistemic uncertainties) were also modelled in finite elements with the use of possibilistic approaches such as random matrix theory, evidence theory, interval probabilities, fuzzy probabilities and Bayesian methods. A review of these methods and their applications can be found in references [20, 21].

Well into the 1990s, Component Mode Synthesis was originally used in conjunction with probabilistic uncertainty by Brown and Ferri [22]. They used the component modes and residual flexibility matrices as random variables and used reliability methods to obtain the statistical characteristics of the responses. Then, Mace and Shorter [23] developed a perturbation method based on Craig-Bampton CMS models. They proposed to quantify uncertainty at a component-modal level and propagate the uncertainty to the full system modes using a perturbation relationships in Monte Carlo simulations. They pointed out that it makes sense to quantify uncertainty at a component level, since different components may come from independent manufacturing processes. Also, statistical properties of the component modes might be easier to measure in modal coordinates, rather than quantified in terms of random fields in physical variables. Nonetheless, component mode statistics may be alternatively obtained from physical uncertainty description using available SFEM methods. Subsequently, Hinke et al. [24] expanded this approach by establishing the perturbation relationships between the covariance matrices of physical parameters, component-modes and global-modes. Hinke [25] also proposed an efficient covariance propagation between the global-modes and the FRF covariance matrices with the use of KL expansion. Recently, Kammer and Krattiger [26] presented a perturbation method that performed covariance propagation directly from components FRFs to full system FRFs using a Craig-Bampton CMS approach. In their method damping was implicitly included in the FRFs.

In the last few years, the use of CMS has been exploited in all kinds of uncertainty analysis. Mencik [27] put together the use of Wave Finite Elements (WFE) and perturbation methods in CMS for the modelling of uncertain junctions. Sarsi et al. [28] used PC expansion for the quantification of uncertainties in the component matrices. The PC expansion for the full matrices in CMS coordinates is obtained using the CMS transformation matrix. Uncertainty analysis is performed using spectral SFEM in CMS coordinates. Possibilistic methods have also started to make use of CMS. For instance, Hiannini and Hanss [29], and De Gersem [30] et al. used CMS in conjunction with fuzzy arithmetic and interval analysis.

A rather new approach to uncertainty is the stochastic reduced basis methods

(SRBM) developed by Nair and Keane [31]; that is, Ritz reduction methods in which the transformation matrix consists of stochastic modes (i.e. modes with uncertainty). Bah et al. [32] first developed the Stochastic Component Mode Synthesis (SCMS). They presented a method in which the Craig-Bampton transformation matrix is formed by stochastic modes based on mode perturbations. Later, Guedri et al. [33] proposed a double-condensation stochastic reduction method. They first reduce the model using the original SCMS method and then, they further condense the stochastic matrices in Craig-Bampton coordinates using the Perturbation expansion in SFEM or the PC expansion in spectral SFEM. Next, Tran et al. [34] presented another SRBM for damped systems. They basically accounted for viscoelastic damping by adding enrichment Ritz vectors to the Craig-Bampton transformation matrix and then used this enriched transformation matrix in the former double-condensation method. Similarly Dohnal et al. [35] developed SRBM for joint uncertainty propagation expressing the stochastically reduced Craig-Bampton matrices in terms of the KL expansion. They also presented enhanced methods for the computation of the stochastic reduced basis.

1.4.2 Component Mode Synthesis and Inverse Problems

Modal truncation based reduction methods have been identified as being the most suitable methods for the reanalysis of indeterminate systems [36]. Among these, Component Mode Synthesis is probably the method that has been used in a broader range of applications. In the last two decades, Component Mode Synthesis has been used in conjunction with reanalysis approximate methods for model identification, updating and optimization.

From the early 1990s, researchers in the model updating and parameter identification fields [37] have been introducing reduction methods. Friswell et al. [36, 38] first considered the use of reduced models for parameter estimation and updating from frequency response functions measurements. In parallel, Huckelbridge et al. [39] pioneered the use of Component Mode Synthesis for parameter identification. They aimed at identifying junctions/interface parameters from estimated/measured modal parameters using a sensitivity method. Component Mode Synthesis allows for a significant reduction of the number of degrees of freedom of the components, and at the same time, the coupling interface DOFs remain unreduced in using the Craig-Bampton method. Later, CMS was used for robust model identification from modal parameters by Link [40]. In this case, CMS local and global parameters are allowed to have uncertainty. Robust identification of joints was attempted. Also,

CMS was used for model identification directly from FRF measurements by Grafe [41]. In his work, identification of proportional viscous damping using a sensitivity method on CMS is presented as well. Then, Morgan et al. [42–44] derived methods for identifying CMS matrices in Craig-Bampton coordinates directly from FRF measurements, both for undamped and damped cases. Takewaki et al. [45] presented an incremental inverse problem for model redesigning based on CMS for updating damped systems from damped modal frequencies.

1.5 Aims and objectives

In this work it is intended to explore new ways to address variations and modifications in dynamic system models when these are heavily damped. The focus is placed on approximate solution methods based on the modal analysis of such systems. Therefore, one is interested in how the damped modes of a system vary.

The literature review above was used to highlight the fact that Component Mode Synthesis is employed in a large variety of situations in which approximate repeated analyses are conducted, with the purpose of reducing the model order and, thus, increasing the reanalysis efficiency. It has also been remarked that specific CMS methods based on damped component modes may be used for the reduction and solution of generally damped systems. Accordingly, the aim in this thesis is to determine how one would proceed to the analysis of heavily damped systems with varying parameters with the use of CMS methods for damped systems.

One question that needs to be addressed is whether the damped modes CMS methods provide a substantial benefit over classical CMS methods. Therefore, one of the objectives is to assess the performance of damped modes CMS in comparison to classical CMS methods in order to evaluate in which situations, i.e. for which damping characteristics, the damped CMS methods may be required for a correct modal solution.

Moreover, an associated concern is that in the damped CMS methods the component modes are formulated in the state-space. Therefore, a consequent objective is to determine the implications of the use of the state-space formulation. This involves the investigation of numerical complexity of state-space solution and quantification of the cost for the modes computation.

Whether the system is reduced or not, the methods for approximate analysis are mainly based on linear approximations. This is the case for sensitivity based meth-

ods, such as the perturbation method, or linear interpolation methods. In the event of using damped CMS methods for reducing a FE model, the solutions to approximate would then be the damped component modes of the system and, eventually, the damped modes of the full system. Therefore, another objective of this work is to critically examine the linear approximation methods when these are used for the analysis of damped vibration modes in order to determine the limitations of these methods. The applicability of the approximate methods is to be assessed with regards to solution cost and admissible range of variation of the parameters for an accurate solution.

The main goal is to formulate the approximate reanalysis of heavily and/or locally damped systems when these are reduced through state-space based damped CMS methods. To this effect, it is necessary to evaluate how amenable the damped CMS methods are for the reanalyses computation based on the kind of component modes to compute, the ease of component coupling, the scalability of the CMS method, etc. In other words, evaluating how easy it is to update the reduced model after parameter variation. The objective is then deriving the approximation expressions and reporting their performance in terms of efficiency and accuracy.

Then, a subsequent objective is to improve the approximate CMS analysis of damped systems. On one hand, it is sought to enhance the accuracy of the approximations so that the range of validity of the approximation methods can be broadened. On the other hand, the lowest possible computation cost for the approximations is also pursued. The combined goal is to accomplish an increase in efficiency which does not result in a degradation in accuracy and, viceversa, that an approximation enhancement does not produce a large increment in computation cost. This may be attempted on the basis of existing CMS approximate reanalysis approaches for undamped/lightly damped systems found in the literature.

Finally, it is a purpose of this thesis to test the performance of the damped CMS approximate solution methods when applied for the intensive analysis of damped dynamic systems, specifically for scenarios in which damping plays an important role in the variation behaviour. That may be the case for uncertainty analysis of locally damped systems, modelling of damped joints, trim damping optimisation, or design search of the placement of damping treatments in built up structures.

1.6 Outline of the thesis

For the purpose of developing approximate reanalysis methods for generally damped systems based on damped CMS reduction this thesis starts by revisiting the state-space formulation. The mathematical properties of the state-space EVP are examined in detail and specific eigenvalue algorithms for the solution of the state-space equations of motion are discussed. Moreover, the determination of error bounds for damped modal solutions is also addressed. On these grounds, the perturbation and interpolation methods for heavily damped systems have been developed in this work. Existing sensitivity functions for damped (state-space) eigensolutions are revisited. Likewise, interpolation of damped (state-space) eigensolutions is proposed. Improved modal estimates are achieved by means of a novel non-linear approximation method for the damped eigenvalues through a Rayleigh quotient for the damped equations of motion.

Then, a generic formulation for the state-space based CMS methods is proposed and their performance is studied through numerical examples. Next, the linear approximate analysis of damped CMS reduced models is formulated. The applicability and limitations of the damped modes approximation in CMS state-space coordinates are further analysed. Finally, original perturbation methods on CMS models are derived. These methods offer enhanced efficiency and they are very well suited for the analysis of systems with localised damping and/or heavy damping characteristics. The application of the CMS perturbation methods to uncertainty analysis is addressed, showing very good performance both in terms of accuracy and efficiency.

A brief overview of the coverage in the thesis is described below:

CHAPTER 1: An introduction chapter. It sets the motivation, the aim and the scope of the thesis. It contains a relevant literature review.

CHAPTER 2: Background theory for the linear modelling of dynamic damped systems is outlined here. Included are sections for the types of linear damping and modal analysis of damped systems. The state-space formulation is explained here, the properties of the state-space eigenvalue problem are discussed and its solution through appropriate eigenvalue algorithms is determined. The implications of the use of state-space formulations on the error analysis of the modal estimates are also discussed.

CHAPTER 3: In this chapter the perturbation and interpolation methods are intro-

duced. Their application for damped modes estimation is presented. The accuracy of the methods is tested numerically and their efficiency through asymptotic analysis. Furthermore, a new formulation of the Rayleigh quotient for damped systems is developed. Its use for enhancing the linear approximations is novel to this work. These methods are to be combined with Component Mode Synthesis to devise more efficient reanalysis methods for damped systems, which are presented in chapter 5.

CHAPTER 4: This chapter is devoted to Component Mode Synthesis. The background theory for model order reduction techniques and substructuring of finite element models is first presented. Component mode synthesis is explained by means of a generic formulation which is valid for all specific CMS methods. The most conventional CMS methods are then described; namely, the fixed-interface with constraint modes and the free-interface with residual attachment modes. Then, a generic formulation for state-space based CMS methods is developed, and two CMS methods for damped systems are described. The CMS methods are tested on two numerical examples in order to evaluate their accuracy and efficiency, and the undamped and damped CMS methods are compared.

CHAPTER 5: In chapter 5 perturbation methods in damped modes CMS are formulated. Two methods, namely the Component Modal-Propagation (CMP) method and the Local Modal Perturbation (LMP) method for damped systems are presented. They are validated using numerical examples so that the accuracy of approximation can be bounded. The range of validity is discussed and a range of potential applications is proposed. The efficiency of the methods is further tested with a large numerical example.

CHAPTER 6: The application of the fixed-interface perturbation method for uncertainty analysis is developed in this chapter. The basic theory for modelling of uncertainty as well as uncertainty quantification is explained. Then the use of perturbation method in Monte Carlo calculations is described. Finally, validation and efficiency of this application is tested through simulations on a ribbed plate example.

CHAPTER 7: Finally chapter 7 summarises the work done and reviews the degree of accomplishment of the thesis objectives. It draws conclusions of the thesis, future research lines, other potential applications and underlines the research achievements of this study.

1.7 Contributions

This section summarises the original contributions coming out of the present thesis, which can be arranged in three main areas of contribution.

A first area concerns the development of the approximate modal analysis of heavily damped systems from the state-space formulation. This involves bringing together the perturbation and interpolation linear approximation methods with the eigensolution of state-space models. On one hand, the exact solution of state-space eigenvalue problem is needed for computing the baseline solutions needed for the linear approximations. Here, a modified version of the Symmetric Indefinite Lanczos Method has been proposed in order to obtain just the relevant (i.e. non-overdamped) modes of vibration. This is very important specially for the proper component reduction in state-space based CMS. On the other hand, damped mode perturbation has been formulated from existing sensitivity expressions and the approximation of damped modes through the interpolation method has been proposed, showing similar efficiency and improved accuracy in comparison to existing methods for linear approximate modal analysis from undamped eigensolutions.

Secondly, the range of validity of the modal approximations has been efficiently broadened by means of the proposed quotient approximation for damped eigenvalues. This damped quotient is derived directly from the state-space EVP and provides optimal eigenvalue estimation given an approximate damped eigenvector. Its use with interpolation methods is preferred given the reduced cost for eigenvector interpolation. Hence, the accuracy in modal damping and modal frequency approximation is highly improved by applying the proposed quotient, which makes quotient approximation suitable for approximating gross modifications in structural design.

In third place, enhanced perturbation methods based on the CMS reduction of state-space models have been proposed. In this thesis, existing state-space based CMS methods have been evaluated, proving their improved performance for the reduction of locally and heavily damped systems. Perturbation approximations in CMS reduced models have been formulated, providing in this way a substructured perturbation scheme that allows for scalable application of the perturbation approximations. From this generic framework two perturbation methods are developed. The Component Modal-Propagation method which is very well suited for the efficient modal approximation of systems with locally varying damping, and the Local Modal Perturbation method whose application is satisfactory for very

efficient modal approximation of heavily damped systems with variability in the medium and high-frequency regimes. In the current work, the (state-space) CMS perturbation methods have shown very good performance when applied to uncertainty analysis applications, and they are regarded equally suitable for their use in other applications requiring intensive reanalysis.

Chapter 2

Linear analysis of damped systems

In this thesis, the dynamic analysis of vibrating systems is considered. Efficient original methods are to be derived for the analysis of damped systems. These efficient methods are required for the case when large systems have to be analysed repeatedly (e.g. for variability investigations), so that the computational cost is bearable for modelling purposes. In subsequent chapters these efficient approximate methods will be presented. Before that, however, examination of the conventional ways to perform the dynamic analysis of damped systems will be presented in this chapter. The theory introduced here will serve as a basis for the derivation of the aforementioned approximate methods.

The linear analysis of dynamic systems is typically performed using the modal superposition method, where the vibration solution is found as the weighted sum of vibration modes. Each mode is defined by its modal frequency, modal damping and mode shape vector. Determination of the modes of a system is not a trivial task and typically it constitutes the most expensive computation in the analysis. In particular, the modal analysis of damped systems is rather complicated because it is difficult to correctly account for the damping using a simple mathematical model.

In this chapter the modal analysis of damped systems with viscous damping is detailed. Two different strategies for finding the damped system modes are presented. First, the classical Rayleigh approach is explained, where the damped modes are obtained from the undamped modes of the system. This approach is only valid under the assumption that the viscous damping is small or proportional to the mass and stiffness properties of the system. The second approach based on the state-space formulation is then explained. The damped modes are obtained directly in this

second approach, with no assumption other than the damping being of the viscous kind.

The computation of dynamic system modes always results in estimated modes with a certain degree of computational error. When one performs modal analysis one has to be aware of the amount of error introduced in the computation. Ways exist to estimate the error in the modal solutions, or at least upper bounds for the error. In this chapter, these error measures and bounds are specified for damped modal analysis. The importance of introducing them is that they will be of use for estimating the approximation error introduced by the approximate methods that are developed in this thesis.

2.1 Damping models for structural vibrations

The classical Rayleigh [46] approach for the modelling of vibrating structures approximates the elastic and inertia properties of the system with the stiffness $\mathbf{K}$ and mass $\mathbf{M}$ matrices respectively. The energy dissipation in the system is analogously represented by the damping matrix $\mathbf{C}$ giving rise to the damped equations of motion

$$\mathbf{M\ddot{u}} + \mathbf{C\dot{u}} + \mathbf{Ku} = \mathbf{f} \tag{2.1}$$

with $\mathbf{u}$ the vector of generalised displacements and $\mathbf{f}$ the vector of external forces. The vectors $\dot{\mathbf{u}}$ and $\ddot{\mathbf{u}}$ stand for the displacements' first and second derivatives with respect to time. In the classical approach, it is assumed that the damping forces are proportional to the instantaneous velocity $\dot{\mathbf{u}}$. Hence, the matrix $\mathbf{C}$ is a viscous damping matrix.

The viscous damping model is not the *only* existing dissipation model. In fact, in equation 2.1 the elastic and inertia forces are known to be well defined by the terms $\mathbf{Ku}$ and $\mathbf{M\ddot{u}}$ respectively. On the contrary, there may be various dissipation mechanisms in a structure (e.g. distributed material damping, frictional micro-slipping and air pumping at joints, fluid in contact with the structure) and, according to Woodhouse [47], it is not clear that the damping forces are proportional to the instantaneous velocity. Nevertheless, viscous damping is the most generally used damping model and it gives good approximate results in the majority of cases, especially for light damping.

Other linear models of damping include the *hysteretic damping* model which is a dissipation-matrix based model [48] for frequency domain analysis. In this model

the damping matrix is frequency dependent $\mathbf{C}(\omega)$ so that damping is not necessarily proportional to the instantaneous velocity. A specific case of hysteretic damping is when the damping matrix is defined as $\mathbf{C}(\omega) = \mathbf{C}/|\omega|$, which implies that it is proportional to the instantaneous harmonic displacement. This model gives frequency independent modal damping, which is in agreement with many material damping testing results. However, the hysteretic damping model is physically inconsistent since it violates considerations of causality [49]. Typically viscoelastic damping is alternatively accounted for by assigning a constant damping ratio to all modes once they have been computed from the undamped equations of motion.

Linear damping models which are not dissipation-matrix models assume that damping is not only proportional to the instantaneous state variables but also to its past time history. These methods use kernel functions which are convoluted with the state variables instead of dissipation matrices. Also, there exist non-linear models such as friction power law damping (e.g. *velocity squared* damping, etc.). The interested reader can refer to [50] for further details on these damping models. In this thesis only the dissipation-matrix models will be used, and the viscous damping model will be assumed throughout unless otherwise stated.

2.2 Modal analysis of viscously damped systems

The modal analysis of a system consists in finding the modes of vibration of the system, so that the vibration response of the system due to external loading can be expressed as a sum of modal contributions. The modes of a system modelled with a Finite Element model can be computed from the dynamic equations of motion.

For a viscously damped system the equations of motion are posed in terms of the mass, stiffness and viscous damping matrices (c.f. equation 2.1) whose free vibration solutions are the vibration modes of the system. The damped equations of motion are a set of N_d coupled second-order differential equations. The solutions to these equations are assumed to be of the following kind

$$\mathbf{u}(t) = \boldsymbol{\phi} e^{\lambda t} \tag{2.2}$$

so that generalized displacement vector is expressed as the product of a constant shape vector $\boldsymbol{\phi}$ and an exponential time function with argument λ.

The modal parameters of the system are obtained from the homogeneous equations of motion, i.e. setting $\mathbf{f} = \mathbf{0}$. In principle, the modal solution to such a system

of equations follows from the solution of the corresponding quadratic eigenvalue problem (QEVP)

$$\left(\lambda^2\mathbf{M} + \lambda\mathbf{C} + \mathbf{K}\right)\boldsymbol{\phi} = \mathbf{0} \tag{2.3}$$

with λ the eigenvalue and $\boldsymbol{\phi}$ the eigenvector solutions. The QEVP has $2N_d$ eigenvalues and $2N_d$ right/left eigenvectors. For $\mathbf{K}$, $\mathbf{M}$ and $\mathbf{C}$ being real and symmetric, the eigenvalues and eigenvectors occur in complex conjugate pairs and the left eigenvector equals the transposed right eigenvector [51].

Each complex conjugate pair represents one vibrational mode m. The eigenvalues of damped systems are therefore complex valued, i.e. $\lambda_m = -\sigma_m \pm i\omega_{d,m}$, with the negative real part accounting for the modal decay rate due to damping and the imaginary part corresponding to the damped modal frequency. The modal damping is usually given in non-dimensional units in terms of the damping ratio $\zeta_m = \sigma_m/|\lambda_m|$. Generally, the eigenvectors $\boldsymbol{\phi}_m$ are also complex valued and they correspond to the mode shape vectors.

In order to avoid dealing with a non-linear EVP whose solution is numerically complicated [51], the QEVP is typically linearized into a standard generalised EVP. This can be done in two ways: either by solving the undamped system EVP under the assumption that the damping is small or proportional to the mass and stiffness matrices; or by transformation of the equations of motion into first order state-space form.

2.2.1 Proportional damping

The classical approach assumes that the viscous damping matrix is proportional to the mass and stiffness matrices, which is known as *Rayleigh damping*, *classical damping* or *proportional viscous damping*. In this case the problem is initially reduced to the solution of the undamped equations of motion.

$$\mathbf{M}\ddot{\mathbf{u}} + \mathbf{K}\mathbf{u} = \mathbf{f} \tag{2.4}$$

The undamped solutions for the generalized displacements $\mathbf{u}$ are assumed to be the product of a shape vector $\boldsymbol{u}$ and an exponential time function with argument $s = i\omega$.

$$\mathbf{u}(t) = \boldsymbol{u}e^{st} \tag{2.5}$$

Then, the linearized EVP corresponding to the undamped equations of motion is solved

$$\left(s^2\mathbf{M} + \mathbf{K}\right)\boldsymbol{u} = \mathbf{0} \tag{2.6}$$

having N_d eigenvalue pairs $s_m^2 = (\pm i\omega_m)^2 = -\omega_m^2$ corresponding to the undamped modal frequencies and N_d real-valued eigenvectors $\boldsymbol{u}_m$ corresponding to the undamped mode shape vectors. Here it must be pointed out that the undamped eigenvalues are generally termed

$$\lambda_m^{\text{undamp}} = \omega_m^2 \tag{2.7}$$

This convention comes from expressing the EVP in equation 2.6 as $\lambda \mathbf{M}\boldsymbol{u} = \mathbf{K}\boldsymbol{u}$. However, one shall not confuse this undamped eigenvalues convention with the damped eigenvalues λ_m coming from the QEVP in equation 2.3.

The mass and stiffness matrices can be transformed into modal coordinates $\mathbf{p}$ by pre and post multiplication with the matrix $\mathbf{U} = [\boldsymbol{u}_1, \boldsymbol{u}_2, \cdots, \boldsymbol{u}_{N_d}]$ consisting of the undamped eigenvectors. This transformation diagonalises the matrices because the eigenvectors form an orthogonal basis. Typically, the eigenvectors are normalised with respect to the mass matrix (c.f. Appendix A.3) so that the modal mass matrix $\bar{\mathbf{M}}$ equals the identity matrix, that is

$$\bar{\mathbf{M}} = \mathbf{U}^T\mathbf{M}\mathbf{U} = \mathbf{I}$$

Correspondingly the mass-normalized modal stiffness matrix $\bar{\mathbf{K}}$ is

$$\bar{\mathbf{K}} = \mathbf{U}^T\mathbf{K}\mathbf{U} = \boldsymbol{\Omega}^2$$

where $\boldsymbol{\Omega} = \text{diag}(\omega_1, \omega_2, \cdots, \omega_{N_d})$ is a diagonal matrix consisting of the N_d undamped modal frequencies.

The proportionality assumption implies that the $\mathbf{C}$ matrix is also diagonalised by the $\mathbf{U}$ matrix. The modal damping matrix $\bar{\mathbf{C}} = \mathbf{U}^T\mathbf{C}\mathbf{U}$ is a diagonal matrix with the m'th element in the diagonal of the modal damping matrix $\bar{C}_{mm}$ corresponding to the modal damping of the mth mode. Therefore, the undamped eigenvectors do uncouple the proportionally-damped equations of motion when transformed into the modal coordinates $\mathbf{p}$, that is

$$\ddot{\mathbf{p}} + \bar{\mathbf{C}}\dot{\mathbf{p}} + \boldsymbol{\Omega}^2\mathbf{p} = \mathbf{Q} \tag{2.8}$$

with $\mathbf{u} = \mathbf{U}\mathbf{p}$ and $\mathbf{Q} = \mathbf{U}^T\mathbf{f}$. This means that the mode shape vectors $\boldsymbol{\phi}_m$ of a proportionally damped system equal the undamped mode shape vectors $\boldsymbol{u}_m$.

Each uncoupled equation of motion in equation 2.8 corresponds to a mode of vibration that can be analysed as a single-degree-of-freedom (SDOF) viscously damped oscillator[1].

[1] A damped SDOF system with mass m, stiffness k and damping constant c has its damped resonance frequency at $\omega_d = \omega_n\sqrt{1-\zeta^2}$, with $\omega_n = \sqrt{\frac{k}{m}}$ the corresponding undamped natural frequency and $\zeta = \frac{c}{2m\omega_n}$ the damping ratio.

Thence, a proportionally damped mode has $\omega_{d,m} = \omega_m\sqrt{1-\zeta_m^2}$ modal frequency and $\zeta_m = \frac{\bar{C}_{mm}}{2\omega_m}$ damping ratio, so that the eigenvalues of a proportionally damped system read

$$\lambda_m = -\zeta_m\omega_m \pm i\omega_m\sqrt{1-\zeta_m^2} \tag{2.9}$$

The steady state response solution is obtained by assuming harmonic vibration response for each mode. Then, the modal displacement vectors $\mathbf{p}$ in equation 2.8 are straightforwardly differentiated with respect to time giving

$$[-\omega^2\mathbf{I} + i\omega\bar{\mathbf{C}} + \mathbf{\Omega}^2]\mathbf{p} = \mathbf{Q} \tag{2.10}$$

so that solving for the modal displacements

$$\mathbf{p} = [-\omega^2\mathbf{I} + i\omega\bar{\mathbf{C}} + \mathbf{\Omega}^2]^{-1}\mathbf{Q} = \bar{\mathbf{H}}\mathbf{Q} \tag{2.11}$$

one finds modal response solution in terms of the modal *receptance* matrix $\bar{\mathbf{H}}$. The modal response $\mathbf{p}$ can be transformed back into physical displacement coordinates by pre-multiplying both sides of equation 2.11 with $\mathbf{U}$, that is

$$\mathbf{u} = \mathbf{U}\bar{\mathbf{H}}\mathbf{U}^T\mathbf{f} = \mathbf{H}\mathbf{f} \tag{2.12}$$

where $\mathbf{H}$ is the receptance matrix in physical coordinates. Hence, the displacement response of the system is found by means of the $\mathbf{H}$ matrix. Each element of the receptance matrix H_{ij} is the frequency response function between the force applied at the i'th physical degree of freedom and the displacement response at the j'th degree of freedom. From equations 2.11 and 2.12 it can be seen that

$$\mathbf{H} = \sum_{m=1}^{N_d} \frac{\boldsymbol{u}_m\boldsymbol{u}_m^T}{-\omega^2 + i2\zeta_m\omega_m\omega + \omega_m^2} \tag{2.13}$$

where it is clear that, in modal analysis, the response of the system is obtained as the sum of the contributions of each mode.

2.2.2 Small damping

In the majority of cases the mode shapes of a system are complex-valued when they are estimated using modal testing [48]. Hence the proportional damping assumption is convenient mathematically, but it does not match with the damping distribution of real systems. In a general case, the viscous damping matrix is *non-proportional* to the mass and stiffness matrices. Performing the analysis with undamped eigenvectors does not uncouple the damped equations of motion, i.e. the $\bar{\mathbf{C}}$ matrix is not diagonal.

Nevertheless, the modal damping matrix $\bar{\mathbf{C}}$ for non-proportional viscous damping is usually diagonal-dominant, and many times the modal damping can be still fairly well estimated using undamped modes for lightly damped systems. Under the assumption of small damping, Rayleigh [46] showed that the damped eigenvectors λ_m can be approximated from the corresponding undamped modal frequencies ω_m and undamped mode shape vectors $\boldsymbol{u}_m$ as

$$\lambda_m \approx -\frac{1}{2}\bar{C}_{mm} \pm i\omega_m \tag{2.14}$$

with $\bar{C}_{mm} = \boldsymbol{u}_m^T \mathbf{C} \boldsymbol{u}_m$. Similarly, the damped eigenvectors $\boldsymbol{\phi}_m$ can be approximated from all undamped modal frequencies ω_k and all undamped mode shape vectors $\boldsymbol{u}_k$ as

$$\boldsymbol{\phi}_m \approx \boldsymbol{u}_m \pm i \sum_{k \neq m} \frac{\omega_m \bar{C}_{km}}{\omega_m^2 - \omega_k^2} \boldsymbol{u}_k \tag{2.15}$$

with $\bar{C}_{km} = \boldsymbol{u}_k^T \mathbf{C} \boldsymbol{u}_m$. Complex valued mode shape vectors are obtained from the small damping approximation.

2.2.3 State-Space formulation

The QEVP in equation 2.3 may be linearised using the *State-Space* formulation instead (see for instance Meirovitch [52]). The damped equations of motion in equation 2.1 can be cast into the first-order state-space form

$$\begin{bmatrix} \mathbf{0} & \mathbf{M} \\ \mathbf{M} & \mathbf{C} \end{bmatrix} \begin{Bmatrix} \ddot{\mathbf{u}} \\ \dot{\mathbf{u}} \end{Bmatrix} + \begin{bmatrix} -\mathbf{M} & \mathbf{0} \\ \mathbf{0} & \mathbf{K} \end{bmatrix} \begin{Bmatrix} \dot{\mathbf{u}} \\ \mathbf{u} \end{Bmatrix} = \begin{Bmatrix} \mathbf{0} \\ \mathbf{f} \end{Bmatrix} \tag{2.16}$$

where the identity $\mathbf{M}\dot{\mathbf{u}} - \mathbf{M}\dot{\mathbf{u}} = \mathbf{0}$ is introduced in the upper row. Introducing the *state* condensed notation

$$\mathbf{x} = \begin{Bmatrix} \dot{\mathbf{u}} \\ \mathbf{u} \end{Bmatrix} \;,\; \mathbf{A} = \begin{bmatrix} \mathbf{0} & \mathbf{M} \\ \mathbf{M} & \mathbf{C} \end{bmatrix} \;,\quad \mathbf{B} = \begin{bmatrix} \mathbf{M} & \mathbf{0} \\ \mathbf{0} & -\mathbf{K} \end{bmatrix} \quad \text{and} \quad \mathbf{f}^x = \begin{Bmatrix} \mathbf{0} \\ \mathbf{f} \end{Bmatrix} \tag{2.17}$$

it can be clearly observed that the equations of motion in state coordinates $\mathbf{x}$ are a set of $2N_d$ first-order differential equations.

$$\mathbf{A}\dot{\mathbf{x}} - \mathbf{B}\mathbf{x} = \mathbf{f}^x \tag{2.18}$$

The state equations of motion may be solved in the same way as for the undamped equations of motion. Assume solutions of the kind

$$\mathbf{x}(t) = \boldsymbol{x} e^{\lambda t} \tag{2.19}$$

with the state vector $\mathbf{x}$ composed as the product of a shape vector $\boldsymbol{x}$ and an exponential time function with complex argument λ. The state solution follows from the solution of a linear EVP in state-coordinates

$$(\lambda\mathbf{A} - \mathbf{B})\,\boldsymbol{x} = \mathbf{0} \tag{2.20}$$

with $\lambda_m = -\sigma_m \pm i\omega_{d,m}$ the complex eigenvalues of the original QEVP, and $\boldsymbol{x}_m = \{\lambda_m \boldsymbol{\phi}_m^T, \boldsymbol{\phi}_m^T\}^T$ the state eigenvectors which contain the original QEVP complex eigenvectors $\boldsymbol{\phi}_m$. The solutions obtained using the state-space formulation are exact and, unlike the expressions in equations 2.14 and 2.15, they are valid regardless of the system being lightly damped or not.

The state equations of motion in equation 2.18 can be decoupled using a matrix $\mathbf{X} = [\boldsymbol{x}_1, \boldsymbol{x}_2, \cdots, \boldsymbol{x}_{2N_d}]$ consisting of the $\mathbf{A}$-normalized state eigenvectors (c.f. Appendix A.4). The modal state matrices are then

$$\bar{\mathbf{A}} = \mathbf{X}^T\mathbf{A}\mathbf{X} = \mathbf{I}$$

$$\bar{\mathbf{B}} = \mathbf{X}^T\mathbf{B}\mathbf{X} = \boldsymbol{\Lambda}$$

with $\boldsymbol{\Lambda} = \mathrm{diag}(\lambda_1, \lambda_2, \cdots, \lambda_{2N_d})$ a diagonal matrix consisting of the $2N_d$ complex eigenvalues. In this way the equations of motion are posed into modal state coordinates $\mathbf{q}$

$$\dot{\mathbf{q}} - \boldsymbol{\Lambda}\mathbf{q} = \mathbf{Q}^x \tag{2.21}$$

with the vectors $\mathbf{x} = \mathbf{X}\mathbf{q}$ and $\mathbf{Q}^x = \mathbf{X}^T\mathbf{f}^x$ having $2N_d$ degrees of freedom (DOFs).

As for the proportionally damped case, the steady state response is obtained assuming harmonic vibration so that the state equations of motion read

$$[s\mathbf{I} - \boldsymbol{\Lambda}]\mathbf{q} = \mathbf{Q}^x \tag{2.22}$$

with $s = i\omega$. Again, solving for the modal state-displacements $\mathbf{q}$

$$\mathbf{q} = [s\mathbf{I} - \boldsymbol{\Lambda}]^{-1}\mathbf{Q}^x = \bar{\mathbf{H}}^x\mathbf{Q}^x \tag{2.23}$$

the modal response solution is posed in terms of a modal *receptance* matrix $\bar{\mathbf{H}}^x = [s\mathbf{I} - \boldsymbol{\Lambda}]^{-1}$. The modal response is transformed back into physical state coordinates $\mathbf{x}$ by pre-multiplication with the $\mathbf{X}$ matrix

$$\mathbf{x} = \mathbf{X}\bar{\mathbf{H}}^x\mathbf{X}^T\mathbf{f}^x \tag{2.24}$$

The physical displacement coordinates $\mathbf{u}$ are a partition of the state coordinates $\mathbf{x}$. The $\mathbf{X}$ matrix can be partitioned accordingly, i.e. $\mathbf{X} = [\boldsymbol{\Lambda}\boldsymbol{\Phi}^T,\ \boldsymbol{\Phi}^T]^T$ with $\boldsymbol{\Phi} =$

$[\boldsymbol{\phi}_1, \boldsymbol{\phi}_2, \cdots, \boldsymbol{\phi}_{2N_d}]$ a matrix consisting of the damped eigenvectors of the original QEVP. Hence, from equation 2.24 we can write

$$\mathbf{u} = \boldsymbol{\Phi}\bar{\mathbf{H}}^x\boldsymbol{\Phi}^T\mathbf{f} = \mathbf{H}\mathbf{f} \tag{2.25}$$

where $\mathbf{H} = \boldsymbol{\Phi}[s\mathbf{I} - \boldsymbol{\Lambda}]^{-1}\boldsymbol{\Phi}^T$ is the receptance matrix in physical coordinates. Notice that here $\boldsymbol{\Phi}$ is a matrix of damped mode shape vectors $\boldsymbol{\phi}_m$ with different normalisation than the mass normalised undamped mode shape vectors $\boldsymbol{u}_m$. Finally, the receptance matrix $\mathbf{H}$ for non-proportionally damped systems is expressed as the sum of the modal contributions

$$\mathbf{H} = \sum_{m=1}^{N_d} \frac{\boldsymbol{\phi}_m\boldsymbol{\phi}_m^T}{s - \lambda_m} + \frac{\boldsymbol{\phi}_m^*\boldsymbol{\phi}_m^H}{s - \lambda_m^*} \tag{2.26}$$

where H is the Hermitian operator and each mode is characterised by the complex conjugate pairs of damped eigenvalues and eigenvectors.

The solutions obtained using the state-space formulation are exact and, unlike the expressions in equations 2.14 and 2.15, they are valid regardless of the system being lightly damped or not. On the contrary, the order of the state EVP in equation 2.20 is doubled with respect to the undamped EVP in equation 2.6.

2.3 The eigenvalue problem in modal analysis

Typically, the dynamic structures for which it is desired to perform modal analysis are characterised by FE models consisting of thousands or millions of degrees of freedom, giving rise to very large sparse system matrices. In turn, one is usually interested in just a few tens or hundreds of vibrational modes. The EVPs corresponding to such large systems are typically solved using *Lanczos* algorithms. These eigenvalue algorithms are the most efficient algorithms for computing just a few number of eigensolutions of large eigenvalue problems.

Although it is not the purpose of this work to gain a deep insight into the details of eigenvalue algorithms, some basic features of the Lanczos algorithms will be briefly highlighted in this section. This will give a general understanding of the nature of these algorithms, so that the associated computational cost of the algorithms can be evaluated. For further algorithm details, the interested reader may find many publications in the literature devoted to numerical algorithms for the solution of eigenvalue problems (e.g. [53–55]).

In this section, the mathematical properties of the EVPs encountered in the modal analysis of dynamic systems are evaluated. It will be seen that the undamped EVP and the state-space EVP have different properties. Consequently, different Lanczos algorithms are used for each case.

2.3.1 Eigenvalue algorithms

The solutions to eigenvalue problems are computed through so called eigenvalue algorithms. Eigenvalue algorithms are very computationally expensive. These are typically iterative algorithms which keep iterating until the solution converges. The computational efficiency of the eigenvalue algorithms depends on the computational cost of each iteration step, and also on the convergence rate of the algorithm, i.e. how many iterations are needed for each modal solution.

Eigenvalue algorithms may be divided into two groups. Those algorithms that may compute one or few eigensolutions only (e.g. Rayleigh quotient iteration, Lanczos algorithms, etc.), and those algorithms that necessarily produce all eigensolutions of the EVP (e.g. QR algorithm, MRRR algorithm, etc.). The former are aimed at solving EVPs defined by large sparse matrices whereas the latter are applied to EVPs defined by smaller densely populated matrices.

In modal analysis the eigenvalue algorithms producing a limited number of solutions to the EVP are of relevance. Among these, the Lanczos algorithms are the ones that achieve the best computational efficiency. The Lanczos algorithms are nothing but efficient implementations of the *Arnoldi iteration* method. In turn, the Arnoldi iteration method was developed from the *power iteration* method.

In the following, the power and inverse iteration methods are explained. Next, the *Arnoldi iteration* method is explained on the grounds the power iteration. In this way, a general overview of the computational complexity and efficiency of the Lanczos algorithms is given. For simplicity, the methods will be described for the standard eigenvalue problem $\mathbf{A}\boldsymbol{b} = \lambda\boldsymbol{b}$, that is, the problem of finding the eigenvalues λ and eigenvectors $\boldsymbol{b}$ of a matrix $\mathbf{A}$.

Power and inverse iteration

The algorithms that compute just some of the eigensolutions have their origin in the *power iteration* method for finding the dominant (largest) eigenvalue of a generic

matrix $\mathbf{A}$.

Power iteration starts from an arbitrary vector $\boldsymbol{b}_0$ (typically a random vector). At each iteration i the $\mathbf{A}$ matrix is applied to the vector resulting from the previous iteration, i.e. $\boldsymbol{b}_i = \mathbf{A}\boldsymbol{b}_{i-1}$. This is equivalent to multiplying the initial vector with increasing order powers of the matrix at each iteration, i.e. $\boldsymbol{b}_i = \mathbf{A}^i\boldsymbol{b}_0$. After several iterations the vector converges to the dominant eigenvector of the matrix. In turn, the norms ratio of two consecutive iterations vectors converges to the dominant eigenvalue.

For a matrix of order N, each iteration has a computational cost of $\mathcal{O}(N^2)$, which is that of performing the matrix-vector multiplication. The rate of convergence is linear and may be very slow if the second larger eigenvalue is of comparable magnitude to the largest one.

In order to find eigensolutions other than the one corresponding to the dominant eigenvalue, the power iteration method may be applied to the inverse matrix $(\mathbf{A} - \mu\mathbf{I})^{-1}$, which is known as the *inverse iteration* method. Inverse iteration converges to the eigenvalue of matrix $\mathbf{A}$ which is closest to the value of the parameter μ at a linear convergence rate. For hermitian matrices (or hermitian generalised EVPs) inverse iteration can be enhanced by updating μ with the Rayleigh quotient at each iteration yielding a cubic convergence rate.

However, the large matrices that arise in structural dynamics are often ill conditioned, so that performing their direct inversion may give rise to large errors in the solution. Hence, it may not be implemented, analogous to the power iteration, as just multiplying the inverted matrix at each step. Instead, a linear system of equations, i.e. $(\mathbf{A} - \mu\mathbf{I})\,\boldsymbol{b}_i = \boldsymbol{b}_{i-1}$, must be solved at each iteration step. This significantly increases the computational cost at each step which may go up to $\mathcal{O}(N^3)$ depending on the structure of the matrix (e.g. sparse, Toeplitz, non-structured...).

Arnoldi iteration and Lanczos algorithms

Much more efficient algorithms have been devised based on the fact that the set of vectors $\boldsymbol{b}_i$ obtained at each iteration in the power iteration method span a *Krylov subspace*.

The central idea of these algorithms is to project the EVP matrix $\mathbf{A}$ onto a Krylov subspace $\mathcal{K}$ of reduced order m generated by the matrix $\mathbf{A}$ and an initial vector $\boldsymbol{b}_0$. This gives as a result a reduced matrix $\mathbf{R}$ with the same order as the $\mathcal{K}^m(\mathbf{A}, \boldsymbol{b}_0)$

subspace, whose eigensolutions correspond to the m dominant eigensolutions of the original matrix $\mathbf{A}$. The order m of the Krylov subspace may be chosen arbitrarily and it is typically set to twice the number of eigensolutions (modes) that are to be computed.

Following this idea, the *Arnoldi iteration* method and the *Lanczos* algorithms were defined. Arnoldi iteration is the method for reducing the EVP matrix ensuring numerical stability, and it is valid for any linear eigenvalue problem. The Lanczos algorithms are efficient implementations of the Arnoldi iteration.

The classic Lanczos algorithm [56] is the most efficient algorithm and applies only to hermitian EVPs. Hermitian EVPs are those that can be transformed into a standard EVP defined by a Hermitian matrix. There also exist less efficient variants of the Lanczos algortihm for non-hermitian EVPs.

Arnoldi iterartion computes the m vectors that span the Krylov subspace performing Gram-Schmidt orthogonalisation at each step, giving rise to an orthonormal basis $\mathbf{V}$ of so called *Arnoldi vectors* $\boldsymbol{v}_i$. The EVP matrix $\mathbf{A}$ is projected onto the Arnoldi vectors basis, so that it gets transformed into a reduced matrix $\mathbf{R}$, i.e. $\mathbf{R} = \mathbf{V}^H\mathbf{A}\mathbf{V}$. The reduced matrix is of *Hessenberg* form for a generic matrix $\mathbf{A}$. If the $\mathbf{A}$ matrix is hermitian, the reduced matrix becomes real-symmetric *tridiagonal*.

The computational cost of the Arnoldi iteration method is the cost of computing the Arnoldi vectors and obtaining the reduced matrix. This is done at a computational cost $\mathcal{O}(N^2)m+2Nm^2$. The Lanczos algorithm is a simplified version of the Arnoldi iteration that takes full advantage of the symmetry of the tridiagonal reduced matrix in hermitian EVPs. It efficiently computes the so called *Lanczos vectors* and the tridiagonal reduced matrix at a cost $\mathcal{O}(N^2)m + 7Nm$.

Then, m eigensolutions can be found by solving the EVP corresponding to the reduced order matrix $\mathbf{R}$. The computed eigenvalues correspond to the m dominant eigenvalues of the original EVP. The corresponding computed eigenvectors are of reduced order and they may be transformed back into full order by pre-multiplication with $\mathbf{V}$.

Efficient algorithms that produce *all* eigensolutions of the reduced EVP may be used since $\mathbf{R}$ is a small matrix. The *QR algorithm* may be used for computing efficiently all eigensolutions of a Hessemberg $\mathbf{R}$ matrix at a cost $\mathcal{O}(6m^3)+\mathcal{O}(m^2)$ per iteration step and with a cubic convergence rate. For a real symmetric tridiagonal $\mathbf{R}$ matrix (i.e. hermitian EVP), the *Multiple Relatively Robust Representations* (MRRR) algorithm may be used instead at a computational cost $\mathcal{O}(m^2)$ per iteration step.

Assuming, as it is usually the case in dynamics, that the order of the matrices N is very large, the computational cost for solving the reduced EVP is very small in comparison with the cost of obtaining the reduced EVP. Moreover, since $m \ll N$, Lanczos algorithms obtain the m dominant eigensolutions of a large matrix roughly at a cost $\mathcal{O}(N^2)$ per eigensolution.

2.3.2 Eigenvalue problem properties

In modal analysis, the eigenvalue problems that need to be solved are generalised eigenvalue problems defined by a pair of matrices, what is known as a *matrix pencil*. The mathematical properties of the matrices defining the eigenvalue problem are of great significance for the computation of the solution. Depending on these properties more or less efficient algorithms can be used for solving the corresponding eigenvalue problem.

The undamped EVP is defined by the $(\mathbf{M}, \mathbf{K})$ pencil whereas the state-space EVP is defined by the $(\mathbf{A}, \mathbf{B})$ pencil. These two pencils have distinct mathematical properties.

The $\mathbf{M}$ and $\mathbf{K}$ matrices are real-symmetric positive-definite matrices. This makes the $(\mathbf{M}, \mathbf{K})$ pencil to be a definite matrix pencil and, consequently, the undamped EVP is of the hermitian kind. These are the less complicated eigenvalue problems to solve.

The $\mathbf{A}$ and $\mathbf{B}$ matrices are real-symmetric as well, but they are not positive-definite. Hence, the $(\mathbf{A}, \mathbf{B})$ pencil is said to be indefinite. This has several implications. To start with, the state-space eigenvalue problem is a non-hermitian eigenvalue problem. Therefore, the EVP solving algorithms become more complicated and therefore less efficient. In turn, the availability of error bounds for the modal solutions of the state-space EVP gets reduced due to the indefiniteness of the pencil, as will be shown in section 2.4.2.

2.3.3 Undamped eigenvalue problem solution computation

As has been described in section 2.3.2 the eigenvalue problem corresponding to the undamped equations of motion is hermitian. Hence, the solution of the undamped EVP is obtained using the standard Lanczos algorithm for the generalised hermitian eigenvalue problem (GHEVP). Implementation of the Lanczos algorithm is publicly

available in the Linear Algebra Package (LAPACK) software library.

As opposed to the $\mathcal{O}(N^2)$ cost per eigensolution of the Lanczos algorithms for the standard EVP, the generalised EVPs involve a solution cost of up to $\mathcal{O}(N^3)$ per eigensolution through the use of Lanczos algorithms. This is because one needs to solve a linear system of equations at each iteration of the Lanczos algorithm for the GHEVP, in addition to the matrix-vector multiplication ($\mathcal{O}(N^2)$ cost) that was already needed in the Lanczos algorithm for the standard EVP (see section 5.5.1 in reference [54] for details). The cost for solving a linear system of equations is of $\mathcal{O}(N^3)$ for a generic matrix.

Sparsity of the matrices

It has to be pointed out, however, that the **M**, **C** and **K** matrices are markedly sparse (and so are the **A** and **B** matrices in the state-space EVP). Most of the elements in sparse matrices are zero valued and, therefore, the computational complexity of sparse matrix operations is significantly smaller than for generic full matrices.

For instance, the cost of sparse matrix-vector products is proportional to the number of non-zero elements rather than to the total number of matrix elements (see [57]). For large systems, the number of non-zero elements N_{NZ} is much smaller than the total number of elements N^2, but larger than the matrix order N since they are of full rank, i.e. $N < N_{\mathrm{NZ}} \ll N^2$. Therefore, the associated computational cost of sparse matrix-vector products is somewhat close above $\mathcal{O}(N)$ rather than $\mathcal{O}(N^2)$.

In a similar way, solving a system of equations determined by large sparse matrices involves a much smaller computational cost than $\mathcal{O}(N^3)$. Estimating the associated computation cost is not a trivial task although, according to [57], the required computational time is proportional to the number of arithmetic operations on nonzero quantities. Hence, the computation cost for solving a sparse system of equations may well be below $\mathcal{O}(N^3)$. In fact, rather than computing the exact solution to the linear system of equations, eigenvalue algorithms for large sparse matrices typically compute a least squares estimate of this solution, which is much more efficiently computed through sparse specific algorithms such as the LSQR algorithm [58].

It can be concluded that the solution of large sparse generalised eigenvalue problems encountered in modal analysis involves a solution cost that scales with the number of non-zero elements in the matrices, and that $\mathcal{O}(N^2)$ may be regarded as a conservative upper bound for the computational cost per eigensolution through

Lanczos algorithms.

Lumped mass approximation

For the undamped EVP, the mass matrix is the matrix involved in the linear system of equations to solve in the Lanczos iterations. Many times, a *lumped mass matrix* approximation is used in order to reduce the solution cost. This approximation replaces the *consistent* element mass matrices obtained in the finite element method with diagonal mass matrices with equivalent total mass. That is, the inertial properties of the elements are approximated by lumped masses at the nodes of the element. Thence, the *lumped* mass matrix is a diagonal matrix and, consequently, it only involves an $\mathcal{O}(N)$ solution cost in the Lanczos algorithm iterations. Thus, by using the lumped mass matrix approximation the solution of the large undamped EVPs encountered in modal analysis involve a cost of just $\mathcal{O}(N_{NZ})$ per eigensolution.

2.3.4 State-space eigenvalue problem solution computation

In contrast to the undamped eigenvalue problem, the eigenvalue problem in the state-space formulation is non-hermitian and is defined with an indefinite pencil. Therefore, the standard Lanczos algorithm for the GHEVP may not be used since it would not converge to any correct solution.

One possibility is to use the Implicitly Restarted Arnoldi (IRA) algorithm [59], whose implementation is publicly available in the Arnoldi Package (ARPACK) software library included in MATLAB. This is a less-efficient eigenvalue algorithm than the Lanczos algorithm, but it can handle non-hermitian eigenvalue problems. However, the Arnoldi iteration presents some limitations when computing the solution of large indefinite GEVPs.

The Implicitly Restarted Arnoldi algorithm is a less stable algorithm than the Lanczos algorithm. It may efficiently compute the outer spectra eigensolutions, i.e. the larger eigenvalues, but it may have much more trouble finding the eigensolutions in the inner spectra of the GEVPs. This implies that the IRA algorithm may break down when computing eigensolutions, e.g. due to loss of orthogonality of the Arnoldi vectors, or may have a extremely slow convergence rate.

This problem is exacerbated for large orders of the state-space matrices, which is

the case in modal analysis. Due to the fact that robust algorithms for solving the state-space EVP had not been available, the use of state-space formulation for modal analysis has traditionally been avoided in practical situations. Despite specific variants of the Lanczos algorithm for non-hermitian GEVPs having been developed in recent decades, the state-space formulation has been customarily left aside.

Thus, it is possible nowadays to perform modal analysis of damped systems through state-space formulation. In particular, a specific variant of the Lanczos algorithm, namely the *Symmetric Indefinite Lanczos Method*, shall be used for solving the state-space EVP.

Symmetric Indefinite Lanczos Method

The solution of the state-space EVP using a Symmetric Indefinite Lanczos Method (SILM) was described by Chen et al. [60, 61] for systems without mode multiplicity (i.e. systems without repeated eigenvalues) and extended to systems with mode multiplicity by Kim et al. [62]. SILM tackles specifically the indefinite GEVP in the state-space formulation, but its implementation is not generally available in most commercial software. Yet, a prototype MATLAB implementation of the Symmetric Indefinite Lanczos Method (named *INSYLAN*) was developed by Thomas Kowalski [54] and is available online.

For large systems, the Symmetric Indefinite Lanczos Method is significantly more stable than the Implicitly Restarted Arnoldi algorithm, making it possible to compute many more inner spectra eigensolutions without breakdown or convergence issues. As for the standard Lanczos algorithm, the computational complexity of SILM is also of $\mathcal{O}(N^2)$ per eigensolution.

Yet, since the state-space formulation involves doubling the degrees of freedom in the equations of motion, the solution of the state-space EVP is at least four times more computationally demanding than the undamped EVP solution, let alone the increase in computational cost due to complex arithmetic operations and lower algorithmic efficiency of the Symmetric Indefinite Lanczos algorithm with respect to the Lanczos algorithm for the GHEVP. Moreover, for the state-space EVP, neither of the two state-space matrices, $\mathbf{A}$ and $\mathbf{B}$, become diagonal if a lumped mass matrix is introduced. Therefore, the lumped mass approximation gives hardly any computational cost reduction when the equations of motion are cast into the state-space form.

All in all, the solution of the state-space EVP through Lanczos algorithms is an order of magnitude more computationally demanding in comparison with the solution of the undamped eigenvalue problem.

2.4 Modal solution error analysis

In section 2.2, the modal analysis method has been described from an analytical point of view. In engineering applications, however, modal analysis is conducted numerically. A numerical representation is inherently an approximation to reality and, consequently, any numerical method produces results subject to a certain degree of error.

There is therefore a need to quantify the amount of error in the computed modal solutions. This quantification is what is known as *error analysis*. Measures of the error are presented in this section. These measures allow one to determine if the numerical solutions are accurate enough for the needs of the damped system analysis.

Specifically, if modal analysis is performed on a finite element model of a vibrating structure, the modal solution is an approximation with two main sources of error. On one hand, the FE model is a numerical model and as such it is already an approximation of the structure's nature. Moreover, the FE model parameters are in practice estimated values, which are usually assumed from partial information about the structure properties. On the other hand, the numerical algorithms for solving the eigenvalue problem always obtain solutions with a certain amount of inaccuracy.

Nevertheless, numerical modal solutions are usually considered to be exact for engineering purposes. That is, it is assumed that the FE model is accurate enough for a correct dynamic analysis, and that the output error in EVP algorithms is negligible. In this thesis, however, the aim is at developing efficient methods for obtaining *cheap* computational modal solutions at the expense of larger approximation errors. Thus, the error measures defined for the error analysis of eigenvalue problems may be used for the quantification of the error in the approximate modal solutions.

2.4.1 Error measures

The most straightforward way of measuring the error in the mode approximation is to compute the absolute error in the eigenvalues and eigenvectors. In order to do so, one must know both the exact and the approximate values for the eigensolutions. Here we introduce the following notation for exact and approximate modes.

Exact eigenvalues are denoted by symbol λ for both damped and undamped EVP, undamped eigenvalues being $\lambda_m = \omega_m^2$ and damped eigenvalues being $\lambda_m = -\sigma_m \pm \omega_{d,m}$. Approximate eigenvalues will be denoted with a tilde, $\tilde{\lambda}_m$ being the approximation to the exact eigenvalue λ_m.

Exact eigenvectors are denoted $\boldsymbol{u}_m$, $\boldsymbol{\phi}_m$ and $\boldsymbol{x}_m$ and their corresponding approximate eigenvectors $\tilde{\boldsymbol{u}}_m$, $\tilde{\boldsymbol{\phi}}_m$ and $\tilde{\boldsymbol{x}}_m$ for undamped, damped and state-space eigenvectors respectively.

Absolute error

The error in the eigenvalues is calculated as the absolute value of the difference of the exact to the approximate eigenvalue, i.e. $\left|\lambda_m - \tilde{\lambda}_m\right|$. In most of the cases, however, it is of interest to know the error in the modal frequencies and modal damping directly. Thence, errors for the undamped modal frequencies $|\omega_m - \tilde{\omega}_m|$, damped modal frequencies $|\omega_{d,m} - \tilde{\omega}_{d,m}|$ and damping ratios $\left|\zeta_m - \tilde{\zeta}_m\right|$ are usually regarded.

The error in eigenvectors can be computed in an analogous way, i.e. $|\boldsymbol{u}_m - \tilde{\boldsymbol{u}}_m|$, $\left|\boldsymbol{\phi}_m - \tilde{\boldsymbol{\phi}}_m\right|$ and $|\boldsymbol{x}_m - \tilde{\boldsymbol{x}}_m|$. However, this error measure does not give any practical information. On one hand, it is a vector quantity which does not give a clear understanding of the amount of error. On the other hand, eigenvectors are scalable solutions, and therefore the absolute error of an eigenvector does not have a unique value, since it depends on an arbitrary scaling factor. Thus, it would be desirable to establish alternative error measures for eigenvectors that express the error as a simple scalar value.

Modal Assurance Criterion

A broadly used measure for eigenvalue errors is the *Modal Assurance Criterion* (MAC). It is a measure of the orthogonality between two vectors. The MAC is

defined in the following way for any two vectors $\mathbf{v}$ and $\mathbf{w}$

$$\mathrm{MAC}\left(\mathbf{v},\mathbf{w}\right)=\frac{\left|\mathbf{v}^{H}\mathbf{w}\right|^{2}}{\left(\mathbf{v}^{H}\mathbf{v}\right)\left(\mathbf{w}^{H}\mathbf{w}\right)}=\frac{\left|\langle\mathbf{v},\mathbf{w}\rangle\right|^{2}}{\left\|\mathbf{v}\right\|^{2}\left\|\mathbf{w}\right\|^{2}} \tag{2.27}$$

The MAC can take values between 0 and 1 since its definition follows from the Cauchy-Schwarz inequality (c.f. Appendix A.1). A MAC value of 1 indicates that the two vectors are identical regardless of their scaling factor. This is clearly proved if $\mathbf{v}=\alpha\mathbf{w}$ is introduced in equation 2.27. A MAC value of 0 indicates that the two vectors are orthogonal. This is straightforward to see since for two orthogonal vectors it holds that $\langle\mathbf{v},\mathbf{w}\rangle=0$.

Therefore, the Modal Assurance Criterion performs an orthogonality test whose result may serve as a measure of the error between an exact and an approximate eigenvector. This measure is given by a simple scalar value and it does not depend on the arbitrary scaling of the eigenvectors.

For instance, for an exact $\boldsymbol{\phi}_m$ and approximate $\tilde{\boldsymbol{\phi}}_m$ damped eigenvectors one can compute $\mathrm{MAC}\left(\boldsymbol{\phi}_m,\tilde{\boldsymbol{\phi}}_m\right)$. The closer the MAC value is to 1, the smaller the error committed in the approximation. Conversely, if one computes $\mathrm{MAC}\left(\boldsymbol{\phi}_n,\tilde{\boldsymbol{\phi}}_m\right)$ with $n\neq m$ the error in $\tilde{\boldsymbol{\phi}}_m$ is smaller as this MAC value tends to 0.

Residual vector

So far, the error measures that have been presented require knowledge of the exact solutions in order to evaluate the error in the approximate ones. These can be calculated for small academic examples when the aim is to validate the approximate solution method itself. However, in practical applications, the exact solutions will not be available, precisely because one wants to avoid computing them. Therefore, alternative estimations of the approximation error are needed to ensure that the deviation of the solution is within an acceptable tolerance.

The accuracy of eigensolution approximations may be determined by substituting them back into the equations for which they are solutions, that is, into the EVP equations. Certainly, if the approximate eigenpairs are introduced in the left hand side of the EVPs in equations 2.3, 2.6 and 2.20, then the right hand side becomes no longer a zero vector $\mathbf{0}$, but an error vector which is known as the *residual vector*.

Explicitly, the residual vectors – $\mathbf{r}$ for the undamped EVP and $\mathbf{s}$ for the state EVP

– for the m'th mode read

$$\mathbf{r}_m = \left(\mathbf{K} - \tilde{\lambda}_m \mathbf{M}\right) \tilde{\boldsymbol{u}}_m \tag{2.28}$$

$$\mathbf{s}_m = \left(\mathbf{B} - \tilde{\lambda}_m \, \mathbf{A}\right) \tilde{\boldsymbol{x}}_m \tag{2.29}$$

with $\tilde{\lambda}_m = \tilde{\omega}_m^2$ in the undamped case. Notice that the state residual vectors are complex valued, unlike the undamped residuals which are real valued. In any case, the smaller the approximation error, the closer to $\mathbf{0}$ are the $\mathbf{r}_m$ and $\mathbf{s}_m$ residual vectors. Conveniently, this may be quantified by a positive scalar quantity using the norm of the residual, i.e.

$$\|\mathbf{r}_m\| = \langle \mathbf{r}_m, \mathbf{r}_m \rangle^{\frac{1}{2}} = \left(\mathbf{r}_m^T \mathbf{r}_m\right)^{\frac{1}{2}} \tag{2.30}$$

$$\|\mathbf{s}_m\| = \langle \mathbf{s}_m, \mathbf{s}_m \rangle^{\frac{1}{2}} = \left(\mathbf{s}_m^H \mathbf{s}_m\right)^{\frac{1}{2}} \tag{2.31}$$

where a smaller residual norm indicates better eigensolution accuracy. Nevertheless, the residuals are scaled accordingly with the arbitrary scaling of $\tilde{\boldsymbol{u}}_m$ and $\tilde{\boldsymbol{x}}_m$. Therefore, in order to compare different approximations accuracies it may be useful to normalise the residual norm with respect to the norm of the corresponding approximate eigenvector.

2.4.2 Error bounds

The residual vector itself gives an indirect measure of the error introduced in the approximation, but it does not quantify explicitly the approximation error in the eigenvalues and eigenvectors. Yet, it is possible to derive error bounds for the approximate eigenvalues from their corresponding residuals.

These error bounds can be found in the literature in publications dedicated to the mathematical and computational aspects of the eigenvalue problem (see for instance references [53–55]). However, most of the time these are only stated for the standard eigenvalue problem. In modal analysis, on the contrary, generalised eigenvalue problems are faced. For this reason, error bounds for the generalised EVP are relevant to this work and their derivations can be found in Appendix B.

For the undamped eigenvalue problem, error bounds for the eigenvalue error $\left|\lambda_m - \tilde{\lambda}_m\right|$ are found in terms of the M-inverse norm of the residual vector $\mathbf{r}_m$, which is defined as

$$\|\mathbf{r}_m\|_{M^{-1}} = \left\langle \mathbf{M}^{-1}\mathbf{r}_m, \mathbf{r}_m \right\rangle^{\frac{1}{2}} = \left(\mathbf{r}_m^T \mathbf{M}^{-1} \mathbf{r}_m\right)^{\frac{1}{2}} \tag{2.32}$$

Assuming that the $\tilde{\boldsymbol{u}}_m$ eigenvectors are mass-normalised, the error in the eigenvalues is bounded according to the inequality

$$\left|\lambda_m - \tilde{\lambda}_m\right| \leq \|\mathbf{r}_m\|_{M^{-1}} \tag{2.33}$$

which is known as the Krylov-Weinstein theorem [63]. This is a simple result that allows one to estimate the error without knowing the exact solution, albeit it may give a coarse bound with respect to the actual error.

An alternative bound may be used when the eigenvalues are computed through the *Rayleigh Quotient*. In such case the error is bounded according to the Kato-Temple theorem [64], i.e.

$$\left|\lambda_m - \tilde{\lambda}_m\right| \leq \frac{\|\mathbf{r}_m\|^2_{M^{-1}}}{d} \tag{2.34}$$

with d the distance from $\tilde{\lambda}_m$ to the closest eigenvalue other than λ_m. Clearly, if the distance d is significantly larger than the $\left|\lambda_m - \tilde{\lambda}_m\right|$ error, Kato-Temple gives a much tighter error bound than the Krylov-Weinstein one.

For the state-space eigenvalue problem, however, analogous error bounds to the ones in equations 2.33 and 2.34 cannot be defined (c.f. Appendix B). Only a more generic bound can be formulated based on the Bauer-Fike theorem [65], i.e.

$$\left|\lambda_m - \tilde{\lambda}_m\right| \leq \text{cond}(\mathbf{X}) \left\|\mathbf{A}^{-1}\right\| \frac{\|\mathbf{s}_m\|}{\|\tilde{\boldsymbol{x}}_m\|} \tag{2.35}$$

with $\text{cond}(\mathbf{X})$ the condition number of the state-eigenvectors matrix $\mathbf{X}$. This bound is of hardly any practical use because it requires knowledge of *all* of the exact state-eigenvector solutions. Nevertheless, it states that the error in the eigenvalues is proportional to the $\mathbf{s}_m$ residual norm.

2.5 Summary

The theory for the linear vibration analysis of damped systems has been covered in this chapter. The main features of the analysis are summarised in the following.

Firstly, it has been seen that the damping properties of dynamic systems depend on a range of energy dissipation mechanisms with different physical nature. These dissipation mechanisms may act conjointly when a structure is vibrating so that the mathematical modelling of the overall damping of a system is rather difficult. For this reason the modelling of damping is addressed using formulations which are mathematically convenient, and that produce a fair approximation to the actual

modal damping of vibrating systems. The most commonly used model is the viscous damping model and it is the one used in this thesis.

Secondly, the modal analysis of viscously damped systems has been explained in detail. The modes of vibration of such systems are found as the solutions of the quadratic eigenvalue problem arising from the corresponding equations of motion. A complication with QEVPs is that there is no canonical form for decoupling the QEVP set of equations, as opposed to the standard EVP[2]. Therefore, the QEVP may be linearised conveniently into a first order EVP in order to find the eigensolutions using well-established EVP solving methods.

The classical approach for modal analysis is to consider the undamped equations of motion, so that their corresponding EVP becomes of first order. The undamped EVP is defined by a definite pencil $(\mathbf{M}, \mathbf{K})$. Therefore, it can be efficiently solved using the well-known Lanczos algorithm. The eigenvalues and eigenvectors obtained in this way are real valued and they correspond to the undamped system modes.

Obtaining the damped system modes can be done a posteriori and only in two circumstances. One is the mathematical assumption of proportional damping, where the undamped mode shapes diagonalise the damping matrix, and thus the corresponding modal damping is found. This assumption, however, is rarely of use in practical situations. The other valid situation is when the system's damping is small, where a first order approximation can be used to find the damped modes from the undamped modes. Obviously, the approximation worsens as the level of damping increases.

The alternative approach for finding the damped modes is to rearrange the equations of motion into the state-space formulation. The corresponding eigenvalue problem is then of first order and its eigensolutions directly correspond to the exact damped modes. However, the transformation into the state-space presents two handicaps. The matrix pencil $(\mathbf{A}, \mathbf{B})$ defining the state-space EVP is indefinite. This means that the standard Lanczos algortihm cannot be directly applied for the EVP solution. A less-efficient *Symmetric Indefinite Lanczos Method* [54, 60, 61] may be used instead. Moreover, the state-space formulation doubles the dimensions of the matrices in the EVP, which significantly increases the solution computation cost. As it has been shown in this chapter, the computational cost for computing each modal solution using Lanczos algorithms is proportional to the square of the matrices order. Hence, the computational cost for solving a state-space EVP is

[2]The case of proportional damping is a special case where precisely the Schur form can be used for decomposing simultaneously the mass, stiffness and damping matrices.

roughly an order of magnitude bigger than the cost for solving the corresponding undamped EVP.

Lastly, ways to estimate the error introduced in the computation of modal solutions have been explained. The error in the computed modes may be measured directly if the exact modes of the system are known. The absolute and relative errors may be calculated for the modal frequencies and modal damping. The error in the mode shape vectors may be assessed through the *Modal Assurance Criterion*.

When the exact modes of the systems are not available – which is typically the case – the error in the computed modal solution may be assessed alternatively through the residual vector. The residual vector does not measure the modal parameters error explicitly, but it does give information about the overall computation error in the corresponding mode.

Moreover, it has been seen that error bounds for the computed eigenvalues can be given in terms of the residual vector norm. The *Krylov-Weinstein* theorem gives an error bound for the eigenvalues of the undamped EVP, so that the error in the natural frequencies may be (roughly) estimated without knowing the exact solution. A tighter error bound for the natural frequencies can be obtained using the *Kato-Temple* theorem, but only when the undamped eigenvalues are computed through the *Rayleigh quotient*. For the state-space EVP, however, analogous error bounds cannot be defined. Therefore, no explicit estimate of the error in modal damping and damped modal frequencies can be given when the exact solutions are not available.

2.6 Concluding remarks

The aim of this thesis is to develop new methods for repeatedly analysing the dynamics of damped vibrating linear systems in an efficient way. The *reanalysis* methods shall obtain cost efficient dynamic solutions at the expense of acceptable approximation error in the solutions. Approximate reanalysis methods for damped systems may be developed based on the mathematical grounds of modal analysis that have been presented in this chapter.

The reanalysis methods that are developed throughout this work stand on the mathematical model for viscous damping. Viscous damping is proportional to instantaneous velocity and it results in frequency dependent modal damping. This may not be the case for all damping mechanisms, e.g. viscoelastic materials usually

show constant modal damping. Nevertheless, for a certain frequency range and an appropriate choice of viscous damping values one can obtain a rather flat characteristic of the modal damping as a function of frequency. On the contrary, one could think of using some kind of hysteretic damping model giving constant modal damping. However, such models are not used in this work because they present inconvenient mathematical properties that impede the derivation of successful reanalysis methods.

The computational cost of any approximate reanalysis method has to be smaller than the cost of performing modal analysis. Since the most expensive task in modal analysis is that of resolving the eigenvalue problem, most of the computation cost reduction may be achieved by calculating cheap approximations of the eigensolutions. Therefore, the reanalysis methods may be based on mathematical approximations for the solutions of either the undamped eigenvalue problem or the state-space eigenvalue problem. Typically, such mathematical approximations involve the system matrices and also some previously computed solutions corresponding to a former analysis of the system that is to be reanalysed.

The question to put forward now is whether an approach based on the undamped eigenvalue problem or an approach based on the state-space eigenvalue problem should be used in order to perform damped systems reanalysis. In modal analysis, even though the state-space formulation yields the exact damped modes, use of the state-space formulation is preferably avoided in practical situations. This is because it involves a much higher computational cost for solving the eigenvalue problem, and also because the eigenvalue algorithms for the indefinite pencils could occasionally fail due to numerical instability. However, this may not be necessarily the case for eigensolution reanalysis.

In the undamped eigenvalue problem the number of degrees of freedom of the eigenvectors and the order of the matrices is that of the equations of motion. On the contrary, these dimensions are doubled in the state-space eigenvalue problem. This fact implies that the cost for computing approximate eigensolutions will be at the very least two times higher for the state-space case than for the undamped case. Yet, the increase in computational cost is not as pronounced as for solving the EVPs, where the solution cost in the state-space case is an order of magnitude higher. Moreover, the undamped eigensolutions do not have direct correspondence to the damped modes of the system, whereas the state-space eigensolutions do. Obtaining the damped modes from the undamped eigensolutions needs extra computation effort, which is that of the Rayleigh approximation for small damping (c.f. section

2.2.2).

Therefore, it is not apparent that reanalysis methods based on the undamped eigensolutions approximations shall be significantly more efficient than reanalysis methods based on state-space eigensolutions approximations. On the other hand, reanalysis methods based on the state-space formulation might produce more accurate results, specially for highly damped systems. Furthermore, no numerical instability issues are expected in reanalysis methods since the solutions are not to be searched for through iterative algorithms. Thus, reanalysis methods based on the state-space formulation are particularly considered in this thesis.

The approximation error of the reanalysis methods may be assessed in the same way as the error introduced by the eigenvalue algorithms. The damped modes error can be measured explicitly by comparison to the exact solution. This way of measuring the approximation error implies that the exact eigensolution must be additionally computed. Certainly, this is not what is aimed to do in practical situations, where the eigensolution computation through eigenvalue algorithms is precisely to be avoided in the reanalysis. When the exact solution is not available the error shall only be assessed through the residual vector. However, it has been seen in this chapter that explicit estimates of the error in damped modes (such as "damped" eigenvalue error bounds) cannot be obtained from the residual vector. This is the case for damped modes obtained through eigenvalue algorithms, and will equally be for damped modes approximated through reanalysis methods, regardless of the use of state-space formulation or small damping assumption.

Nevertheless, in this work, approximate solutions obtained through the reanalysis methods will be compared to the exact solutions for small academic examples, so that the error introduced by the reanalysis approximations can be estimated. For engineering purposes, the modal solutions computed through eigenvalue algorithms are considered to be error free. Thence, the direct error measures may be used to estimate the error in the modal solutions coming from approximate reanalysis methods if one regards the eigenvalue algorithms solutions as exact solutions. In this way, the accuracy of the reanalysis methods themselves will be evaluated.

Chapter 3

Approximate methods for the modal analysis of damped systems

This chapter addresses methods for computing the dynamics of damped vibrating systems without necessarily solving the eigenvalue problems arising in modal analysis.

When the parameters of a system model are prone to vary one is interested in the corresponding variation in dynamic response. Computing the dynamic response for each possible variation through the solution of eigenvalue problems is in general too demanding. Instead, the dynamic response can be computed fully for one or few deterministic cases, and the remaining range of possible dynamic responses may be computed coming out from the former at a much lower cost using approximate reanalysis methods.

Here, the *perturbation method* and the *interpolation method* are considered. In this chapter these methods are defined for undamped systems and also for systems with general viscous damping. Subsequently, the accuracy and efficiency of the methods that are being presented in this chapter will be assessed through simple academic numerical examples.

The perturbation method is an approximate reanalysis method that computes variations in the system response. The idea of the method is that if the response of the system is known for a given set of parameters, the variations in the response due to variations in the parameters may be computed through first order approximations, under the assumption that the variations are small. The use of this method in dynamics was first proposed by Liu et al. [66] in order to perform the analysis of

systems subject to uncertainty.

The interpolation method is an approximate reanalysis method that computes rough estimates of the response of a system by interpolation of already available modal solutions. It was proposed by Bhaskar et al. [67] as a method for obtaining very computationally cheap estimates of the modal frequencies of a system whose parameters are allowed to vary, so that these estimates may be used in design search and optimisation problems of large dynamic systems.

Also in this chapter, the use of the *Rayleigh quotient* in combination with perturbation and interpolation methods is proposed. The Rayleigh quotient is an important quantity in modal analysis. It is used in the methods that solve the equations of motion of the system in order to find its modes of vibration. Here, however, we are mainly interested in its use as a modes approximant.

The classical Rayleigh quotient is defined for undamped systems. Therefore, its use as an approximant is restricted to undamped modal solutions. For this reason, a new Rayleigh Quotient for damped systems is defined in this chapter, as proposed by Bhaskar [68]. The properties of this quotient are analysed in detail and its potential use as a novel damped modes approximant is studied for the first time.

3.1 Response variation in dynamic systems

The reanalysis methods presented in this chapter approximate the variation of the dynamic response of a system when the system model parameters vary. The variation in dynamic response may be approximated following two different approaches. On one hand, one may attempt to update the response function of a system from previously computed response functions. On the other hand, one may update the system modal parameters from previously computed modal parameters, and then compute the corresponding response function from the updated modal parameters.

It is desirable that the reanalyses take the lowest possible computation time. Thence, linear approximations are to be used in the reanalysis methods, since they are the most simple approximations one can use and, therefore, the ones that present the lowest computational complexity. However, the accuracy of linear approximations depend crucially on how close to linear is the rate of change of the variable being approximated.

In this section, the rate of change of response functions and modal parameters are

qualitatively analysed in order to determine which approximation approach (i.e. response function or modal parameter approximation) is best for approximating variations in the system dynamics. Recall that vibration modes behave analogously to single degree of freedom (SDOF) oscillators. Therefore, the rate of variation of the dynamic response of a generic system shall be similar to the response variation of a SDOF system.

An example of varying response for a SDOF damped system is illustrated in figure 3.1. In this example the stiffness value k in figure 3.1a varies in a $\pm 20\%$ range of its nominal value. In figure 3.1b the frequency response function for the nominal value of k is drawn along with several frequency response functions corresponding to equidistant k variations inside the variation interval. The response function resonance peak is located roughly at 5 Hz, and incurs significant variations in frequency and amplitude when k varies.

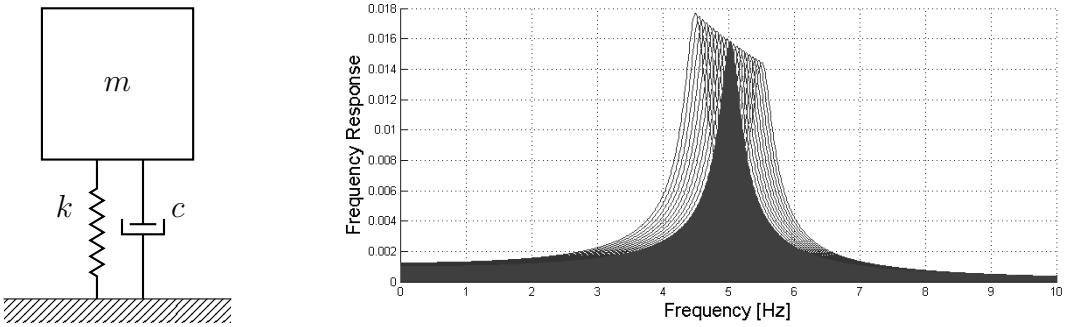

a) Damped SDOF system. b) Frequency response variation.

Figure 3.1: Example of response variation of a single degree of freedom system with $\pm 20\%$ variation range in stiffness value.

For the same example, the rate of change of the response function and the modal parameters with respect to the variations in stiffness is illustrated in figure 3.2. The frequency response function variation is shown at 5 Hz because it is the frequency around which the resonance peak varies. It can be observed that the variation in the response function has a completely non-linear shape. On the contrary, the variations in modal frequency and modal damping are much more smooth, showing a monotonic and quasi-linear shape.

The response functions of a generic system with multiple degrees of freedom (MDOF) will show resonance peaks for each mode of vibration behaving similar to the resonance peak in figure 3.1b when subjected to variations. The rate of change of such response functions will be very non-linear especially around the resonance peaks, as is the case for the SDOF example. On the contrary, the modal parameters of each

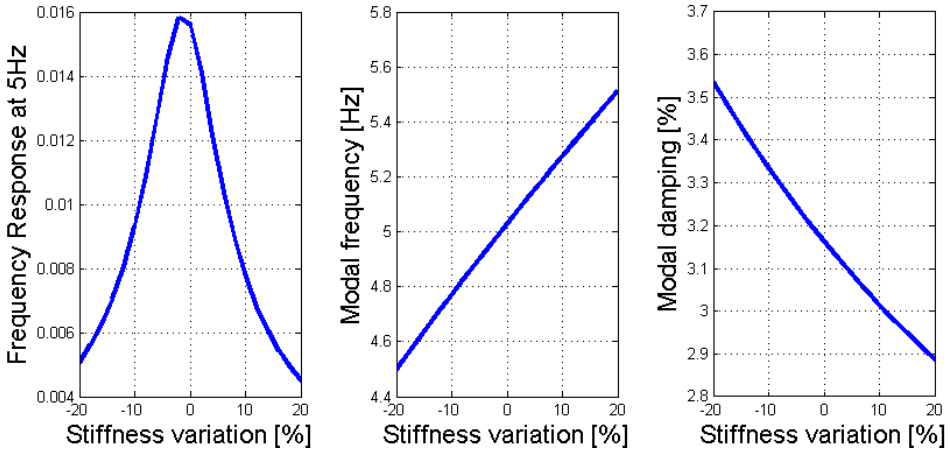

Figure 3.2: Variations in frequency response at 5Hz, modal damping and modal frequency of the SDOF system for a $\pm 20\%$ variation range in stiffness value.

mode will vary smoothly as in figure 3.2. Therefore, the rate of change of modal parameters will be fairly well approximated using linear approximations, whereas approximating response function variations through linear approximations will give very poor results. Thus, the modal approximation reanalysis approach is considered best and, for this reason, it is the one developed in this work.

3.1.1 Variation in modal parameters

The rate of variation of modal parameters with respect to system model parameter changes is analysed here with further detail. In Appendix C the rate of change of the modal parameters of a SDOF system are analysed. From the analysis on undamped resonance frequency in section C.1, it can be stated that variations in the undamped modal frequencies are rather smooth, although the rate of change with respect to mass and stiffness variations is non-linear. On the contrary, undamped eigenvalues (i.e. $\lambda_m = \omega_m^2$) show a linear rate of change with respect to stiffness variations and a flat quasi-linear rate of change with respect to mass variations.

As for the undamped modes, the variation of the modal parameters for a damped SDOF system has been analysed in Appenix C. The rates of change of the damped modal frequencies and modal damping show very different characteristics depending on whether the system is lightly or heavily damped.

Lightly damped modal frequencies incur smooth non-linear variations for mass and stiffness variations (like undamped modal frequencies), and are almost invariant for (low) damping variations. In turn, modal damping varies proportionally to

damping constant variations, and incurs very small quasi-linear variations due to mass or stiffness variations for low levels of damping.

On the contrary, heavily damped modal frequencies vary in a very non-linear way for variations in any of the dynamic system parameters: mass, stiffness and damping. Moreover, although modal damping varies proportionally to damping constant variations, variations in mass or stiffness produce significant non-linear variations in modal damping for high levels of damping.

The rate of change of mode shape vectors may not be analysed from a SDOF system analogy. However, the shape of a mode is a rather invariant quantity with respect to physical parameter variations. Only significant variations in the geometry of the system would change the mode shapes strongly. Essentially, a mode of vibration is an oscillating displacement shape. Variations in mass or stiffness make such a (mode) *shape* to resonate at one frequency or another. In turn, variations in the damping constant introduce small shifts in the phase of the mode shapes, i.e. the difference in vibration phase at two distinct degrees of freedom varies slightly. Therefore, although their rate of change may not be linear, the variations in mode shape vectors are expected to be very small in comparison to modal frequency and modal damping variations.

3.2 Perturbation Method

The perturbation method needs a baseline model to be solved once. The dynamics of the system when model parameters vary are then calculated as the original dynamic response plus the corresponding response variation, which is computed using sensitivity functions. Sensitivity functions relate the change in the dynamic behaviour of the system to the variation in model parameters.

Consider a generic system model defined by a set of model parameters $\boldsymbol{\theta}$ (e.g. physical dimensions, mass density, elastic modulus, etc). The response of the system is characterised by a set of output quantities $\boldsymbol{z}$ (e.g. modal frequencies and mode shapes, or displacement responses) which depend on the model parameters. For the baseline system, the model parameters have a given value $\boldsymbol{\theta}_0$ for which the corresponding response $\boldsymbol{z}_0$ is known.

For an output quantity $z(\theta)$ depending on a model parameter θ, a perturbation

(variation) $\Delta\theta$ in the parameter induces a perturbation Δz in the output, i.e.

$$z(\theta_0 + \Delta\theta) = z_0 + \Delta z \tag{3.1}$$

The perturbation method consists in approximating the Δz perturbation using a Taylor series expansion truncated after the linear term, i.e.

$$z(\theta_0 + \Delta\theta) \approx z_0 + \tilde{\Delta} z = z_0 + [S_z(\theta)]_{\theta=\theta_0} \Delta\theta \tag{3.2}$$

where $S_z(\theta) = \frac{\partial z}{\partial \theta}$ is the linear sensitivity function to be evaluated at $\theta = \theta_0$. Generically, for a set of varying parameters $\boldsymbol{\theta}$ and a set of outputs $\mathbf{z}$ the perturbation relationship reads

$$\mathbf{z}(\boldsymbol{\theta}) \approx \mathbf{z}_0 + [\mathbf{S}_\mathbf{z}(\boldsymbol{\theta})]_{\boldsymbol{\theta}=\boldsymbol{\theta}_0} \Delta\boldsymbol{\theta} \tag{3.3}$$

with $\mathbf{S}_\mathbf{z}(\boldsymbol{\theta})$ a matrix of sensitivity functions.

The sensitivity functions may be formulated analytically, and therefore, the computational cost of the method is that of evaluating linear functions for the varying parameters. This implies that the computational cost for obtaining the perturbed system response is significantly reduced with respect to that of solving the corresponding EVP.

On the contrary, the perturbation method linearly approximates the generally nonlinear relationship between the outputs and the parameters of the model. Therefore, the perturbation method is restricted to *small* variations in the parameters, since the error in the linear approximation increases as the parameters deviate from the baseline model values. This is shown in the qualitative example in Figure 3.3.

3.2.1 Sensitivity functions in dynamics

In dynamic analysis the output quantities to be evaluated are the frequency responses of the system. The perturbations in the frequency responses may be computed in two ways depending on which sensitivity functions are used.

Analytical sensitivity functions for undamped modes were first described by Fox and Kapoor [69] for systems *without* eigenvalue multiplicity, and by Nelson [70] for systems with eigenvalue multiplicity. Analytical sensitivity functions for damped modes were first proposed by Bhaskar [71] for the eigenvalues of viscously damped systems and, later, sensitivities for the corresponding eigenvectors were derived following the same idea [72]. Other sensitivities may be found in the literature for the

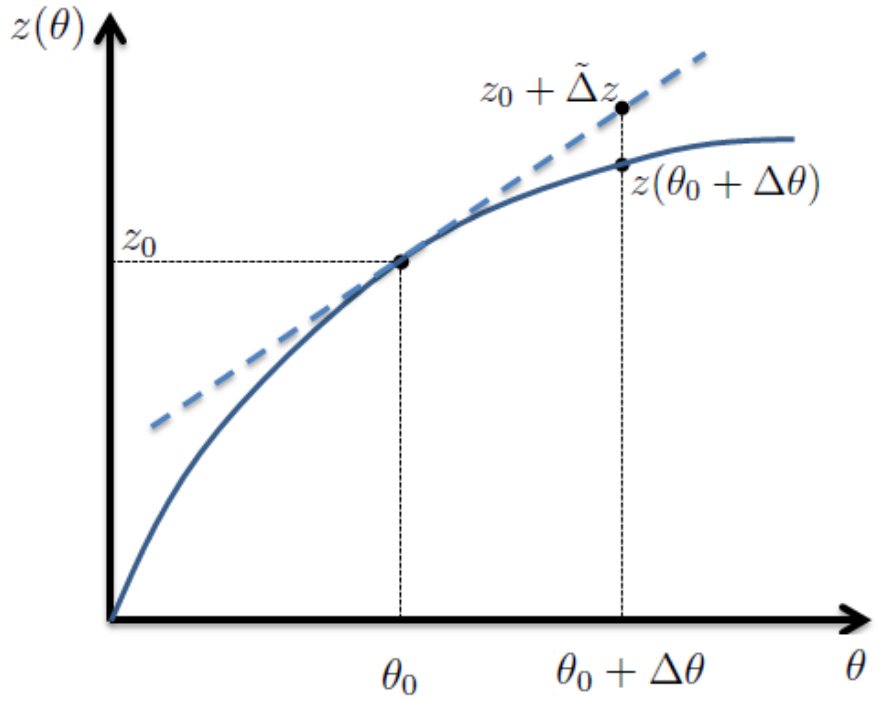

Figure 3.3: Perturbation method qualitative example. Solid line: Exact variation of the output quantity. Dashed line: Perturbation approximation.

modes of non-viscously damped systems, e.g. [73–75]. Analytical sensitivity functions for the frequency response are easily obtained through the partial derivation of the response matrix.

The analytical sensitivity functions for undamped modes, damped modes and response functions are described in Appendix D for brevity. These analytical sensitivities are posed in terms of the sensitivities of the system matrices $S_{\mathbf{M}}(\theta) = \frac{\partial \mathbf{M}}{\partial \theta}$, $S_{\mathbf{C}}(\theta) = \frac{\partial \mathbf{C}}{\partial \theta}$ and $S_{\mathbf{K}}(\theta) = \frac{\partial \mathbf{K}}{\partial \theta}$ with respect to model parameters variations. This may be expressed as

$$S_z(\theta) = S_z(S_{\mathbf{M}}(\theta), S_{\mathbf{C}}(\theta), S_{\mathbf{K}}(\theta)) \tag{3.4}$$

In a finite element model, the system matrices are obtained by assembly of the element matrices. Hence, the dependency of system matrices to physical model parameters depends on the element types used to describe the physics of the systems. Therefore, generic expressions for the matrices' sensitivities cannot be given since they are completely case specific. Nevertheless, perturbations in model parameters can be propagated to the system matrices and further propagated into the output quantities as we shall see next.

3.2.2 Perturbation propagation

Let an approximate output quantity be noted $\tilde{z}$ and an approximate perturbation be noted $\tilde{\Delta}z$ so that

$$\tilde{z} = z_0 + \tilde{\Delta}z \tag{3.5}$$

Hence, the perturbation in an output quantity z with respect to a perturbation in a model parameter θ is approximated as

$$\tilde{\Delta}z = S_z(\theta)\Delta\theta \tag{3.6}$$

where the evaluation of the sensitivity function at $\theta = \theta_0$ (c.f. equation 3.2) has been omitted for clarity.

Due to the fact that first order sensitivities are used, $S_z(\theta)$ in equation 3.4 is just a linear combination of the matrices sensitivities. Therefore, the parameter perturbation $\Delta\theta$ may be directly applied to the matrices sensitivities $S_{\mathbf{M}}(\theta)$, $S_{\mathbf{C}}(\theta)$ and $S_{\mathbf{K}}(\theta)$, i.e.

$$S_z(\theta)\Delta\theta = [\alpha S_{\mathbf{M}}(\theta) + \beta S_{\mathbf{C}}(\theta) + \gamma S_{\mathbf{K}}(\theta)]\Delta\theta = P_z(\tilde{\Delta}\mathbf{M}, \tilde{\Delta}\mathbf{C}, \tilde{\Delta}\mathbf{K}) \tag{3.7}$$

where $\tilde{\Delta}\mathbf{M} = S_{\mathbf{M}}(\theta)\Delta\theta$, $\tilde{\Delta}\mathbf{C} = S_{\mathbf{C}}(\theta)\Delta\theta$ and $\tilde{\Delta}\mathbf{K} = S_{\mathbf{K}}(\theta)\Delta\theta$ are first order approximations of the exact system matrices perturbations $\Delta\mathbf{M}$, $\Delta\mathbf{C}$ and $\Delta\mathbf{K}$ respectively.

Since generic sensitivities for the system matrices are not generally available, the actual perturbations in system matrices may be directly calculated at a bearable computation cost through FE matrices re-assembly instead. Therefore, the perturbation in an output quantity z may be expressed directly in terms of the system matrices perturbations $\Delta\mathbf{M}$, $\Delta\mathbf{C}$ and $\Delta\mathbf{K}$.

$$\tilde{\Delta}z = P_z(\Delta\mathbf{M}, \Delta\mathbf{C}, \Delta\mathbf{K}) \tag{3.8}$$

Here, $P_z(\Delta\mathbf{M}, \Delta\mathbf{C}, \Delta\mathbf{K})$ is no longer a sensitivity function but a perturbation propagation function. The perturbation in the system matrices is computed from the perturbation in model parameters, then, the system matrices perturbations are *propagated* to the output quantities through the perturbation propagation function.

If several model parameters are perturbed at the same time and these are uncorrelated, a perturbation propagation needs to be computed for each perturbed parameter. The total perturbation in an output quantity is the sum of the propagated perturbations. Let N_θ be the number of perturbed parameters and θ_n the

nth perturbed parameter, the total perturbation in an output quantity z is

$$\Delta z \approx \sum_{n=1}^{N_\theta} \tilde{\Delta} z(\Delta\theta_n) = \sum_{n=1}^{N_\theta} P_z(\Delta\mathbf{M}(\Delta\theta_n), \Delta\mathbf{C}(\Delta\theta_n), \Delta\mathbf{K}(\Delta\theta_n)) \tag{3.9}$$

where $\Delta\mathbf{M}(\Delta\theta_n)$, $\Delta\mathbf{C}(\Delta\theta_n)$ and $\Delta\mathbf{K}(\Delta\theta_n)$ are the matrices perturbations for the nth parameter perturbation $\Delta\theta_n$.

In the following the perturbation propagation functions for the modal parameters are presented. The dependency on the nth parameter perturbation $\Delta\theta_n$ will be omitted for brevity. Nevertheless, it should be kept in mind that the following expressions hold for a single parameter perturbation and that, if multiple parameters are perturbed, these expressions would be summed up as in equation 3.9.

Perturbation functions for frequency responses may also be formulated. However, the perturbation approximation yields very large approximation error at the resonance peaks of response functions for the reasons that have been presented in section 3.1. Thus, direct perturbation approximation of response functions is discarded beforehand.

3.2.3 Modal perturbation

In this section, the perturbation propagation functions for the modal parameters are presented in explicit form. These expressions are obtained from the corresponding analytical sensitivity functions, which can be consulted in Appendix D.

Perturbation functions for undamped modes

The perturbation functions for undamped modes are based on the sensitivity functions derived by Fox and Kapoor [69] and described in section D.1. The sensitivities for the undamped eigenvalues S_{λ_m} (equation D.2) and the undamped eigenvectors S_{u_m} (equation D.3) depend on the mass and stiffness matrices sensitivities only, so that the corresponding perturbation functions are of the form

$$\tilde{\Delta}\lambda_m = P_{\lambda_m}(\Delta\mathbf{M}, \Delta\mathbf{K}) \tag{3.10}$$

$$\tilde{\Delta}\boldsymbol{u}_m = P_{u_m}(\Delta\mathbf{M}, \Delta\mathbf{K}) \tag{3.11}$$

Then, assuming the undamped eigenvectors to be mass-normalised, the explicit first order perturbation propagation expression for the undamped eigenvalues is

$$\tilde{\Delta}\lambda_m = \boldsymbol{u}_m^T \left[\Delta\mathbf{K} - \lambda_m \Delta\mathbf{M}\right] \boldsymbol{u}_m \tag{3.12}$$

and for the undamped eigenvectors

$$\tilde{\Delta}\boldsymbol{u}_m = -\frac{1}{2}\left(\boldsymbol{u}_m^T \Delta\mathbf{M}\boldsymbol{u}_m\right)\boldsymbol{u}_m - \sum_{i\neq m}\frac{\boldsymbol{u}_i^T\left[\Delta\mathbf{K} - \lambda_m\Delta\mathbf{M}\right]\boldsymbol{u}_m}{\lambda_i - \lambda_m}\boldsymbol{u}_i \tag{3.13}$$

Recalling that the undamped eigenvalues correspond to the squared natural frequencies, i.e. $\lambda_m = \omega_m^2$, the perturbed undamped modal frequencies may be approximated as

$$\tilde{\omega}_m = \sqrt{\lambda_m + \tilde{\Delta}\lambda_m} \tag{3.14}$$

Logically, the undamped modes give no information on the system damping. Hence, when the undamped modes perturbation functions are used, the modal damping of a perturbed damped system needs to be computed a posteriori. Using the small damping approximation in section 2.2.2 together with the approximate perturbation of the undamped modes, the perturbed modal damping may be approximated as

$$\tilde{\zeta}_m = \frac{\tilde{\boldsymbol{u}}_m^T(\mathbf{C}+\Delta\mathbf{C})\tilde{\boldsymbol{u}}_m}{|\tilde{\boldsymbol{u}}_m^T(\mathbf{C}+\Delta\mathbf{C})\tilde{\boldsymbol{u}}_m \pm i2\tilde{\omega}_m|} \tag{3.15}$$

which is valid as long as the small damping assumption is fulfilled.

Perturbation functions for damped modes

The sensitivity functions for damped eigenvalues S_{λ_m} (equation D.7) and damped eigenvectors S_{ϕ_m} (equation D.10) are used to derive the perturbation functions for damped modes. In this case the sensitivity functions depend on the damping matrix sensitivity as well as the sensitivities of the mass and stiffness matrices, i.e.

$$\tilde{\Delta}\lambda_m = P_{\lambda_m}(\Delta\mathbf{M}, \Delta\mathbf{C}, \Delta\mathbf{K}) \tag{3.16}$$

$$\tilde{\Delta}\boldsymbol{\phi}_m = P_{\phi_m}(\Delta\mathbf{M}, \Delta\mathbf{C}, \Delta\mathbf{K}) \tag{3.17}$$

Assuming **A**-normalisation, the explicit perturbation propagation expression for the damped eigenvalues is

$$\tilde{\Delta}\lambda_m = -\boldsymbol{\phi}_m^T\left[\lambda_m^2\Delta\mathbf{M} + \lambda_m\Delta\mathbf{C} + \Delta\mathbf{K}\right]\boldsymbol{\phi}_m \tag{3.18}$$

and for the damped eigenvectors

$$\tilde{\Delta}\boldsymbol{\phi}_m = -\frac{1}{2}\left(\boldsymbol{\phi}_m^T\left[2\lambda_m\Delta\mathbf{M} + \Delta\mathbf{C}\right]\boldsymbol{\phi}_m\right)\boldsymbol{\phi}_m + \sum_{i\neq m}\frac{\boldsymbol{\phi}_i^T\left[\lambda_m^2\Delta\mathbf{M} + \lambda_m\Delta\mathbf{C} + \Delta\mathbf{K}\right]\boldsymbol{\phi}_m}{\lambda_i - \lambda_m}\boldsymbol{\phi}_i \tag{3.19}$$

Recalling that the expression for the damped eigenvalues is $\lambda_m = -\sigma_m \pm i\omega_{d,m}$, the perturbation approximations for damped modal frequency and modal damping are

$$\tilde{\Delta}\omega_{d,m} = \Im\{\tilde{\Delta}\lambda_m\} \tag{3.20}$$

$$\tilde{\Delta}\zeta_m = \frac{\Re\{\tilde{\Delta}\lambda_m\}}{|\tilde{\lambda}_m|} \tag{3.21}$$

3.2.4 The cost of modal perturbation

So far, the modal perturbation method has been presented and some considerations on the approximation accuracy have been discussed. Now, the computational complexity of the modal perturbation method is analysed in this section.

If a look is taken into the modal perturbation equations in section 3.2.3 (c.f. equations 3.12, 3.13, 3.18 and 3.19), one can see that all perturbation functions involve operations of the kind vector-matrix-vector product. These products involve the perturbed matrices ($\Delta\mathbf{M}$, $\Delta\mathbf{C}$ or $\Delta\mathbf{K}$) and the eigenvectors ($\boldsymbol{u}_m$ or $\boldsymbol{\phi}_m$) which have dimensions $N \times N$ and $N \times 1$ respectively, with N corresponding to the number of degrees of freedom defined. For large systems the dimensions of the matrices and vectors are big enough that the computational cost of their products dominate over any other operation cost. Thus, the computational complexity of the modal perturbation method will scale as of the cost of the eigenvector-perturbation matrix-eigenvector products (*Δ-matrix products* for brevity).

The cost of a vector-matrix-vector product is the cost of a matrix-vector product plus the cost of the subsequent vector-vector product. Generically, the cost of a matrix-vector product is of $\mathcal{O}(N^2)$ scalar floating point operations (flops) and the cost of a vector-vector product is of $\mathcal{O}(N)$ scalar flops. However, the products computation cost may vary dramatically depending on whether the matrix involved is a full matrix, a sparse matrix or any other sort of structured matrix.

The system matrices that define the equations of motion for a large FE model present very large sparsity. This means that most of the entries are zero valued. The number of non-zero entries may be characterised by the average number b of non-zero entries per matrix row. For large systems the number degrees of freedom greatly exceeds this quantity, i.e. $b << N$.

Moreover, whenever a model parameter is perturbed (e.g. a design modification, a material property uncertainty, ...), not all entries in the system matrices are necessarily perturbed. In fact, for large systems it is more probable that the perturbation

is localised in a rather small region. Thence, the Δ-matrices involved in the vector-matrix-vector products may show even much higher sparsity than the already sparse system matrices. A number p of perturbed degrees of freedom may be defined to characterise the sparsity of the matrices, so that for localised perturbations the number of perturbed DOFs p is smaller than total number of degrees of freedom N, i.e. $p < N$.

In table 3.1 the computational cost of the vector-matrix-vector product operation is shown for three different cases, namely for a full matrix, for a sparse matrix and for a sparse perturbation matrix. Only those non-zero entries in sparse matrices need to be multiplied. In the table it can be seen that the cost of the product involving a Δ-matrix scales as of $\mathcal{O}(p)$ flops in contrast with the $\mathcal{O}(N^2)$ computational cost for full vector-matrix-vector products. Assuming that both quantities b and p for a perturbation matrix are much smaller than the total number of degrees of freedom N, it is apparent that the computational cost of the Δ-matrix product is orders of magnitude smaller than the full matrix product cost.

	Matrix-Vector product		Vector-Vector product	Vector-Matrix-Vector product	
	Operations/row	Rows	Operations	Total operations	Complexity
Full matrix	N products + $N-1$ sums	N	N products + $N-1$ sums	$2N^2+N-1$	$\mathcal{O}(N^2)$
Sparse matrix	b products + $b-1$ sums	N	N products + $N-1$ sums	$2(b+1)N-1$	$\mathcal{O}(N)$
Sparse Δ-matrix	b products + $b-1$ sums	p	p products + $p-1$ sums	$2(b+1)p-1$	$\mathcal{O}(p)$

Table 3.1: The computational cost of a vector-matrix-vector product for full matrices, sparse matrices and sparse perturbation matrices.

The overall cost of the modal perturbation method will be proportional to the cost of the Δ-matrices products involved in the eigensolutions perturbation functions.

In particular, the undamped eigenvalues perturbation function in equation 3.12 involves 2 Δ-matrix products plus 2 extra scalar operations. Therefore the cost for computing each undamped eigenvalue perturbation scales as $\mathcal{O}(p)$ operations.

Similarly, the undamped eigenvectors perturbation function in equation 3.13 involves a weighted sum of all unperturbed eigenvectors. Each weight is computed through Δ-matrix products, i.e. at an $\mathcal{O}(p)$ cost. With M being the total number of computed modes and N the size of the vectors, the cost for scaling and summing up all vectors is M times an $\mathcal{O}(N)$ number of flops. In summary, the total cost for computing an undamped eigenvector perturbation scales as M times an $\mathcal{O}(p)$ cost plus M times an $\mathcal{O}(N)$ cost.

Yet, an extra vector-matrix-vector product involving the full system damping matrix is needed to compute the corresponding perturbed modal damping (c.f. equation

3.15). This will be computed at a cost of $\mathcal{O}(N)$ operations, and only after having previously computed both the eigenvalue and eigenvector perturbations.

The total cost of the undamped modes perturbation method is summarised in table 3.2. The perturbed modal frequencies are obtained at a cost proportional to the Δ-matrix products. The computation is very efficient specially if the perturbations occur in a reduced set of DOFs. On the contrary, the computational cost for the perturbed mode shapes scales as the size and number of the eigenvectors. This supposes a much higher computational cost compared to the eigenvalues perturbation.

Nevertheless, in a worst case scenario where all degrees of freedom are perturbed at a time, i.e. $p = N$, the cost of the perturbation method scales as $2(M+1)$ times $\mathcal{O}(N)$ operations (see table 3.2). Recall that the cost of solving the EVP through Lanczos algorithms (c.f. section 2.3.3) scales as of $\mathcal{O}(N^2)$ operations. Thus, since the number of computed modes M will always be much smaller than the system model order N, the cost for computing eigensolution perturbations through the modal perturbation method is much smaller than the cost for solving the perturbed EVP.

	Undamped Modes Perturbation	
	Operations	Complexity
Modal frequency	2 Δ-matrix products + 2 flops	$\mathcal{O}(p)$
Mode shape vector	M times (Δ-matrix products + vector operations)	$M[\mathcal{O}(p) + \mathcal{O}(N)]$
Modal damping	1 sparse-matrix product + 2 flops	$\mathcal{O}(N)$

Table 3.2: The computational cost of the undamped modal perturbation method.

Analogous to the undamped case, the damped eigenvalues perturbation function in equation 3.18 involves 3 Δ-matrix products plus 4 extra scalar operations. Hence, the cost associated with the computation of damped eigenvalue perturbations also scales as $\mathcal{O}(p)$ operations. Here, however, both the modal frequencies and the modal damping perturbations are directly obtained. This implies that the modal damping perturbations may be computed without the need of previously computing the eigenvector perturbations.

In turn, the damped eigenvector perturbation function in equation 3.19 involves a weighted sum of all damped eigenvectors. Again, the weights correspond to Δ-matrix products with $\mathcal{O}(p)$ computational cost. With M_d the number of damped eigensolutions computed, M_d vector operations are needed to perform the vector sum. Notice that each mode corresponds to a complex conjugate pair of damped eigensolutions so that $M_d = 2M$. Thus each damped mode shape vector perturbation is obtained at a cost of $2M$ times an $\mathcal{O}(p)$ cost weighting operation plus $2M$

times an $\mathcal{O}(N)$ cost vector operation.

The total cost of the damped modes perturbation method is summarised in table 3.3. The computational complexity of the damped modes perturbation is the same as for the undamped modes perturbation, but scaling with the double number of eigenvectors. If one is not intending to compute the eigenvector perturbations but just the perturbations in modal frequencies and modal damping, damped mode perturbation is a much more efficient and accurate method.

	Damped Modes Perturbation	
	Operations	Complexity
Modal frequency/damping	3 Δ-matrix products + 4 flops	$\mathcal{O}(p)$
Mode shape vector	$2M$ times (Δ-matrix products + vector operations)	$2M[\mathcal{O}(p) + \mathcal{O}(N)]$

Table 3.3: The computational cost of the damped modal perturbation method.

Finally, it should be mentioned that the costs shown in table 3.3 assume that just one model parameter is perturbed. If several uncorrelated parameters are perturbed these costs apply for each of the varying parameters (c.f. section 3.2.2). Thus, for n varying parameters, the overall cost is n times the cost presented in table 3.3.

3.2.5 Numerical example

In this section, the modal perturbation method is tested through a simple example. The two degrees of freedom system in figure 3.4 is used for this purpose. The system is damped by means of the c_1 and c_3 viscous dampers. Specifically, the c_3 damper has a prominently high damping value which makes the system overall heavily damped in a non-proportional way.

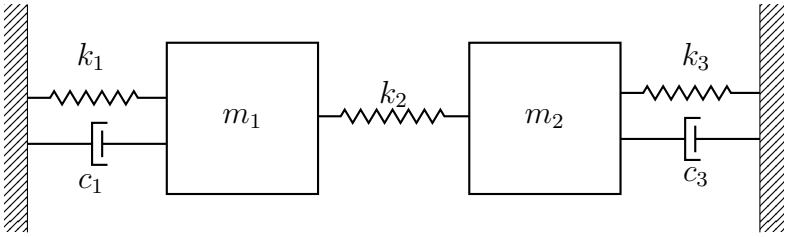

Figure 3.4: Damped two degrees of freedom system. Parameters: $m_1 = 0.12$ kg, $m_2 = 0.1$ kg, $k_1 = 1.5$ kN/m, $k_2 = 1$ kN/m, $k_3 = 2$ kN/m, $c_1 = 2$ Ns/m, $c_3 = 10$ Ns/m.

The free-vibration equations of motion of the 2-DOFs system are

$$\begin{bmatrix} m_1 & 0 \\ 0 & m_2 \end{bmatrix} \ddot{\mathbf{u}} + \begin{bmatrix} c_1 & 0 \\ 0 & c_3 \end{bmatrix} \dot{\mathbf{u}} + \begin{bmatrix} k_1 + k_2 & -k_2 \\ -k_2 & k_2 + k_3 \end{bmatrix} \mathbf{u} = \mathbf{0}$$

These equations of motion have been coded into MATLAB so that the dynamics of the system can be solved. The exact modal solution is obtained by solving the eigenvalue problem corresponding to the equations of motion cast into the state-space formulation. Two modes of vibration are encountered for the 2-DOFs: the first mode at 20.1 Hz modal frequency and 15.7% modal damping ratio; the second mode at 28.3 Hz modal frequency and 21.0% modal damping ratio.

In this numerical example the k_3 spring and the c_3 damper will be allowed to vary. Variations from -50% to +50% around their nominal value will be applied in steps of 10%. However, the two parameters will not vary simultaneously, only one parameter, either k_3 or c_3, will vary at a time and the rest of the parameters will be kept constant.

For each variation in the value of k_3 or c_3 the modal solutions of the perturbed system are computed in two ways. On one hand, the exact eigensolutions of the perturbed system are computed by solving the corresponding state-space EVP. On the other hand, the perturbed system approximate eigensolutions are computed using the perturbation propagation expressions in section 3.2.3. In this way, the accuracy of the undamped and damped modal perturbation approximations can be evaluated through comparison with the exact modal solutions.

The exact and approximate modal solutions for the aforementioned k_3 and c_3 variations are compared in figures 3.5, 3.6 and 3.7. Figure 3.5 shows the variation in the modal frequency of the two modes introduced by the k_3 stiffness variation (left) and the c_3 damping variation (right). Likewise, figure 3.6 shows the corresponding variation in the modal damping. In both figures, the top plots present the exact and approximate values of the modal frequencies and damping, and the bottom plots present the relative error of the approximate values with respect to the corresponding exact values. In figure 3.7, the MAC between the exact and the approximate mode shapes, i.e. $\text{MAC}(\boldsymbol{\phi}_m, \tilde{\boldsymbol{\phi}}_m)$ and $\text{MAC}(\boldsymbol{\phi}_m, \tilde{\boldsymbol{u}}_m)$, is shown for the k_3 stiffness variations (left) and the c_3 damping variations (right).

Damped modes exact perturbation

The baseline system modal frequencies and modal damping are indicated with a red circle (at 0% parameter variation) in figures 3.5 and 3.6 respectively. When stiffness

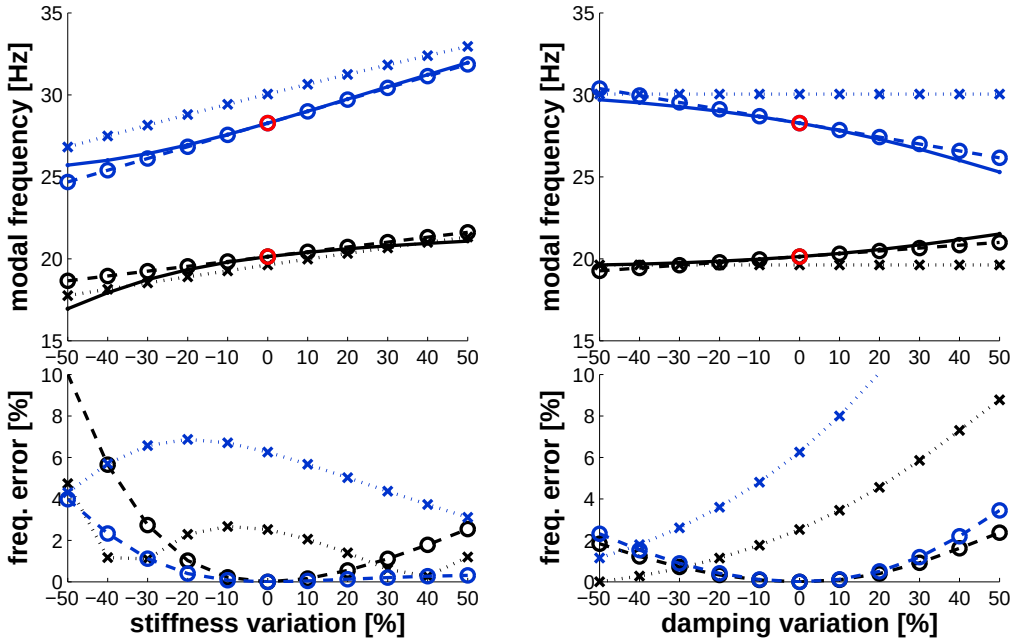

Figure 3.5: Variation and error in modal frequencies with respect to k_3 and c_3 variations:
1st mode: — exact —○— damped perturbation ··×·· undamped perturbation
2nd mode: — exact —○— damped perturbation ··×·· undamped perturbation

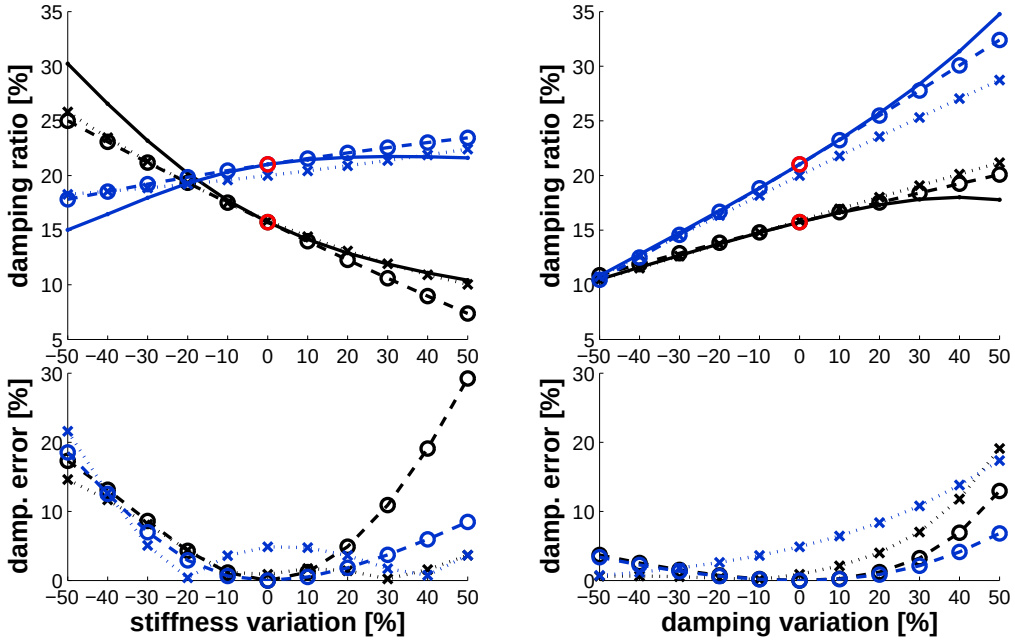

Figure 3.6: Variation and error in modal damping with respect to k_3 and c_3 variations:
1st mode: — exact —○— damped perturbation ··×·· undamped perturbation
2nd mode: — exact —○— damped perturbation ··×·· undamped perturbation

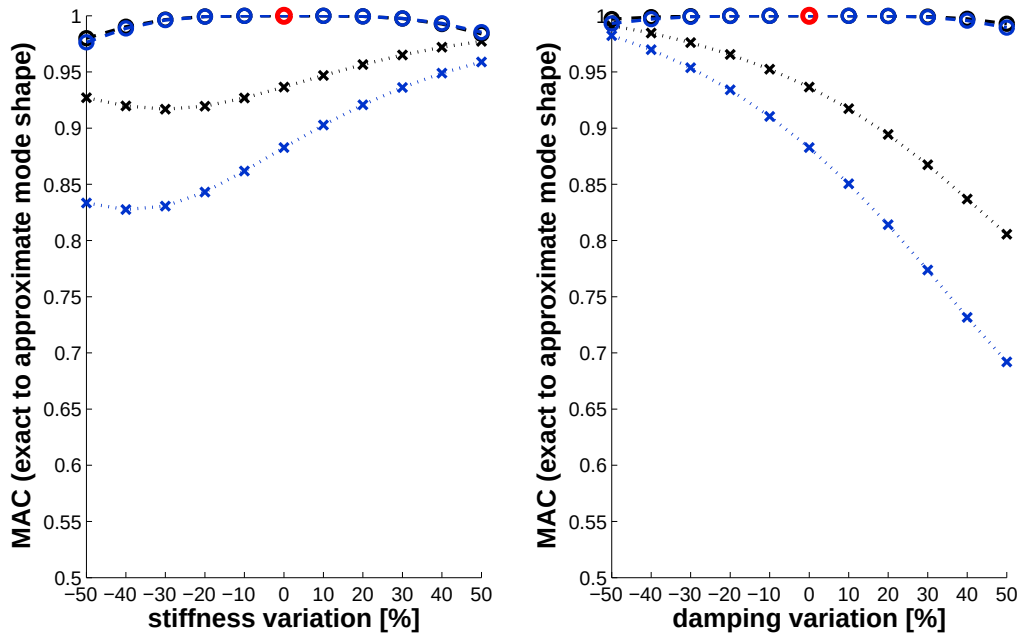

Figure 3.7: Exact to approximate eigenvectors' MAC with respect to k_3 and c_3 variations:
1^{st} mode: $-\circ-$ damped perturbation $\cdots\times\cdots$ undamped perturbation
2^{nd} mode: $-\circ-$ damped perturbation $\cdots\times\cdots$ undamped perturbation

or damping perturbations are introduced, the exact modal frequencies and damping vary in a slightly non-linear manner (solid lines). For stiffness variations, both modes increase their modal frequency as the stiffness increases. On the contrary, the modal damping of the first mode decreases whereas the modal damping of the second mode increases with respect to stiffness increments. For damping variations the converse behaviour is observed, that is, for both modes the modal damping increases together with damping increments but, while the first mode increases its frequency, the second mode frequency decreases.

Damped modes perturbation approximation

The damped modes perturbation functions approximate the exact modal parameter variations as linear variations proportional to the varying parameter as can be observed in the top plots of figures 3.5 and 3.6 (dashed-circle lines). Consequently, the corresponding approximation error (bottom plots) grows polynomially with the stiffness or damping perturbation magnitude. A fair approximation error is obtained in the $\pm 20\%$ perturbation range, with modal frequency errors below 1% and modal damping errors below 5% for Δk_3 and below 1% for Δc_3. Beyond $\pm 20\%$

perturbation in k_3 or c_3 the approximation error in the perturbed modal parameters may be considered too large. For this reason, the validity of the perturbation method is said to be restricted to small variations in the parameters.

So far, modal frequencies and modal damping have been evaluated, but little attention has been paid to the mode shapes. The accuracy of the mode shapes perturbation approximation may be evaluated by means of the Modal Assurance Criterion (MAC). In figure 3.7 it can be observed how the MAC values corresponding to damped modes perturbation functions approximation (dashed-circle lines) are all very close to unity. This means that the error in the approximate (damped) mode shapes is very small for the full ±50% perturbation range. This fact corroborates the idea that mode shape vectors vary at relatively slow variation rate, so that the range of validity of the perturbation approximation method will be rather delimited by the modal frequencies and modal damping errors.

Undamped modes perturbation approximation

Finally, the results for the undamped modes perturbation approximation are discussed separately. The undamped modes diverge from the damped modes as the level of damping increases. Damping reduces the resonance frequencies and the mode shape vectors become more complex valued. In consequence, the accuracy of the undamped modes perturbation approximation shows a great dependency on the overall system level of damping.

As is appreciable in figures 3.5 and 3.6, the modal parameters obtained from the undamped system eigensolutions (dotted-cross lines) present significant approximation error with respect to the exact solution even before applying any perturbation (2-3% errors in mode 1 and 5-6% errors in mode 2). This is due to the fact that the 2-DOF system is heavily damped ($\zeta_1 = 15.7\%$ and $\zeta_2 = 21.0\%$). Similarly, it can be observed in figure 3.7 that the MAC between the undamped and damped mode shapes of the baseline system $\mathrm{MAC}(\boldsymbol{\phi}_m, \boldsymbol{u}_m)$ have values well below unity already.

For stiffness variation, the undamped approximate modal frequencies (dotted-cross lines in figure 3.5) show a similar rate of change to that of the damped approximate modal frequencies (dashed-circle lines), shifted in frequency due to the baseline undamped modal frequencies error. This results in an always present significant error level for the full variation range. Likewise, the undamped approximate mode shape vectors incur a similar behaviour. The wide ranging error in the undamped approximate mode shapes is noticeable in figure 3.7 (dotted-cross lines) where the

MAC values are around 0.8-0.9 for the full variation range. Incidentally, the MAC values converge to unity for the highest positive variation in stiffness. The reason for this is that the system becomes closer to being proportionally damped, i.e. the prominence of c_3 is matched by the prominence of the perturbed k_3.

For damping variation, the undamped approximate modal frequencies show no variation (dotted-cross lines in figure 3.5). However, the approximation error diminishes as the damping diminishes (errors<2% at -50% Δc_3) and increases otherwise (errors>8% at +50% Δc_3), since the actual damped modes tend to converge with the undamped ones as the damping becomes small. The undamped approximate mode shapes show the same behaviour; that is, no perturbation is produced by damping variations, but the approximation errors varies according to overall damping level. In figure 3.7 close to unity MAC values are observed for -50% damping variation, whereas for +50% variation low MAC values around 0.7-0.8 are encountered.

The corresponding modal damping variation has been computed a posteriori from the undamped mode approximate perturbations using the small damping approximation (c.f. equation 3.15). The larger errors in modal damping (>15%) occur precisely when the undamped mode perturbation approximation shows more error with respect to the exact damped modes. Conversely, minimum modal damping errors (<3%) occur when the undamped modes perturbation approximation shows less error. The latter has happened for +50% stiffness perturbation (close to proportional damping condition) and -50% damping perturbation (close to the undamped condition).

3.3 Interpolation method

The interpolation method considers a limited interval of variation of the model parameters. Then the system model is solved at each of the interval extremes. The rest of the solutions throughout the range of variation are approximated by interpolation of the exact solutions at the interval extremes. The method is aimed at moderate variations of the model parameters.

3.3.1 Linear interpolation

As for the perturbation method, consider a system model defined by a set of model parameters $\boldsymbol{\theta}$. For each model parameter θ an interval in which the parameter is

assumed to vary is determined, i.e. $\theta \in [\theta_o,\ \theta_f]$. Then, the values for the output quantities $z(\theta)$ at the interval extremes are computed, i.e. $z(\theta_o) = z_o$ and $z(\theta_f) = z_f$.

The interpolation method considers that an output quantity $z(\theta)$ corresponding to a parameter value θ inside the defined interval can be approximated as a combination of z_o and z_f. Since a priori we do not have any information on how $z(\theta)$ may vary, the simplest approximation is to perform linear interpolation, that is

$$z(\theta) \approx (1-\varepsilon)z_o + \varepsilon z_f = \tilde{z}(\theta) \tag{3.22}$$

with ε a normalised value for the varying parameter, i.e.

$$\varepsilon(\theta) = \frac{\theta - \theta_o}{\theta_f - \theta_o} \tag{3.23}$$

so that ε takes values between 0 and 1 in the $[\theta_o,\ \theta_f]$ interval.

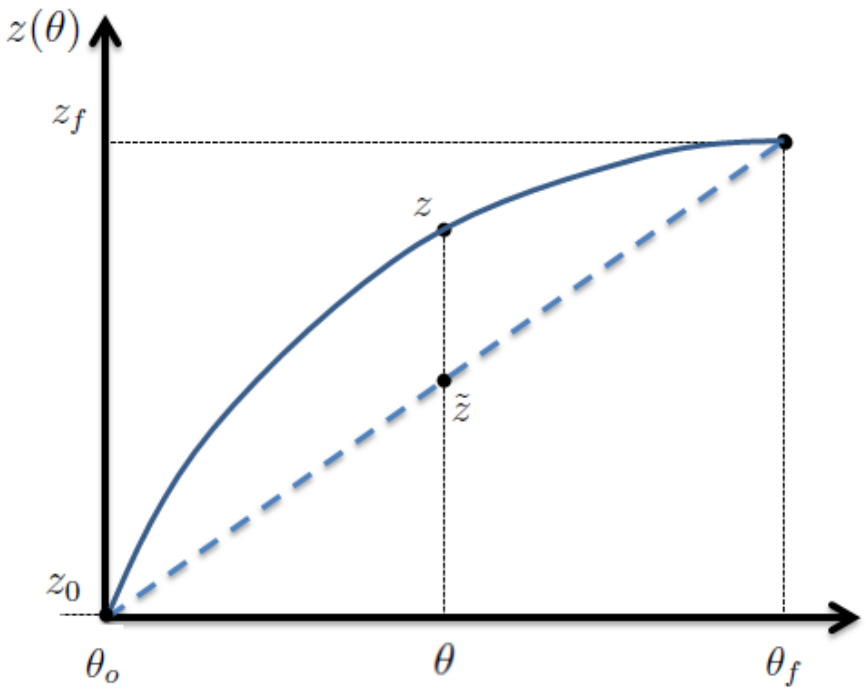

Figure 3.8: Linear interpolation qualitative example. Solid line: Exact variation of the output quantity. Dashed line: Interpolation approximation.

In this way, the approximated output $\tilde{z}(\theta)$ is obtained as a weighted sum of the exact outputs z_o and z_f at the interval extremes. For a θ value close to θ_o, ε is close to zero, and therefore most of the contribution to $\tilde{z}(\theta)$ comes from z_o. For a θ value close to θ_f, ε is close to unity, and therefore most of the contribution to $\tilde{z}(\theta)$ comes from z_f. At $\theta = \theta_o$ and $\theta = \theta_f$ the interpolation yields the exact solution.

The maximum error in the interpolation approximation is expected to be around the centre of the interval because $z(\theta)$ will differ from both z_o and z_f. This can be observed in the qualitative plot shown in figure 3.8.

Linear interpolation provides a rough approximation whose accuracy depends on the degree of linearity of the relation between the model parameters and the output quantities in the defined interval. Therefore, for a generally non-linearly dependent output, the interpolation approximation may be too imprecise for large variations of the model parameters.

On the contrary, it will give good accuracy for small variations of the parameters, like the perturbation method, but with a reversed distribution of the approximation error along an interval of variation, i.e. smaller error at the interval extremes than in the centre. However, the need to compute at least two exact solutions to perform the interpolation puts in question its computational efficiency benefits with respect to the perturbation method in the case of small variations.

Nonetheless, linear interpolation might be very beneficial if one considers moderate variations of the model parameters. For such variations, the perturbation method is definitely going to result in large errors away from the baseline solution. On the contrary, the interpolation method may provide a fair approximation since the error is constrained at both extremes. Thence, the interpolation method could be used in search processes where one explores design modifications, at a very low computational cost, in order to meet some design requirements.

3.3.2 Multivariate linear interpolation

The interpolation method may be also applied when more than one parameter varies. For instance, consider two parameters θ_1 and θ_2 whose intervals of variation are $\theta_1 \in [\theta_{1o},\ \theta_{1f}]$ and $\theta_2 \in [\theta_{2o},\ \theta_{2f}]$ respectively. In such case, the joint variation of the two parameters may be combined together in a two dimensional coordinate space $\boldsymbol{\theta} = (\theta_1,\ \theta_2)$, so that the two intervals of variation define a rectangular-shape area of variation. The area of variation is limited by four coordinate values corresponding to the four corners of the rectangle, i.e. $\boldsymbol{\theta}_1 = (\theta_{1o}, \theta_{2o})$, $\boldsymbol{\theta}_2 = (\theta_{1o}, \theta_{2f})$, $\boldsymbol{\theta}_3 = (\theta_{1f}, \theta_{2o})$ and $\boldsymbol{\theta}_4 = (\theta_{1f}, \theta_{2f})$.

Thence, an output quantity $z(\boldsymbol{\theta})$ that varies along the area may be approximated by *bilinear interpolation* of the output quantity at the four corners coordinates, i.e.

$$\tilde{z}(\boldsymbol{\theta}) = (1-\varepsilon_1)(1-\varepsilon_2)z_1 + (1-\varepsilon_1)\varepsilon_2 z_2 + \varepsilon_1(1-\varepsilon_2)z_3 + \varepsilon_1\varepsilon_2 z_4 \tag{3.24}$$

where z_i is the value of the output quantity at the i'th corner coordinate $\boldsymbol{\theta}_i$, and ε_j is the normalised value of the j'th varying parameter θ_j (c.f. equation 3.23).

In the same way, if three varying parameters are considered an output quantity may be approximated by *trilinear interpolation*. In this case the joint variation of the three parameters span a three dimensional space with variations inside a cube-shaped volume determined by the intervals of variation of each parameter. Output quantities at the eight vertices of the cube need to be computed in order to interpolate output quantities inside the volume of variation.

Generalising, for a set of output quantities $\mathbf{z}(\boldsymbol{\theta})$ depending on a set of n varying parameters $\boldsymbol{\theta} = (\theta_1, \ldots, \theta_n)$, the output quantities at 2^n extreme values $\boldsymbol{\theta}_i$ are needed in order to obtain the interpolated approximations $\tilde{\mathbf{z}}(\boldsymbol{\theta})$, i.e.

$$\tilde{\mathbf{z}}(\boldsymbol{\theta}) = \sum_{i=1}^{2^n} a_i(\boldsymbol{\varepsilon})\mathbf{z}_i \tag{3.25}$$

with $\mathbf{z}_i = \mathbf{z}(\boldsymbol{\theta}_i)$ the set of output quantities at the i'th extreme value $\boldsymbol{\theta}_i$, and $a_i(\boldsymbol{\varepsilon})$ the corresponding interpolation weighting factor depending on the set of normalised parameters $\boldsymbol{\varepsilon} = (\varepsilon_1, ..., \varepsilon_n)$.

The computational cost of the interpolation method grows exponentially with the number n of varying parameters, since 2^n solutions must be computed before actually performing the interpolation. Therefore, as the number of varying parameters increase, the interpolation method provides smaller gain in computational efficiency. This fact together with the expectation of roughly approximate results may not justify the use of interpolation method when more than, say, 2 or 3 simultaneously varying parameters are considered.

3.3.3 Modal interpolation

In dynamic analysis we may consider as output quantities either the modal parameters or the frequency responses. Here, the interpolation method is specified for the computation of approximate modal parameters when the model parameters vary. Application of the interpolation method to frequency responses is discarded beforehand because of the way the frequency responses vary[1].

[1]Consider that one knows the frequency response for the two extreme values of the varying parameter. Now consider that at a certain frequency none of the two known responses show resonance, but that the response shows resonance for an intermediate value of the varying parameter. Clearly, interpolation of the two extreme responses will not show any resonance giving a completely wrong approximation for certain range of variation of the parameter.

Interpolation of undamped modes

Starting with undamped systems, one may think on interpolating modal frequencies. Variations in undamped modal frequencies are non-linear but rather smooth when the mass or stiffness in the system vary. Therefore, undamped modal frequencies may be interpolated directly.

However, as has been seen in section 3.1.1 and Appendix C, the rate of change of undamped eigenvalues (i.e. $\lambda_m = \omega_m^2$) is linear with respect to stiffness variations and quasi-linear with respect to mass variations. This observation suggests that linear interpolation of undamped eigenvalues may yield better approximations in modal frequencies than direct modal frequency interpolation. Therefore, undamped eigenvalue linear interpolation is preferred over undamped modal frequency linear interpolation.

For a generic varying parameter θ, the exact eigenvalues $\lambda_m(\theta_o)$ and $\lambda_m(\theta_f)$ at the extremes of the interval of variation shall be computed. Then, linear interpolation of eigenvalues is used to approximate the intermediate eigenvalues, that is

$$\tilde{\lambda}_m(\theta) = (1-\varepsilon)\lambda_m(\theta_f) + \varepsilon\lambda_m(\theta_o) \tag{3.26}$$

Next, one may contemplate interpolating the undamped eigenvectors for the same variation interval. Typically, the rate of variation in mode shape vectors is small compared to variations in modal frequencies. This means that for moderate variations of model parameters, the relative change from the eigenvector at one of the extremes of the interval to the eigenvector at the other extreme is relatively small. Hence, linear interpolation may be a fair approximation of the eigenvectors inside the interval of variation. This can be posed as

$$\tilde{\boldsymbol{u}}_m(\theta) = (1-\varepsilon)\boldsymbol{u}_m(\theta_f) + \varepsilon\boldsymbol{u}_m(\theta_o) \tag{3.27}$$

with $\boldsymbol{u}_m(\theta_o)$ and $\boldsymbol{u}_m(\theta_f)$ the undamped eigenvectors at the variation interval extremes.

The approximate undamped mode shape vectors correspond directly to the interpolated undamped eigenvectors $\tilde{\boldsymbol{u}}_m$. The approximate undamped modal frequencies $\tilde{\omega}_m$ correspond to the square root of the interpolated eigenvalues $\tilde{\lambda}_m$.

Interpolation of damped modes

Modal interpolation may be used for approximating damped systems dynamics as well. The question here is whether to treat modal damping ζ_m and damped modal frequencies $\omega_{d,m}$ independently, or if it is preferable to interpolate directly the damped eigenvalues which contain both quantities, i.e. $\lambda_m = -\zeta_m|\lambda_m| \pm i\omega_{d,m}$.

For lightly damped systems, the rate of change in modal frequencies is almost invariant with respect to damping (moderate) variations, and show the same variation rate as undamped modal frequencies. Conversely, modal damping is almost invariant with respect to mass or stiffness (moderate) variations, and varies linearly with system damping variations. Therefore, the variations in modal damping and modal frequencies are uncorrelated, so that interpolating each modal parameter independently may be a good idea.

Lightly damped modal frequencies may be treated as undamped modal frequencies and, in consequence, linear interpolation of their squared values shall give the most accurate approximations. For a generic varying parameter θ, one may compute the exact modal frequencies $\omega_{d,m}(\theta_o)$ and $\omega_{d,m}(\theta_f)$ at the extremes of the interpolation interval. Then, linear interpolation of the squared modal frequencies is used to approximate the intermediate modal frequencies, that is

$$\tilde{\omega}^2_{d,m}(\theta) = (1-\varepsilon)\omega^2_{d,m}(\theta_f) + \varepsilon\omega^2_{d,m}(\theta_o) \tag{3.28}$$

Likewise, knowing the modal damping $\zeta_m(\theta_o)$ and $\zeta_m(\theta_f)$ at the intervals extremes, the intermediate modal damping values may be approximated fairly through linear interpolation, i.e.

$$\tilde{\zeta}_m(\theta) = (1-\varepsilon)\zeta_m(\theta_f) + \varepsilon\zeta_m(\theta_o) \tag{3.29}$$

Logically, modal frequencies interpolation (equation 3.28) would be used for mass or stiffness variations and modal damping interpolation (equation 3.29) for damping variations, when the system is lightly damped.

Damped eigenvectors show the same behaviour of small variation compared to the damped modal frequencies than the one explained for undamped systems. The only difference is that the variations happen in the relative phase and amplitude between the shape positions, not only relative amplitudes as in the undamped case. Thus, linear interpolation of damped eigenvectors is sought to be a fair approximation of the variation of damped eigenvectors for moderate variations in the system model parameters. The linear interpolation of damped eigenvectors is made explicit in equation 3.30.

$$\tilde{\boldsymbol{\phi}}_m(\theta) = (1-\varepsilon)\boldsymbol{\phi}_m(\theta_f) + \varepsilon\boldsymbol{\phi}_m(\theta_o) \tag{3.30}$$

For heavily damped systems both modal frequencies and modal damping vary strongly and in a non-linear way for variations in any of the system parameters: mass, stiffness and damping. Since no further specific information on the rate of change of these modal parameters can be known beforehand when the system is heavily damped, the simplest choice is to directly interpolate the damped eigenvalues $\lambda_m = -\sigma_m \pm i\omega_{d,m}$ as in equation 3.26. However, this may not yield very accurate results.

Mode shape vectors of heavily damped systems also vary at a higher rate than for lightly damped systems, especially the relative phase between shape positions. Nevertheless, the variations may still remain relatively small. Linear interpolation of heavily damped mode shape vectors may be performed in the same way as given in equation 3.30 for the lightly damped ones.

3.3.4 The cost of modal interpolation

The modal interpolation method has been presented. After having discussed the approximation goodness of the modal interpolation method, it is now time to evaluate its presumed efficiency. Reanalysis through modal interpolation involves two main processes that contribute to the overall computational cost.

On one hand, there is the cost associated with computing exact modal solutions for each of the extremes of the variation domain of the varying model parameters. For instance, if only one varying parameter is considered, two exact modal solutions are needed, that is, two eigenvalue problems must be solved. For n varying parameters, 2^n EVPs have to be solved.

The computational cost for solving the eigenvalue problem in modal analysis has been largely discussed in the previous chapter (see section 2.3.3), and it depends on the order N of the involved system matrices. The cost for finding each vibration mode scales as of $\mathcal{O}(N^2)$ floating point operations (flops) if the undamped EVP is solved, or $\mathcal{O}\left(4N^2\right)$ flops if the state-space EVP is solved.

On the other hand, there is the computational cost associated with the interpolation expressions exposed in the previous section. The interpolation of eigenvalues (equation 3.26), damped modal frequencies (equation 3.28) or modal damping (equation 3.29) involves only a few scalar operations, so that the associated computational cost is trivial.

The interpolation of mode shape vectors (equations 3.27 and 3.30) corresponds to a

weighted sum of N-sized vectors. For a single varying parameter only two extreme mode shape vectors must be summed up, but for multivariate interpolation 2^n vectors should be summed up. Each weighted eigenvector to be summed supposes a computational cost proportional to $\mathcal{O}(N)$ flops.

	Computing exact modal solutions		Each modal reanalysis	
	Operations	Complexity	Operations	Complexity
Undamped eigensolutions	2^n EVP solutions	$2^n\mathcal{O}(N^2)$	2^n vector operations + $\mathcal{O}(2^n)$ flops	$2^n\mathcal{O}(N)$
Damped eigensolutions	2^n S-S EVP solutions	$2^n\mathcal{O}(4N^2)$		

Table 3.4: The computational cost of the modal interpolation method.

All in all, the computational cost of the modal interpolation method is that of computing the extreme exact solutions twice, plus the cost of interpolation of the eigensolutions at each reanalysis. This is summarised in table 3.4.

Each reanalysis is performed at a very low computational cost in comparison with the perturbation method. The cost for interpolating the scalar modal parameters (eigenvalues or modal frequencies/damping) is negligible. The cost for computing mode shape vectors scales as of $\mathcal{O}(N)$. In contrast, the cost of eigenvalue perturbation was proportional to the number of perturbed DOFs, and the cost of eigenvector perturbation proportional to the number of modes M times $\mathcal{O}(N)$. That is, the interpolation reanalysis obtains approximate eigenvalues at a cost up to N times smaller, and approximate eigenvectors at a cost M times smaller than perturbation reanalysis.

That being said, one must take into account the cost of computing exact solutions at the interval extremes. This cost may be extremely large in comparison with the reanalysis cost. The factor that makes it worth incurring such large extra cost is the number of reanalyses one intends to perform, since the exact solutions are to be computed only once.

3.3.5 Numerical example

The modal interpolation method is tested here using the same two degrees of freedom examples used for the modal perturbation method (see figure 3.4 in section 3.2.5). In this case, however, exact modal solutions for the damped system are computed at the extremes of the variation intervals. Only Damped modes interpolation is considered in this example.

The k_3 and c_3 parameters are allowed to vary in a $\pm 50\%$ range around their nominal

value as in the perturbation method numerical example. Variations from -50% to +50% around their nominal value are applied in steps of 10%. Although simultaneous variation of k_3 and c_3 may be handled using multivariate interpolation, non-simultaneous variation is chosen here so that the interpolation results can be compared to the results obtained using the perturbation method.

For each variation in the value of k_3 or c_3 the modal solutions of the system are computed in two ways. On one hand, the exact eigensolutions of the perturbed system are computed by solving the corresponding state-space EVP. On the other hand, the approximate modal solutions are computed through interpolation of the exact damped modal solutions at the interval extremes. The approximate modal frequencies and modal damping are computed twice: once by interpolation of squared modal frequencies $\omega_{d,m}^2$ and interpolation of modal damping ζ_m separately, and once again by interpolation of damped eigenvalues λ_m directly.

The exact and approximate modal solutions for the k_3 and c_3 variations are compared in figures 3.9, 3.10 and 3.11. Figure 3.9 shows the variations in the modal frequencies induced by the k_3 stiffness variation (left) and the c_3 damping variation (right) respectively. Figure 3.10 shows the corresponding variation in the modal damping. In both figures, the top plots present the exact and approximate values of the modal frequencies and modal damping, and the bottom plots present the relative error of the approximate values with respect to the corresponding exact values. In figure 3.11, the MAC between the exact and the approximate mode shapes, i.e. $\text{MAC}(\boldsymbol{\phi}_m, \tilde{\boldsymbol{\phi}}_m)$, is shown for the k_3 stiffness variations (left) and the c_3 damping variations (right) respectively.

The solid lines in figures 3.9 and 3.10 show the exact variation in modal frequencies and modal damping respectively. Logically, the exact solutions coincide with the example in section 3.2.5 since the same variations in k_3 and c_3 have been defined (c.f. figures 3.5 and 3.6). In the same figures, the dashed-circle lines show the results for the direct interpolation of damped eigenvalues λ_m as defined in equation 3.26. In figure 3.9, the dotted-cross lines show the results for the squared damped modal frequencies $\omega_{d,m}^2$ interpolation as defined in equation 3.28; whereas in figure 3.10 the dotted-cross lines show the results for the modal damping ζ_m interpolation as defined in equation 3.29.

The first thing one can realise by inspecting figures 3.9 and 3.10 is that, as expected, the error in the interpolation approximation is minimum at the extremes of the variation intervals and maximum in the central range of variation. This characteristic in the error is opposite to that of the perturbation method.

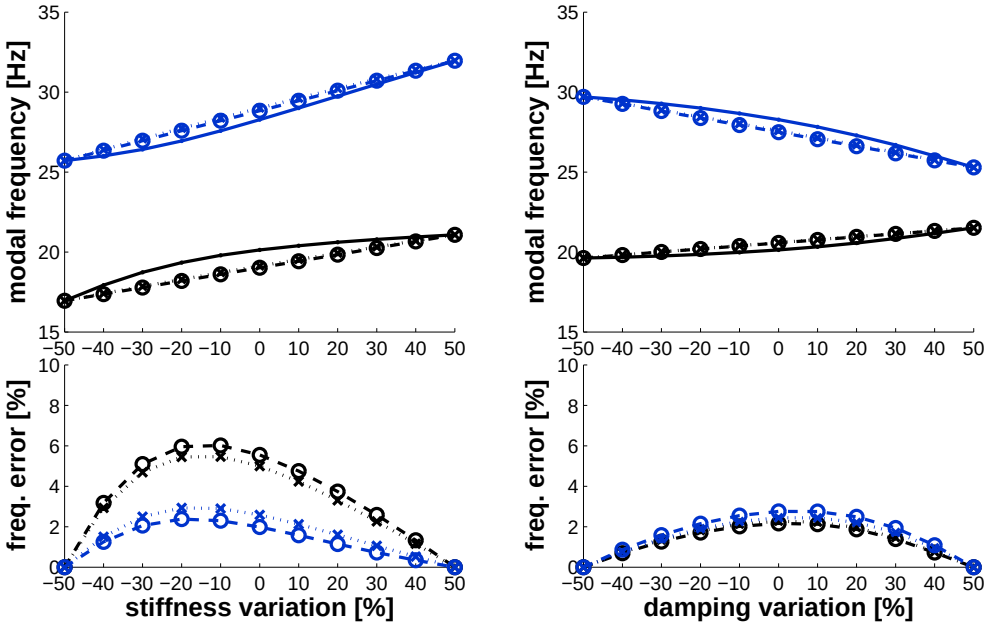

Figure 3.9: Variation and error in modal frequencies with respect to k_3 and c_3 variations:
1st mode: — exact —○— damped λ_m interpolation ··×·· $\omega_{d,m}^2$ interpolation
2nd mode: — exact —○— damped λ_m interpolation ··×·· $\omega_{d,m}^2$ interpolation

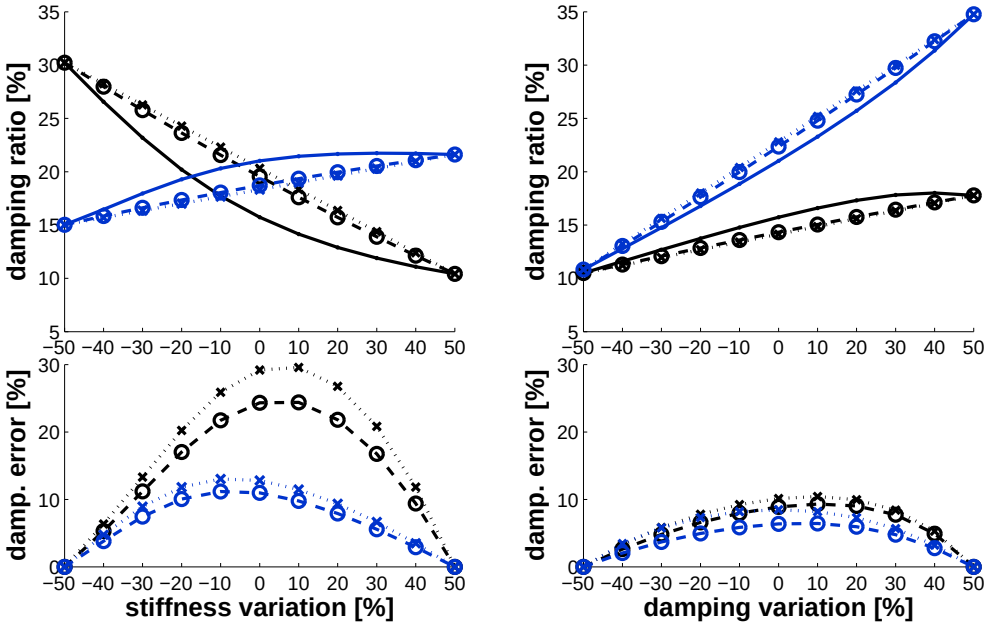

Figure 3.10: Variation and error in modal damping with respect to k_3 and c_3 variations:
1st mode: — exact —○— damped λ_m interpolation ··×·· ζ_m interpolation
2nd mode: — exact —○— damped λ_m interpolation ··×·· ζ_m interpolation

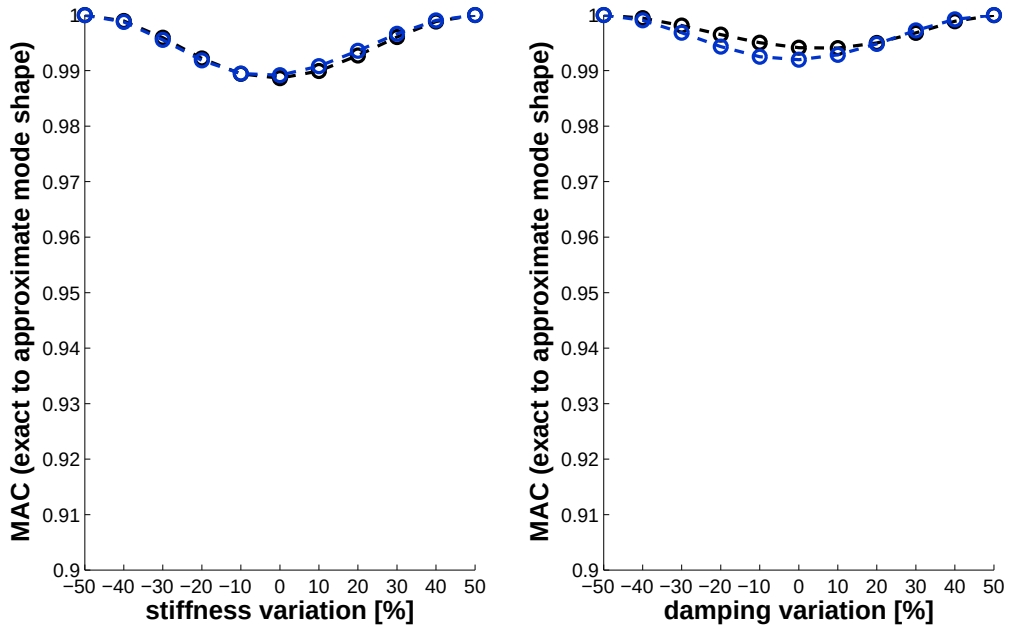

Figure 3.11: Interpolated to exact eigenvectors' MAC values variation with respect to k_3 and c_3 variations: $-\circ-$ 1st mode $-\circ-$ 2nd mode

Looking at the modal frequencies interpolation results in figure 3.9, the approximations obtained through λ_m interpolation and through $\omega_{d,m}^2$ interpolation are almost coincident. For stiffness variations maximum approximation errors are of 6% in the first mode and 2% in the second mode. For damping variations maximum approximation errors are of 2% for both modes. These approximation errors are of comparable magnitude to those of the perturbation method[2].

Despite it having been argued in the previous section that the $\omega_{d,m}^2$ interpolation should give better approximation for lightly damped systems, the results of this example show that for moderate to high damping (as is the case here) the $\omega_{d,m}^2$ interpolation does not show any substantial advantage over the more straightforward λ_m interpolation.

As can be observed in figure 3.9, the modal damping interpolation results obtained through ζ_m interpolation also show little differences with respect to λ_m interpolation results. The latter results produce slightly smaller error than the former. This fact reaffirms the convenience of using λ_m interpolation for damped systems. Again,

[2]In the numerical example for the perturbation method described in section 3.2.5, the maximum errors in damped modal frequencies obtained at the interval extremes were: 10% error in the first mode and 4% in the second mode for stiffness variation; 2% error in the first mode and 3% error in the second mode for damping variation. See figure 3.5

the maximum amount of error in the interpolation approximation occurs at the central range of variation, with comparable magnitude to that of the damped modes perturbation errors.

Finally, the error in the interpolated mode shape vectors may be evaluated through the Modal Assurance Criterion. Here it has to be remarked that the eigenvector interpolation results will vary depending on the difference in *absolute phase* of the complex valued eigenvectors at the extremes of the variation range. Care has to be taken when interpolating them. Since the absolute phase of eigenvectors may have any arbitrary value, there is the need to *put in phase* the two interval extremes eigenvectors before performing the interpolation. Otherwise, the relative amplitudes and phase shifts between different DOF positions in the interpolated mode shape are wrongly computed.

It can be seen in figure 3.11 that, for both modes and in the whole range of variation of k_3 and c_3, the MAC of the interpolated mode shapes to the exact mode shapes is permanently above a value of 0.99. Therefore, very good accuracy is obtained when interpolating complex mode shape vectors even for heavily damped systems. The limiting factor in the usage of the modal perturbation method is therefore the approximation error in modal frequencies and modal damping.

3.4 Rayleigh quotient eigenvalue approximation

The Rayleigh quotient is a key concept in the analysis of dynamic systems. It was defined for conservative systems (i.e. undamped systems) within Rayleigh's variational approach for solving the generalised eigenvalue problem that arises from the equations of motion [46]. The main application of the Rayleigh quotient is its usage in algorithms for solving the eigenvalue problem. However, this is not the only application it may have. For the purpose of this thesis, the Rayleigh quotient holds some properties that means it presents itself as a candidate to be used in approximate reanalysis methods. For instance, Bhaskar et al. [67, 76] combined the Rayleigh quotient with interpolation methods. Thus, the Rayleigh quotient is introduced in this section and the properties relevant to this work are outlined.

Then, it is also shown in this section that a very good approximation of an eigenvalue may be obtained when the Rayleigh quotient is applied to an approximate corresponding eigenvector. Hence, it is proposed to use Rayleigh quotient approximation in conjunction with approximate reanalysis methods (specifically the perturbation

and interpolation methods presented in the previous sections).

3.4.1 The Rayleigh quotient

The Rayleigh quotient $R(\boldsymbol{u})$ is a functional over a real vector space $\mathcal{V}$ defined as the ratio of two quadratic forms involving the stiffness $\mathbf{K}$ and mass $\mathbf{M}$ matrices respectively. In other words, the Rayleigh quotient $R(\boldsymbol{u})$ is a scalar associated to any shape vector $\boldsymbol{u} \in \mathcal{V}$, with respect to the $(\mathbf{M}, \mathbf{K})$ matrix pencil.

$$R(\boldsymbol{u}) = R(\boldsymbol{u}; \mathbf{M}, \mathbf{K}) = \frac{\boldsymbol{u}^T \mathbf{K} \boldsymbol{u}}{\boldsymbol{u}^T \mathbf{M} \boldsymbol{u}} \tag{3.31}$$

The Rayleigh quotient is specifically defined so that it equals a system eigenvalue when applied to its corresponding eigenvector, i.e.

$$R(\boldsymbol{u}_m) = \lambda_m = \omega_m^2 \tag{3.32}$$

This may be easily proved by pre-multiplying with $\boldsymbol{u}_m^T$ the undamped EVP equation, i.e.

$$\boldsymbol{u}_m^T \left(\lambda_m \mathbf{M} \boldsymbol{u}_m\right) = \boldsymbol{u}_m^T \left(\mathbf{K} \boldsymbol{u}_m\right) \tag{3.33}$$

In effect, isolating for the λ_m eigenvalue in equation 3.33 yields the $R(\boldsymbol{u}_m)$ Rayleigh quotient expression.

It can also be proved that for any trial vector $\boldsymbol{u}$ the Rayleigh quotient is an upper bound for the smallest eigenvalue of the system, and a lower bound for the largest eigenvalue of the system. Moreover, if a trial vector $\boldsymbol{u}$ is orthogonal to the N lowest eigenvectors, then its Rayleigh quotient is an upper bound for the $N+1$ eigenvalue (see section 4-11 in [52]).

The importance of the Rayleigh quotient lies in the fact that it is *stationary* for any trial vector $\boldsymbol{u}$ in the neighbourhood of an eigenvector $\boldsymbol{u}_m$. This means that the rate of change of the Rayleigh quotient is zero at the system eigenvectors, i.e.

$$\delta R(\boldsymbol{u})_{|\boldsymbol{u}=\boldsymbol{u}_m} = 0 \tag{3.34}$$

where δ is the first variation of a functional, as encountered in variational calculus.

The stationarity property implies that if a vector $\boldsymbol{u}$ differs from an eigenvector $\boldsymbol{u}_m$ by a small quantity ϵ, the corresponding Rayleigh quotient $R(\boldsymbol{u})$ will differ from the corresponding eigenvalue λ_m by a small quantity $\mathcal{O}(\epsilon^2)$. This is proved in section E.1 of Appendix E, where the properties of the Rayleigh quotient are demonstrated separately.

The stationarity of the Rayleigh quotient has implications of practical use. For example, consider an eigenvector is calculated using an approximate method. Thence, this eigenvector is an approximation to the true eigenvector. Assume that the Rayleigh quotient is used to compute the corresponding eigenvalue. Then, due to stationarity, the eigenvalue approximation error will be much smaller than the error in the eigenvector. This implies that very good approximations in the modal frequencies can be obtained from much less accurate mode shape vectors.

Not only is the Rayleigh quotient a *better than deserved* approximation of an eigenvalue, but the best approximation one can get from any trial vector $\boldsymbol{u}$. In Chapter 2 it has been seen that the eigenvalue error for the undamped EVP may be bounded using the Krylov-Weinstein or the Kato-Temple error bounds. These bounds for generalised eigenvalue problems are given in terms of the M-inverse norm of the residual vector $\|\mathbf{r}\|_{M^{-1}}$. As is shown in section E.2 of Appendix E, the Rayleigh quotient of a vector $\boldsymbol{u}$ minimises the M-inverse norm of the corresponding residual vector $\mathbf{r}(\boldsymbol{u})$. Thus, the Rayleigh quotient provides the best possible approximation of an eigenvalue for a given approximate eigenvector.

The Rayleigh quotient gives rise to yet another important property. When an eigenvalue is approximated through the Rayleigh quotient, the residual vector $\mathbf{r}(R(\boldsymbol{u}), \boldsymbol{u})$ becomes orthogonal to the corresponding trial eigenvector $\boldsymbol{u}$ (see proof in section E.3 in Appendix E). In turn, residual to eigenvector orthogonality is the property that makes it possible to define the Kato-Temple bound. For this reason this error bound only holds when the Rayleigh Quotient is used for eigenvalue approximation.

3.4.2 Eigenvalue approximation

When one wants to perform repeated analysis of dynamic systems, one can perform the modal analysis of the system. Then, in each modal reanalysis the mode shape vectors may be approximated fairly well using perturbation or interpolation methods, and the modal frequencies may be approximated with much better accuracy through the Rayleigh quotient.

Consider an undamped system defined by a set of parameters $\boldsymbol{\theta}$. The dynamics of that system are governed by the corresponding mass-stiffness matrix pencil $(\mathbf{M}, \mathbf{K})$. Then, the modal solution of such system will consist of a set of $\lambda_m - \boldsymbol{u}_m$ pairs.

When the $\boldsymbol{\theta}$ parameters vary, the modal pairs may be computed accurately at a high computational cost or, alternatively, they may be approximated using computation-

ally cost-efficient approximate reanalysis methods. Rayleigh quotient eigenvalue approximation brings together cost-efficient computations with accurate solutions.

For a varying parameter θ, an approximate eigenvalue $\lambda_m(\theta)$ is computed by applying the Rayleigh quotient to a corresponding approximate eigenvector, i.e.

$$\tilde{\lambda}_m(\theta) = R(\tilde{\boldsymbol{u}}_m(\theta)) \tag{3.35}$$

where the $\tilde{\boldsymbol{u}}_m(\theta)$ eigenvector may have been obtained through perturbation of the $\mathbf{M}(\theta)$ and $\mathbf{K}(\theta)$ matrices, or by interpolation of certain known exact solutions $\boldsymbol{u}_m(\theta_i)$.

Since the eigenvectors are computed through approximate methods they are obtained at a small computational cost. In turn, the eigenvalues are approximated using the Rayleigh quotient, which also involves a small computational cost. At the same time, the Rayleigh quotient provides a highly accurate estimate of the true eigenvalue due to the stationarity and optimality of the the Rayleigh quotient. Furthermore, good estimates of the approximation error can be computed using the Kato-Temple error bound.

However, the Rayleigh quotient approximation is only applicable to undamped eigenpairs. Thence, a novel Rayleigh quotient for damped systems is explored in the next section in order to apply Rayleigh quotient eigenvalue approximation to the modal solutions of damped systems.

3.4.3 A Rayleigh quotient for damped systems

The Rayleigh quotient as defined in the previous section is only applicable to undamped eigenvalue problems with real valued eigenvalues and eigenvectors. Therefore, its use for damped system is limited only to cases where the damping may be modelled using small or proportional damping assumptions. Since it is intended to develop approximate methods for generally damped systems, it would be desirable to have a Rayleigh quotient that could be used for the complex-valued eigenvectors corresponding to the damped eigenvalue problem. In this section, the possibilities for defining a Rayleigh quotient for damped systems are explored. In order to do so, the state-space EVP defined by the matrix pencil $(\mathbf{A}, \mathbf{B})$ is considered.

Previously, the mathematical definition of the Rayleigh quotient for undamped systems has been given as the ratio of two quadratic forms. This definition can be naturally extended to EVPs defined by hermitian (i.e. conjugate symmetric)

matrices which have complex eigenvectors. The Rayleigh quotient is defined then as the ratio of two hermitian forms. For a definite pencil $(\mathbf{D}, \mathbf{F})$ and a complex trial eigenvector $\boldsymbol{v}$ this is explicitly stated as

$$R(\boldsymbol{v}) = R(\boldsymbol{v}; \mathbf{D}, \mathbf{F}) = \frac{\boldsymbol{v}^H \mathbf{F} \boldsymbol{v}}{\boldsymbol{v}^H \mathbf{D} \boldsymbol{v}} \tag{3.36}$$

This definition of the Rayleigh quotient is mathematically consistent with respect to the classical Rayleigh Quotient for undamped systems.

However, a Rayleigh quotient like the one in equation 3.36 is not applicable to the state-space eigenvalue problem. Even though the $\mathbf{A}$ and $\mathbf{B}$ matrices are real-symmetric matrices they are not positive-definite. Accordingly, the $(\mathbf{A}, \mathbf{B})$ pencil is indefinite. These properties of the state-space EVP result in the state-eigenvectors $\boldsymbol{x}_m$ being orthogonal to their complex conjugate pair with respect to the $\mathbf{A}$ and $\mathbf{B}$ matrices. Consequently, a Rayleigh quotient of the kind $R(\boldsymbol{x}; \mathbf{A}, \mathbf{B})$ would give an indeterminate result when applied to the state-eigenvectors, that is

$$R(\boldsymbol{x}_m) = \frac{\boldsymbol{x}_m^H \mathbf{B} \boldsymbol{x}_m}{\boldsymbol{x}_m^H \mathbf{A} \boldsymbol{x}_m} = \frac{0}{0} \tag{3.37}$$

All in all, there does not exist a quotient based on $(\mathbf{A}, \mathbf{B})$ that strictly matches the mathematical definition of the Rayleigh quotient while providing useful results.

Nevertheless, the idea of approximating eigenvalues using a Rayleigh quotient for damped system may be still possible. Bhaskar [68] proposed a *Rayleigh* quotient in the state-space for non-conservative systems.

$$Q(\boldsymbol{x}) = Q(\boldsymbol{x}; \mathbf{A}, \mathbf{B}) = \frac{\boldsymbol{x}^T \mathbf{B} \boldsymbol{x}}{\boldsymbol{x}^T \mathbf{A} \boldsymbol{x}} \tag{3.38}$$

In this case, the quotient is defined as a ratio of two bilinear forms – $B_B(\mathbf{v}, \mathbf{w}) = \mathbf{w}^T \mathbf{B} \mathbf{v}$ and $B_A(\mathbf{v}, \mathbf{w}) = \mathbf{w}^T \mathbf{A} \mathbf{v}$ – applied to a complex trial vector $\boldsymbol{x}$. This implies that $Q(\boldsymbol{x})$ does not conform exactly with the mathematical definition of the Rayleigh quotient. However, this quotient retains most of the properties of the Rayleigh quotient for undamped systems, as shall be proven in the following section.

Properties of the proposed quotient

To start with, the quotient applied to a state-eigenvector $\boldsymbol{x}_m$ results in its corresponding eigenvalue $\lambda_m = -\sigma_m \pm i\omega_{d,m}$, that is

$$Q(\boldsymbol{x}_m) = \lambda_m \tag{3.39}$$

which is straightforwardly proved by pre-multiplying the state-space EVP with $\boldsymbol{x}_m^T$, i.e.

$$\boldsymbol{x}_m^T \left(\lambda_m \mathbf{A}\boldsymbol{x}_m\right) = \boldsymbol{x}_m^T \left(\mathbf{B}\boldsymbol{x}_m\right) \tag{3.40}$$

This is analogous to the classical Rayleigh quotient.

The Q quotient also shows stationarity for any trial vector $\boldsymbol{x}$ in the neighbourhood of a state-eigenvector $\boldsymbol{x}_m$. This is proved as follows. Regarding that $Q(\boldsymbol{x})$ is a functional one can compute its first variation δ, i.e.

$$\delta Q(\boldsymbol{x}) = \frac{\delta(\boldsymbol{x}^T\mathbf{B}\boldsymbol{x})\boldsymbol{x}^T\mathbf{A}\boldsymbol{x} - \delta(\boldsymbol{x}^T\mathbf{A}\boldsymbol{x})\boldsymbol{x}^T\mathbf{B}\boldsymbol{x}}{(\boldsymbol{x}^T\mathbf{A}\boldsymbol{x})^2} \tag{3.41}$$

where $\delta(\boldsymbol{x}^T\mathbf{B}\boldsymbol{x}) = 2\delta\boldsymbol{x}^T\mathbf{B}\boldsymbol{x}$ and $\delta(\boldsymbol{x}^T\mathbf{A}\boldsymbol{x}) = 2\delta\boldsymbol{x}^T\mathbf{A}\boldsymbol{x}$. The stationary points of $Q(\boldsymbol{x})$ are those that accomplish $\delta Q(\boldsymbol{x}) = 0$; and it turns out that this happens for $\delta Q(\boldsymbol{x})$ evaluated at the state-eigenvectors.

$$\delta Q(\boldsymbol{x})_{|\boldsymbol{x}=\boldsymbol{x}_m} = \frac{2\delta\boldsymbol{x}_m^T(\mathbf{B}\boldsymbol{x}_m - \lambda_m\mathbf{A}\boldsymbol{x}_m)}{(\boldsymbol{x}_m^T\mathbf{A}\boldsymbol{x}_m)^2} = 0 \tag{3.42}$$

Since the Q quotient is stationary around the state-eigenvectors, for an approximate state-eigenvector the quotient gives a better approximation of the corresponding eigenvalue than the present eigenvector approximation. Again, this property is in agreement with the stationarity of the classical Rayleigh quotient.

Therefore, the quotient proposed in equation 3.38 serves as a Rayleigh quotient for damped systems posed in the state-space. For its use as an eigenvalue approximation it does fulfill the properties that make the Rayleigh quotient relevant, namely, it is stationary in the neighbourhood of the eigenvectors and its value converges to the damped eigenvalues when meeting the true eigenvectors.

The quotient in physical coordinates

The proposed quotient may be transformed back from the state-space into physical coordinates as suggested in [68]. Since the state-eigenvectors are of the form $\boldsymbol{x}_m = \{\lambda_m\boldsymbol{\phi}_m^T, \boldsymbol{\phi}_m^T\}^T$, the trial state-vectors $\boldsymbol{x}$ may be restricted to be of the form $\boldsymbol{x} = \{\beta\boldsymbol{\phi}^T, \boldsymbol{\phi}^T\}^T$, so that they are defined by a trial pair $(\beta, \boldsymbol{\phi})$. Using this well-founded restriction, the Rayleigh quotient for damped systems is defined alternatively in terms of the system matrices and shape vectors in physical coordinates.

$$Q(\beta, \boldsymbol{\phi}) = Q(\beta, \boldsymbol{\phi}; \mathbf{M}, \mathbf{C}, \mathbf{K}) = \frac{\beta^2\boldsymbol{\phi}^T\mathbf{M}\boldsymbol{\phi} - \boldsymbol{\phi}^T\mathbf{K}\boldsymbol{\phi}}{2\beta\boldsymbol{\phi}^T\mathbf{M}\boldsymbol{\phi} + \boldsymbol{\phi}^T\mathbf{C}\boldsymbol{\phi}} \tag{3.43}$$

Obviously, this second definition possesses eigenvalue convergence and stationarity properties, i.e. $Q(\lambda_m, \boldsymbol{\phi}_m) = \lambda_m$ and $\delta Q(\beta, \boldsymbol{\phi})_{|\beta=\lambda_m,\, \boldsymbol{\phi}=\boldsymbol{\phi}_m} = 0$. The quotient in terms of the $(\beta, \boldsymbol{\phi})$ trial pair may be beneficial when it has to be computed intensively, since the size of the trial vectors is reduced to half the number of degrees of freedom in comparison to the state-space vectors. This would be the case for solution search algorithms such as the EVP iterative solvers.

Quotient bounds

So far, the $Q(\boldsymbol{x})$ quotient has been introduced as an alternative Rayleigh quotient for damped systems. It has been proved that damped eigenvalues may be approximated using this quotient. Yet, the accuracy of this approximation has not been assessed. Thence, it would be convenient to quantify the approximation error.

Previously in chapter 2, eigenvalue approximation error bounds have been presented in section 2.4.2. General error bounds for damped eigenvalues have proved to be of no practical use. On the contrary, it has been seen that the error committed by a Rayleigh quotient approximation of undamped eigenvalues is bounded by the Kato-Temple inequality. Here, we ask ourselves whether an analogous bound can be defined for the $Q(\boldsymbol{x})$ quotient approximation of damped eigenvalues.

The Kato-Temple theorem follows from Temple's inequality, whose derivation can be found in section B.4 of Appendix B. In turn, Temple's inequality follows from the orthogonality property of the Rayleigh quotient. Section E.3 in Appendix E shows that the residual vector $\mathbf{r}(\alpha, \boldsymbol{u})$ is orthogonal to the corresponding undamped trial eigenvector $\boldsymbol{u}$ when the trial eigenvalue α equals the Rayleigh quotient $R(\boldsymbol{u})$.

The orthogonality property implies that for two residual vectors $\mathbf{r}_a$ and $\mathbf{r}_b$ with trial eigenvalues a and b respectively it holds that

$$\langle \mathbf{r}_a, \mathbf{r}_b \rangle_{M^{-1}} = \mathbf{r}_b^T \mathbf{M}^{-1} \mathbf{r}_a = \|\mathbf{r}\|_{M^{-1}}^2 + (R(\boldsymbol{u}) - a)\,(R(\boldsymbol{u}) - b) \tag{3.44}$$

with $\mathbf{r} = \mathbf{r}(R(\boldsymbol{u}), \boldsymbol{u})$. Temple's theorem states that the $\langle \mathbf{r}_a, \mathbf{r}_b \rangle_{M^{-1}}$ product in equation 3.44 is positive valued for any interval (a, b) containing $R(u)$ but no exact eigenvalue. This conforms Temple's inequality, i.e.

$$\|\mathbf{r}\|_{M^{-1}}^2 \leq (R(\boldsymbol{u}) - a)\,(b - R(\boldsymbol{u})) \tag{3.45}$$

Similarly, for a damped trial eigenpair $\beta - \boldsymbol{x}$ a state-space residual vector $\mathbf{s}$ can be considered, that is

$$\mathbf{s} = (\mathbf{B} - \beta \mathbf{A})\, \boldsymbol{x} \tag{3.46}$$

Now, assume that β equals the $Q(\boldsymbol{x})$ quotient. In this case it does not hold that the residual vector $\mathbf{s}$ is orthogonal to the trial eigenvector $\boldsymbol{x}$, i.e. $\langle \mathbf{s}, \boldsymbol{x} \rangle \neq 0$. This is not the case because $Q(\boldsymbol{x})$ is defined mathematically as a quotient of two bilinear forms, as opposed to the classical Rayleigh quotient which is a quotient of two quadratics.

However, if a bilinear form B is defined such that $B(\mathbf{v}, \mathbf{w}) = \mathbf{w}^T\mathbf{v}$, and is applied to the $\mathbf{s}$ and $\boldsymbol{x}$ vectors

$$B(\mathbf{s}, \boldsymbol{x}) = B(\mathbf{B}\boldsymbol{x} - \beta\mathbf{A}\boldsymbol{x}, \boldsymbol{x}) = B_B(\boldsymbol{x}, \boldsymbol{x}) - \beta B_A(\boldsymbol{x}, \boldsymbol{x}) \tag{3.47}$$

one finds out that when $\beta = Q(\boldsymbol{x})$ the B form vanishes. That is, the state-space residual vector and trial eigenvector are orthogonal with respect to the B form when the trial eigenvalue is $\beta = Q(\boldsymbol{x})$.

Analogously to the undamped case (c.f. the Temple's inequality derivation in section B.4), the orthogonality property implies that for two residual vectors $\mathbf{s}_a$ and $\mathbf{s}_b$ with trial eigenvalues a and b respectively it holds that

$$B_{A^{-1}}(\mathbf{s}_a, \mathbf{s}_b) = \mathbf{s}_b^T\mathbf{A}^{-1}\mathbf{s}_a = B_{A^{-1}}(\mathbf{s}, \mathbf{s}) + (Q(\boldsymbol{x}) - a)(Q(\boldsymbol{x}) - b) \tag{3.48}$$

with $\mathbf{s} = \mathbf{s}(Q(\boldsymbol{x}), \boldsymbol{x})$. On the contrary, the spectral expansion of the expression in equation 3.48 reads

$$B_{A^{-1}}(\mathbf{s}_a, \mathbf{s}_b) = \sum_m c_m^2 (\lambda_m - a)(\lambda_m - b) \tag{3.49}$$

where c_m, λ_m, a and b are in general complex valued. Hence, it cannot be said that the form $B_{A^{-1}}(\mathbf{s}_a, \mathbf{s}_b)$ in equation 3.48 is positive valued for any restricted values of a and b. This gives no opportunity for a sort of Temple's inequality to exist in this case, and one might discard the idea of finding an specific error bound for the $Q(\boldsymbol{x})$ quotient.

Optimality of the quotient

The classical Rayleigh quotient is said to be optimal because it minimizes the M-inverse residual norm $\|\mathbf{r}\|_{M^{-1}}$ which guarantees the tightest possible eigenvalue error bound. In the previous section it can be observed that the $B_{A^{-1}}(\mathbf{s}, \mathbf{s})$ form in equation 3.48 plays an analogous role to the squared $\|\mathbf{r}\|_{M^{-1}}$ norm with respect to the classical Rayleigh quotient (see equation E.14).

In fact, as it is the case of the Rayleigh quotient with respect to the $\|\mathbf{r}\|_{M^{-1}}$ norm, the $Q(\boldsymbol{x})$ quotient does minimise the $B_{A^{-1}}(\mathbf{s}, \mathbf{s})$ form. As for the undamped case

(see section E.2), $B_{A^{-1}}(\mathbf{s},\mathbf{s})$ may be expanded as a function of the trial value β

$$B_{A^{-1}}(\mathbf{s},\mathbf{s}) = \beta^2 \boldsymbol{x}^T\mathbf{A}\boldsymbol{x} - 2\beta\boldsymbol{x}^T\mathbf{B}\boldsymbol{x} + \boldsymbol{x}^T\mathbf{B}\mathbf{A}^{-1}\mathbf{B}\boldsymbol{x} = f(\beta) \tag{3.50}$$

whose minimum is found by setting to zero its first derivative with respect to β

$$f'(\beta) = 2\beta\boldsymbol{x}^T\mathbf{A}\boldsymbol{x} - 2\boldsymbol{x}^T\mathbf{B}\boldsymbol{x} = 0 \tag{3.51}$$

which clearly corresponds to $\beta = Q(\boldsymbol{x})$.

However, the $B_{A^{-1}}(\mathbf{s},\mathbf{s})$ form does not appear in the error bounds formulations, nor it has been possible to establish analogous inequalities based on bilinear forms. Yet, it can be expressed in an inner product fashion as

$$B_{A^{-1}}(\mathbf{s},\mathbf{s}) = \mathbf{s}^T\mathbf{A}^{-1}\mathbf{s} = \langle \mathbf{A}^{-1}\mathbf{s}, \mathbf{s}^* \rangle \tag{3.52}$$

Then, making use of the Cauchy-Schwarz inequality (c.f. Appendix A.1), the $B_{A^{-1}}(\mathbf{s},\mathbf{s})$ form may be related to the residual norm $\|\boldsymbol{s}\|$ encountered in the Bauer-Fike error bound (c.f. equation 2.35), i.e.

$$|B_{A^{-1}}(\mathbf{s},\mathbf{s})| = \left|\langle \mathbf{A}^{-1}\mathbf{s}, \mathbf{s}^* \rangle\right| \leq \left\|\mathbf{A}^{-1}\boldsymbol{s}\right\| \|\boldsymbol{s}^*\| \leq \left\|\mathbf{A}^{-1}\right\| \|\mathbf{s}\|^2 \tag{3.53}$$

Equation 3.53 indicates that the lower the $B_{A^{-1}}(\mathbf{s},\mathbf{s})$ form is, the lower the $\|\boldsymbol{s}\|$ norm can potentially be. In other words, a small $B_{A^{-1}}(\mathbf{s},\mathbf{s})$ is a necessary condition for a small residual norm, although it is not a sufficient condition. Therefore, the minimum $B_{A^{-1}}(\mathbf{s},\mathbf{s})$ induced by the $Q(\boldsymbol{x})$ quotient may not yield a minimum $\|\boldsymbol{s}\|$. Nevertheless, the minimum for $\|\boldsymbol{s}\|$ shall correspond to a β value which may not be far from $Q(\boldsymbol{x})$ due to the necessary condition specified in equation 3.53. Thus, the $Q(\boldsymbol{x})$ quotient is the best guess (close to optimal) one can do for a damped trial eigenvalue in terms of the eigenvalue error bound.

3.4.4 Approximation of damped system eigenvalues

The Q quotient has been defined as a Rayleigh quotient equivalent for damped systems. Its stationarity and convergence towards the exact eigenvalues of the damped system have been proved in the previous section. Hence, in this work it is proposed to use such a Q quotient for the first time in the approximate reanalysis of damped vibrating systems.

Analogous to the approximation of undamped eigenvalues through the Rayleigh quotient described in section 3.4.2, when the system model parameters $\boldsymbol{\theta}$ vary, the

damped eigenvalues $\lambda_m(\boldsymbol{\theta})$ may be directly approximated with great accuracy by means of the Q quotient. The quotient has been defined for vectors and matrices in the state-space domain, i.e. $Q(\boldsymbol{x}; \mathbf{A}, \mathbf{B})$, but it may be also expressed in physical coordinates, i.e. $Q(\beta, \boldsymbol{\phi}; \mathbf{M}, \mathbf{C}, \mathbf{K})$.

In order to use the $Q(\boldsymbol{x})$ definition for approximating the system eigenvalues one needs to have beforehand a fair approximation to the corresponding state eigenvectors $\boldsymbol{x}_m(\boldsymbol{\theta})$. These may be obtained using the modal perturbation method if one uses the sensitivity function for state eigenvectors (equation D.9) that can be found in Appendix D. Alternatively, state eigenvectors may be approximated through linear interpolation in the same way that it is done for the mode shape vectors (c.f. equation 3.30). Then, accurate approximations for the damped eigenvalues $\tilde{\lambda}_m$ may be computed as

$$\tilde{\lambda}_m(\boldsymbol{\theta}) = Q(\tilde{\boldsymbol{x}}_m(\boldsymbol{\theta})) \tag{3.54}$$

with $\tilde{\boldsymbol{x}}_m$ the prior approximation for the state eigenvectors.

On the contrary, for using the $Q(\beta, \boldsymbol{\phi})$ counterpart one needs a priori fair approximations of both the damped eigenvalues and the damped eigenvectors. These may be obtained through the damped modes perturbation or interpolation methods described in this chapter. Then, a second more accurate eigenvalue approximation $\tilde{\lambda}_m$ may be computed as

$$\tilde{\lambda}_m(\boldsymbol{\theta}) = Q(\tilde{\lambda}_m(\boldsymbol{\theta}), \tilde{\boldsymbol{\phi}}_m(\boldsymbol{\theta})) \tag{3.55}$$

with $\tilde{\lambda}_m$ and $\tilde{\boldsymbol{\phi}}_m$ inside the quotient the prior approximations for the damped eigenvalues and eigenvectors respectively.

3.4.5 The cost of the quotient approximation

Approximating eigenvalues through the Rayleigh quotient or its damped equivalent, the Q quotient, involves the computation of the approximate eigenvectors to be quotient-evaluated, and the computation of the quotient itself. The cost for computing approximate eigenvectors has been already evaluated for the perturbation method in section 3.2.4, and for the interpolation method in section 3.3.4. Therefore, in this section focus will be taken mainly on the cost of computing the quotient.

The Rayleigh quotient involves the computation of two quadratics, i.e. $\boldsymbol{u}^T\mathbf{K}\boldsymbol{u}$ and $\boldsymbol{u}^T\mathbf{M}\boldsymbol{u}$. Each of them corresponds to a vector-sparse matrix-vector multiplication as the ones that have been described previously when analysing the computational

cost of the perturbation method (c.f. table 3.1). Due to the sparsity of the matrices of large dynamic systems, such operation shall be computed at a cost of $\mathcal{O}(N)$ floating point operations (flops), with N the order of the involved vectors and matrices which corresponds to the number of degrees of freedom of the system model.

The Q quotient involves the computation of bilinear forms which are essentially vector-sparse matrix-vector multiplications as well. For the quotient expressed in the state space domain $Q(\boldsymbol{x})$ two bilinear forms, $\boldsymbol{x}^T\mathbf{B}\boldsymbol{x}$ and $\boldsymbol{x}^T\mathbf{A}\boldsymbol{x}$, must be computed. The order of the state space matrices and vectors is $2N$. Thus, the computational complexity of the quotient evaluation scales as of $\mathcal{O}(4N)$ flops. On the contrary, the quotient expressed in physical coordinates $Q(\beta, \boldsymbol{\phi})$ involves three bilinear forms $\boldsymbol{\phi}^T\mathbf{K}\boldsymbol{\phi}$, $\boldsymbol{\phi}^T\mathbf{C}\boldsymbol{\phi}$ and $\boldsymbol{\phi}^T\mathbf{M}\boldsymbol{\phi}$, with N-sized matrices and vectors. Therefore, the associated computational complexity is proportional to $\mathcal{O}(N)$ flops instead.

Summarising, undamped eigenvalue approximation through the Rayleigh quotient involves the cost of computing approximate undamped eigenvectors plus the cost of evaluating the Rayleigh quotient. Damped eigenvalues approximation through the $Q(\boldsymbol{x})$ quotient involves the cost for computing approximate state eigenvectors plus the cost for evaluating the quotient. Also, damped eigenvalue approximation through the $Q(\beta, \boldsymbol{\phi})$ quotient involves the cost for computing approximate damped eigenvectors and damped eigenvalues plus the cost for evaluating the quotient. The associated computational complexity for the three cases is summarised in table 3.5. In all cases the computational cost is much lower (for large systems) than the cost of performing an entire EVP solution which scales as $\mathcal{O}(N^2)$ operations.

Prior approximation	Perturbation cost	Interpolation cost	Quotient	Complexity
$\tilde{\boldsymbol{u}}_m$	$n\ M\ \mathcal{O}(N)$	$2^n\ \mathcal{O}(N)$	$R(\boldsymbol{u})$	$\mathcal{O}(N)$
$\tilde{\boldsymbol{x}}_m$	$n\,2M\ \mathcal{O}(2N)$	$2^n\ \mathcal{O}(2N)$	$Q(\boldsymbol{x})$	$\mathcal{O}(2N)$
$\tilde{\boldsymbol{\phi}}_m$ / $\tilde{\lambda}_m$	$n\,2M\ \mathcal{O}(N)$ / $n\ \mathcal{O}(p)$	$2^n\ \mathcal{O}(N)$ / $\mathcal{O}(2^n)$	$Q(\beta, \boldsymbol{\phi})$	$\mathcal{O}(N)$

Table 3.5: The computational complexity of Rayleigh quotient eigenvalue approximation.

3.4.6 Numerical example

The same two degrees of freedom damped system that has been used in the numerical examples for the perturbation and interpolation methods is considered here again. In this case, the objective will be to obtain the damped system modes through quotient approximation for the same variations in the k_3 stiffness and the

c_3 damping parameters. That is, variations from -50% to +50% of their nominal values in steps of 10% variations.

Since the damped modes are to be computed, the Q quotient will be used for the approximation. Recall that the Rayleigh quotient only provides undamped eigenvalue solutions. In particular the $Q(\beta, \boldsymbol{\phi})$ form of the quotient is used here. On one hand, because of the more efficient computation with respect to the $Q(\boldsymbol{x})$ and, on the other hand, because the approximate damped solutions from the previous numerical examples are already available.

Hence, the approximate damped eigenvalues $\tilde{\lambda}_m^p$ and eigenvectors $\tilde{\boldsymbol{\phi}}_m^p$ obtained through damped modes perturbation in section 3.2.5 have been used to obtain approximate modal frequencies and modal damping through the Q quotient. Likewise, the approximate damped eigenvalues $\tilde{\lambda}_m^i$ and eigenvectors $\tilde{\boldsymbol{\phi}}_m^i$ obtained through damped modes interpolation in section 3.3.5 have also been used to approximate modal frequencies and modal damping using the Q quotient.

The exact and approximate modal solutions for the k_3 and c_3 variations are compared in figures 3.12 and 3.13. Figure 3.12 shows the variations in the modal frequencies induced by the k_3 stiffness variation (left) and the c_3 damping variation (right) respectively. Figure 3.13 shows the corresponding variation in the modal damping. In both figures, the top plots present the exact and approximate values of the modal frequencies and modal damping, and the bottom plots present the relative error of the approximate values with respect to the corresponding exact values.

The solid lines in figures 3.12 and 3.13 show the exact variation in modal frequencies and modal damping respectively. In the same figures, the dashed-circle lines show the results for the quotient evaluated at the interpolation approximated eigensolutions, and the dotted-cross lines show the results for the quotient evaluated at the perturbation approximation eigensolutions. Yet, the exact and approximate f_m and ζ_m curves are barely distinguished by naked eye since they almost overlap.

As can be observed in the error curves of figures 3.12 and 3.13, the quotient results obtained from the interpolation approximate modes show the interpolation method error characteristic, that is, zero error at the interval extremes and maximum error in the central range of the interval. Conversely, the quotient results obtained from the perturbed approximate modes show the perturbation method error characteristic, namely zero error over the broad mid-range parameters solution and maximum error at the interval extremes. Yet, the quotient approximation error is remarkably

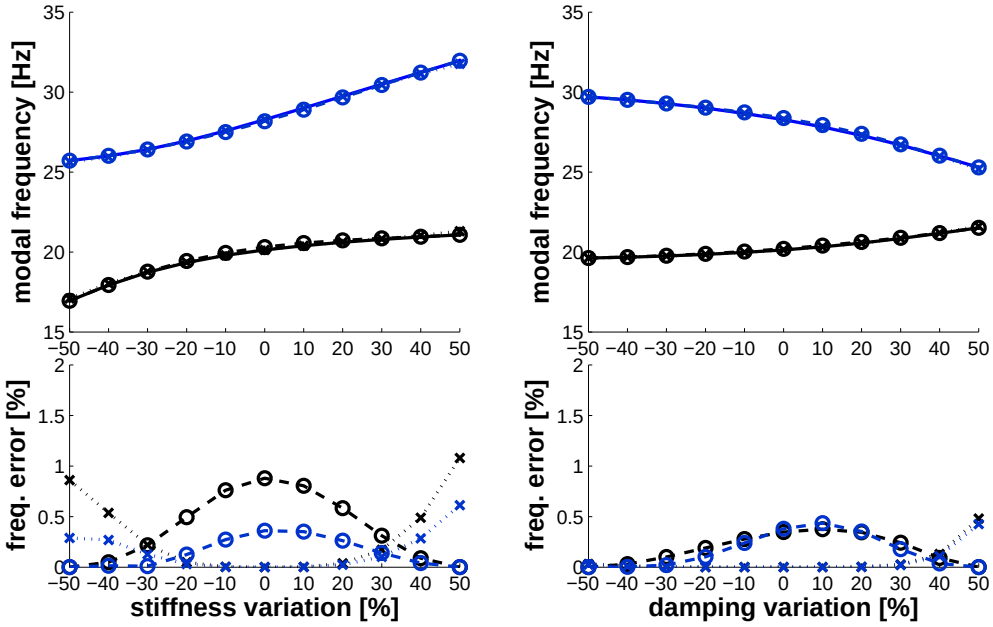

Figure 3.12: Variation and error in modal frequency with respect to k_3 and c_3 variations:
1st mode: — exact $-\circ-$ $Q(\tilde{\lambda}_m^i, \tilde{\phi}_m^i)$ $\cdot\cdot\times\cdot\cdot$ $Q(\tilde{\lambda}_m^p, \tilde{\phi}_m^p)$
2nd mode: — exact $-\circ-$ $Q(\tilde{\lambda}_m^i, \tilde{\phi}_m^i)$ $\cdot\cdot\times\cdot\cdot$ $Q(\tilde{\lambda}_m^p, \tilde{\phi}_m^p)$

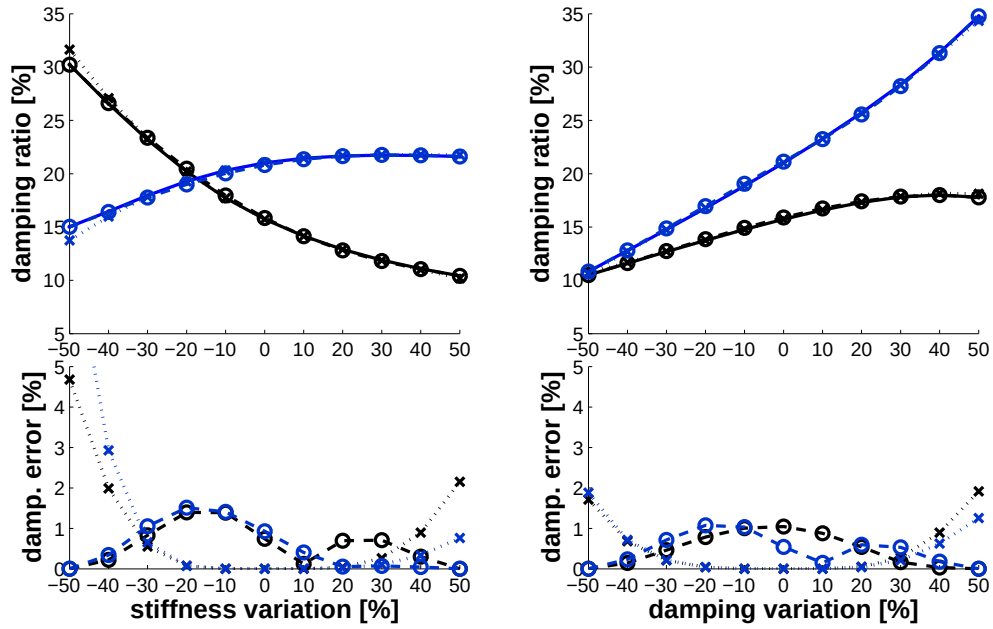

Figure 3.13: Variation and error in modal damping with respect to k_3 and c_3 variations:
1st mode: — exact $-\circ-$ $Q(\tilde{\lambda}_m^i, \tilde{\phi}_m^i)$ $\cdot\cdot\times\cdot\cdot$ $Q(\tilde{\lambda}_m^p, \tilde{\phi}_m^p)$
2nd mode: — exact $-\circ-$ $Q(\tilde{\lambda}_m^i, \tilde{\phi}_m^i)$ $\cdot\cdot\times\cdot\cdot$ $Q(\tilde{\lambda}_m^p, \tilde{\phi}_m^p)$

smaller than the error of the prior approximate eigenvalues.

The Q quotient approximation obtains modal frequencies with error under 1% for the full variation range of k_3 and error under 0.5% for the full variation range of c_3, as can be appreciated in figure 3.12. The modal frequency errors were under 6% and under 3% for k_3 and c_3 variations respectively when using perturbation or interpolation method as can be recalled from figure 3.14. These are six times more accurate results.

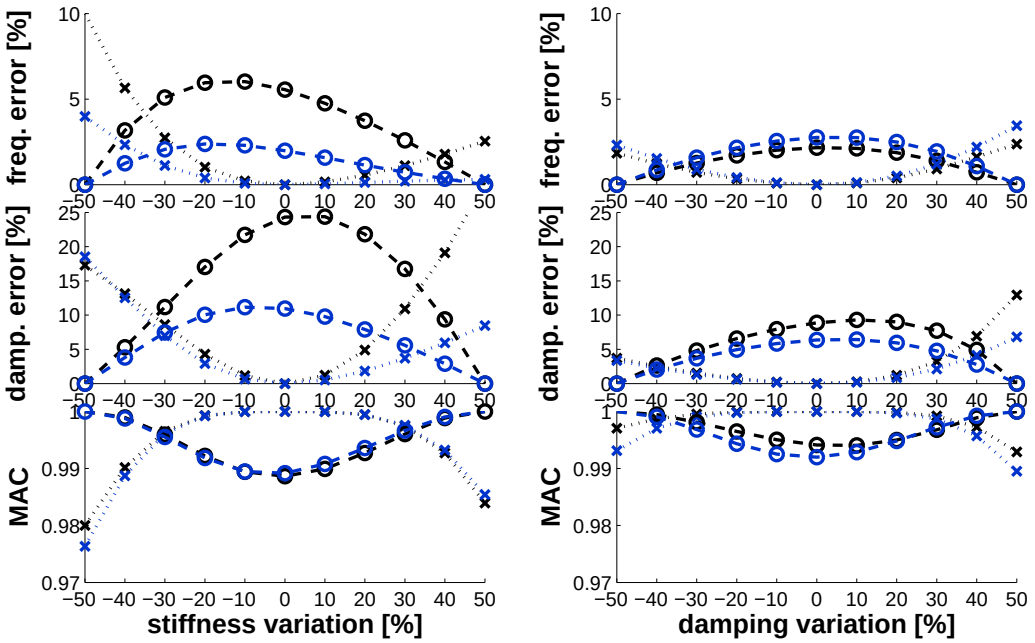

Figure 3.14: Error and MAC values for the prior approximate eigensolutions:
1st mode: — ○ — damped interpolation · · × · · damped perturbation
2nd mode: — ○ — damped interpolation · · × · · damped perturbation

As can be observed in figure 3.13, the $Q(\tilde{\lambda}_m^i, \tilde{\phi}_m^i)$ approximation obtains modal damping with error under 2% for the full variation range of k_3 and c_3. This is a great improvement in accuracy in contrast with the modal damping error obtained through the interpolation method. For k_3 variations the interpolated modal damping error was as high as 25% (see damping error in figure 3.14). This supposes a ten times reduction in the approximation error when using the Q quotient approximation.

Also in figure 3.13, it can be observed that the $Q(\tilde{\lambda}_m^p, \tilde{\phi}_m^p)$ approximation results in modal damping with approximation error below 2% for most of the variation range in k_3 and the full variation range in c_3. Only in the lowest values of k_3 does it get around 5% modal damping error. Notice that this corresponds to the

"worse" values fpr the approximate to exact mode shapes MAC (see MAC values in figure 3.14). In any case, these error values are much lower than the error in modal damping obtained through the perturbation method. As can be observed in figure 3.14, these were over 25% error for stiffness variation and over 10% for damping variation. Again this results in a ten times reduction in the approximation error when using the Q quotient approximation in most of the variation range.

3.5 Conclusions

In this chapter several methods have been presented for reanalysing the dynamics of damped vibrating systems when these are subject to structural variations. These methods are aimed at reducing the computational cost of the reanalyses, since the computational cost might be prohibitive for very large system models. However, approximation error is the price to pay for obtaining efficient methods.

The focus has been placed on methods that linearly approximate the variations in dynamic behaviour of a damped system, namely, the perturbation method and the interpolation method. Linear approximations have the advantage that they are the simplest mathematical approximations one can use and consequently the ones that can be computed at a lower cost. However, they incur large error whenever the variation curve being approximated possesses a non-linear characteristic. In structural dynamics, the relation between the parameters that define the system model and the quantities that characterise its dynamic behaviour is typically non-linear. For this reason, the validity of the linear reanalysis methods is in general restricted to small variations in the parameters.

The first thing that has been analysed in this chapter is the rate of change of the quantities that characterise the dynamics of a system. The dynamic response of a system may be evaluated through its time or frequency response. Yet, these response functions are highly non-linear so that only incredibly narrow variations in the model parameters might be reanalysed through linear methods. In particular, for the frequency response functions, linearly approximating the response variation in the vicinity of resonance peaks yields completely erroneous predictions. On the contrary, the dynamic response of a system may be characterised alternatively by its modal parameters, i.e. modal frequencies, modal damping and mode shapes. Although the rate of change of the modal parameters is also non-linear, the variation in modal parameters is quite smooth, so that linearly approximating them is a much more reasonable option. Thus, the perturbation and the interpolation methods are

applied here to the modal parameters.

In fact, the modal perturbation and interpolation methods compute approximations to the eigensolutions of the EVP corresponding to the equations of motion of the varying system. If the undamped EVP is considered, approximate undamped eigensolutions are obtained, and the damped system modes must be obtained through further small damping approximation. Undamped eigenvalues computations is a rather standard way of proceeding when computing damped system modes in finite element analysis. However, for approximate reanalysis methods, undamped eigensolution approximations yield quite poor accuracy in damped modal solutions as has been proved in this chapter's numerical examples. On the contrary, damped eigensolution linear approximations show much fairer accuracy to the actual (damped) modal parameters. Therefore, in this work it is chosen to proceed with the less-conventional linear approximations of the complex valued eigensolutions arising in the quadratic EVP, or the equivalent state-space EVP.

With regard to the reanalysis efficiency, the computational cost of each of the modal approximate reanalysis methods has been evaluated analytically. In both cases, the cost for computing the approximate eigenvalues is much smaller than the cost of computing the approximate eigenvectors. Hence the efficiency of the methods is mainly determined by the complexity of the eigenvectors computation. The eigenvector approximations involve computations whose computational cost is of the order of the total number of degrees of freedom N which, for very large system models, may be a very large number. Nevertheless, the exact solution of an eigenvalue problem involves a cost of the order of N^2 operations. Thus, the approximate methods are way more efficient than exact reanalysis in any case.

Together with linear eigensolution approximations, the use of the Rayleigh quotient has been proposed in order to further improve the accuracy of the reanalyses. Improving the eigenvalues accuracy implies that the approximation methods may be used for much wider ranges of variation in the model parameters. The Rayleigh quotient performs a non-linear eigenvalue approximation, which means that its computational cost for computing the eigenvalues exceeds that of the linear approximate reanalysis methods. Yet, the cost for evaluating the Rayleigh quotient is also of the order of N, so that it does not exceed the cost for linearly approximating the eigenvectors through perturbation or interpolation method. Therefore, performing the Rayleigh quotient approximation does not introduce much extra cost in a reanalysis where the mode shapes are also approximated. However, the Rayleigh quotient approximation is only applicable to undamped eigenvalues.

Damped eigenvalues cannot be approximated through the Rayleigh quotient as has been proved in section 3.4.3. For this reason it is proposed here to use an alternative ad-hoc quotient that serves as a damped eigenvalues approximation, equivalent to the Rayleigh quotient approximation. This quotient was first defined by Bhaskar in [68] and here it is referred to as the Q quotient. Its use as damped eigenvalues approximation for eigensolution reanalysis is original to this work.

It has been shown in this chapter that the Q quotient upholds the properties of the Rayleigh quotient that qualifies it as an eigenvalue approximant, i.e. convergence and stationarity. Yet, it has also been proved that, unlike the Rayleigh quotient, error bounds for the Q quotient may not be formulated. Nonetheless, it has been justified analytically that this quotient approximation is close to optimal in an eigenvalue error bound sense, and this argument has been corroborated by the accurate results obtained in the numerical example.

Finally, recall that the approximate methods described in this chapter are intended to be used in processes such as uncertainty analysis or model optimisation. The claimed efficiency of these methods might not be sufficiently high for such processes that require very intensive reanalysis calculations. Thence, there is the need to explore ways to increase the efficiency of the methods. Noticing that the efficiency of linear approximation methods and quotient approximations is limited by the number of degrees of freedom of the model to reanalyse, a logical option is to explore the use of these methods on smaller models.

A finite element model may be reduced into a dynamic equivalent model with reduced number of degrees of freedom by means of model order reduction and substructuring techniques. Hence, model reduction methods for damped systems are presented in the next chapter, and the use of approximate reanalysis methods described here will be applied in the reduced models which will be developed in the following chapters.

Chapter 4

Component Mode Synthesis for damped dynamic systems

When designing engineering structures, the dynamics of vibrating systems may be assessed at an early design stage through numerical computations. At low frequencies, this may be typically done through finite element analysis (FEA) provided that a finite element (FE) model for the structure is created.

The computational cost for performing finite element analyses is always dependent on the size of the model generated. As the frequency range at which one aims at conducting a vibration analysis increases, more and more degrees of freedom are needed in the FE model in order to obtain accurate analysis results. That is, the FE model becomes larger.

For large engineering structures, very large FE models are needed for the analyses, especially as the target frequencies approach the mid-frequency range. In order to handle FEA of such large models one often attempts to circumvent the direct analysis of the full FE model. Otherwise, the computational cost will be prohibitive.

One possible way of reducing the computational cost of a FEA is to follow a substructuring strategy. One may chose to split a structure model into smaller substructures and conduct the FEA of each substructure separately. Then, the full structure dynamics are resolved by consistently coupling the dynamics of each of the substructures.

Another possible way of handling the FEA of very large models is to devise a dynamic equivalent FE model with a much reduced number of degrees of freedom. This may be done through model order reduction methods. For large built-up

structures Component Mode Synthesis may be used for reducing the order of the corresponding finite element model.

Component Mode Synthesis (CMS) combines model substructuring and model order reduction methods. In CMS, the FE model of the structure is split into several smaller FE models corresponding to the structure subsystems. These are referred to as the system *components*. Then, the modes of each component are computed when the components are uncoupled. In this way, the component models are reduced by transformation into the component modal coordinate space. Next, the reduced component models are coupled together. This gives a reduced model of the full system in terms of the modes of the different subsystems. Thus, this reduced CMS model can be used for the FEA of the original system and, also, for the solution reanalysis using approximate methods.

In the previous chapter, approximate reanalysis methods for the modal analysis of (large) damped systems have been explored. It has been seen that these approximate methods are very efficient in comparison with computing the exact modal solution from an FE model (typically by solving a corresponding eigenvalue problem). However, for processes that require intense reanalyses (e.g. model optimization, uncertainty analysis...) it would be desirable to further increase their efficiency. As it has been already pointed out, this may be possible if the approximate reanalyses are performed on reduced order models.

Keeping in mind that in this thesis efficient reanalysis methods are to be developed, Component Mode Synthesis offers a very convenient framework for reducing large system models that are to be intensively reanalysed through approximate reanalysis methods. There exist many methods for performing Component Mode Synthesis and these are generally based on undamped component modes. Yet, considering that in chapter 3 emphasis has been placed on the reanalysis methods for damped systems, CMS methods based on damped component modes are regarded here.

Having said that, this chapter addresses model order reduction methods as well as substructuring methods, and focuses particularly on the description of Component Mode Synthesis. The main purpose is to give a comprehensive background in order to introduce CMS methods for damped systems. These CMS methods based on damped component modes are very rare, and typically are not found in commercial software.

In this chapter the use of Component Mode Synthesis for locally or heavily damped structures is recalled. CMS methods based on damped component modes are re-

visited and studied through numerical examples. Further, the use of CMS reduced models in conjunction with approximate reanalysis methods is addressed in the following chapters.

4.1 Model order reduction methods

A reduced order model is a projection of a full model into a coordinate space with fewer degrees of freedom. The reduced model is therefore an approximation of the full model. Reduction methods imply a loss of information but, if the truncated information is unimportant or redundant, the dynamics of the reduced model are a very good approximation for the full model dynamics. Thus, a model reduction method aims at achieving the maximum accuracy possible with a minimum order of the reduced model.

Several reduction methods exist depending on the basis used for the reduction of the model. In Component Mode Synthesis it is common to use reduction methods based on Ritz vectors. These may be modal truncation methods [46, 77–79] and condensation methods [80–83]. There exist other reduction methods which are not based on Ritz vectors (e.g. Krylov Subspace Method [84], Padé approximations [85, 86], Balancing-related truncation techniques [87],...). However, these latter approaches are less frequently used in Component Mode Synthesis, and are not required for the component reduction through damped component modes. Therefore, a brief overview of reduction methods based on Ritz vectors only is given in the following.

Consider the finite element model of a dynamic system defined by its equations of motion, that is

$$\mathbf{D}\mathbf{u} = \mathbf{f} \tag{4.1}$$

with $\mathbf{D} = \mathbf{M}\frac{\partial^2}{\partial t^2} + \mathbf{C}\frac{\partial}{\partial t} + \mathbf{K}$ the dynamic stiffness matrix. Typically, model order reduction methods are Rayleigh-Ritz methods in which the full model coordinate space $\mathbf{u}$ is transformed into a new coordinate space spanned by *Ritz vectors*. The full set of Ritz vectors is an orthogonal basis that defines a coordinate space $\mathbf{v}$ of the same order as $\mathbf{u}$. The relation between the two sets of coordinates is given by the coordinate transformation matrix $\mathbf{T}^v$

$$\mathbf{u} = \mathbf{T}^v\mathbf{v} \tag{4.2}$$

where the transformation matrix columns are the Ritz vectors. In equation 4.2, the $\mathbf{T}^v$ matrix has as many columns as the number of DOFs in $\mathbf{u}$. If only a subset of

Ritz vectors is considered, a reduced coordinate space $\mathbf{w}$ can be defined, so that the full model coordinate space may be approximated by a linear combination of these vectors.

$$\mathbf{u} \approx \mathbf{T}^w \mathbf{w} \tag{4.3}$$

with $\mathbf{T}^w$ the transformation matrix associated to $\mathbf{w}$. Candidate Ritz vectors to use in a reduced basis should contain the maximum amount of relevant information for the scope of the analysis.

Then, the equations of motion of the full system may be transformed into a reduced set of equations of motion by means of the $\mathbf{T}^w$ matrix, that is

$$\mathbf{D}^w \mathbf{w} = \mathbf{f}^w \tag{4.4}$$

with $\mathbf{D}^w = \mathbf{T}^{wT} \mathbf{D} \mathbf{T}^w$ and $\mathbf{f}^w = \mathbf{T}^{wT} \mathbf{f}$. The solution of the reduced model may be transformed back into the full model coordinates by means of equation 4.3. The accuracy of the full solution will depend on the chosen reduced basis.

4.1.1 Modal Reduction

Rayleigh-Ritz methods are in fact a generalisation of the Rayleigh method for modal analysis. It can be observed that the coordinate transformation in equation 4.2 is analogous to the modal coordinates transformation in modal analysis

$$\mathbf{u} = \mathbf{\Phi} \mathbf{p} \tag{4.5}$$

with $\mathbf{\Phi}$ the modal transformation matrix and $\mathbf{p}$ the modal coordinates. Therefore, mode shape vectors are appropriate vectors to use as candidate Ritz vectors.

Accordingly, one of the methods for reduction of the model order is the modal transformation using a reduced set of modes. This is known as *modal reduction*. The modes of vibration contribute significantly to the system response in the vicinity of their corresponding modal frequency, and their contribution vanishes far away from it. Since a dynamic analysis is typically aimed at a confined frequency range, the response of the system can be approximated by the weighted sum of those modes that contribute significantly in this frequency range. These modes are kept for the modal transformation, while the rest of the modes are not included, that is, truncated or removed.

Generally, truncated modes are termed *higher order* modes because the kept modes include all low frequency modes up to the truncation limit frequency. Hence, the

modal transformation matrix $\mathbf{\Phi}$ can be split into the kept modes partition $\mathbf{\Phi}_k$ and the higher order modes partition $\mathbf{\Phi}_h$. Thus, the full model coordinates $\mathbf{u}$ can be approximated by the transformation into the reduced modal coordinate space $\mathbf{p}_k$.

$$\mathbf{u} \approx \mathbf{\Phi}_k \mathbf{p}_k \tag{4.6}$$

The process of mode truncation inevitably introduces error in the predicted response. Generally, the accuracy obtained for the displacement response is satisfactory including only the modes with lowest modal frequency [88] (e.g. up to one and a half times the maximum frequency of the analysis). However, the higher modes may have significant influence in the internal forces and stresses related to local effects. A greater number of modes must be included in order to have the same accuracy for the forces and stresses [77].

Residual flexibility correction

The modal reduction method can be enhanced using corrections accounting for the static effects of the truncated modes. This is known generically as the Modal Acceleration Method (MAM) [89]. Several versions of the MAM exist in the literature [77–79] with the *residual flexibility* method being the simpler and more widespread.

In the residual flexibility method the static equations of motion $\mathbf{Ku} = \mathbf{f}$ are considered. The solution to the static equations of motion may be expressed in terms of the flexibility matrix $\mathbf{G} = \mathbf{K}^{-1}$, that is

$$\mathbf{u} = \mathbf{Gf} \tag{4.7}$$

It can be proved[1] that the flexibility matrix $\mathbf{G}$ of a dynamic system can be expressed in terms of the modal parameters as

$$\mathbf{G} = \mathbf{\Phi}\mathbf{\Lambda}^{-1}\mathbf{\Phi}^T \tag{4.8}$$

Hence, by splitting the modes into kept and higher order modes one may decompose the flexibility matrix as the sum of the kept modes flexibility matrix $\mathbf{G}^k = \mathbf{\Phi}_k\mathbf{\Lambda}_k^{-1}\mathbf{\Phi}_k^T$ plus the *residual flexibility matrix* $\mathbf{G}^h = \mathbf{\Phi}_h\mathbf{\Lambda}_h^{-1}\mathbf{\Phi}_h^T$ corresponding to the higher

[1] Consider the modal transformation matrix $\mathbf{\Phi} = \mathbf{U}$ of an undamped system, where $\mathbf{U}$ is the full set of undamped eigenvectors $\boldsymbol{u}_m$. The flexibility matrix $\mathbf{G} = \mathbf{K}^{-1}$ of a dynamic system may be expressed in modal form by pre and post multiplying the inverse of the stiffness matrix with the identity $\mathbf{\Phi}\mathbf{\Phi}^{-1} = \mathbf{I}$, i.e. $\mathbf{G} = (\mathbf{\Phi}\mathbf{\Phi}^{-1})\mathbf{K}^{-1}(\mathbf{\Phi}\mathbf{\Phi}^{-1})^T = \mathbf{\Phi}\mathbf{\Lambda}^{-1}\mathbf{\Phi}^T$

order modes. In practical situations the residual flexibility matrix $\mathbf{G}^h$ is obtained as the flexibility matrix in which the contribution of the kept modes is subtracted.

$$\mathbf{G}^h = \mathbf{G} - \mathbf{\Phi}_k \mathbf{\Lambda}_k^{-1} \mathbf{\Phi}_k^T \tag{4.9}$$

In this way, the static solution may be decomposed into the kept modes static contribution $\mathbf{G}^k\mathbf{f}$ and the truncated modes static contribution $\mathbf{G}^h\mathbf{f}$.

$$\mathbf{u} = \mathbf{G}^k\mathbf{f} + \mathbf{G}^h\mathbf{f} \tag{4.10}$$

Therefore, a modal transformation may be enriched with the static contribution of the truncated modes, i.e.

$$\mathbf{u} \approx \mathbf{\Phi}_k\mathbf{p}_k + \mathbf{G}^h\mathbf{f} \tag{4.11}$$

In this way, exact static responses are ensured along with more accurate dynamic responses. The error in the modal reduction transformation is minimised through the static correction provided by the residual flexibility matrix.

Inertia-relief projection

When a component has rigid body freedoms - i.e. it is not fully constrained - the stiffness matrix is singular and therefore it cannot be inverted. Instead, the flexibility matrix may be computed in an alternative way.

Assuming there are N_r rigid body modes, the component may be *temporarily restrained* at a set r of degrees of freedom to avoid rigid body motion. The stiffness matrix for the remaining *unrestrained* degrees of freedom u can be then inverted. A pseudo-flexibility matrix $\mathbf{G}'$ is assembled by inserting zeros in the rows and columns for the temporary restrained degrees of freedom.

$$\mathbf{G}' = \begin{bmatrix} \mathbf{K}_{uu}^{-1} & \mathbf{0}_{ur} \\ \mathbf{0}_{ru} & \mathbf{0}_{rr} \end{bmatrix} \tag{4.12}$$

The flexibility matrix $\mathbf{G}'$ is singular and it has the same rank as the unconstrained stiffness matrix. This means that it describes both the elastic and rigid body behaviour of the component. In [90] the inertia-relief loading matrix $\mathbf{P}$ was introduced to filter out the rigid body characteristic of the flexibility matrix as

$$\mathbf{P} = \mathbf{I} - \mathbf{M}\mathbf{\Phi}_r\mathbf{\Phi}_r^T \tag{4.13}$$

where $\mathbf{\Phi}_r$ is the (mass-normalised) rigid body modes' partition of the modal transformation matrix. The rigid body modes $\boldsymbol{\phi}_r$ are those modes that are solution to the static equation $\mathbf{K}\boldsymbol{\phi}_r = \mathbf{0}$.

It can be proved that an *elastic* flexibility matrix $\mathbf{G}^e$ may be obtained by pre and post multiplying the flexibility matrix $\mathbf{G}'$ with the projector $\mathbf{P}$. The same $\mathbf{G}^e$ matrix is obtained regardless of which degrees of freedom r have been chosen to be temporarily restrained.

$$\mathbf{G}^e = \mathbf{P}^T \mathbf{G}' \mathbf{P} \tag{4.14}$$

4.1.2 Condensation methods

Other kinds of reduction methods based on Ritz vectors are the *condensation* methods. In condensation methods the reduced coordinate space $\mathbf{w}$ is a subset of the physical coordinates $\mathbf{u}$. Condensation methods split the physical coordinates into *master* $\mathbf{u}_M$ and *slave* $\mathbf{u}_S$ degrees of freedom and uses the master DOFs as the reduced coordinates

$$\mathbf{u} \approx \mathbf{T}^M \mathbf{u}_M = \begin{bmatrix} \mathbf{I}_{MM} \\ \mathbf{T}_{SM} \end{bmatrix} \mathbf{u}_M \tag{4.15}$$

with $\mathbf{I}_{MM}$ an identity matrix of rank equal to the number of master DOFs, and $\mathbf{T}_{SM}$ a transformation matrix relating the slave DOFs to the master DOFs.

Static reduction

The Guyan reduction method [80] was the first condensation method to appear. This reduction method was developed for the analysis of the static response. The static equations of motion may be arranged in terms of the master and slave degrees of freedom, i.e.

$$\begin{bmatrix} \mathbf{K}_{MM} & \mathbf{K}_{MS} \\ \mathbf{K}_{SM} & \mathbf{K}_{SS} \end{bmatrix} \begin{bmatrix} \mathbf{u}_M \\ \mathbf{u}_S \end{bmatrix} = \begin{bmatrix} \mathbf{f}_M \\ \mathbf{f}_S \end{bmatrix} \tag{4.16}$$

If one considers the slave DOFs to be unforced, that is $\mathbf{f}_S = \mathbf{0}_S$, the lower row in equation 4.16 reads

$$\mathbf{K}_{SM}\mathbf{u}_M + \mathbf{K}_{SS}\mathbf{u}_S = \mathbf{0}_S \tag{4.17}$$

so that the response at the slave DOFs may be expressed as a linear combination of the master DOFs response. A static transformation matrix relating the master and the slave DOFs is computed from the homogeneous static equations of motion.

$$\mathbf{T}_{SM} = -\mathbf{K}_{SS}^{-1}\mathbf{K}_{SM} \tag{4.18}$$

By solving the statically condensed equations of motion the exact static response at the master DOFs is found, and the static response at the slave DOFs is approximated through the $\mathbf{T}_{SM}$ matrix.

Dynamic reduction

The condensation method was later extended for dynamic analysis [81]. A dynamic transformation matrix relating master and slave DOFs can be computed for a fixed value of frequency.

If one considers harmonic vibration, the equations of motion in equation 4.1 may be expressed in terms of the the dynamic stiffness matrix

$$\mathbf{D}(\omega) = -\omega^2\mathbf{M} + \omega\mathbf{C} + \mathbf{K} \tag{4.19}$$

Thence, the dynamic stiffness matrix at a certain fixed frequency ω_0 may be regarded as a static stiffness matrix. Therefore, pseudo-static equations of motion may be formulated for the $\mathbf{D}(\omega_0)$ matrix as in Guyan's method.

Proceeding in this way, a dynamic condensation matrix may be obtained from the homogeneous dynamic equations of motion corresponding to the unforced slave DOFs

$$\mathbf{T}_{SM} = -\mathbf{D}_{SS}^{-1}\mathbf{D}_{SM} \tag{4.20}$$

The dynamic response of the reduced model is computed exactly at the master DOFs. The response in the slave DOFs is approximated through multiplication of this matrix with the response in the master DOFs. The error in the approximation increases as the analysis frequencies move away from the fixed frequency chosen to create the transformation matrix. It can be noticed that Guyan's original static reduction method is the specific case when the fixed frequency is chosen to be zero.

IRS and SEREP methods

Improved condensation methods were developed by O'Callahan et al. for analysis of dynamic systems. The Improved Reduction System (IRS) method [82] is an extension to the Guyan method to increase its accuracy when used for dynamic analysis. IRS adds some adjustment terms to the Guyan transformation matrix in equation 4.18 to account for inertial effects of the slave DOFs, increasing the accuracy for the higher order modes.

The System Equivalent Reduction-Expansion Process (SEREP) method [83] uses the modes of the full order system to compute a transformation matrix relating the master and the slave DOFs.

$$\mathbf{T}_{SM} = \mathbf{\Phi}_{Sk}\mathbf{\Phi}_{Mk}^{-1} \tag{4.21}$$

As many modes $\boldsymbol{\phi}_k$ as master DOFs $\mathbf{u}_M$ are required for inverting $\boldsymbol{\Phi}_{Mk}^{-1}$. Therefore, the SEREP transformation may be computationally expensive to produce. On the other hand, the eigensolution of the reduced system is exact and the SEREP transformation gives great accuracy for the slave DOFs response.

4.2 Substructuring and coupling of models

Dynamic systems are usually built-up structures consisting of several coupled substructures. Hence, a finite element model of a dynamic system may be is split into N_s submodels corresponding to each of the substructures. The submodels may be treated as independent models which are connected to one or more adjacent substructures by redundant interfaces. For a substructure $s \in \{1, N_s\}$ the equations of motion in physical coordinates $\mathbf{u}$ read

$$\mathbf{D}_s \mathbf{u}_s = \mathbf{f}_s \tag{4.22}$$

with $\mathbf{D}_s = \mathbf{M}_s \frac{\partial^2}{\partial t^2} + \mathbf{C}_s \frac{\partial}{\partial t} + \mathbf{K}_s$ the subsystem matrices, $\mathbf{u}_s$ the substructure's displacement vector and $\mathbf{f}_s$ the vector of external forces in physical coordinates. The physical degrees of freedom consist of the FE-nodal displacements and rotations in the considered dimensions, i.e. x, y, z, θ_x, θ_y and/or θ_z.

In each substructure the degrees of freedom may be split into two subsets. On one hand, those degrees of freedom corresponding to nodes located at the coupling interface with other substructures. On the other hand, those degrees of freedom of the substructure that do not correspond to the coupling interface nodes. The former are termed *coupling* degrees of freedom $\mathbf{u}_{c,s}$ and the later are termed *interior* degrees of freedom $\mathbf{u}_{i,s}$. The substructure equations of motion may be rearranged according to this nomenclature, that is

$$\begin{bmatrix} \mathbf{D}_{ii} & \mathbf{D}_{ic} \\ \mathbf{D}_{ci} & \mathbf{D}_{cc} \end{bmatrix}_s \begin{Bmatrix} \mathbf{u}_i \\ \mathbf{u}_c \end{Bmatrix}_s = \begin{Bmatrix} \mathbf{f}_i \\ \mathbf{f}_c \end{Bmatrix}_s \tag{4.23}$$

.

When the substructures are assembled together, the equations of motion for the full structure may be obtained by coupling of the equations of motion for each of the substructures. The substructure coupling is performed by applying coupling constraints into the equations. Namely, the constraints for coupling the models are displacement continuity and force equilibrium at the coupling interface nodes.

Displacement continuity implies equal displacement at coupling interfaces DOFs of two adjacent substructures α and β, i.e.

$$\mathbf{u}_{c,\alpha} = \mathbf{u}_{c,\beta} \tag{4.24}$$

Force equilibrium implies that the internal forces that the two adjacent substructures exert on each other at the coupling interfaces are mutually reactive, so that the internal forces balance at the coupling interfaces, that is

$$\mathbf{f}^{\text{int}}_{c,\alpha} + \mathbf{f}^{\text{int}}_{c,\beta} = \mathbf{0} \tag{4.25}$$

Now, the substruture's displacements may be merged together into a generalised coordinates displacement vector $\mathbf{s}$, and the substructures matrices and forces may be merged accordingly, i.e.

$$\mathbf{s} = \begin{Bmatrix} \mathbf{u}_1 \\ \vdots \\ \mathbf{u}_{N_s} \end{Bmatrix} \qquad \mathbf{D}^s = \begin{bmatrix} \mathbf{D}_1 & \mathbf{0} & \mathbf{0} \\ \mathbf{0} & \ddots & \mathbf{0} \\ \mathbf{0} & \mathbf{0} & \mathbf{D}_{N_s} \end{bmatrix} \qquad \mathbf{f}^s = \begin{Bmatrix} \mathbf{f}_1 \\ \vdots \\ \mathbf{f}_{N_s} \end{Bmatrix} \tag{4.26}$$

Notice, however, that the generalised displacements $\mathbf{s}$ contains redundant coupling interface DOFs, so that it is not equivalent to the physical displacements $\mathbf{u}$ of the full system.

Thence, the displacement continuity constraint can be put into a matrix form in generalised coordinates as

$$\boldsymbol{\mathcal{C}}\mathbf{s} = \mathbf{0} \tag{4.27}$$

where $\boldsymbol{\mathcal{C}}$ is the coupling matrix. For instance, for a two coupled substructures system the coupling matrix would read $\boldsymbol{\mathcal{C}} = \begin{bmatrix} \mathbf{0}_{ci,1} & \mathbf{I}_{cc,1} & \mathbf{0}_{ci,2} & -\mathbf{I}_{cc,2} \end{bmatrix}$.

The coupled system equations of motion may be formulated in generalised coordinates by application of Lagrange's equation as it is done in Lagrangian mechanics (e.g. see section 7.4 in reference [52]), i.e.

$$\mathbf{D}^s\mathbf{s} = \mathbf{f}^s + \lambda\boldsymbol{\mathcal{C}} \tag{4.28}$$

with λ the Lagrange multipliers. The coupling internal forces are conservative forces and therefore they cancel out in the Lagrangian expression. However, it is more convenient to formulate the coupled equations of motion in the full system's physical coordinates.

Due to the constraint equation (equation 4.27) the generalised coordinates s are not linearly independent. The coupling generalised coordinate set s_c contains redundant

degrees of freedom so that half of the set is dependent on the redundant counterpart. Therefore, the generalised displacements may be split into a dependent d and a linearly independent l coordinates sets, i.e.

$$\mathbf{s} = \begin{Bmatrix} \mathbf{s}_d \\ \mathbf{s}_l \end{Bmatrix} \tag{4.29}$$

where the dependent displacement vector $\mathbf{s}_d$ involves the redundant set $\mathbf{u}_c^\beta$, and the independent displacement vector $\mathbf{s}_l$ involves $\mathbf{u}_i$ and $\mathbf{u}_c^\alpha$, that is the assembled system physical coordinates, i.e. $\mathbf{s}_l = \mathbf{u}$.

Accordingly, the constraint equation (equation 4.27) may be rewritten

$$\boldsymbol{\mathcal{C}}_{dl}\mathbf{s}_l + \boldsymbol{\mathcal{C}}_{dd}\mathbf{s}_d = \mathbf{0} \tag{4.30}$$

Thus, a condensation transformation may be established between the physical coordinates displacements and the generalised displacements as

$$\mathbf{s} = \begin{Bmatrix} \mathbf{s}_d \\ \mathbf{s}_l \end{Bmatrix} = \begin{bmatrix} -\boldsymbol{\mathcal{C}}_{dd}^{-1}\boldsymbol{\mathcal{C}}_{dl} \\ \mathbf{I}_{ll} \end{bmatrix} \mathbf{s}_l = \mathbf{S}\mathbf{u} \tag{4.31}$$

where $\mathbf{S}$ is the transformation matrix involving the dependent coordinates partition of the coupling matrix $\boldsymbol{\mathcal{C}}_{dd}$ and the independent coordinates partition $\boldsymbol{\mathcal{C}}_{dl}$. This condensation is a lossless transformation since only redundant information is reduced.

Pre-multiplying equation 4.28 with $\mathbf{S}^T$ one obtains the full system equations of motion, i.e.

$$\mathbf{D}\mathbf{u} = \mathbf{f} \tag{4.32}$$

with $\mathbf{D} = \mathbf{S}^T\mathbf{D}^s\mathbf{S}$, and $\mathbf{f} = \mathbf{S}^T\mathbf{f}^s$. Consequently, the coupled equations of motion may be directly obtained by transformation of the matrices and vectors in generalised coordinates. The coupling term $\lambda\boldsymbol{\mathcal{C}}$ in equation 4.28 vanishes since $\mathbf{S}^T\boldsymbol{\mathcal{C}} = \mathbf{0}$ by its own definition.

In fact, the matrix condensation transformation ($\mathbf{D} = \mathbf{S}^T\mathbf{D}^s\mathbf{S}$) corresponds to the finite element assembly of superelements matrices. However, formalising the assembly process in terms of a coordinate transformation matrix is of interest in this work because it will allow one to formulate the coupling and assembly of reduced order models.

4.3 Component Mode Synthesis

Component Mode Synthesis (CMS) is a method for solving/computing the dynamics of large built-up systems in an efficient way. It combines substructuring and model

order reduction techniques for this purpose. Figure 4.1 shows a block diagram outlining the procedures involved in the CMS method.

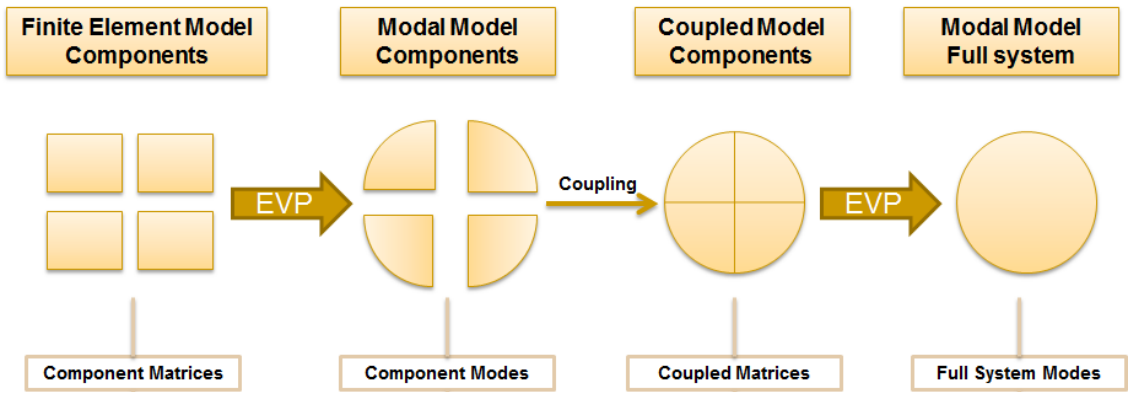

Figure 4.1: Component Mode Synthesis schematic

In CMS, a structural model is split into several substructures or *components*. A finite element model is defined for each component being uncoupled from the rest of the system. The dynamic equations of motion are defined in terms of the component mass, damping and stiffness matrices in *component-physical* coordinates.

Then, a coordinate transformation is applied to each component model by means of a set of component basis functions. Typically, the basis functions set consists of the component normal modes plus a series of attachment or constraint modes. Accordingly, the equations of motion may be posed in terms of these *component-modal* coordinates. Model order reduction is achieved by truncation of the set of basis functions. This results in a much reduced order of the component-modal coordinates.

The components' reduced models are then coupled together by enforcing displacement continuity and force equilibrium at the coupling interface degrees of freedom. These coupling conditions are applied to the reduced component models through a modal constraint equation. In this way a reduced coupled model for the full system is obtained in terms of the *coupled-modal* coordinates. This process is known as the *synthesis* of components.

The equations of motion of the full system in coupled-modal coordinates are still a set of linear dependent equations. These may be uncoupled by means of the *global* modes of the full system. The global modes are obtained from the solution of the corresponding (reduced) eigenvalue problem. Using the global modes as a set of basis functions, the equations of motion can be transformed into a set of linearly independent equations in *global-modal* coordinates. The dynamics of the full system

are fully characterized by the global modes that contribute to the response in the target frequency range.

The efficiency of the CMS method derives from the fact that the cost for solving an EVP scales as of the squared number of degrees of freedom in the EVP matrices. Consequently, the solution of an EVP for each component reduction will be much more cost-efficient than the solution of an EVP for the full system finite element model. Then, for large models, the cost for coupling the modal components and solving the much reduced coupled-modal EVP involves a trivial cost.

4.3.1 Component modes

Several kinds of component modes may be defined (e.g. normal modes, constraint modes, attachment modes...) and these will be obtained from the component equations of motion. In the following, the most common kinds of component modes are summarised. Their corresponding mathematical definitions may be consulted in Appendix F.

The component *normal modes* are the solution of the eigenvalue problem (EVP) defined from the component equations of motion. These may be free-interface component modes or fixed-interface component modes.

Free-interface modes $\boldsymbol{\phi}$ are the normal modes of a component whose coupling interface DOFs are considered force-free.

Fixed-Interface modes $\boldsymbol{\phi}^F$ are the normal modes of a component whose coupling interface DOFs are considered fixed, i.e. with zero displacement and rotation.

Constraint modes $\boldsymbol{\psi}^C$ describe the static deformation of the component when a unit displacement is applied to one coupling degree of freedom while all other coupling degrees of freedom are held fixed. There are as many constraint modes as component coupling degrees of freedom. The set of constraint modes $\boldsymbol{\Psi}^C$ is obtained as the static transformation matrix in Guyan's reduction when the coupling DOFs are considered to be the master degrees of freedom, i.e.

$$\boldsymbol{\Psi}^C = \begin{bmatrix} -\mathbf{K}_{ii}^{-1}\mathbf{K}_{ic} \\ \mathbf{I}_{cc} \end{bmatrix} \tag{4.33}$$

The set of constraint modes spans all possible displacement boundary conditions that any adjacent component might impose to its interface, and they are linearly independent of the fixed-interface normal modes.

Attachment modes $\boldsymbol{\psi}^A$ describe the static deformation of the component when a unit force is applied to one coupling degree of freedom while all other coupling degrees of freedom are force free. As for the constraint modes, there exist as many attachment modes as component coupling degrees of freedom. The set of attachment modes $\boldsymbol{\Psi}^A$ is computed from the static equations of motion with the described force boundary conditions at the component interface, giving rise to

$$\boldsymbol{\Psi}^A = \begin{bmatrix} \mathbf{G}_{ic} \\ \mathbf{G}_{cc} \end{bmatrix} \tag{4.34}$$

where $\mathbf{G}_{ic}$ and $\mathbf{G}_{cc}$ are partitions of the flexibility matrix. The set of attachment modes spans all possible force boundary conditions that any adjacent component might impose on its interface.

Residual attachment modes $\boldsymbol{\psi}^R$ are obtained if the residual flexibility matrix $\mathbf{G}^h$ is used in equation 4.34 instead. The residual attachment modes are linearly independent of the free-interface normal modes, because they only account for the contribution of the higher order normal modes that have been discarded for the modal reduction.

The choice of the modes to use in the component transformation matrix must be such that the dynamics of the component are described with completeness, and that the coupling constraints can be imposed consistently. This is usually accomplished by choosing a transformation basis consisting of a reduced number of the component normal modes, plus the full set of attachment or constraint modes that relate the motion in the component coupling interface degrees of freedom to the motion in the rest of component (interior) degrees of freedom. In CMS, it is common to use the constraint modes together with fixed-interface normal modes, and (residual) attachment modes together with free-interface normal modes.

4.3.2 Component modal reduction

Initially, a finite element model must be available for each component. Hence, each component's equations of motion are those defined for the substructuring method in section 4.2, i.e.

$$\mathbf{D}_s \mathbf{u}_s = \begin{bmatrix} \mathbf{D}_{ii} & \mathbf{D}_{ic} \\ \mathbf{D}_{ci} & \mathbf{D}_{cc} \end{bmatrix}_s \begin{Bmatrix} \mathbf{u}_i \\ \mathbf{u}_c \end{Bmatrix}_s = \begin{Bmatrix} \mathbf{f}_i \\ \mathbf{f}_c \end{Bmatrix}_s = \mathbf{f}_s$$

with $\mathbf{D}_s = \mathbf{M}_s \frac{\partial^2}{\partial t^2} + \mathbf{C}_s \frac{\partial}{\partial t} + \mathbf{K}_s$ the component matrices, $\mathbf{u}_s$ the component displacements and $\mathbf{f}_s$ the component external forces.

Then each component is reduced by means of a coordinate transformation. The component physical displacements $\mathbf{u}_s$ are transformed into component modal displacements $\mathbf{v}_s$ by means of a component modal transformation matrix $\mathbf{\Psi}_s$, i.e.

$$\mathbf{u}_s = \mathbf{\Psi}_s \mathbf{v}_s \tag{4.35}$$

where the transformation matrix consists of a reduced set of component modes.

Thence, the reduced model equations of motion in component modal coordinates v read

$$\mathbf{D}_s^v \mathbf{v}_s = \mathbf{f}_s^v \tag{4.36}$$

with $\mathbf{D}_s^v = \mathbf{\Psi}_s^T \mathbf{D}_s \mathbf{\Psi}_s = \mathbf{M}_s^v \frac{\partial^2}{\partial t^2} + \mathbf{C}_s^v \frac{\partial}{\partial t} + \mathbf{K}_s^v$ the reduced modal component matrices and $\mathbf{f}_s^v = \mathbf{\Psi}_s^T \mathbf{f}_s$ the reduced modal force vector.

4.3.3 Synthesis of modal components

Once the component models have been reduced into component-modal coordinates, the components may be coupled together following the coupling process described in section 4.2. In Component Mode Synthesis, the coupling of modal components is referred to as *synthesis* of components (or component modes), which gives the name to the method.

The coupling constraints for two adjacent components α and β, i.e. $\mathbf{u}_{c,\alpha} = \mathbf{u}_{c,\beta}$, may be formulated in component-modal coordinates as

$$\mathbf{\Psi}_{c,\alpha} \mathbf{v}_\alpha - \mathbf{\Psi}_{c,\beta} \mathbf{v}_\beta = \mathbf{0} \tag{4.37}$$

with c standing for the coupling DOFs partition.

Then, the components modal displacements $\mathbf{v}_s$ may be merged together into generalised modal displacements $\mathbf{v}$, and the modal component matrices and modal forces may be merged accordingly, that is

$$\mathbf{v} = \begin{Bmatrix} \mathbf{v}_1 \\ \vdots \\ \mathbf{v}_{N_s} \end{Bmatrix} \qquad \mathbf{D}^v = \begin{bmatrix} \mathbf{D}_1^v & \mathbf{0} & \mathbf{0} \\ \mathbf{0} & \ddots & \mathbf{0} \\ \mathbf{0} & \mathbf{0} & \mathbf{D}_{N_s}^v \end{bmatrix} \qquad \mathbf{f}^v = \begin{Bmatrix} \mathbf{f}_1^v \\ \vdots \\ \mathbf{f}_{N_s}^v \end{Bmatrix} \tag{4.38}$$

so that a modal constraint equation can be posed in generalised modal coordinates v as

$$\boldsymbol{\mathcal{C}}^v \mathbf{v} = \mathbf{0} \tag{4.39}$$

where $\boldsymbol{\mathcal{C}}^v$ is the modal coupling matrix. For instance, for a system comprising two components the modal coupling matrix would be $\boldsymbol{\mathcal{C}}^v = \begin{bmatrix} \boldsymbol{\Psi}_{c,1} & -\boldsymbol{\Psi}_{c,2} \end{bmatrix}$.

As for the physical generalised coordinates used in section 4.2, the modal generalised coordinates in general show redundancy. For instance, if constraint modes are used for the component reduction, the static displacement at the coupling interface DOFs is described twice, once by the constraint modes of one of the components and once again by the constraint modes of the adjacent component.

Therefore, the generalised component-modal coordinates may be split into a subset of independent modal coordinates l and a subset of dependent modal coordinates d, so that the modal constraint equation (equation 4.39) may be rewritten accordingly, i.e.

$$\boldsymbol{\mathcal{C}}^v_{dl}\mathbf{v}_l + \boldsymbol{\mathcal{C}}^v_{dd}\mathbf{v}_d = \mathbf{0} \tag{4.40}$$

Thence, based on the modal constraint equation, one may condense the generalised component modal displacements $\mathbf{v}$ into coupled-modal displacements $\mathbf{w}$ in linearly independent coordinates, that is

$$\mathbf{v} = \begin{Bmatrix} \mathbf{v}_d \\ \mathbf{v}_l \end{Bmatrix} = \begin{bmatrix} -\boldsymbol{\mathcal{C}}^{v\ -1}_{dd}\boldsymbol{\mathcal{C}}^v_{dl} \\ \mathbf{I}_{ll} \end{bmatrix} \mathbf{v}_l = \mathbf{S}^w\mathbf{w} \tag{4.41}$$

where $\mathbf{S}^w$ is the modal condensation matrix. Notice that $\mathbf{S}^w$ is analogous to the condensation matrix $\mathbf{S}$ used in the substructure coupling process.

Thereupon, the equations of motion of the full system can be formulated in modal-coupled coordinates w through the use of the modal condensation matrix $\mathbf{S}^w$, i.e.

$$\mathbf{D}^w\mathbf{w} = \mathbf{f}^w \tag{4.42}$$

with $\mathbf{D}^w = \mathbf{S}^{wT}\mathbf{D}^v\mathbf{S}^w = \mathbf{M}^w\frac{\partial^2}{\partial t^2} + \mathbf{C}^w\frac{\partial}{\partial t} + \mathbf{K}^w$ the coupled-modal system matrices, $\mathbf{w}$ the coupled-modal displacements, and $\mathbf{f}^w = \mathbf{S}^{wT}\mathbf{f}^v$ the coupled-modal external forces.

4.3.4 Global modal solution

Finally, the modes of vibration of the full system are computed from the reduced equations of motion in coupled-modal coordinates. The modal solutions are obtained from the eigenvalue problem[2] corresponding to equation 4.42, i.e.

$$\lambda^2\mathbf{M}^w\boldsymbol{\phi}^w + \lambda\mathbf{C}^w\boldsymbol{\phi}^w + \mathbf{K}^w\boldsymbol{\phi}^w = \mathbf{0} \tag{4.43}$$

[2]Component Mode Synthesis methods are typically formulated for the undamped equations of motion. Therefore, a reduced undamped EVP is to be solved instead of the reduced QEVP.

The modes of vibration of the full system are fully characterised by the eigensolution pairs λ_m– $\boldsymbol{\phi}_m^w$.

The total number of modes that can be correctly computed in this way will depend on the accuracy of the reduced coupled-modal model, that is on the amount and type of component modes used for the reduction and synthesis of components. In the same way, the cost for solving this EVP will depend on the number of DOFs of the reduced coupled-modal modal.

The reduced equations of motion of the full coupled system can now be transformed into a set of linearly independent equations, that is into *global-modal* equations of motion. Using the set of coupled-modal eigenvectors $\boldsymbol{\Phi}^w$ as the modal transformation matrix one obtains

$$\bar{\mathbf{D}}\mathbf{p} = \mathbf{Q} \tag{4.44}$$

with $\bar{\mathbf{D}} = \boldsymbol{\Phi}^{wT}\mathbf{D}^w\boldsymbol{\Phi}^w = \bar{\mathbf{M}}\frac{\partial^2}{\partial t^2} + \bar{\mathbf{C}}\frac{\partial}{\partial t} + \bar{\mathbf{K}}$ the (global-)modal system matrices, $\mathbf{p}$ the (global-)modal displacements, and $\mathbf{Q} = \boldsymbol{\Phi}^{wT}\mathbf{f}^w$ the (global-)modal external forces.

Summarising, the component models are reduced by means of a component-modal transformation $\mathbf{u}_s = \boldsymbol{\Psi}_s\mathbf{v}_s$. The component-modal models are coupled and reduced into a coupled-modal model by means of the synthesis transformation $\mathbf{v} = \mathbf{S}^w\mathbf{w}$. Finally, the modal model of the full system is found by means of the modal transformation $\mathbf{w} = \Phi^w\mathbf{p}$.

4.3.5 Global modes back-transformation

Notice that the $\boldsymbol{\phi}_m^w$ eigenvectors are of reduced size since they are expressed in coupled-modal coordinates w. However, one will be interested in knowing the mode shape vectors of the system in physical coordinates (e.g. for visually displaying the mode shapes, for computing the frequency response functions, etc.). Nevertheless, the full system mode shape vectors in physical coordinates $\boldsymbol{\phi}_m$ may be recovered from the reduced eigenvector solutions $\boldsymbol{\phi}_m^w$.

The relation between the reduced and the full mode shape vectors may be obtained by concatenating the different coordinate transformations that have been defined in Component Mode Synthesis. The transformation from global-modal displacements $\mathbf{p}$ to component-physical displacements $\mathbf{u}_s$ is then

$$\mathbf{u}_s = \boldsymbol{\Psi}_s\mathbf{v}_s = \boldsymbol{\Psi}_s\mathbf{S}_s^w\mathbf{w} = \boldsymbol{\Psi}_s\mathbf{S}_s^w\boldsymbol{\Phi}^w\mathbf{p} \tag{4.45}$$

However, in this chapter it is aimed at describing CMS methods for damped systems. Thus, the reduced QEVP is formulated here in order to maintain generality.

where $\mathbf{S}_s^w$ is the partition of the modal condensation matrix mapping the component modes of the s'th component. Then, since the $\mathbf{u}_s$ displacements correspond to uncoupled components, these may be merged into a generalised-physical coordinates displacement vector $\mathbf{s}$ as described in section 4.2, i.e.

$$\mathbf{s} = \begin{Bmatrix} \mathbf{u}_1 \\ \vdots \\ \mathbf{u}_{N_s} \end{Bmatrix} = \begin{Bmatrix} \mathbf{s}_d \\ \mathbf{u} \end{Bmatrix} = \mathbf{S}\mathbf{u} \tag{4.46}$$

which is related to the full model displacements $\mathbf{u}$ by the condensation matrix $\mathbf{S}$. Hence, a component-modal matrix $\mathbf{\Psi}^s$ in generalised component-physical coordinates may be formulated as

$$\mathbf{\Psi}^s = \text{diag}(\mathbf{\Psi}_1, \ldots, \mathbf{\Psi}_{N_s}) \tag{4.47}$$

which, in turn, can be transformed into a component-modal matrix $\mathbf{\Psi}^u$ in full system physical coordinates by pre-multiplication with the inverse condensation matrix

$$\mathbf{\Psi}^u = \mathbf{S}^{-1}\mathbf{\Psi}^s \equiv \mathbf{\Psi} \tag{4.48}$$

Thence, using the full system component-modal matrix $\mathbf{\Psi}$ one can establish a direct relation from the global-modal displacements $\mathbf{p}$ to the full system physical displacements $\mathbf{u}$

$$\mathbf{u} = \mathbf{\Psi}\mathbf{S}^w\mathbf{\Phi}^w\mathbf{p} = \mathbf{\Phi}\mathbf{p} \tag{4.49}$$

where $\mathbf{\Phi} = \mathbf{\Psi}\mathbf{S}^w\mathbf{\Phi}^w$ is in fact the modal matrix of the full system. From equation 4.49 it is apparent that the relation between the global-reduced mode shapes $\boldsymbol{\phi}_m^w$ and the full system mode shapes $\boldsymbol{\phi}_m$ is

$$\boldsymbol{\phi}_m = \mathbf{T}^w\boldsymbol{\phi}_m^w \tag{4.50}$$

with $\mathbf{T}^w = \mathbf{\Psi}\mathbf{S}^w$ the transformation matrix that provides a transformation back from the reduced modes to the full system modes.

4.3.6 The coupled-modal reduced model

The coupled-modal system matrices $\mathbf{M}^w$, $\mathbf{C}^w$ and $\mathbf{K}^w$ fully describe the coupled-modal model. The dynamics of the actual physical system can be described by this reduced model with more or less accuracy depending on the amount and type of component modes that have been used for the reduction.

The amount of component normal-modes to keep in each component will depend on the modal frequency of the component modes in relation to the frequency range of interest for the full system analysis. Typically, the higher the number of kept component normal-modes, the better the accuracy of the model. Conversely, the higher the amount of component modes, the lower the reduction of the model. Therefore, there should be a compromise regarding how many component modes need to be kept in order to optimally reduce the model without incurring significant inaccuracies.

At the same time, the type of component modes chosen for the component reduction also compromises the accuracy and reduction of the coupled-modal model. With the same amount of component modes, some component mode combinations may describe with more completeness the components and the coupling dynamics. In other words, an accurate coupled-modal model may be achieved with larger or smaller reduced model order depending on the component modes chosen.

Furthermore, another factor that should be taken into account when evaluating the goodness of CMS methods is the computation time required to obtain the coupled-modal matrices. Some CMS methods may result in certain structured disposition of the matrices that make their computation more cost-efficient, reducing in this way the overall time for solving the dynamics of a system through Component Mode Synthesis.

4.4 Undamped Component Mode Synthesis methods

Many Component Mode Synthesis methods may be described depending on the type of component modes used for the components reduction, each of them having its pros and cons in this regard. The most commonly used methods are the Craig-Bampton [5] method and the Craig-Chang [7] method which are based on fixed-interface and free-interface component modes respectively. In the following, these classic CMS methods are described.

Focus will be placed on principles that ensure consistent synthesis of the modal components. The features that define these methods (e.g. structure of the component matrices, structure of the coupled-modal matrices, etc.) and distinguish them from any other CMS method are also presented. Otherwise, the specific mathematical derivation of the particular CMS transformations are omitted for brevity, since

these two methods are quite standard methods. In any case, the transformation expressions in any of the two methods are specific forms of the generic Component Mode Synthesis described in the previous section.

4.4.1 The Craig-Bampton method

The Craig-Bampton (CB) method [5] uses fixed interface normal modes and static constraint modes for the component's reduction basis. The definition of these component modes may be consulted in sections F.1 and F.2 of the appendix.

Craig-Bampton component model reduction

For a component s, consider the reduced set $\mathbf{U}_s^F$ of component fixed-interface (undamped) normal modes, and the set $\mathbf{\Psi}_s^C$ of component constraint modes. Then, the component modes transformation matrix $\mathbf{\Psi}_s$ in the CB method is

$$\mathbf{\Psi}_s = \begin{bmatrix} \mathbf{U}_{ik}^F & \mathbf{\Psi}_{ic}^C \\ \mathbf{0}_{ck} & \mathbf{I}_{cc} \end{bmatrix}_s \tag{4.51}$$

where the i, c and k subindices stand for the *interior*, *coupling* and *kept normal-modal* component DOFs. Notice that the coupling DOFs of the fixed-interface modes are all zero. This implies that the component modal coordinates involve the coupling set of physical coordinates. Hence, the component modal displacements $\mathbf{v}_s$ may be expressed as

$$\mathbf{v}_s = \begin{Bmatrix} \mathbf{p}^F \\ \mathbf{u}_c \end{Bmatrix}_s \tag{4.52}$$

with $\mathbf{p}_s^F$ the component fixed-modal displacements and $\mathbf{u}_{c,s}$ the component coupling-physical displacements. Accordingly, the undamped component-modal matrices $\mathbf{K}_s^v$ and $\mathbf{M}_s^v$ read

$$\mathbf{K}_s^v = \begin{bmatrix} \mathbf{\Lambda}_{kk}^F & \mathbf{0}_{kc} \\ \mathbf{0}_{ck} & \mathbf{K}_{cc}^v \end{bmatrix}_s \qquad \mathbf{M}_s^v = \begin{bmatrix} \mathbf{I}_{kk} & \mathbf{M}_{kc}^v \\ \mathbf{M}_{ck}^v & \mathbf{M}_{cc}^v \end{bmatrix}_s \tag{4.53}$$

where $\mathbf{\Lambda}_{kk,s}^F = \mathrm{diag}(\lambda_1, \ldots, \lambda_{N_k})_s$ is a diagonal matrix containing the eigenvalues corresponding to the kept fixed-interface modes. Notice that the matrices coupling partitions $\mathbf{K}_{cc,s}^v$ and $\mathbf{M}_{cc,s}^v$ remain in physical coordinates. On the contrary, the $\mathbf{M}_{kc,s}^v$ and $\mathbf{M}_{ck,s}^v$ partitions of the component-modal mass matrix are expressed in modal-physical hybrid coordinates. The corresponding partitions for the component-modal stiffness matrix become zero matrices due to the specific definition of the constraint modes in terms of the stiffness matrix (c.f. equation 4.33).

The Craig-Bampton coupled-modal model

The fact that the coupling partitions remain in physical coordinates is what makes the coupling of components so easy in the CB method. The constraint equation can be formulated from displacement continuity in physical coordinates (equation 4.24), rather than from its modal counterpart in equation 4.37. This means that the synthesis of components is performed through condensation of the physical coupling DOFs. Therefore, the coupled-modal displacements form a vector involving all the component's fixed-modal displacements $\mathbf{p}^F$ plus the non-redundant set of physical coupling-interface displacements $\mathbf{u}_c$, that is

$$\mathbf{w} = \begin{Bmatrix} \mathbf{p}^F \\ \mathbf{u}_c \end{Bmatrix} \qquad \text{with} \quad \mathbf{p}^F = \begin{Bmatrix} \mathbf{p}_1^F \\ \vdots \\ \mathbf{p}_{N_s}^F \end{Bmatrix} \tag{4.54}$$

Thence, the coupled-modal CB system matrices $\mathbf{K}^w$ and $\mathbf{M}^w$ may be simply obtained through the assembly of the component-modal matrices. Accordingly the coupled-modal CB system matrices have the following structure

$$\mathbf{K}^w = \begin{bmatrix} \mathbf{\Lambda}_{kk}^F & \mathbf{0}_{kc} \\ \mathbf{0}_{ck} & \mathbf{K}_{cc}^w \end{bmatrix} \qquad \mathbf{M}^w = \begin{bmatrix} \mathbf{I}_{kk} & \mathbf{M}_{kc}^w \\ \mathbf{M}_{ck}^w & \mathbf{M}_{cc}^w \end{bmatrix} \tag{4.55}$$

$$\begin{aligned} \text{with} \quad & \mathbf{\Lambda}_{kk}^F = \text{diag}(\mathbf{\Lambda}_{kk,1}^F, \ldots, \mathbf{\Lambda}_{kk,N_s}^F) && \mathbf{M}_{kc}^w = \text{vect}(\mathbf{M}_{kc,1}^v, \ldots, \mathbf{M}_{kc,N_s}^v) = \mathbf{M}_{ck}^{w\,T} \\ & \mathbf{K}_{cc}^w = \text{assembly}(\mathbf{K}_{cc,1}^v, \ldots, \mathbf{K}_{cc,N_s}^v) && \mathbf{M}_{cc}^w = \text{assembly}(\mathbf{M}_{cc,1}^v, \ldots, \mathbf{M}_{cc,N_s}^v) \end{aligned}$$

where $\mathbf{\Lambda}_{kk}^F$ is a diagonal matrix containing the eigenvalues corresponding to the component modes of all components, $\mathbf{K}_{cc}^w$ and $\mathbf{M}_{cc}^w$ are the assembly of the component matrices' coupling interface partitions in physical coordinates, and $\mathbf{M}_{kc}^w$ and $\mathbf{M}_{ck}^w$ are the sub-matrices containing the corresponding partitions of all component-modal mass matrices.

In turn, the CB reduced to physical global modes transformation matrix $\mathbf{T}^w$ is also constructed through assembly of the component modal transformation matrices $\mathbf{\Psi}_s$ as

$$\mathbf{T}^w = \begin{bmatrix} \mathbf{U}_{ik}^F & \mathbf{\Psi}_{ic}^C \\ \mathbf{0}_{ck} & \mathbf{I}_{cc} \end{bmatrix} \tag{4.56}$$

$$\text{with} \qquad \mathbf{U}_{ik}^F = \text{diag}(\mathbf{U}_{ik,1}^F, \ldots, \mathbf{U}_{ik,N_s}^F) \qquad \mathbf{\Psi}_{ic}^C = \text{vect}(\mathbf{\Psi}_{ic,1}^C, \ldots, \mathbf{\Psi}_{ic,N_s}^C)$$

where $\mathbf{U}_{ik}^F$ contains the fixed-interface component normal modes interior partitions of all of the components and $\mathbf{\Psi}_{ic}^C$ contains the constraint modes' interior partitions of all of the components.

Pros and cons of the Craig-Bampton method

The Craig-Bampton (CB) method performs the synthesis of components and the recovery of the full system modes without the need of performing complicated coordinate transformations, i.e. $\mathbf{v} = \mathbf{S}^w\mathbf{w}$ and $\mathbf{T}^w = \mathbf{S}^{-1}\mathbf{\Phi}^s\mathbf{S}^w$. Instead, it simply assembles the component-modal matrices and the transformation matrices as if they were finite element superelements. This supposes very good scalability of the CB method, since the components may be coupled systematically.

However, the ease of coupling of the CB method comes at the price of non optimal reduction of the model. On one hand, all coupling degrees of freedom are not being reduced into compact modal coordinates. On the other hand, the modal reduction of the components needs a sufficient number of fixed-interface modes in order to ensure good accuracy in the coupled model. This supposes that the CB coupled-modal model involves a moderate number of fixed-interface modal DOFs and a large number of coupling-interface physical DOFs.

Characteristic constraint modes reduction

One possible way for reducing the number of DOFs of the CB coupled-modal model is to use *characteristic constraint* (CC) modes [91]. After assembling together the component matrices, the coupling interface physical DOFs may be reduced by means of a modal reduction of the coupling DOFs.

An undamped EVP may be formulated for the coupling interface matrices $\mathbf{K}^w_{cc}$ and $\mathbf{M}^w_{cc}$, i.e.

$$\lambda^{CC}\mathbf{M}^w_{cc}\boldsymbol{u}^{CC} = \mathbf{K}^w_{cc}\boldsymbol{u}^{CC} \tag{4.57}$$

so that the coupling interface displacements are transformed into modal coordinates, that is

$$\mathbf{u}_c = \mathbf{U}^{CC}\mathbf{p}^{CC} \tag{4.58}$$

with $\mathbf{U}^{CC}$ the reduced set of characteristic constraint modes. Thence, the CB coupled-modal displacements $\mathbf{w}^{CB}$ may be reduced using the CC modes as

$$\mathbf{w}^{CB} = \begin{Bmatrix}\mathbf{p}^F\\ \mathbf{u}_c\end{Bmatrix} = \begin{bmatrix}\mathbf{I} & \mathbf{0}\\ \mathbf{0} & \mathbf{U}^{CC}\end{bmatrix}\begin{Bmatrix}\mathbf{p}^F\\ \mathbf{p}^{CC}\end{Bmatrix} = \mathbf{T}^\nu\boldsymbol{\nu} \tag{4.59}$$

where $\boldsymbol{\nu}$ is the much reduced set of coupled-modal displacements involving the fixed-interface modal DOFs and the characteristic constraint modal DOFs. Thus, the coupled-modal CB system matrices $\mathbf{K}^w$ and $\mathbf{M}^w$ can be further reduced through the CC modal transformation, i.e. $\mathbf{K}^\nu = \mathbf{T}^{\nu T}\mathbf{K}^w\mathbf{T}^\nu$ and $\mathbf{M}^\nu = \mathbf{T}^{\nu T}\mathbf{M}^w\mathbf{T}^\nu$.

This transformation reduces greatly the number of coupling interface DOFs of the CB coupled-modal model. In turn it makes the reduced coupled-modal stiffness matrix $\mathbf{K}^{\nu}$ diagonal since $\mathbf{U}^{CC^T}\mathbf{K}^{w}_{cc}\mathbf{U}^{CC} = \mathbf{\Lambda}^{CC}$.

4.4.2 The Craig-Chang method

The Craig-Chang (CCH) method [7] uses free-interface normal modes and great reduction and accuracy in the coupled-modal model is achieved through the use of residual attachment modes. The definition of these component modes may be consulted in sections F.1 and F.3 of the appendix.

Craig-Chang component model reduction

For a component s, consider the reduced set $\mathbf{U}_s$ of component free-interface (undamped) normal modes, and the set $\mathbf{\Psi}^R_s$ of component residual attachment modes. Then, the component modes transformation matrix $\mathbf{\Psi}_s$ in the CCH method is

$$\mathbf{\Psi}_s = \begin{bmatrix} \mathbf{U}_{ik} & \mathbf{\Psi}^R_{ia} \\ \mathbf{U}_{ck} & \mathbf{\Psi}^R_{ca} \end{bmatrix}_s \tag{4.60}$$

where the i and c subindices stand for the *interior*, *coupling* physical component DOFs, and the k and a subindices stand for the *kept normal* and (residual) *attachment* component DOFs. This implies that the component modal coordinates v involve a reduced set of free interface normal-modal coordinates and the set of attachment coordinates. Hence, the component modal displacements $\mathbf{v}_s$ may be expressed as

$$\mathbf{v}_s = \begin{Bmatrix} \mathbf{p} \\ \mathbf{v}_a \end{Bmatrix}_s \tag{4.61}$$

with $\mathbf{p}_s$ the component free-interface normal-modal displacements and $\mathbf{v}_{a,s}$ the component attachment displacements. The set of attachment displacements $\mathbf{v}_{a,s}$ is of the same size to the set of coupling physical displacements $\mathbf{u}_{c,s}$. However, this does not mean that the attachment coordinates a are interchangeable with physical coupling coordinates c.

Thus, the undamped component-modal reduced matrices $\mathbf{K}^v_s$ and $\mathbf{M}^v_s$ may be computed through the CCH component modes transformation matrix. Assuming (for simplicity) that the components have no rigid body freedom, the component-modal

matrices read

$$\mathbf{K}_s^v = \begin{bmatrix} \mathbf{\Lambda}_{kk} & \mathbf{0}_{ka} \\ \mathbf{0}_{ak} & \mathbf{K}_{aa}^v \end{bmatrix}_s \qquad \mathbf{M}_s^v = \begin{bmatrix} \mathbf{I}_{kk} & \mathbf{0}_{ka} \\ \mathbf{0}_{ak} & \mathbf{M}_{aa}^v \end{bmatrix}_s \tag{4.62}$$

where $\mathbf{\Lambda}_{kk,s} = \text{diag}(\lambda_1, \ldots, \lambda_{N_k})_s$ is a diagonal matrix containing the eigenvalues corresponding to the kept free-interface modes. In this case, the matrices attachment partitions $\mathbf{K}_{aa}^v$ and $\mathbf{M}_{aa}^v$ are transformed into attachment coordinates, as opposed to the CB method. Moreover, since by definition the residual attachment modes are linearly independent to the kept free-interface modes, the remaining partitions of the component-modal matrices become zero matrices.

Attachment pseudo-static approximation

This specific structure of the component matrices was exploited by Craig and Chang in [7] in order to find a pseudo-static approximation that allows reduction of all of the attachment component DOFs in the coupled-modal model.

Since the normal-modal partitions and the attachment partitions of the component matrices in equation 4.62 are linearly independent, the component-modal equations of motion for the attachment coordinates subset may be formulated separately, i.e.

$$\mathbf{M}_{aa,s}^v \dot{\mathbf{v}}_{a,s} + \mathbf{K}_{aa,s}^v \mathbf{v}_{a,s} = {\mathbf{\Psi}_{ca,s}^R}^T \mathbf{f}_{c,s} \tag{4.63}$$

Then, it is further shown in [7] that the attachment partition of the component modal stiffness matrix $\mathbf{K}^v$ equals indeed the coupling partition of the residual attachment modes set $\mathbf{\Psi}_s^R$, i.e.

$$\mathbf{K}_{aa,s}^v = \mathbf{\Psi}_{ca,s}^R$$

Thence, since by definition $\mathbf{\Psi}_{ca,s}^R = \mathbf{G}_{cc,s}^h$ is a symmetric matrix, the component *static* equations of motion for the attachment DOFs read

$$\mathbf{\Psi}_{ca,s}^R \mathbf{v}_{a,s} = \mathbf{\Psi}_{ca,s}^R \mathbf{f}_{c,s} \tag{4.64}$$

From this last equation, and regarding that $\mathbf{\Psi}_{ca,s}^R$ is a non-singular matrix, a pseudo-static approximation for the attachment displacements $\mathbf{v}_{a,s}$ can be established as

$$\mathbf{v}_{a,s} = \mathbf{f}_{c,s} \tag{4.65}$$

The attachment displacements pseudo-static approximation is then used to formulate the force equilibrium constraint at the coupling interfaces of two adjacent components α and β in terms of the attachment displacements, that is

$$\mathbf{v}_{a,\alpha} + \mathbf{v}_{a,\beta} = 0 \tag{4.66}$$

This pseudo-static constraint together with the displacement continuity modal constraint, i.e.

$$\boldsymbol{\Psi}_{c,\alpha}\mathbf{v}_{\alpha} - \boldsymbol{\Psi}_{c,\beta}\mathbf{v}_{\beta} = 0$$

are combined into a single constraint equation $\boldsymbol{\mathcal{C}}^{v}\mathbf{v} = \mathbf{0}$ in modal coordinates. For instance, for a two component system the constraint equation would read

$$\begin{bmatrix} \mathbf{0}_{ck} & \mathbf{I}_{ca} & \mathbf{0}_{ck} & \mathbf{I}_{ca} \\ \mathbf{U}_{ck,1} & \boldsymbol{\Psi}^{R}_{ca,1} & -\mathbf{U}_{ck,2} & -\boldsymbol{\Psi}^{R}_{ca,2} \end{bmatrix} \begin{Bmatrix} \mathbf{p}_1 \\ \mathbf{v}_{a,1} \\ \mathbf{p}_2 \\ \mathbf{v}_{a,2} \end{Bmatrix} = \mathbf{0} \tag{4.67}$$

where the upper row corresponds to force equilibrium and the bottom row to displacement continuity.

The Craig-Chang coupled-modal model

The fact that two complementary constraints can be formulated in terms of component-modal displacements supposes that all component attachment DOFs become linearly dependent with respect to the free-interface component modal DOFs, that is, the attachment DOFs are redundant. Therefore, the resulting modal condensation matrix $\mathbf{S}^{w}$ does condense all attachment DOFs, meaning that the Craig-Chang coupled-modal displacements consist of just the free-interface modal displacements of all components, that is

$$\mathbf{w} = \begin{Bmatrix} \mathbf{p}_1 \\ \vdots \\ \mathbf{p}_{N_s} \end{Bmatrix} \tag{4.68}$$

However, the attachment partition of the modal condensation matrix $\mathbf{S}^{w}_{ak}$ turns out to be a rather complicated expression in terms of the coupling partitions $\mathbf{U}_{ck,s}$ and $\boldsymbol{\Psi}^{R}_{ca,s}$ of the component modal transformation matrices $\boldsymbol{\Psi}_s$. Consequently, the CCH coupled-modal matrices $\mathbf{K}^{w}$ and $\mathbf{M}^{w}$ become fully populated non-structured matrices that are function of the $\boldsymbol{\Psi}_s$ and $\mathbf{K}^{v}_{aa,s}$ or $\mathbf{M}^{v}_{aa,s}$ matrices.

On the contrary, the normal modal partition of the modal condensation matrix $\mathbf{S}^{w}_{kk}$ is just an identity matrix $\mathbf{I}_{kk}$. Hence, the mathematical expressions for coupled-modal matrices may be decomposed into the sum of two distinct matrices, one corresponding to the normal modal DOFs of the component matrices, and the second one corresponding to the condensation of the component matrices (residual)

attachment DOFs, that is

$$\mathbf{K}^w = \mathbf{\Lambda}_{kk} + \mathbf{K}^R_{kk} \qquad\qquad \mathbf{M}^w = \mathbf{I}_{kk} + \mathbf{M}^R_{kk} \tag{4.69}$$

with $\mathbf{\Lambda}_{kk} = \text{diag}(\mathbf{\Lambda}_{kk,1}, \ldots, \mathbf{\Lambda}_{kk,N_s})$, $\mathbf{K}^R_{kk} = {\mathbf{S}^w_{ak}}^T \mathbf{K}^v_{aa} \mathbf{S}^w_{ak}$ and $\mathbf{M}^R_{kk} = {\mathbf{S}^w_{ak}}^T \mathbf{M}^v_{aa} \mathbf{S}^w_{ak}$.

The $\mathbf{\Lambda}_{kk}$ matrix contains the eigenvalues corresponding to the free-interface normal modes of all components. The $\mathbf{K}^R_{kk}$ and $\mathbf{M}^R_{kk}$ matrices are fully populated, whereas the $\mathbf{\Lambda}_{kk}$ and $\mathbf{I}_{kk}$ matrices are diagonal.

The CCH reduced to physical global modes transformation matrix $\mathbf{T}^w$ may be also decomposed into component normal-modal and condensed residual attachment matrices as

$$\mathbf{T}^w = \mathbf{U}^w + \mathbf{T}^R \tag{4.70}$$

$$\text{with} \quad \mathbf{U}^w = \begin{bmatrix} \text{diag}(\mathbf{U}_{ik,1}, \ldots, \mathbf{U}_{ik,N_s}) \\ \frac{1}{2}[\mathbf{U}_{ck,1} \ \ldots \ \mathbf{U}_{ck,N_s}] \end{bmatrix}, \quad \mathbf{T}^R = \begin{bmatrix} \text{diag}(\mathbf{\Psi}^R_{ia,1}\mathbf{S}^w_{ak,1}, \ldots, \mathbf{\Psi}^R_{ia,N_s}\mathbf{S}^w_{ak,N_s}) \\ \frac{1}{2}[\mathbf{\Psi}^R_{ca,1}\mathbf{S}^w_{ak,1} \ \ldots \ \mathbf{\Psi}^R_{ca,N_s}\mathbf{S}^w_{ak,N_s}] \end{bmatrix}$$

Pros and cons of the Craig-Chang method

The Craig-Chang coupled-modal model describes with very good accuracy the dynamics of the full physical system. This is because the component-modal model is obtained through a modal reduction with residual flexibility correction. Thence, the residual static effects of the higher order component modes discarded for the reduction are accounted for through the residual attachment modes. This contrasts with the CB method, where the contribution of the higher order fixed-interface modes is simply trimmed off.

Consequently, for the same number of component modes covering a target frequency range, better accuracy is obtained with the CCH method than with the CB method. In other words, the same accuracy may be achieved with a slightly smaller number of component modes. In turn, the CCH coupled-modal model consists only of the free-interface component normal-modal coordinates. Therefore, the CCH reduced model is of significantly reduced order since no coupling (or characteristic constraint) DOFs remain in the coupled-modal model. Thus, the Craig-Chang method optimally reduces the full model into a minimum order coupled-modal model.

Conversely, the CCH coupled-modal matrices do not show a structured composition. Therefore, the coupling of components is not as straightforward as in the CB method. In turn, this implies that the coupled-modal matrices necessarily need to be computed through the modal-condensation matrix pre and post-multiplication.

Accordingly, the global modes back-transformation matrix is non-structured and needs also to be computed through modal-condensation matrix pre-multiplication. This fact implies a much greater computation time for the coupled model reduction and the recovery of the full order global modes.

4.5 Damped Component Mode Synthesis methods

The two *classic* CMS methods described in the previous section - namely the Craig-Bampton and the Craig-Chang methods - are based on the component undamped normal modes. Consequently they are aimed at systems with light damping that may be modelled as undamped systems or systems with classical damping. For these kinds of systems the classic CMS methods produce results with sufficient accuracy. Yet, heavily damped systems or systems with the damping being localized will show non-proportional damping characteristics and may be poorly estimated by the classic CMS methods.

For the purpose of analysing systems with non classical damping, CMS methods based on damped component modes were likewise developed. Typically, these methods write the component equations of motion in state-space form to find the component damped modes. However, these state-space methods are not commonly adopted by most of the engineering community. Here, the damped CMS methods are recovered/revisited here in order to put them together with the damped modes reanalysis methods that have been explored in the previous chapter.

In this thesis, these latter damped CMS methods – namely the Morgan method [14] with fixed-interface complex modes and constraint modes in the state-space, and the Craig-Ni method [13] with free-interface complex modes and attachment modes in the state-space – are proposed for reducing large damped systems with varying parameters. These methods are not standard methods and for this reason they will be explained thoroughly in this section. Before that, the specific notation for CMS methods in the state-space is introduced in the following.

4.5.1 Component Mode Synthesis in state-space formulation

The Component Mode Synthesis method performs the reduction of the components through linear modal transformations. When a dynamic system is generally damped, the modal components reduction will involve damped modes of vibration. As has been explained in chapter 2, damped modes are mathematically described through complex conjugate eigensolution pairs. Therefore, a generally damped component (or full system) modal transformation matrix should contain both complex conjugate eigensolutions of the kept damped modes used for the reduction. The most convenient way to find these eigensolution pairs is to transform the equations of motion into the state space. Thence, Component Mode Synthesis methods for generally damped systems typically start by posing the component equations of motion in state-space form, i.e.

$$\mathbf{A}_s\dot{\mathbf{x}}_s - \mathbf{B}_s\mathbf{x}_s = \mathbf{f}_s^x \tag{4.71}$$

$$\text{with} \quad \mathbf{x}_s = \begin{Bmatrix} \dot{\mathbf{u}} \\ \mathbf{u} \end{Bmatrix}_s, \quad \mathbf{A}_s = \begin{bmatrix} \mathbf{0} & \mathbf{M} \\ \mathbf{M} & \mathbf{C} \end{bmatrix}_s, \quad \mathbf{B}_s = \begin{bmatrix} \mathbf{M} & \mathbf{0} \\ \mathbf{0} & -\mathbf{K} \end{bmatrix}_s \quad \text{and} \quad \mathbf{f}_s^x = \begin{Bmatrix} \mathbf{0} \\ \mathbf{f} \end{Bmatrix}_s$$

where $\mathbf{x}_s$ is the component state-displacements vector, consisting of the component physical displacements and velocities.

Henceforth, all steps are analogous to the standard Component Mode Synthesis but working with duplicated number of DOFs. State-coordinates contain displacement and velocity physical DOFs, and the corresponding modal state-coordinates involve double the amount of DOFs, accounting for the complex conjugate modal pairs. Here, the CMS explicit formulation for damped systems is introduced with specific notation for the state-space variables.

To begin with, the component state-displacements are split into interior and coupling degrees of freedom. Accordingly, the component equations of motion may be partitioned as

$$\begin{bmatrix} \mathbf{A}_{ii} & \mathbf{A}_{ic} \\ \mathbf{A}_{ci} & \mathbf{A}_{cc} \end{bmatrix}_s \begin{Bmatrix} \dot{\mathbf{x}}_i \\ \dot{\mathbf{x}}_c \end{Bmatrix}_s - \begin{bmatrix} \mathbf{B}_{ii} & \mathbf{B}_{ic} \\ \mathbf{B}_{ci} & \mathbf{B}_{cc} \end{bmatrix}_s \begin{Bmatrix} \mathbf{x}_i \\ \mathbf{x}_c \end{Bmatrix}_s = \begin{Bmatrix} \mathbf{f}_i^x \\ \mathbf{f}_c^x \end{Bmatrix}_s \tag{4.72}$$

Then, a set $\boldsymbol{\Upsilon}_s$ of component modes in state-space coordinates (including damped state-normal modes, state-constraint modes, state-attachment modes, etc.) is used for transforming the component state-displacement $\mathbf{x}_s$ into modal state-displacements $\mathbf{y}_s$, that is

$$\mathbf{x}_s = \boldsymbol{\Upsilon}_s\mathbf{y}_s \tag{4.73}$$

where $\mathbf{y}_s$ is the state-space equivalent of the component-modal displacements $\mathbf{v}_s$ described in section 4.3.

Therefore, the state-space component equations of motion may be reduced into modal state-coordinates

$$\mathbf{A}_s^y \dot{\mathbf{y}}_s - \mathbf{B}_s^y \mathbf{y}_s = \mathbf{f}_s^y \tag{4.74}$$

with $\mathbf{A}_s^y = \boldsymbol{\Upsilon}_s^T \mathbf{A}_s \boldsymbol{\Upsilon}_s$ and $\mathbf{B}_s^y = \boldsymbol{\Upsilon}_s^T \mathbf{B}_s \boldsymbol{\Upsilon}_s$ the component-modal state-matrices and $\mathbf{f}_s^y = \boldsymbol{\Upsilon}_s^T \mathbf{f}_s$ the component external forces in modal state-coordinates. Notice that the damped normal-eigenvectors that are used for the modal reduction will generally be complex valued. Therefore the reduced component matrices are generally complex valued.

Then, the coupling modal constraints for the full system can be formulated in generalised component-modal state-coordinates,

$$\boldsymbol{\mathcal{C}}^y \mathbf{y} = \mathbf{0} \tag{4.75}$$

with the generalised component-modal state-displacements, state-matrices and state-forces being

$$\mathbf{y} = \begin{Bmatrix} \mathbf{y}_1 \\ \vdots \\ \mathbf{y}_{N_s} \end{Bmatrix} \quad \mathbf{A}^y = \begin{bmatrix} \mathbf{A}_1^y & \mathbf{0} & \mathbf{0} \\ \mathbf{0} & \ddots & \mathbf{0} \\ \mathbf{0} & \mathbf{0} & \mathbf{A}_{N_s}^y \end{bmatrix} \quad \mathbf{B}^y = \begin{bmatrix} \mathbf{B}_1^y & \mathbf{0} & \mathbf{0} \\ \mathbf{0} & \ddots & \mathbf{0} \\ \mathbf{0} & \mathbf{0} & \mathbf{B}_{N_s}^y \end{bmatrix} \quad \mathbf{y} = \begin{Bmatrix} \mathbf{f}_1^y \\ \vdots \\ \mathbf{f}_{N_s}^y \end{Bmatrix} \tag{4.76}$$

In this case, the constraints must ensure that the coupling is consistent for both the displacement and the velocity DOFs. Therefore, the modal constraint equation shall impose displacement and velocity continuity at the coupling interfaces, i.e.

$$\mathbf{x}_{c,\alpha} = \mathbf{x}_{c,\beta} \tag{4.77}$$

Subsequently, the synthesis of components is carried out through a modal condensation transformation

$$\mathbf{y} = \mathbf{S}^z \mathbf{z} \tag{4.78}$$

where $\mathbf{z}$ is the state-space equivalent of the coupled-modal displacements $\mathbf{w}$, and $\mathbf{S}^z$ is the modal condensation state-matrix

$$\mathbf{S}^z = \begin{bmatrix} -{\boldsymbol{\mathcal{C}}_{dd}^y}^{-1} \boldsymbol{\mathcal{C}}_{dl}^y \\ \mathbf{I}_{ll} \end{bmatrix} \tag{4.79}$$

Thus, coupled-modal equations of motion in the state-space may be formulated as

$$\mathbf{A}^z \dot{\mathbf{z}} - \mathbf{B}^z \mathbf{z} = \mathbf{f}^z \tag{4.80}$$

with $\mathbf{A}^z = \mathbf{S}^{zT}\mathbf{A}^y\mathbf{S}^z$ and $\mathbf{B}^z = \mathbf{S}^{zT}\mathbf{B}^y\mathbf{S}^z$ the coupled-modal state-matrices, and $\mathbf{f}^z = \mathbf{S}^{zT}\mathbf{f}^y$ the full system external forces in coupled-modal state-coordinates.

Finally, a reduced EVP in coupled-modal state-coordinates may be solved in order to find the global modes of the system

$$\lambda\mathbf{A}^z\boldsymbol{z} = \mathbf{B}^z\boldsymbol{z} \tag{4.81}$$

with the corresponding eigensolutions being the full system damped eigenvalues $\lambda_m = -\sigma_m \pm i\omega_{d,m}$ and the full system damped eigenvectors $\boldsymbol{z}_m$ in coupled-modal state-coordinates.

Notice that the matrices in equation 4.81 will be complex valued and symmetric, i.e. the reduced EVP is non-hermitian. Therefore, the solution of this reduced EVP shall be tackled with an appropriate eigenvalue algorithm.

The full system damped mode shape vectors $\boldsymbol{\phi}_m$ in physical displacement coordinates may be recovered through a corresponding back-transformation matrix

$$\boldsymbol{\phi}_m = \mathbf{T}_D^z\boldsymbol{z}_m \tag{4.82}$$

which is just the physical displacement partition of the back transformation from modal global state-eigenvectors $\boldsymbol{z}_m$ to state-eigenvectors $\boldsymbol{x}_m$, i.e.

$$\boldsymbol{x}_m = \begin{Bmatrix} \lambda_m\boldsymbol{\phi}_m \\ \boldsymbol{\phi}_m \end{Bmatrix} = \mathbf{T}^z\boldsymbol{z}_m \tag{4.83}$$

with $\mathbf{T}^z = \boldsymbol{\Upsilon}\mathbf{S}^z$ the state-modal to state-space back transformation matrix.

4.5.2 The Morgan-Craig-Bampton method

The CMS methods developed by Morgan et. al [14, 42–44] are based on the state-space formulation. In these methods, component constraint and attachment modes in the state-space are derived from the standard constraint and attachment modes in physical coordinates.

In particular, one of the methods' formulations uses state-constraint modes and combines them with fixed-interface state-normal modes, which is in effect the extension of the classical Craig-Bampton method into the state-space formulation. Therefore, in this thesis, this CMS method for damped system is referred to as the Morgan-Craig-Bampton (MCB) method, which is described next.

MCB component modes

As has just been introduced, the modal reduction basis of each component s consist of a reduced set $\mathbf{X}_s^F$ of fixed-interface state-normal modes and a set $\boldsymbol{\Upsilon}_s^C$ of state-constraint modes.

The fixed-interface state-normal modes $\boldsymbol{x}_{k,s}^F$ may be computed from the eigenvalue problem corresponding to the interior degrees of freedom of the component state-space equations of motion. The interior DOFs eigenvalue problem

$$\mathbf{B}_{ii,s}\boldsymbol{x}_{i,s} = \lambda_s^F \mathbf{A}_{ii,s}\boldsymbol{x}_{i,s} \tag{4.84}$$

has complex conjugate eigensolution pairs $(\lambda_s^F, \boldsymbol{x}_{i,s})_k$ and $(\lambda_s^{*F}, \boldsymbol{x}_{i,s}^*)_k$ corresponding to the k'th fixed-interface damped component mode. Thence, mode shapes for the fixed-interface state-normal modes $\boldsymbol{x}_{k,s}^F$ are obtained as

$$\boldsymbol{x}_{k,s}^F = \begin{Bmatrix} \boldsymbol{x}_i \\ \mathbf{0}_c \end{Bmatrix}_{k,s} \tag{4.85}$$

The reduced set of fixed-interface state-normal modes consist of a number N_k of kept complex conjugate mode pairs, i.e.

$$\mathbf{X}_s^F = \begin{bmatrix} \boldsymbol{x}_1^F & \dots & \boldsymbol{x}_{2N_k}^F \end{bmatrix}_s \tag{4.86}$$

The set of state-constraint modes is obtained from the standard constraint modes. Constraint modes relate the displacement at the coupling interface DOFs to the displacement at all physical DOFs of the component, that is

$$\mathbf{u}_s = \begin{Bmatrix} \mathbf{u}_{i,s} \\ \mathbf{u}_{c,s} \end{Bmatrix} = \begin{bmatrix} -\mathbf{K}_{ii,s}^{-1}\mathbf{K}_{ic,s} \\ \mathbf{I}_{cc} \end{bmatrix} \mathbf{u}_{c,s} = \boldsymbol{\Psi}_s^C \mathbf{u}_{c,s} \tag{4.87}$$

Now, Morgan et al. made the observation that, since the constraint modes conform to a static transformation, they are time independent. Therefore, by differentiating the constraint modes relation in equation 4.87 with respect to time one obtains a constraint relation in terms of the velocity DOFs, i.e.

$$\dot{\mathbf{u}}_s = \frac{\partial}{\partial t}\left(\boldsymbol{\Psi}_s^C \mathbf{u}_{c,s}\right) = \boldsymbol{\Psi}_s^C \dot{\mathbf{u}}_{c,s} \tag{4.88}$$

Hence, a state-constraint relation may be posed as

$$\mathbf{x}_s = \begin{bmatrix} \boldsymbol{\Psi}^C & \mathbf{0} \\ \mathbf{0} & \boldsymbol{\Psi}^C \end{bmatrix}_s \begin{Bmatrix} \dot{\mathbf{u}}_c \\ \mathbf{u}_c \end{Bmatrix}_s = \boldsymbol{\Upsilon}_s^C \mathbf{x}_{c,s} \tag{4.89}$$

where $\boldsymbol{\Upsilon}_s^C = \mathrm{diag}(\boldsymbol{\Psi}_s^C \ \boldsymbol{\Psi}_s^C)$ is the set of constraint modes in the state-space, which is directly obtained from the standard constraint modes set $\boldsymbol{\Psi}_s^C$.

Component MCB state-modal reduction

Thus, the component modal reduction for the MCB method may be finally formulated in terms of the component-modal transformation state-matrix $\boldsymbol{\Upsilon}_s = [\mathbf{X}_s^F \ \boldsymbol{\Upsilon}_s^C]$, that is

$$\mathbf{x}_s = \begin{bmatrix} \mathbf{X}_{ik}^F & \boldsymbol{\Upsilon}_{ic}^C \\ \mathbf{0}_{ck} & \mathbf{I}_{cc} \end{bmatrix}_s \begin{Bmatrix} \mathbf{q}^F \\ \mathbf{x}_c \end{Bmatrix}_s = \boldsymbol{\Upsilon}_s \mathbf{y}_s \tag{4.90}$$

where the component-modal state-displacements $\mathbf{y}_s$ involve a reduced set of fixed-interface modal state-displacements $\mathbf{q}_s^F$ and the set of coupling state-displacements $\mathbf{x}_{c,s}$.

Accordingly, the component state-matrices may be reduced into component modal coordinates by pre and post-multiplying them with $\boldsymbol{\Upsilon}_s^T$ and $\boldsymbol{\Upsilon}_s$. Thence, the MCB component-modal state-matrices read

$$\mathbf{B}_s^y = \begin{bmatrix} \boldsymbol{\Lambda}_{kk}^F & \mathbf{B}_{kc}^y \\ \mathbf{B}_{ck}^y & \mathbf{B}_{cc}^y \end{bmatrix}_s \qquad \mathbf{A}_s^y = \begin{bmatrix} \mathbf{I}_{kk} & \mathbf{A}_{kc}^y \\ \mathbf{A}_{ck}^y & \mathbf{A}_{cc}^y \end{bmatrix}_s \tag{4.91}$$

with

$$\boldsymbol{\Lambda}_{kk,s}^F = \mathrm{diag}(\lambda_1^F, \ldots, \lambda_{1N_k}^F)$$

$$\mathbf{B}_{kc,s}^y = {\mathbf{X}_s^F}^T \mathbf{B}_s \boldsymbol{\Upsilon}_s^C = {\mathbf{B}_{ck}^y}^T \qquad \mathbf{A}_{kc,s}^y = {\mathbf{X}_s^F}^T \mathbf{A}_s \boldsymbol{\Upsilon}_s^C = {\mathbf{A}_{ck}^y}^T$$

$$\mathbf{B}_{cc,s}^y = {\boldsymbol{\Upsilon}_s^C}^T \mathbf{B}_s \boldsymbol{\Upsilon}_s^C \qquad \mathbf{A}_{cc,s}^y = {\boldsymbol{\Upsilon}_s^C}^T \mathbf{A}_s \boldsymbol{\Upsilon}_{kc}^C$$

As in the classic Craig-Bampton method, the modal partition of the reduced component-modal state-matrices are diagonal matrices. Assuming the state-normal modes to be $\mathbf{A}_s$-normalised, the diagonal entries of the $\boldsymbol{\Lambda}_{kk}^F$ sub-matrix correspond to the complex conjugate eigenvalue pairs of the EVP in equation 4.84. Accordingly, the modal partition in matrix $\mathbf{A}_s^y$ is just the identity matrix.

Moreover, analogous to the CB method, the coupling partitions $\mathbf{B}_{cc,s}^y$ and $\mathbf{A}_{cc,s}^y$ remain in state-space coordinates, which implies that the synthesis of state-modal components shall be performed through simple assembly of the reduced matrices.

Synthesis of MCB state-modal reduced components

Once the components have been reduced into component-modal state-coordinates one may proceed with the synthesis of components. For simplicity, the synthesis process is here specified for a system consisting of two components, namely component 1 and component 2.

The state-displacement continuity constraint, i.e. $\mathbf{x}_{c,1} = \mathbf{x}_{c,2}$, expressed in generalised component-modal state-coordinates yields the constraint equation $\boldsymbol{\mathcal{C}}^y\mathbf{y} = \mathbf{0}$. Explicitly, the constraint equation in the MCB method reads

$$\begin{bmatrix}\mathbf{0}_{ck,1} & \mathbf{I}_{cc,1} & -\mathbf{0}_{ck,2} & -\mathbf{I}_{cc,2}\end{bmatrix}\begin{Bmatrix}\mathbf{q}_1^F\\ \mathbf{x}_{c,1}\\ \mathbf{q}_2^F\\ \mathbf{x}_{c,2}\end{Bmatrix} = \mathbf{0} \tag{4.92}$$

where $\mathbf{x}_{c,2}$ is the set of dependent DOFs. Therefore, since $\boldsymbol{\mathcal{C}}_{dd}^y = -\mathbf{I}_{cc,2}$, the MCB synthesis transformation has explicit form

$$\mathbf{y} = \begin{Bmatrix}\mathbf{q}_1^F\\ \mathbf{x}_{c,1}\\ \mathbf{q}_2^F\\ \mathbf{x}_{c,2}\end{Bmatrix} = \begin{bmatrix}\mathbf{I} & \mathbf{0} & \mathbf{0}\\ \mathbf{0} & \mathbf{0} & \mathbf{I}\\ \mathbf{0} & \mathbf{I} & \mathbf{0}\\ \mathbf{0} & \mathbf{0} & \mathbf{I}\end{bmatrix}\begin{Bmatrix}\mathbf{q}_1^F\\ \mathbf{q}_2^F\\ \mathbf{x}_c\end{Bmatrix} = \mathbf{S}^z\mathbf{z} \tag{4.93}$$

By virtue of such a simple modal condensation matrix $\mathbf{S}^z$, the synthesis of components is straightforwardly implemented as the assembly of component-modal state-matrices. The generic computation of the coupled-modal state-matrices, i.e. $\mathbf{A}^z = \mathbf{S}^{zT}\mathbf{A}^y\mathbf{S}^z$ and $\mathbf{B}^z = \mathbf{S}^{zT}\mathbf{B}^y\mathbf{S}^z$, may be substituted with the easier and more efficient assembly of matrices as encountered in any finite element commercial software. For the two component system, the assembled coupled-modal state-matrices read

$$\mathbf{B}_s^z = \begin{bmatrix}\boldsymbol{\Lambda}_{kk,1}^F & \mathbf{0}_{kc} & \mathbf{B}_{kc,1}^y\\ \mathbf{0}_{ck} & \boldsymbol{\Lambda}_{kk,2}^F & \mathbf{B}_{kc,2}^y\\ \mathbf{B}_{ck,1}^y & \mathbf{B}_{ck,2}^y & \mathbf{B}_{cc,1}^y + \mathbf{B}_{cc,2}^y\end{bmatrix}_s \quad \mathbf{A}_s^z = \begin{bmatrix}\mathbf{I}_{kk,1} & \mathbf{0}_{kc} & \mathbf{A}_{kc,1}^y\\ \mathbf{0}_{ck} & \mathbf{I}_{kk,2} & \mathbf{A}_{kc,2}^y\\ \mathbf{A}_{ck,1}^y & \mathbf{A}_{ck,2}^y & \mathbf{A}_{cc,1}^y + \mathbf{A}_{cc,2}^y\end{bmatrix}_s \tag{4.94}$$

The state-modal reduced model in the MCB method consist of the coupled-modal state-equations of motion previously presented in equation 4.80 with the $\mathbf{A}^z$ and $\mathbf{B}^z$ matrices having the structure shown in equation 4.94.

In the MCB method, the coupled-modal state-coordinates involve a reduced set of modal DOFs, but also a large number of coupling-interface state-space DOFs. This is analogous to the classic CB method, where the ease of coupling comes at a price of non-optimally reduced coupled-model. However, in the state-space case the coupled-modal state-matrices are complex valued. So, when it comes to solve the reduced EVP corresponding to the coupled-modal state-equations of motion, the concurrence of complex matrices with a not-so-reduced order of the matrices may result in a significant computation cost for solving the reduced EVP.

Global modes MCB back-transformation

In any case, the global (damped) modes of the coupled system correspond to the complex conjugate eigensolution pairs $(\lambda_m, \boldsymbol{z}_m)$ and $(\lambda_m^*, \boldsymbol{z}_m^*)$ of the reduced coupled-modal state-EVP. The obtained eigenvectors $\boldsymbol{z}_m$, however, are in coupled-modal state-coordinates.

The global modes back-transformation performs the coordinate transformation $\mathbf{x} = \mathbf{T}^z\mathbf{z}$, where the $\mathbf{T}^z$ matrix may be obtained as $\mathbf{T}^z = \boldsymbol{\Upsilon}\mathbf{S}^z$ with $\boldsymbol{\Upsilon} = \mathbf{S}^{-1}\boldsymbol{\Upsilon}^y$. For the MCB method this results in

$$\mathbf{x} = \begin{Bmatrix} \mathbf{x}_{i,1} \\ \mathbf{x}_{i,2} \\ \mathbf{x}_c \end{Bmatrix} = \begin{bmatrix} \mathbf{I} & \mathbf{0} & \mathbf{0} & \mathbf{0} \\ \mathbf{0} & \mathbf{0} & \mathbf{I} & \mathbf{0} \\ \mathbf{0} & \frac{1}{2}\mathbf{I} & \mathbf{0} & \frac{1}{2}\mathbf{I} \end{bmatrix} \begin{bmatrix} \mathbf{X}_{I,1}^F & \boldsymbol{\Upsilon}_{I,1}^C & \mathbf{0} & \mathbf{0} \\ \mathbf{0} & \mathbf{I} & \mathbf{0} & \mathbf{0} \\ \mathbf{0} & \mathbf{0} & \mathbf{X}_{I,2}^F & \boldsymbol{\Upsilon}_{I,2}^C \\ \mathbf{0} & \mathbf{0} & \mathbf{0} & \mathbf{I} \end{bmatrix} \begin{bmatrix} \mathbf{I} & \mathbf{0} & \mathbf{0} \\ \mathbf{0} & \mathbf{0} & \mathbf{I} \\ \mathbf{0} & \mathbf{I} & \mathbf{0} \\ \mathbf{0} & \mathbf{0} & \mathbf{I} \end{bmatrix} \begin{Bmatrix} \mathbf{q}_1^F \\ \mathbf{q}_2^F \\ \mathbf{x}_c \end{Bmatrix} = \mathbf{T}^z\mathbf{z} \tag{4.95}$$

where the I subindex denotes interior partition of the state-normal modes $\mathbf{X}_s^F$ and state-constraint modes $\boldsymbol{\Upsilon}_s^C$ matrices. Hence, the $\mathbf{T}^z$ matrix results in the following compact expression

$$\mathbf{T}^z = \begin{bmatrix} \mathbf{X}_{ik,1}^F & \mathbf{0} & \boldsymbol{\Upsilon}_{ic,1}^C \\ \mathbf{0} & \mathbf{X}_{ik,2}^F & \boldsymbol{\Upsilon}_{ic,2}^C \\ \mathbf{0} & \mathbf{0} & \mathbf{I}_{cc} \end{bmatrix} \tag{4.96}$$

which may be efficiently obtained by assembly of the component-modal transformation state-matrices $\boldsymbol{\Upsilon}_s$. In order to obtain the global modes $\boldsymbol{\phi}_m$ in physical coordinates rather than the global modes $\boldsymbol{x}_m$ in state-space coordinates, the displacement partition of the $\mathbf{T}^z$ matrix shall be used, that is

$$\mathbf{T}_D^z = \begin{bmatrix} \boldsymbol{\Phi}_{ik,1}^F & \mathbf{0} & \boldsymbol{\Psi}_{ic,1}^C \\ \mathbf{0} & \boldsymbol{\Phi}_{ik,2}^F & \boldsymbol{\Psi}_{ic,2}^C \\ \mathbf{0} & \mathbf{0} & \mathbf{I}_{cc} \end{bmatrix} \tag{4.97}$$

with $\boldsymbol{\Phi}^F = \mathbf{X}^{D,F}$ and $\boldsymbol{\Psi}^C = \boldsymbol{\Upsilon}^{D,C}$ the displacement partitions of the state-normal modes and state-constraint modes respectively. Thus, the global modes are recovered through the $\boldsymbol{\phi}_m = \mathbf{T}_D^z\boldsymbol{z}_m$ transformation.

4.5.3 The Craig-Ni method

The Craig-Ni (CN) CMS method [13] for generally damped systems is also based on the state-space formulation. In this method, a state-space equivalent of the residual flexibility matrix is defined, so that residual attachment modes in the state-space

may be defined analogously to the standard residual attachment modes. Consequently, the CN method combines these residual state-attachment modes with free-interface state-normal modes, deriving in this way a consistent extension into the state-space formulation of the Craig-Chang (CCH) method.

CN component modes

In the Craig-Ni method, the modal reduction basis of each component s consist of a reduced set $\mathbf{X}_s$ of free-interface state-normal modes and a set $\boldsymbol{\Upsilon}_s^R$ of residual state-attachment modes.

The free-interface state-normal modes $\boldsymbol{x}_{k,s}$ may be computed from the eigenvalue problem corresponding to the full component state-space equations of motion. The component state-eigenvalue problem

$$\mathbf{B}_s \boldsymbol{x}_s = \lambda_s \mathbf{A}_s \boldsymbol{x}_s \tag{4.98}$$

has complex conjugate eigensolution pairs $(\lambda_s, \boldsymbol{x}_s)_k$ and $(\lambda_s^*, \boldsymbol{x}_s^*)_k$ corresponding to the k'th free-interface damped component mode. The reduced set of free-interface state-normal modes consist of a number N_k of kept complex conjugate mode pairs, i.e.

$$\mathbf{X}_s = \begin{bmatrix} \boldsymbol{x}_{1,s} & \dots & \boldsymbol{x}_{2N_k,s} \end{bmatrix} \tag{4.99}$$

The set of residual state-attachment modes is obtained from a state-space equivalent of the residual flexibility matrix. Component attachment modes relate the motion in the interior DOFs to the motion in the coupling interface DOFs when a unit force is applied at a coupling interface DOF and the remaining DOFs are force-free.

The forcing conditions for the state-attachment modes set may be expressed by means of a forcing matrix in the state-space $\mathbf{F}_{a,s}^x$,

$$\mathbf{F}_{a,s}^x = \begin{bmatrix} \mathbf{0}_{ia}^V \\ \mathbf{0}_{ca}^V \\ \mathbf{0}_{ia}^D \\ \mathbf{I}_{ca}^D \end{bmatrix}_s \tag{4.100}$$

where the V superscript indicates the *velocity* partition and the D superscript indicates the displacement partition of the state-space coordinates. The attachment modes definition supposes that forces are only applied in the displacement partition coupling DOFs.

Then, the residual state-attachment modes $\boldsymbol{\Upsilon}_s^R$ correspond to the solution of the set of static (residual) state-equations of motion

$$-\mathbf{B}_s^h \boldsymbol{\Upsilon}_s^R = \mathbf{F}_{a,s}^x$$

with $\mathbf{B}_s^h = \mathbf{X}_s^{h^T} \boldsymbol{\Lambda}_s^h \mathbf{X}_s^h$ the higher order modes contribution to the $\mathbf{B}_s$ state-matrix. Using the residual flexibility state-matrix $\mathbf{G}_s^{x,h}$ defined by Craig and Ni [13], the attachment modes are directly obtained as

$$\boldsymbol{\Upsilon}_s^R = \mathbf{G}_s^{x,h} \mathbf{F}_{a,s}^x. \tag{4.101}$$

The $\mathbf{G}_s^{x,h}$ matrix may be partitioned in terms of the interior i and attachment a DOFs of the velocity V and displacement D state-coordinates partitions, that is

$$\mathbf{G}_s^{x,h} = \begin{bmatrix} \mathbf{G}_{ii}^{VV} & \mathbf{G}_{ia}^{VV} & \mathbf{G}_{ii}^{VD} & \mathbf{G}_{ia}^{VD} \\ \mathbf{G}_{ai}^{VV} & \mathbf{G}_{aa}^{VV} & \mathbf{G}_{ai}^{VD} & \mathbf{G}_{aa}^{VD} \\ \mathbf{G}_{ii}^{DV} & \mathbf{G}_{ia}^{DV} & \mathbf{G}_{ii}^{DD} & \mathbf{G}_{ia}^{DD} \\ \mathbf{G}_{ai}^{DV} & \mathbf{G}_{aa}^{DV} & \mathbf{G}_{ai}^{DD} & \mathbf{G}_{aa}^{DD} \end{bmatrix}_s^{x,h} \tag{4.102}$$

Consequently, combining equations 4.100, 4.101 and 4.102, the set of residual state-attachment modes $\boldsymbol{\Upsilon}_s^R$ of component s is just partition of the $\mathbf{G}_s^{x,h}$ matrix, i.e.

$$\boldsymbol{\Upsilon}_s^R = \begin{bmatrix} \mathbf{G}_{ia}^{VD} \\ \mathbf{G}_{aa}^{VD} \\ \mathbf{G}_{ia}^{DD} \\ \mathbf{G}_{aa}^{DD} \end{bmatrix}_s^{x,h} \tag{4.103}$$

Before proceeding with the description of the CN method itself, explicit derivation of the $\mathbf{G}_s^{x,h}$ matrix is presented next.

The residual flexibility state-matrix

The flexibility state-matrix may be defined from the "static" state-equations of motion

$$-\mathbf{B}_s \mathbf{x}_s = \mathbf{f}_s^x \tag{4.104}$$

of a component s. The component flexibility state-matrix $\mathbf{G}_s^x$ must be such that $\mathbf{x}_s = \mathbf{G}_s^x \mathbf{f}_s^x$ holds. Hence, it is defined as minus the inverse of the component's $\mathbf{B}_s$ state-matrix, that is

$$\mathbf{G}_s^x = -\mathbf{B}_s^{-1} = \begin{bmatrix} -\mathbf{M}^{-1} & \mathbf{0} \\ \mathbf{0} & \mathbf{K}^{-1} \end{bmatrix}_s \tag{4.105}$$

Then, the residual flexibility state-matrix $\mathbf{G}_s^{x,h}$ is obtained by subtracting the contribution of the kept free-interface state-normal modes from the flexibility state-matrix $\mathbf{G}_s^x$. This may be done in an analogous way as for the standard flexibility matrix defined in section 4.1.1, that is

$$\mathbf{G}_s^{x,h} = \mathbf{G}_s^x - \mathbf{X}_s \mathbf{\Lambda}_s^{-1} \mathbf{X}_s^T \tag{4.106}$$

The residual attachment modes correspond to the pertinent partition of this $\mathbf{G}_s^{x,h}$ matrix.

In the case that the component is not constrained, it will be subject to rigid body motion and, consequently the $\mathbf{K}_s$ matrix will be singular and non-invertible. To overcome this problem, the inertia relief method that has been explained in section 4.1.1 was formulated in the state space. The inertia relief projection may be defined in the state-space as

$$\mathbf{P}_s^x = \mathbf{I} - \mathbf{A}_s \mathbf{X}_{r,s} \mathbf{X}_{r,s}^T \tag{4.107}$$

where $\mathbf{X}_{r,s}$ is the set of ($\mathbf{A}_s$-normalised) rigid-body state-component modes. In a separate article [92] Craig and Ni defined the set of generalised rigid body modes in the state-space as

$$\mathbf{X}_{r,s} = \begin{bmatrix} \mathbf{\Phi}_r & \mathbf{0} \\ \mathbf{0} & \mathbf{\Phi}_r \end{bmatrix}_s \tag{4.108}$$

with $\mathbf{\Phi}_{r,s}$ the set of physical domain rigid body modes accomplishing $\mathbf{K}_s \mathbf{\Phi}_{r,s} = \mathbf{0}$. Hence, the flexibility state-matrix $\mathbf{G}_s^x$ may be obtained by pre and post multiplying a pseudo-flexibility state-matrix with the inertia relief projector $\mathbf{P}_s^x$, i.e.

$$\mathbf{G}_s^x = \mathbf{P}_s^{xT} \begin{bmatrix} -\mathbf{M}^{-1} & \mathbf{0} \\ \mathbf{0} & \mathbf{G}' \end{bmatrix}_s \mathbf{P}_s^x \tag{4.109}$$

with $\mathbf{G}'$ the pseudo-flexibility matrix as defined in section 4.1.1.

Component CN state-modal reduction

The component modal reduction for the CN method may be formulated in terms of the component-modal transformation state-matrix $\mathbf{\Upsilon}_s = [\mathbf{X}_s \ \mathbf{\Upsilon}_s^R]$, that is

$$\mathbf{x}_s = \begin{Bmatrix} \mathbf{x}_i \\ \mathbf{x}_c \end{Bmatrix}_s = \begin{bmatrix} \mathbf{X}_{ik} & \mathbf{\Upsilon}_{ia}^R \\ \mathbf{X}_{ck} & \mathbf{\Upsilon}_{ca}^R \end{bmatrix}_s \begin{Bmatrix} \mathbf{q} \\ \mathbf{y}_a \end{Bmatrix}_s = \mathbf{\Upsilon}_s \mathbf{y}_s \tag{4.110}$$

where the component-modal state-displacements $\mathbf{y}_s$ involve a reduced set of modal state-displacements $\mathbf{q}_s$ and the set of attachment displacements $\mathbf{y}_{a,s}$.

The attachment coordinates correspond to the same FE nodes as the state-space coupling interfaces coordinates. However, from equation 4.110 it is evident that the attachment displacement $\mathbf{y}_{a,s}$ do not equal the coupling interface state-displacements $\mathbf{x}_{c,s}$. In fact, the attachment coordinates have as many DOFs as physical displacement DOFs at the component coupling interface (i.e. $\mathbf{y}_{a,s}$ has half the number of DOFs than $\mathbf{x}_{c,s}$). Thence, the coupling interface state-coordinates are not equivalent to the attachment coordinates.

Here, it is convenient to make a clear distinction between the velocity and the displacement DOFs in the coupling interface state-coordinates. Velocity V and displacement D partitions have already been used for the definition of the residual state-attachment modes, and they are recurrently used in the formulation of the CN method. The component modal transformation for the coupling interface state-displacements $\mathbf{x}_{c,s}$ is specified in the lower row of equation 4.110. This lower row may be decomposed into the velocity and displacement partitions as

$$\mathbf{x}_{c,s} = \begin{Bmatrix} \dot{\mathbf{u}}_c \\ \mathbf{u}_c \end{Bmatrix}_s = \begin{bmatrix} \mathbf{X}_{ck}^{V} & \boldsymbol{\Upsilon}_{ca}^{V,R} \\ \mathbf{X}_{ck}^{D} & \boldsymbol{\Upsilon}_{ca}^{D,R} \end{bmatrix}_s \begin{Bmatrix} \mathbf{q} \\ \mathbf{y}_a \end{Bmatrix}_s \tag{4.111}$$

In the following, the coupling-displacement partitions $\mathbf{X}_{ck,s}^{D}$ and $\boldsymbol{\Upsilon}_{ca,s}^{D,R}$ appear frequently in the component state-matrices reduction and synthesis processes. For this reason they are made explicit in equation 4.111.

The component state-matrices reduced into component modal coordinates are obtained by pre and post-multiplying them with $\boldsymbol{\Upsilon}_s^T$ and $\boldsymbol{\Upsilon}_s$.In the CN method these read

$$\mathbf{B}_s^y = \begin{bmatrix} \bar{\mathbf{B}}_{kk} & \mathbf{0}_{ka} \\ \mathbf{0}_{ak} & \mathbf{B}_{aa}^y \end{bmatrix}_s \qquad \mathbf{A}_s^y = \begin{bmatrix} \bar{\mathbf{A}}_{kk} & \mathbf{0}_{ka} \\ \mathbf{0}_{ak} & \mathbf{A}_{aa}^y \end{bmatrix}_s \tag{4.112}$$

with

$$\bar{\mathbf{B}}_{kk,s} = \mathbf{X}_s^T \mathbf{B}_s \mathbf{X}_s \qquad \bar{\mathbf{A}}_{kk,s} = \mathbf{X}_s^T \mathbf{A}_s \mathbf{X}_s$$

$$\mathbf{B}_{aa,s}^y = \boldsymbol{\Upsilon}_s^{R^T} \mathbf{B}_s \boldsymbol{\Upsilon}_s^R = -\boldsymbol{\Upsilon}_{ca,s}^{D,R} \qquad \mathbf{A}_{aa,s}^y = \boldsymbol{\Upsilon}_s^{R^T} \mathbf{A}_s \boldsymbol{\Upsilon}_s^R$$

Since the residual flexibility state-matrix is a flexibility matrix from which the contribution of the kept free-interface state-normal modes has been removed, the residual state-attachment modes $\boldsymbol{\Upsilon}_s^R$ are linearly independent to the free-interface state-normal modes $\mathbf{X}_s$ (including rigid body modes). Consequently, the component state-matrices partitions corresponding to modal to attachment coordinates coupling are zero-valued matrices.

The $\bar{\mathbf{B}}_{kk,s}$ and $\bar{\mathbf{A}}_{kk,s}$ sub-matrices are modal matrices which in general are not diagonal, but have Jordan form due to repeated rigid body zero-valued eigenvalues. Assuming that the free-interface normal modes are $\mathbf{A}_s$-normalised, the diagonal entries of $\bar{\mathbf{B}}_{kk,s}$ contain the eigenvalues of the component, and the diagonal entries of $\bar{\mathbf{A}}_{kk,s}$ equal unity. Moreover, the $\mathbf{B}^y_{aa,s}$ sub-matrix is of special form. It may be demonstrated[3] that it is equivalent to minus the coupling-displacement partition of the residual attachment modes matrix $\boldsymbol{\Upsilon}^R_s$.

Attachment pseudo-static approximation

As in the Craig-Chang method for undamped systems, the Craig-Ni method component modal state-matrices in equation 4.112 present zero-valued partitions. This implies that the attachment DOFs are linearly independent with respect to the free-interface normal-modal DOFs. Therefore, the component-modal state-equations of motion for the attachment coordinates subset may be formulated separately, i.e.

$$\mathbf{A}^y_{aa,s}\dot{\mathbf{y}}_{a,s} - \mathbf{B}^y_{aa,s}\mathbf{y}_{a,s} = \boldsymbol{\Upsilon}^{R\ T}_{ca,s}\mathbf{f}^x_{c,s} \tag{4.113}$$

In view of the fact that the velocity DOFs are always force-free, the right hand side in equation 4.113 may be simply expressed in physical coordinates, i.e.

$$\boldsymbol{\Upsilon}^{R\ T}_{ca,s}\mathbf{f}^x_{c,s} = \boldsymbol{\Upsilon}^{D,R^T}_{ca,s}\mathbf{f}_{c,s}$$

Then, since $\mathbf{B}^y_{aa,s} = -\boldsymbol{\Upsilon}^{D,R}_{ca,s}$ is a symmetric matrix, the component *static* equations of motion for the coupling-displacement DOFs read

$$\boldsymbol{\Upsilon}^{D,R}_{ca,s}\mathbf{y}_{a,s} = \boldsymbol{\Upsilon}^{D,R}_{ca,s}\mathbf{f}_{c,s} \tag{4.114}$$

From this last equation, and regarding that $\boldsymbol{\Upsilon}^{D,R}_{ca,s}$ is a non-singular matrix, a pseudo-static approximation for the state-attachment displacements $\mathbf{y}_{a,s}$ can be established as

$$\mathbf{y}_{a,s} = \mathbf{f}_{c,s} \tag{4.115}$$

Synthesis of CN state-modal reduced components

The synthesis of components in the Craig-Ni method is performed by enforcing the coupling constraints on the component modal displacements. Both the displacement

[3] The $\boldsymbol{\Upsilon}^{R^T}_s\mathbf{B}_s\boldsymbol{\Upsilon}^R_s$ product may be understood as a partition of a more general matrix product $\mathbf{G}^{x,h^T}_s\mathbf{B}_s\mathbf{G}^{x,h}_s = -\mathbf{G}^{x,h^T}_s$. The corresponding partition is $-[\mathbf{G}^{DD}_{aa}]^{x,h^T}_s = -[\mathbf{G}^{DD}_{aa}]^{x,h}_s = -\boldsymbol{\Upsilon}^{D,R}_{ca,s}$.

continuity condition and the force equilibrium condition at the coupling interfaces may be applied to modal displacements by virtue of the attachment pseudo-static approximation. As in the MCB method, the synthesis process is specified next for a two components system.

Consider a system with two components, namely component 1 and component 2, that share a common coupling interface. By using the displacement partition D in the bottom row of equation 4.111, the displacement continuity constraint $\mathbf{u}_{c,1} = \mathbf{u}_{c,2}$ may be expressed in component modal coordinates as

$$\mathbf{X}^{D}_{ck,1}\mathbf{q}_1 + \boldsymbol{\Upsilon}^{D,R}_{ca,1}\mathbf{y}_{a,1} = \mathbf{X}^{D}_{ck,2}\mathbf{q}_2 + \boldsymbol{\Upsilon}^{D,R}_{ca,2}\mathbf{y}_{a,2} \tag{4.116}$$

The force equilibrium constraint $\mathbf{f}_{c,1} + \mathbf{f}_{c,2} = 0$ in terms of the attachment displacements is straightforwardly formulated from the attachment pseudo-static approximation, that is

$$\mathbf{y}_{a,1} + \mathbf{y}_{a,2} = 0 \tag{4.117}$$

Thus, the two coupling constraints may be unified in a single constraint equation $\boldsymbol{\mathcal{C}}^{y}\mathbf{y} = \mathbf{0}$ in component modal coordinates. The explicit constraint equation for the two components system is

$$\begin{bmatrix} \mathbf{0}_{ck} & \mathbf{I}_{ca} & \mathbf{0}_{ck} & \mathbf{I}_{ca} \\ \mathbf{X}^{D}_{ck,1} & \boldsymbol{\Upsilon}^{D,R}_{ca,1} & -\mathbf{X}^{D}_{ck,2} & -\boldsymbol{\Upsilon}^{D,R}_{ca,2} \end{bmatrix} \begin{Bmatrix} \mathbf{q}_1 \\ \mathbf{y}_{a,1} \\ \mathbf{q}_2 \\ \mathbf{y}_{a,2} \end{Bmatrix} = \mathbf{0} \tag{4.118}$$

where the upper row corresponds to force equilibrium and the bottom row to displacement continuity[4]. The component attachment coordinates form a linearly dependent set with respect to the set of component free-interface modal coordinates, so that the constraint equation may be rewritten as

$$\boldsymbol{\mathcal{C}}^{y}_{dl}\mathbf{y}_l + \boldsymbol{\mathcal{C}}^{y}_{dd}\mathbf{y}_d = \begin{bmatrix} \mathbf{0}_{ck} & \mathbf{0}_{ck} \\ \mathbf{X}^{D}_{ck,1} & -\mathbf{X}^{D}_{ck,2} \end{bmatrix} \begin{Bmatrix} \mathbf{q}_1 \\ \mathbf{q}_2 \end{Bmatrix} + \begin{bmatrix} \mathbf{I}_{ca} & \mathbf{I}_{ca} \\ \boldsymbol{\Upsilon}^{D,R}_{ca,1} & -\boldsymbol{\Upsilon}^{D,R}_{ca,2} \end{bmatrix} \begin{Bmatrix} \mathbf{y}_{a,1} \\ \mathbf{y}_{a,2} \end{Bmatrix} = \mathbf{0} \tag{4.119}$$

Therefore, from the constraint equation, the modal condensation matrix $\mathbf{S}^{z}$ may be formulated as in equation 4.79 giving rise to the synthesis transformation

$$\mathbf{y} = \begin{Bmatrix} \mathbf{q}_1 \\ \mathbf{y}_{a,1} \\ \mathbf{q}_2 \\ \mathbf{y}_{a,2} \end{Bmatrix} = \begin{bmatrix} \mathbf{I} & \mathbf{0} \\ -\mathbf{Y}\mathbf{X}^{D}_{ck,1} & \mathbf{Y}\mathbf{X}^{D}_{ck,2} \\ \mathbf{0} & \mathbf{I} \\ \mathbf{Y}\mathbf{X}^{D}_{ck,1} & -\mathbf{Y}\mathbf{X}^{D}_{ck,2} \end{bmatrix} \begin{Bmatrix} \mathbf{q}_1 \\ \mathbf{q}_2 \end{Bmatrix} = \mathbf{S}^{z}\mathbf{z} \tag{4.120}$$

[4]Generally, for multiple component systems, coupling DOFs may appertain to several components. Then, the constraint equation involves 1 force equilibrium equation and $N_c - 1$ displacement continuity equations for each coupling DOF connecting N_c components.

with $\mathbf{Y} = \left(\boldsymbol{\Upsilon}_{ca,1}^{D,R} + \boldsymbol{\Upsilon}_{ca,2}^{D,R}\right)^{-1}$.

The coupled modal state-matrices are finally obtained by applying the synthesis transformation, i.e. $\mathbf{A}^z = \mathbf{S}^{zT}\mathbf{A}^y\mathbf{S}^z$ and $\mathbf{B}^z = \mathbf{S}^{zT}\mathbf{B}^y\mathbf{S}^z$. Using the modal condensation matrix in equation 4.120, the CN method coupled modal state-matrices read

$$\mathbf{B}^z = \begin{bmatrix} \bar{\mathbf{B}}_{kk,1} & \mathbf{0} \\ \mathbf{0} & \bar{\mathbf{B}}_{kk,2} \end{bmatrix} + \begin{bmatrix} \mathbf{B}_{11}^R & \mathbf{B}_{12}^R \\ \mathbf{B}_{21}^R & \mathbf{B}_{22}^R \end{bmatrix} \qquad \mathbf{A}^z = \begin{bmatrix} \bar{\mathbf{A}}_{kk,1} & \mathbf{0} \\ \mathbf{0} & \bar{\mathbf{A}}_{kk,2} \end{bmatrix} + \begin{bmatrix} \mathbf{A}_{11}^R & \mathbf{A}_{12}^R \\ \mathbf{A}_{21}^R & \mathbf{A}_{22}^R \end{bmatrix} \tag{4.121}$$

$$\text{with} \qquad \begin{aligned} \mathbf{B}_{st}^R &= {\mathbf{X}_{ck,s}^D}^T \mathbf{Y}^T (\mathbf{B}_{aa,1}^y + \mathbf{B}_{aa,2}^y) \mathbf{Y} \mathbf{X}_{ck,t}^D \\ \mathbf{A}_{st}^R &= {\mathbf{X}_{ck,s}^D}^T \mathbf{Y}^T (\mathbf{A}_{aa,1}^y + \mathbf{A}_{aa,2}^y) \mathbf{Y} \mathbf{X}_{ck,t}^D \end{aligned}$$

Hence, the coupled-modal state-matrices are composed of the sum of two matrices, i.e. $\mathbf{B}^z = \bar{\mathbf{B}}_{kk} + \mathbf{B}_{kk}^R$ and $\mathbf{A}^z = \bar{\mathbf{A}}_{kk} + \mathbf{A}_{kk}^R$. The $\bar{\mathbf{B}}_{kk}$ and $\bar{\mathbf{A}}_{kk}$ matrices are block diagonal matrices containing the free-interface modal matrices of all components. The $\mathbf{B}_{kk}^R$ and $\mathbf{A}_{kk}^R$ matrices correspond to the condensation into coupled-modal coordinates of the component modal state-matrices (residual) attachment DOFs.

Thus, in the CN method, the coupled-modal state-matrices are reduced into a set of coordinates that involve only the component free interface modal DOFs. This is analogous to the standard Craig-Chang method but with double the amount of modal DOFs, since the damped eigensolutions come in complex conjugate pairs. Additionally, the coupled-modal state-matrices are complex valued, which shall make the solution of the full system EVP in coupled-modal coordinates less cost-efficient. In any case, the CN yields a coupled-modal model of optimally reduced order. On the contrary, the computation of the reduced coupled-modal model is not systematic as in the MCB method. Therefore, much more computational effort is required for constructing the CN coupled-modal state-matrices.

Global modes back-transformation

The global (damped) modes of the coupled system correspond to the complex conjugate eigensolution pairs $(\lambda_m, \boldsymbol{z}_m)$ and $(\lambda_m^*, \boldsymbol{z}_m^*)$ of the reduced coupled-modal state-EVP. The $\boldsymbol{z}_m$ eigenvectors, however, are in coupled-modal state-coordinates.

The global modes back-transformation performs the coordinate transformation $\mathbf{x} = \mathbf{T}^z\mathbf{z}$, where the $\mathbf{T}^z$ matrix may be obtained as $\mathbf{T}^z = \boldsymbol{\Upsilon}\mathbf{S}^z$ with $\boldsymbol{\Upsilon} = \mathbf{S}^{-1}\boldsymbol{\Upsilon}^y$. For

the CN method the $\mathbf{T}^z$ matrix reads

$$\mathbf{T}^z = \begin{bmatrix} \mathbf{X}_{ik,1} & \mathbf{0} \\ \mathbf{0} & \mathbf{X}_{ik,2} \\ \frac{1}{2}\mathbf{X}_{ck,1} & \frac{1}{2}\mathbf{X}_{ck,2} \end{bmatrix} + \begin{bmatrix} -\mathbf{T}^R_{ik,11} & \mathbf{T}^R_{ik,12} \\ \mathbf{T}^R_{ik,21} & -\mathbf{T}^R_{ik,22} \\ \frac{1}{2}(-\mathbf{T}^R_{ck,11} + \mathbf{T}^R_{ck,21}) & \frac{1}{2}(\mathbf{T}^R_{ck,12} - \mathbf{T}^R_{ck,22}) \end{bmatrix} \tag{4.122}$$

$$\text{with} \qquad \mathbf{T}^R_{ik,st} = \boldsymbol{\Upsilon}^R_{ia,s}\mathbf{Y}\mathbf{X}^D_{ck,t} \qquad \mathbf{T}^R_{ck,st} = \boldsymbol{\Upsilon}^R_{ca,s}\mathbf{Y}\mathbf{X}^D_{ck,t}$$

In order to obtain the global modes $\boldsymbol{\phi}_m$ in physical coordinates rather than the global modes $\boldsymbol{x}_m$ in state-space coordinates, the displacement partition of the $\mathbf{T}^z$ matrix shall be used, that is

$$\mathbf{T}^z_D = \begin{bmatrix} \boldsymbol{\Phi}_{ik,1} & \mathbf{0} \\ \mathbf{0} & \boldsymbol{\Phi}_{ik,2} \\ \frac{1}{2}\boldsymbol{\Phi}_{ck,1} & \frac{1}{2}\boldsymbol{\Phi}_{ck,2} \end{bmatrix} + \begin{bmatrix} -\mathbf{T}^{D,R}_{ik,11} & \mathbf{T}^{D,R}_{ik,12} \\ \mathbf{T}^{D,R}_{ik,21} & -\mathbf{T}^{D,R}_{ik,22} \\ \frac{1}{2}(-\mathbf{T}^{D,R}_{ck,11} + \mathbf{T}^{D,R}_{ck,21}) & \frac{1}{2}(\mathbf{T}^{D,R}_{ck,12} - \mathbf{T}^{D,R}_{ck,22}) \end{bmatrix} \tag{4.123}$$

$$\text{with} \qquad \mathbf{T}^{D,R}_{ik,st} = \boldsymbol{\Upsilon}^{D,R}_{ia,s}\mathbf{Y}\boldsymbol{\Phi}_{ck,t} \qquad \mathbf{T}^{D,R}_{ck,st} = \boldsymbol{\Upsilon}^{D,R}_{ca,s}\mathbf{Y}\boldsymbol{\Phi}_{ck,t}$$

with $\boldsymbol{\Phi}_s = \mathbf{X}^D_s$ the component normal modes in physical coordinates. Thus, the global modes are recovered through the $\boldsymbol{\phi}_m = \mathbf{T}^z_D\boldsymbol{z}_m$ transformation.

4.6 Numerical Validation of Component Mode Synthesis methods

Up to this point, different Component Mode Synthesis methods have been presented. The Craig-Bampton (fixed-interface with contraint modes) and the Craig-Chang (free-interface with residual attachment modes) classical methods have been explained and their pros and cons have been outlined. Yet, since it is aimed in this work to introduce Component Mode Synthesis for the modelling of *damped systems*, CMS methods for general damped systems based on the state-space formulation have been revisited. It is now time to validate the usefulness of these latter CMS methods.

In this section, the accuracy of the different CMS methods is evaluated through numerical examples. The modal solutions of finite element models for two test problems will be computed using Component Mode Synthesis and compared to the exact modal solutions. The accuracy gain when using state-space based CMS methods is evaluated by comparing the resulting modal solution error to that of the classical CMS methods.

On the other hand, finding eigensolutions from the equations of motion posed in the state-space presents some numerical challenges. Some practical issues that arise when computing the component and the global modes in the state-space will be addressed here. Moreover, the numerical complexity of the CMS methods will be evaluated in terms of the computation time for performing the Component Mode Synthesis solution.

4.6.1 Example 1: A damped cantilever

The first example is a damped cantilever beam with uniform cross section, shown in figure 4.2, which is modelled using 2-noded *beam bending elements*[5] with 2 degrees of freedom per node (i.e. transverse displacement z and rotation θ_y).

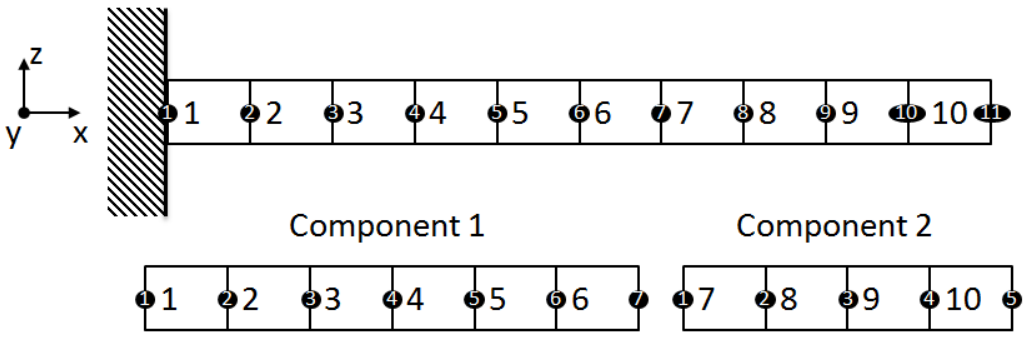

Figure 4.2: Uniform cantilever beam example having ten elements with $\frac{EI}{\rho A L_e^4} = 1$, and description of its substructuring into two components.

The cantilever beam model consists of ten elements, which give rise to a system with 20 unconstrained degrees of freedom (40 DOFs in state-space form). The model is split into two components: component 1 comprising elements 1 to 6, and component 2 comprising elements 7 to 10. Thus, component 1 has 12 DOFs (24 state-space DOFs) and component 2 has 10 DOFs (20 state-space DOFs), and they have a 2 DOFs redundant coupling interface.

The beam's dynamic properties are described by each element's constant parameters satisfying

$$\frac{EI}{\rho A L_e^4} = 1 \tag{4.124}$$

[5]The beam bending element complies with the Euler-Bernouilli beam theory and its description may be found in [1], which has been coded into MATLAB.

with E the elastic modulus, I the second moment of area of the beam's cross section A about the y axis, ρ the mass density and L_e the beam element's length. Damping properties are described by each element damping matrix $\mathbf{C}_e$ being proportional to the corresponding element stiffness matrix $\mathbf{K}_e$. Note that this does not imply that either the beam or the components are proportionally damped unless all of the elements' proportionality factors coincide. This way of describing the general damped beam properties has been recurrently used as a test problem for damped component mode synthesis validation[6].

In the present example, all elements possess the same damping proportionality factor except for elements 5 and 8, which have a ten times bigger proportionality factor. In this way the cantilever beam as well as each of the components show a locally heavily damped characteristic, as if (massless) damping patches were placed on elements 5 and 8.

Here, the first 10 modes of the full system have been computed for different levels of system damping. The full system eigenvalue problem in the state-space is initially solved and is regarded as the *exact* solution. Then the same 10 modes are computed using the CMS methods explained in the previous section, namely the Craig-Bampton (CB), the Craig-Chang (CCH), the Morgan-Craig-Bampton (MCB) and the Craig-Ni (CN) methods. The former two are CMS methods based on undamped component modes whereas the latter are state-space CMS methods based on damped component modes.

The component modes computed in each CMS method are summarised in Table 4.1. The same number of (elastic) vibration modes is computed in all methods, 8 modes for component 1 and 5 modes for component 2, so that their performance may be compared under equal conditions. For the CMS methods using free-interface normal modes (i.e. the CCH and the CN methods), component 2 shows rigid body freedom, therefore two extra rigid body modes need to be computed. In the case of the state-space based methods (i.e. the MCB and the CN methods), the number of normal modes to be computed is doubled since each vibration mode is characterised by a complex conjugate pair of eigensolutions. Notice as well that double number of state-space constraint modes are needed in the MCB method (i.e. for the displacement and for the velocity coupling DOFs), whereas this is not the case for state-space residual attachment modes in the CN method.

[6] A free-free beam example defined in this way was evaluated in [13, 93, 94]). The present work implementation of the Craig-Ni method has been tested against the free-free beam example in [13] yielding identical results.

	Component 1				Component 2			
	CB	CHH	MCB	CN	CB	CHH	MCB	CN
Elastic modes	8	8	8×2	8×2	5	5	5×2	5×2
Rigid body modes	-	-	-	-	-	2	-	2×2
Constraint modes	2	-	4	-	2	-	4	-
Attachment modes	-	2	-	2	-	2	-	2
Total component modes	10	10	20	18	7	9	14	16

Table 4.1: Number of component modes computed for the damped cantilever example.

In the following, the first 10 modes of the damped cantilever computed through CMS methods will be evaluated for two different damping conditions.

Lightly damped cantilever

First of all, the cantilever modes are computed for the cantilever being lightly damped. The damping distribution over the beam is as described previously, with element damping being $\mathbf{C}_e = 0.05\mathbf{K}_e$ for elements 5 and 8 and $\mathbf{C}_e = 0.005\mathbf{K}_e$ for the remaining elements.

Figure 4.3 shows the resulting damped modal frequencies for the first ten modes and, likewise, Figure 4.4 shows the resulting modal damping ratios. On the left hand side plots, a solid black line indicates the exact values for the damped modal frequencies and modal damping ratios. The corresponding results obtained through Component Modes Synthesis are overlayed. On the right hand side plots the relative error between each of the CMS methods (CB, CCH, MCB and CN) and the exact modal values is shown in a logarithmic scale.

It can be seen in Figure 4.3 that the modal frequency results for all CMS methods practically coincide with the exact modal frequency solution. Since the system is lightly damped, the system damping hardly influences the values of the modal frequencies, so that the damped modal frequencies are almost equal to the undamped modal frequencies. Consequently, modal frequencies are accurately estimated through all of the CMS methods considered (damped or undamped), with all modal frequency errors below 1%. Yet, it can be noted from the error plot that the state-space based CMS methods (in dashed lines) show relative error values around an order of magnitude smaller than the classical CMS methods (in dotted lines). It can also be observed from the error plot that, for all CMS methods, the relative errors increase as the modal frequency values rise. This is consistent with the fact

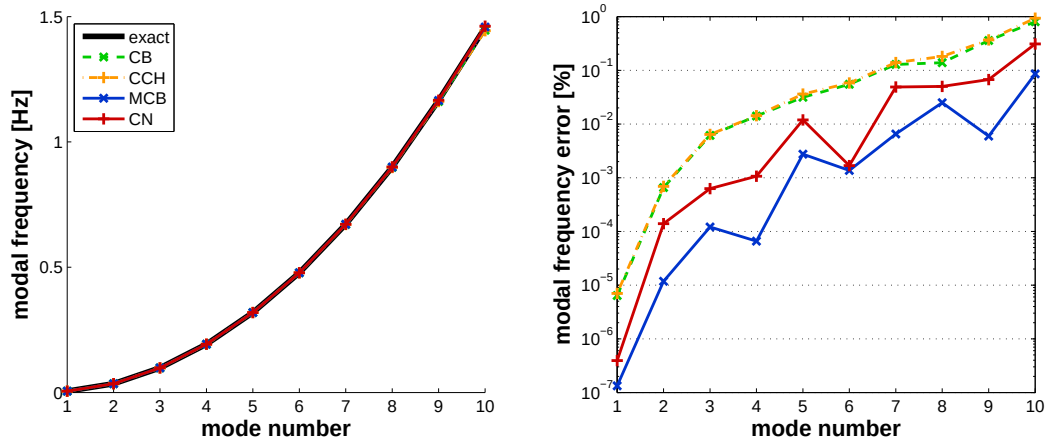

Figure 4.3: Damped modal frequency for the first 10 modes of the lightly damped cantilever, and relative error in the CMS-computed damped modal frequencies.

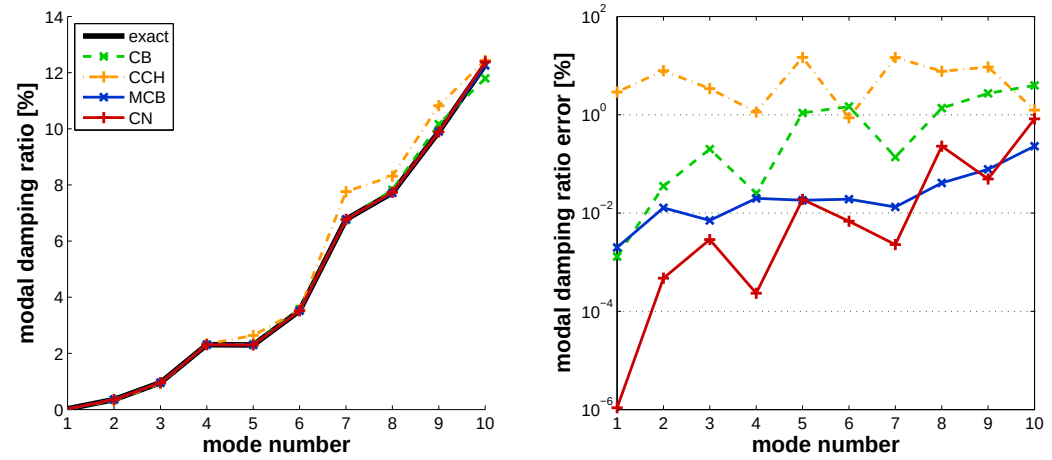

Figure 4.4: Modal damping for the first 10 modes of the lightly damped cantilever, and relative error in the CMS-computed modal damping ratios.

that both the constraint and the residual attachment modes represent static corrections for the contribution of higher order modes. Recall that static correction is less accurate as the modal frequency values fall further away from zero, thus yielding increased modal frequency errors.

On the other hand, as can be observed in Figure 4.4, not all damping ratio values obtained through the CMS methods match the exact solution. Whereas the modal damping values obtained through state-space based CMS methods do coincide with the exact solution, several of the modal damping values obtained from the classical CB and CCH methods show significant deviation. In these latter methods, the modal damping is estimated a-posteriori from the undamped system modes (c.f.

small damping approximation in chapter 2). Since the system is non-classically damped, the undamped mode shape vectors do not diagonalise the damping matrix so that modal damping is incorrectly estimated. Modal damping error values for the undamped CMS methods lie around the 1% to 10% error range. In contrast, modal damping ratio estimates through state-space based CMS methods present errors well below 1%.

In view of these results it can be concluded that, when computing the vibration modes of locally (i.e. non-classically) damped systems, the Morgan-Craig-Bampton and the Craig-Ni methods are significantly more precise than their classical counterparts, the Craig-Bampton and the Craig-Chang methods respectively. Yet, for low modal damping values, the CB and CCH modal frequency predictions may be considered accurate enough since they show errors below 1%. On the contrary, errors in modal damping obtained through undamped CMS methods are significant. Therefore, the use of the state-space based CMS methods implies a sensible gain in accuracy when estimating modal damping values.

Heavily damped cantilever

A second evaluation of the locally damped cantilever modes is considered here for increased values of the system damping. In this case, the element damping matrices are $\mathbf{C}_e = 0.2\mathbf{K}_e$ for elements 5 and 8 and $\mathbf{C}_e = 0.02\mathbf{K}_e$ for the remaining elements. This supposes the same distribution of damping but with four times more overall damping, so that the system becomes heavily damped (i.e. with modal damping values exceeding 20% modal damping ratio for modes 7 to 10).

The first 10 modes of the heavily damped cantilever have been computed using the four CMS methods considered (CB, CCH, MCB and CN). The resulting damped modal frequency and modal damping ratio values are presented in Figures 4.5 and 4.6 respectively, together with the relative error with respect to the exact solution.

Starting with the modal damping results in Figure 4.6, the most noticeable fact is that for the modes which are largely damped, in this case modes 7 to 10 show modal damping between 25% and 35% damping ratio, the estimation error of the classical CMS methods is very large, with relative error values exceeding 40% error in the 10th mode. Conversely, state-space CMS methods estimate modal damping with very good accuracy for all modes with errors in modal damping below 1% of the ratio value. For the first 6 modes, which are not so highly damped, the modal damping error does not seem to be so excessive when looking at the absolute

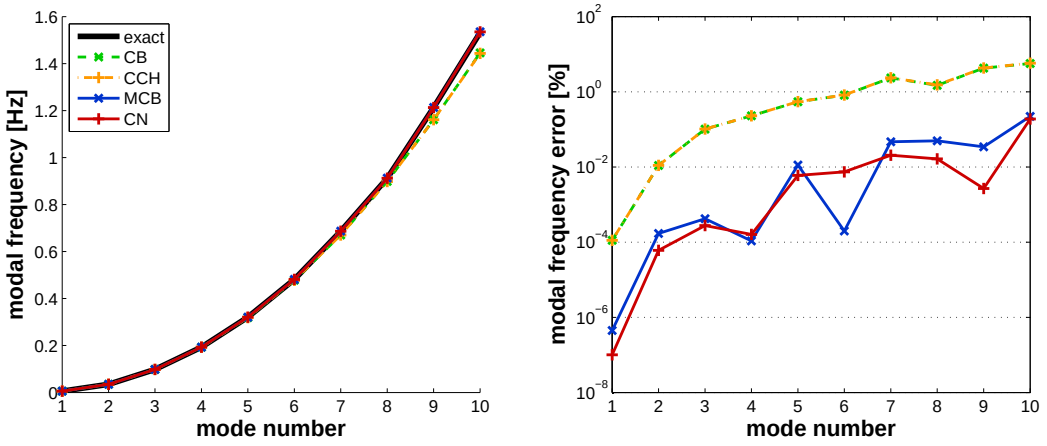

Figure 4.5: Damped modal frequency for the first 10 modes of the heavily damped cantilever, and relative error in the CMS-computed damped modal frequencies.

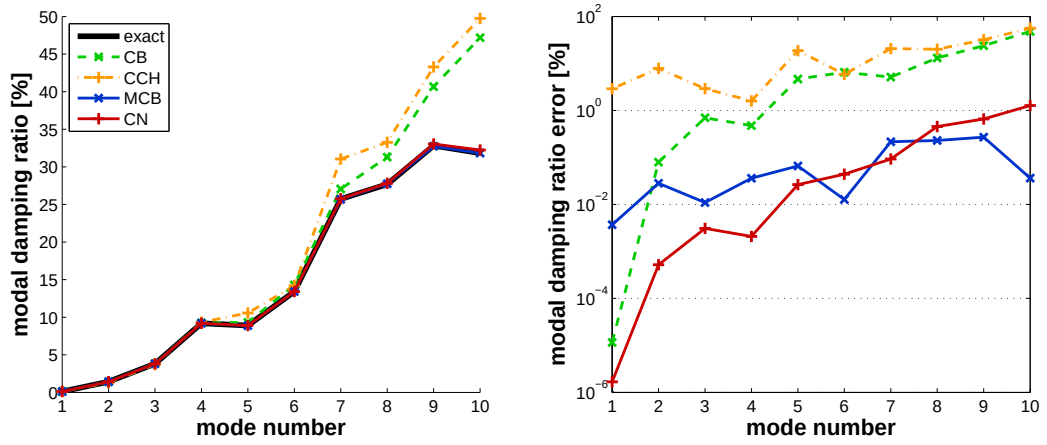

Figure 4.6: Modal damping for the first 10 modes of the heavily damped cantilever, and relative error in the CMS-computed modal damping ratios.

damping values in the left hand plot. Yet, the relative errors lie between 1% and 10% values for the classical CMS methods, while the same modes are estimated with errors below 0.1% with the state-space methods. Thus, the relative difference in accuracy between the classical and the state-space CMS methods shows a constant gap in the error levels of about two orders of magnitude.

The effect on the modal damping errors are reflected in the modal frequency results shown in Figure 4.5. For high levels of damping the damped modal frequencies are strongly dependent on the corresponding modal damping values. In this case it can be observed how the modal frequencies for modes 7 to 10 estimated through the CB and the CCH methods deviate significantly from the exact damped modal frequencies solution, reaching modal frequency errors between 1% and 10%. This

amount of error in modal frequency estimation may be regarded to be beyond acceptable tolerance. On the contrary, this is not the case for the MCB and the CN methods, which show very good accuracy even for the highly damped modes with errors far below 1%, that is, errors two orders of magnitude smaller than the CB and CCH methods once again.

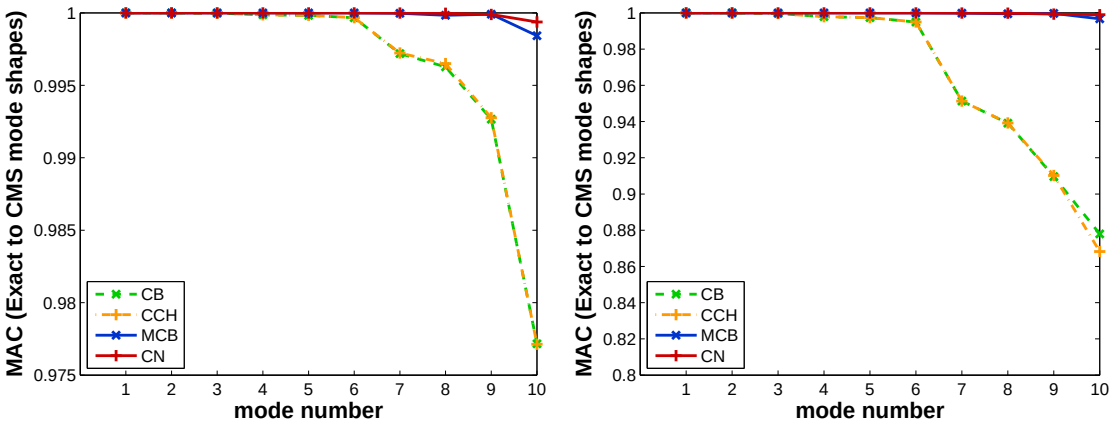

Figure 4.7: MAC value between exact and CMS computed mode shape vectors for the first 10 modes of the lightly (left) and heavily (right) damped cantilever.

Finally, the cantilever mode shape vectors obtained through the different CMS methods may be compared to the exact mode shape vectors by means of the Modal Assurance Criterion (MAC). In Figure 4.7 the MAC values for the CMS computed mode shape vectors compared with their matching exact mode shape vector are presented for the lightly damped case (left) and for the heavily damped case (right). In both cases, the MAC values for the MCB and CN methods are closer to one than the MAC values for the CB and CCH methods. Nevertheless, the loss of orthogonality with respect to the exact modes is very small in the lightly damped case (all MAC values above 0.98). On the contrary, since highly damped modes become more complex valued, the orthogonality of the (undamped) mode shapes computed through the CB and CCH methods with respect to the highly damped cantilever exact mode shapes is severely lost. Therefore, the increased accuracy of the state-space based CMS methods is also decisive for the correct damped mode shape estimation in highly damped systems.

With the locally damped cantilever example it has been illustrated that the Morgan-Craig-Bampton and the Craig-Ni state-space based CMS methods estimate the modes of vibration of general damped systems with much improved accuracy with respect to their classical counterparts, the Craig-Bampton and the Craig-Chang methods. Regardless of the system being lightly or heavily damped, the computa-

tion error in the modes is sensibly smaller. Yet, the need for such accurate CMS methods is better justified for highly damped systems where the amount of error incurred with the CB and CCH methods clearly exceeds the error tolerance for dynamic analysis purposes. Nevertheless, the use of state-space based CMS methods is also convenient for lightly damped systems if accurate modal damping estimation is of major interest in the purpose of the analysis. Although the modal frequencies and mode shape vectors are reasonably well estimated through the classical CMS methods when the damping is low, the corresponding modal damping ratios are still estimated with a significant amount of error.

4.6.2 Example 2: Coupled plates with damping patches

The second validation example is a set of four aluminium plates which are coupled together as shown in Figure 4.8, each of the plates having a damping patch attached on its surface.

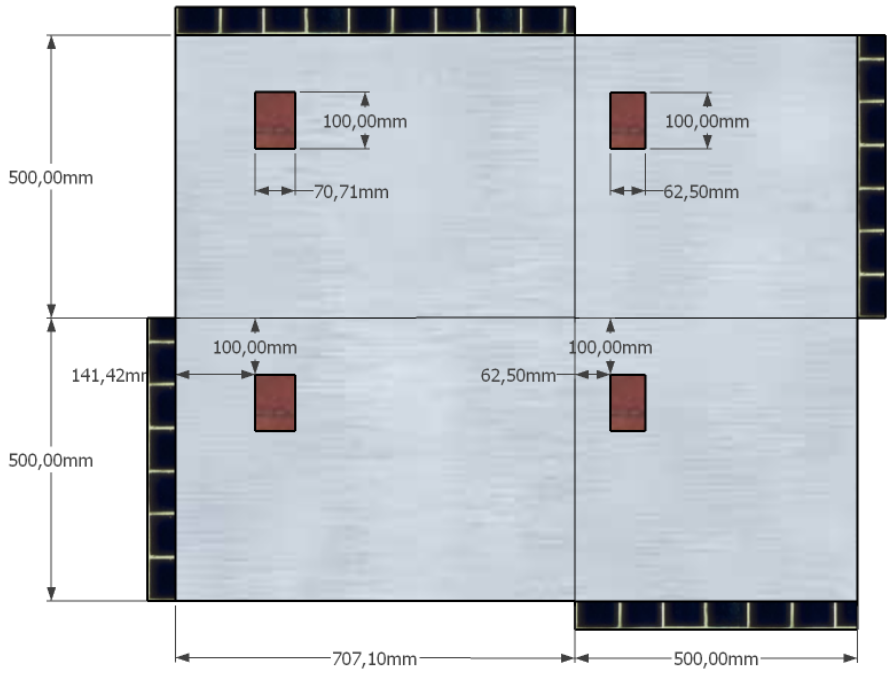

Figure 4.8: Description of the locally damped coupled plates example and its dimensions.

The dimensions of the four aluminium plates are indicated in Figure 4.8, all of them having 3mm thickness, and their mechanical properties are listed in Table 4.2. Likewise, the area of the damping patches and their position over the aluminium plates are also indicated in Figure 4.8. The system's edges are partially clamped

(represented by black walls in Figure 4.8) and partially free.

	Elastic Modulus	Mass Density	Poisson Ratio	Thickness	Proportional Damping Factor
Aluminium Plates	70 GPa	2700 Kg/m^3	0.3	3 mm	10^{-4}
Damping Patches	negligible	negligible	-	negligible	10^{-2}

Table 4.2: Material properties for the locally damped coupled plates example.

Although it seems a rather simple example, locally damped metal plates are recurrently found in industrial design. For instance, in the car industry damping pads may be attached to the car body panels in order to reduce sound and vibration levels. Whereas the cantilever example in the previous section provided a simple test problem on which to prove the accuracy and correct implementation of the CMS methods, this second validation example will serve for analysing the CMS methods in a more realistic problem.

The coupled plates system is meshed using 4-noded isotropic *thin plate elements* [7] with 3 degrees of freedom per node (i.e. transverse displacement z and rotations θ_x and θ_y). Initially, each of the 4 plates is meshed with elements of the size of the corresponding damping patch as shown in Figure 4.9, and 4 components coinciding with the physical plates are defined. Later in this section, the meshing of the coupled plates system will be refined in order to obtain FE models with increasing number of DOFs.

The coupled plates FE model illustrated in Figure 4.9 gives rise to a system of 627 DOFs. Its division into components results in components 1 and 3 having 198 DOFs, components 2 and 4 having 162 DOFs, and the components coupling interface consisting of 87 DOFs. Whenever the state-space formulation is introduced, the described number of DOFs is doubled.

For the sake of simplicity, the damping patches are modelled in an analogous way to the damping in the cantilever example. That is, they are considered massless and their damping properties are accounted for through a proportional damping factor. Hence, the underlying aluminium plate elements will have added damping proportional to their element stiffness matrix by a factor of 0.01 (see Table 4.2), i.e. a hundred times more damping than plate elements with only baseline low damping and no damping patch. Clearly, the coupled system and also all of the components are very locally damped due to the damping patches.

[7] The thin plate element description may be found in [1], which has been coded into MATLAB.

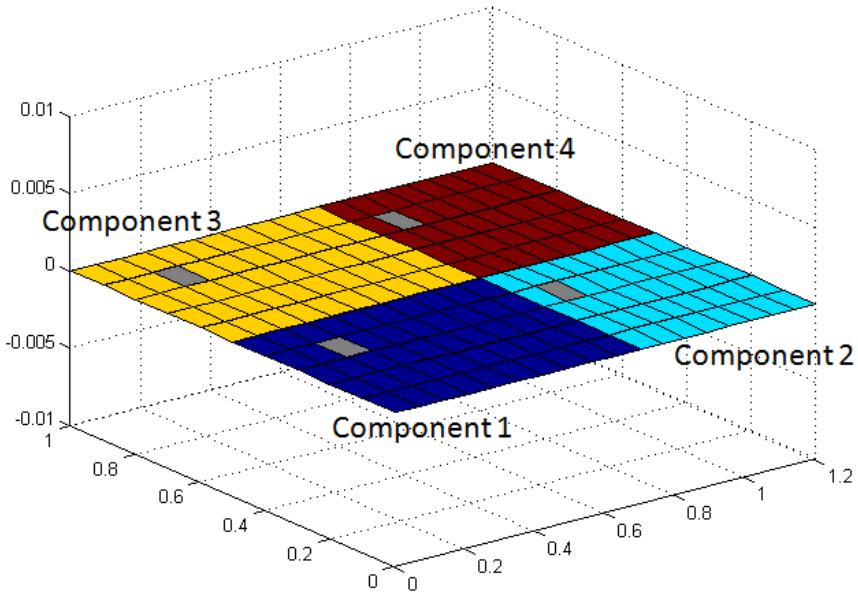

Figure 4.9: Element meshing and component division for the coupled plates example.

The coupled plates example presents several challenging features that were not encountered in the cantilever example. To start with, the overall number of degrees of freedom is larger. This implies that the solution of the eigenvalue problems is not as trivial as for the small matrices in the previous example. In addition, this will allow for the evaluation of the model order reduction capabilities of the CMS methods.

Furthermore, the system model is two dimensional and is split into several components, which yields more complex coupling interfaces than a 1-noded interface. The coupling interface in this example presents components having common interface with more than one component at a time, coupling DOFs belonging to 2 or even 4 (the central node) different components and coupling DOFs which correspond to clamped edges. This supposes a demanding test that will prove the correct implementation of the coupling and synthesis processes.

In this example, the first 100 modes of the full system are computed through the Craig-Bampton (CB), the Craig-Chang (CCH), the Morgan-Craig-Bampton (MCB) and the Craig-Ni (CN) methods, and compared to the *exact* solution obtained from the full system equations of motion in the state-space.

In the CMS methods, 50 component normal modes are computed for each component (100 component normal eigensolutions in the state-space based methods). In this case, since all components have a clamped edge, no rigid body motion is ex-

pected. The number of constraint modes (for fixed-interface methods) and residual attachment modes (for free-interface methods) in each component are proportional to the number of unbounded coupling DOFs in each component, and they are summarised in Table 4.3 for the initial mesh (Mesh 1).

	Component 1	Component 2	Component 3	Component 4
Normal modes	50 (100)	50 (100)	50 (100)	50 (100)
Constraint modes	42 (84)	36 (72)	42 (84)	36 (72)
Attachment modes	42 (42)	36 (36)	42 (42)	36 (36)
Total component modes	92 (184/142)	86 (172/136)	92 (184/142)	86 (172/136)

Table 4.3: Number of component modes computed for the coupled plates example. In brackets: number of state-space component modes.

The results for the first 100 modes of the coupled plates system are presented in Figures 4.10, 4.11 and 4.12. Figure 4.10 shows the CMS computed modal frequency values and errors. Likewise, Figure 4.11 shows the CMS computed modal damping values and errors. Lastly, Figure 4.12 shows the MAC value between the CMS computed mode shape vector and the corresponding exact mode shape vector.

First, the modal characteristics of the coupled plates system are evaluated. The first 100 modes have modal frequencies from 20 up to 760 Hz. It can be observed in Figure 4.10 that the number of modes grows linearly with increasing frequency. Thus, the coupled plates system shows a constant modal density, with an average spacing 7.5 Hz between contiguous modes. Modal damping values range from 2.5% values in the lowest modes till 50% damping values in the higher modes as can be observed in Figure 4.11.

The relatively high modal density together with high damping condition indicates that the system modal overlap shall also be high. These conditions indicate that undamped modal solutions will be far from uncoupling the damped equations of motion, i.e. strong coupling will occur between close undamped modes due to off diagonal terms in the modal damping matrix. In other words, modal parameters (specially modal damping values) computed from undamped modal solutions will be markedly erroneous. Therefore, it is expected that the CB and CCH methods, which are based on undamped component modes, are not capable of correctly estimating the damped modes of the system.

Now, the modal results obtained through the different CMS methods may be analysed. In the error plot in Figure 4.10 it can be observed that the CB and CCH methods obtain the damped modal frequencies values with errors in the 1% to 5%

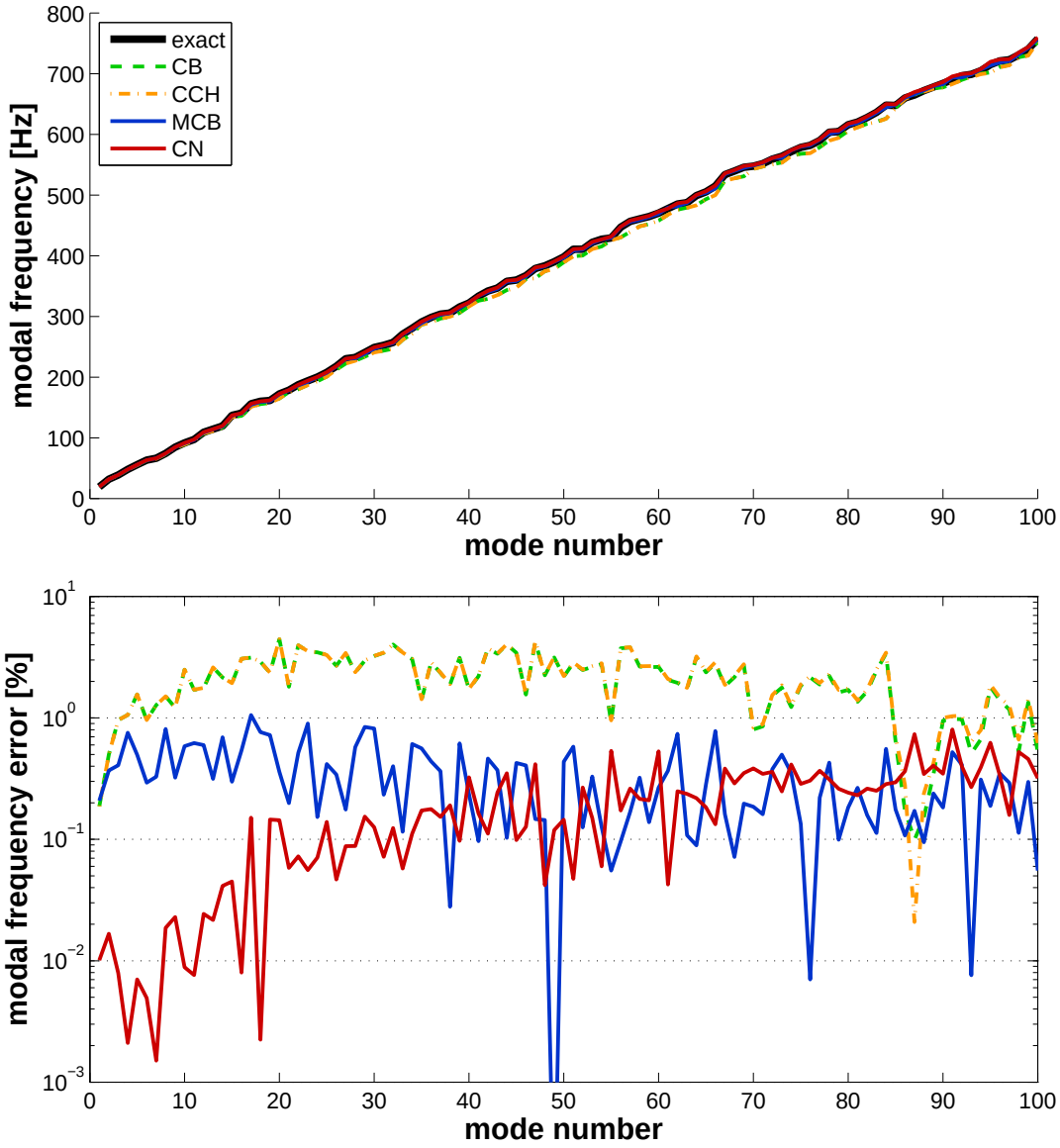

Figure 4.10: Modal frequency for the first 100 modes of the locally damped coupled plates system, and relative error in the CMS-computed modal frequencies.

relative error range. As expected, they get a significant amount of error, which may be excessive (over 1%) for most practical situations. On the contrary, the state-space based CMS methods obtain modal frequencies with errors below 1%. The MCB method shows errors between 0.1% and 1% of the modal frequency value over the 100 computed modes. The CN method shows errors below 0.1% in the lowest modes, which proves that the static correction applied by the state-space residual attachment modes is very accurate. As the frequency increases, the error in the modal frequency estimations lies in the 0.1% - 1% range, similar to the MCB method.

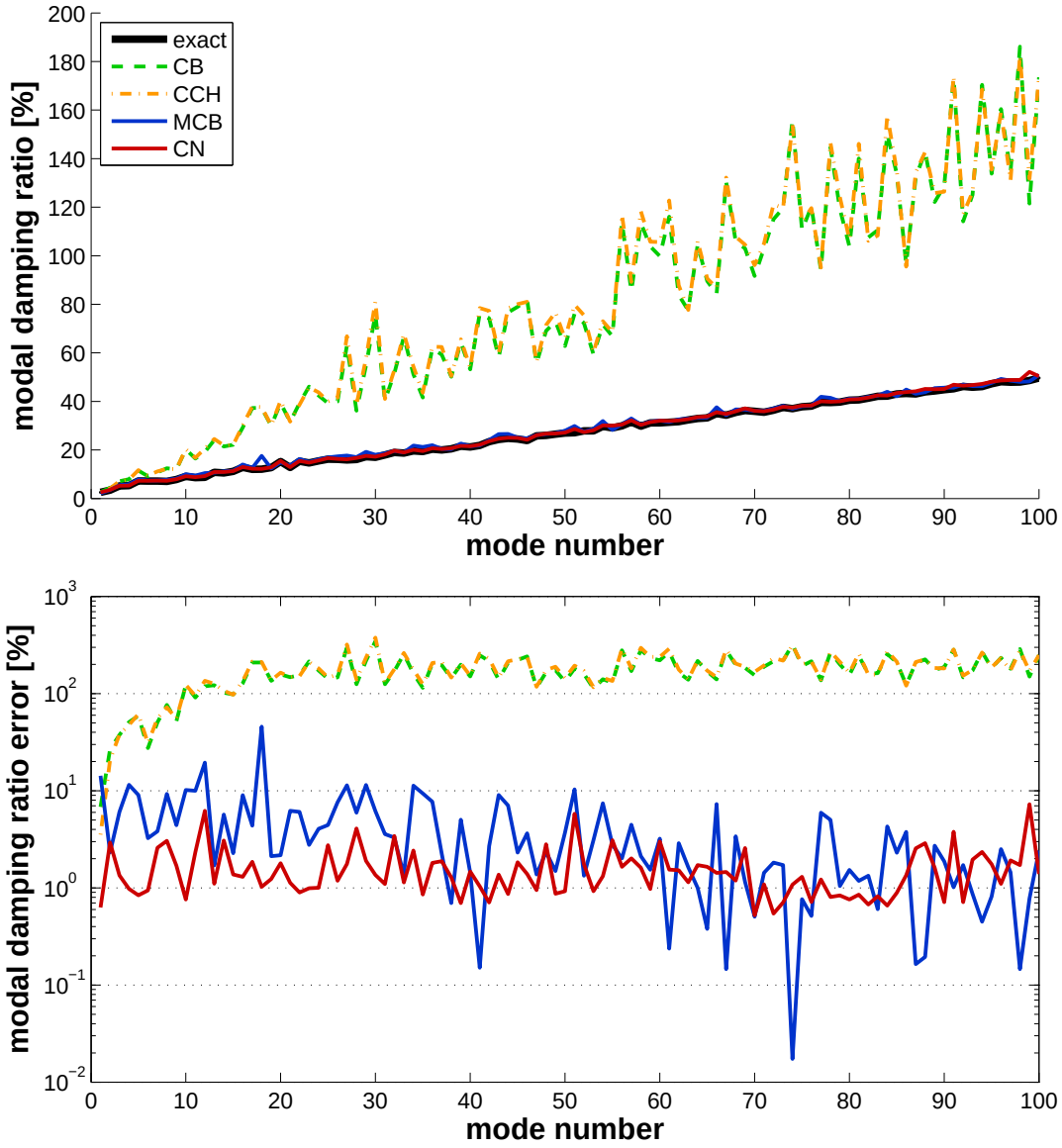

Figure 4.11: Modal damping for the first 100 modes of the locally damped coupled plates system, and relative error in the CMS-computed modal damping ratios.

The results for modal damping of the 100 modes are even more divergent. Whereas the MCB and CN methods fairly well estimate the modal damping values, the CB and CCH methods give completely erroneous results with errors exceeding 100% of the damping ratio value. What is more, half of the modes computed through CB and CCH methods show overdamped conditions, i.e. over 100% damping ratio, while the actual modes are highly damped but not overdamped.

In contrast, the modal damping ratios computed through the CN method agree fairly well with the exact values, with errors ranging from 0.5% to 5%. The MCB

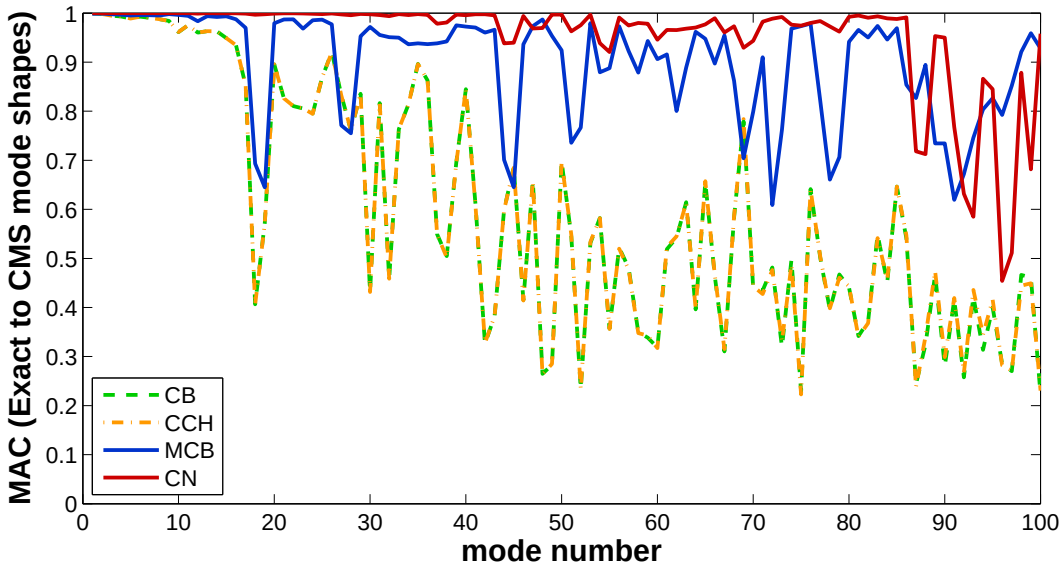

Figure 4.12: MAC value between exact and CMS computed mode shape vectors for the first 100 modes of the locally damped coupled plates system.

method also estimates fairly well the modal damping values. However, the relative errors in damping estimation vary strongly from one mode to another. In general, damping errors range from 0.1 % to 10% error, but with some specific modes clearly exceeding the 10% relative error in modal damping.

The reasons for such an uneven accuracy in modal damping estimation through the MCB method may be disclosed by looking at the MAC values plot in Figure 4.12. There, it may be observed that along the lowest 85 modes the CN method obtains mode shapes which accurately match the exact ones (MAC values very close to unity). Yet, the mode shapes computed through the MCB method do not match so closely (smaller average MAC values than the CN method ones), and the MAC values plot shows clear dips in some specific modes. The cause for such dips, which involve in most of the cases two contiguous modes, is that pairs of modes are very close in frequency, so that the mode shapes for the two modes are mixed up in the MCB computation.

Both the CN and the MCB computed modes are in poor correlation with the exact mode shapes above the 85th mode. It might happen that a larger number of component modes is needed to correctly account for the highest system modes. Another option is that the eigenvalue algorithm loses vectors orthogonality as the amount of modes to compute increases. At the moment, no clear explanation has been found for why these low MAC values are found in this example. In any case, the MAC values obtained for the MCB and CN methods are close to unity for most of the

modes, whereas for CB and CCH methods this only happens for the first 15 modes.

This second example has provided a further insight into the level of acceptance of the different CMS methods in terms of accuracy. On one hand, the superiority of the state-space based CMS methods over the classical CMS methods based on undamped component modes has been confirmed once again for a general damped system. On the other hand, it has been possible to evaluate the CMS estimated results in the mid-frequency regime rather than just in the few first modes of vibration.

After the first 10 or 15 modes, modal frequencies were in the hundreds of Hertz, with modal damping ratio over 10% and modal spacing below 10 Hz. That is, in the mid-frequency regime, with moderately high modal overlap. It has been seen that under these circumstances the modal frequencies and modal damping values computed through the MCB and CN methods are still fairly well estimated. However, it has been seen that neighbouring modes with very close modal frequencies are not always fully distinguished, especially for the Morgan-Craig-Bampton method.

The Craig-Ni method appears to be more accurate for the lower modes (first 50 modes), and it resolves better the discrimination of neighbouring global modes. Nevertheless, as the number of computed modes increases, both the Morgan-Craig-Bampton and the Craig-Ni methods show similar accuracy.

4.6.3 Computational issues when solving the eigenvalue problems in state-space based CMS methods

Up to this point, the focus has been only on how accurate results are obtained when computing the modal solution of the cantilever and the coupled plates examples through CMS methods. It has been proved that fair estimates may be obtained through the state-space based methods. However, no attention has yet been paid to the computational needs for obtaining such results. In this section, some difficulties which are faced when working in the state-space formulation are discussed, and the computational solutions that have been adopted are stated.

For the state-space based CMS methods, most of the computational issues come from the complication in solving the state-space eigenvalue problem. In chapter 2, eigenvalue algorithms for the solution of the state-space EVP have been discussed (c.f. section 2.3.4). There, it has been stated that for large systems the Implicitly Restarted Arnoldi algorithm, which is included in the `eigs` MATLAB function, fails

at converging to the desired solutions. Alternatively, the Symmetric Indefinite Lanczos Method (SILM) may be used for tackling the state-space EVP. However, this latter algorithm is not coded in any commercial software library.

Here, the coupled plates example is used as a basis for studying numerical issues in the solution of the state-space eigenvalue problem. The plate's mesh is increasingly refined in order to obtain corresponding finite element models with increasing numbers of degrees of freedom. The initial mesh (Mesh 1) shown in Figure 4.9 has an element size equalling the area of the damping patches. Successive meshes have been created having elements with edge lengths being a fraction of the damping patch edge lengths. For instance, Mesh 2 in Figure 4.13 has 4 elements per damping patch area, Mesh 3 (also in Figure 4.13) has 9 elements per damping patch area, and so on.

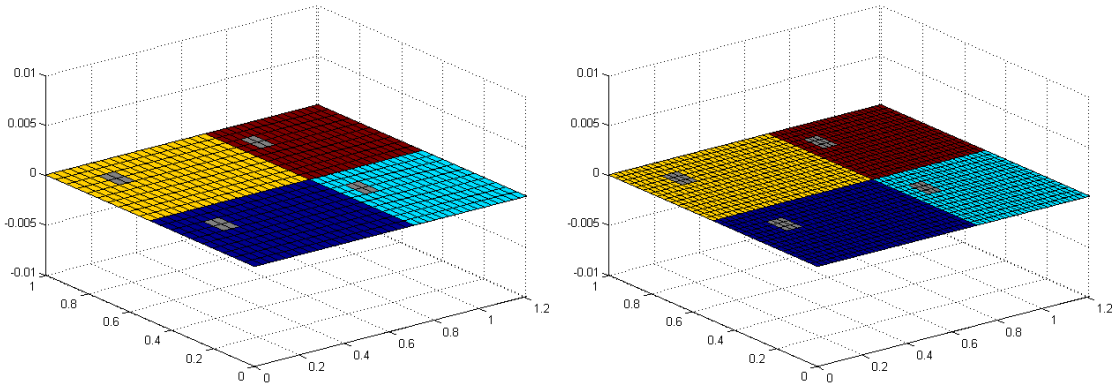

Mesh 2 Mesh 3

Figure 4.13: Refined meshes for the coupled plates example.

In this way 6 meshes have been defined having 627, 2331, 5115, 8979, 13923 and 19947 physical degrees of freedom respectively. When the state-space formulation is introduced these figures are doubled, i.e. system corresponding to meshes 1 to 6 contain 1254, 4662, 10230, 17958, 27846, and 39894 state-space DOFs respectively. Meshes 3 to 6 already represent systems of considerably large size in terms of number of degrees of freedom.

On the eigenvalue algorithms for solving state-space eigenvalue problems

Now, the first 10 full system modes are computed for the 6 different meshes and the computation time for solving the corresponding EVPs is recorded. Here, the first 10 modes were computed from the full system equations of motion, i.e. Component

Mode Synthesis is not used in this test. This has been done 3 times: first by solving the undamped EVP in physical coordinates through the standard Lanczos algorithm (`eigs` function in MATLAB), second by solving the state-space EVP through the Implicitly Restarted Arnoldi (IRA) algortihm (`eigs` function in MATLAB), and last by solving the state-space EVP through the Symmetric Indefinite Lanczos Method (ad-hoc implementation of SILM in MATLAB). In the undamped case 10 eigensolutions are computed, whereas in the state-space cases 20 eigensolutions (10 complex conjugate pairs) are required.

In Figure 4.14 the time records obtained in this test are presented. The computation time records for solving the undamped and state-space eigenvalue problems are plotted in logarithmic scale as a function of the number of degrees of freedom of the mesh (also in logarithmic scale). Obviously, the undamped EVP requires much less computation since the size of the matrices and the number of wanted eigensolutions is halved with respect to the state-space EVP.

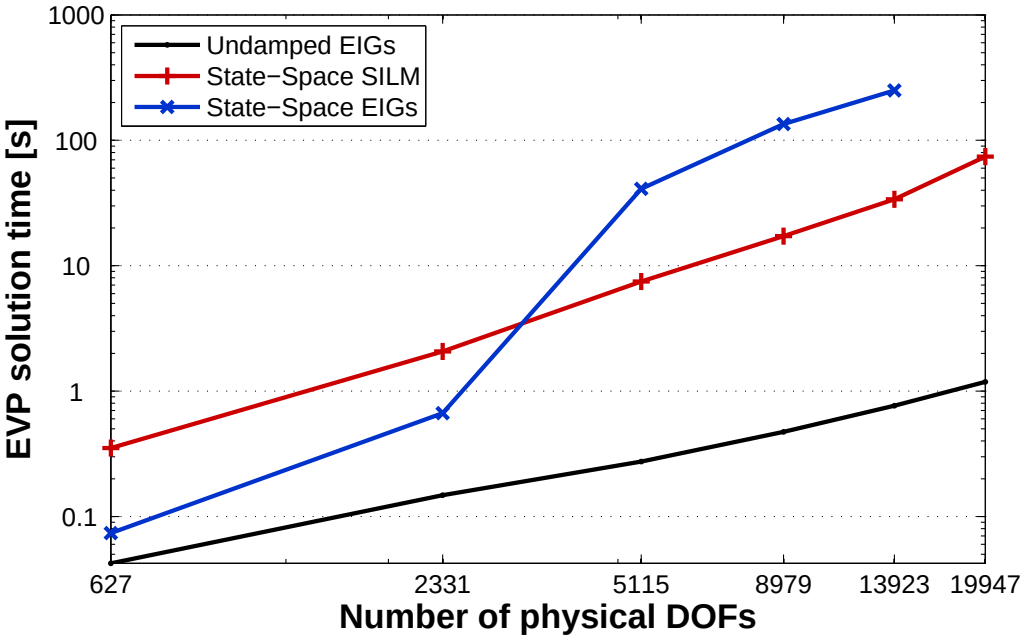

Figure 4.14: Eigenvalue problem solution time as a function of the number of physical degrees of freedom of the full system.

Solution times for the undamped EVP (black solid line) range from hundredths of a second for Mesh 1 until close above 1 second for Mesh 6. Solution times for the state-space EVP (blue line for IRA, red line for SILM) are much larger than those figures.

The Implicity Restarted Arnoldi algorithm (blue crossed line in Figure 4.14) solves

the 10 system modes for Meshes 1 and 2 in times under 1 second, which are indeed solution times that are less than an order of magnitude above the undamped EVP solution time. Yet, this trend is disrupted for Meshes 3 to 5 where solution times rise up to hundreds of seconds. This is a consequence of the loss of convergence of the algorithm. Over 10,000 state-space DOFs, the IRA algorithm struggles at finding just 20 converged eigensolutions. For mesh 6 (close to 40,000 state-space DOFs) the situation is even worse, and the algorithm is unable to find 20 converged eigensolutions[8].

The Symmetric Indefinite Lanczos Method (red crossed line in Figure 4.14) does not incur any convergence issues, as can be seen by the smooth increase in computational time as the number of DOFs increase. However, since SILM is programmed here in MATLAB code rather than in a lower level programming language such as Fortran (contrarily to the built-up algorithms in the `eigs` function), its execution time is shifted up overall. The solution time goes from below half a second for Mesh 1 up to almost 100 seconds for Mesh 6. If an efficient (Fortran) implementation of the SILM algorithm were available, computation time might be an order of magnitude lower, matching the state-space EVP solution time of the `eigs` MATLAB function (IRA algorithm) for Mesh 1 and Mesh 2.

In conclusion, the Symmetric Indefinite Lanczos Method algorithm needs to be used for the computation of large system modes in the state-space. Hence, for performing state-space based Component Mode Synthesis in large systems, the component modes must be computed through the SILM algorithm. On the contrary, once the system model is reduced into coupled-modal coordinates, either by the Morgan-Craig-Bampton method or the Craig-Ni method, the corresponding EVP in coupled modal coordinates is no longer an indefinite GEVP, but a generic complex-valued non-hermitian GEVP. Therefore, since the coupled-modal coordinates are of reduced size, the corresponding EVP may be solved through the IRA algorithm, i.e. using the `eigs` MATLAB function.

On the overdamped modal solutions in state-space eigenvalue problems

In the test that has been just described, 20 eigensolutions have been computed for the state-space EVPs in order to find 10 vibration modes. The reality is, however, that these 20 eigensolutions do not all correspond to the 10 first modes of vibration. Despite having found 20 converged solutions, just a few of them correspond to the

[8] If 100 modes are to be computed as in the previous section, the IRA algorithm fails at finding them already in Mesh 3 with about 10,000 state-space DOFs.

complex conjugate pairs of eigensolutions that were being searched and found.

Starting with the IRA solution for Mesh 1, just 4 out of the 20 converged eigensolutions showed complex valued eigenvalues coming in complex conjugate pairs. The remaining 16 converged eigensolutions presented (negative) real-valued eigenvalues. With the imaginary part of the eigenvalues accounting for modal frequency and the negative real part of the eigenvalues accounting for modal damping, these negative real-valued eigenvalues may only correspond to overdamped modal solutions, i.e. non-vibrating modes which get rapidly attenuated. This means that only the lowest two damped modes of vibration have been found in this case. In turn, the SILM algorithm has obtained 8 complex-valued eigensolutions and 12 negative real-values eigensolutions out of the 20 converged eigesolutions for Mesh 1. Hence, only the first four modes of vibration have been encountered through SILM. That is, slightly better than IRA but absolutely insufficient.

With these results, one must understand why all of these overdamped solutions are found, and how to proceed for computing the sought vibration modes. For the sake of analysing the reason for these overdamped results, a second test was conducted using the coupled plates example.

Instead of looking for just 10 modes of vibration, successive solutions of the state-space EVP for mesh 1 and mesh 2 were computed for increasing number of requested eigensolutions. The SILM algorithm has been executed targeting 20, 40, 60, 80, 100, 120, 140, 160, 180 and 200 converged eigensolutions respectively in each run. This has been done both for Mesh 1 and for Mesh 2. In Table 4.4 the number of resulting overdamped solutions in each run are summarised.

	Requested eigensolutions	20	40	60	80	100	120	140	160	180	200
Overdamped	Mesh 1	12	20	32	36	36	36	36	36	36	36
Eigensolutions	Mesh 2	12	18	34	51	68	82	96	96	96	96

Table 4.4: Number of overdamped eigensolutions for SILM solution of the full system state-space EVP.

It can be observed in Table 4.4 that as the number of requested eigensolutions increases more overdamped solutions are being found. Yet, it comes a point where this tendency gets clipped to a maximum number of overdamped solutions. For mesh 1, 36 overdamped solutions are found among the 80 first converged solutions, and from there on all additional converged solutions come in complex conjugate pairs. For mesh 2, a maximum of 96 overdamped solutions are found among the

first 140 converged solutions and, from that point no more overdamped solutions are found. These results were obtained through the SILM algorithm, but similar results with identical maximum number of overdamped solutions were obtained through the IRA algorithm.

In fact, the maximum number of overdamped modes appears to increase as the mesh is refined, i.e. as the number of DOFs grows. Refining the mesh implies that modes with higher frequency may be computed, which could not be included in a model with a coarser mesh. These higher frequency modes are most likely overdamped, given the damping characteristics of the coupled plates examples.

As presented in the previous section, the modal damping was larger for the higher order modes, and the low frequency modes (even when computed from the undamped eigensolutions) were moderately damped. Consequently, the overdamped modes do not correspond to low frequency modes with high modal damping. Thus, these overdamped solutions will correspond to high frequency modes.

The reason for these high order overdamped modes being found among the first eigensolutions by the eigenvalue algorithms for the state-space EVP is unclear. Overdamped modes in the state-space should be double rooted eigensolutions with zero frequency. However, overdamped solutions do not occur in pairs of solutions with identical eigenvalues. Perhaps, the damping of these presumably double roots is not computed evenly due to some numerical instabilities, making them appear among the first computed eigensolutions.

In view that superfluous overdamped eigensolutions are encountered, these need to be filtered out when solving state-space eigenvalue problems. In fact, the results shown in section 4.6.2 do not include overdamped modes, which have been discarded. The solutions adopted for eliminating overdamped state-space eigensolutions are presented in the following.

Computational solutions adopted

In the context of state-space based Component Mode Synthesis, overdamped modal solutions are unwanted solutions. On one hand, they are of no use for the order reduction because they would only be added basis vectors that carry no relevant information. On the other hand, these solutions are not examined in any vibration analysis because they do not resonate and also because they fall out of the frequency range of interest.

One possible approach for finding a certain number of resonant eigensolutions, e.g. a predefined number of state-space component modes, is to compute many more eigensolutions than the required amount, and then filter out the overdamped solutions a posteriori. The problem, however, is that the number of overdamped solutions is not known beforehand so that one may not know how many extra eigensolutions are needed. Hence, this may involve a trial and error search of the overhead number of eigensolutions needed to obtain the requested number resonant modes.

As been shown before, the number of overdamped solutions increases as the number of requested modes increases, and the maximum number of overdamped solutions also varies with the mesh size. This makes the number of overdamped converged eigensolutions that one may obtain very unpredictable. Therefore, it is desirable to filter out overdamped eigensolutions in another way.

A modification in the Symmetric Indefinite Lanczos Method has been devised for this purpose. Lanczos algorithms keep iterating until a requested number of eigensolutions converge. At each iteration a new Lanczos vector is computed and added to the basis of Lanczos vectors. Then, the original problem is projected into the Lanczos vectors basis and the eigensolutions of the projected problem are computed. Finally, a convergence check is performed in order to validate whether the computed solutions are actual eigensolutions of the original problem. Therefore, the idea here is to modify the convergence criterion of the Lanczos algorithm.

The Modified SILM (MSILM) includes a new condition in the convergence check at each iteration. A converged eigensolution in terms of residual vector is unflagged as converged if its associated Ritz value (eigenvalue) indicates that this solution is overdamped, i.e. if it has zero imaginary part and non-zero negative real part. The consequence is that the algorithm keeps iterating until sufficient numbers of *converged* eigensolutions are found.

The MATLAB code for the SILM algorithm has been modified in order to include this new convergence condition. Then, the same test which computed increasing number of eigensolutions (from 20 to 200 requested eigensolutions) has been repeated for mesh 1 using MSILM. The resulting converged eigensolutions are all resonant, coming in complex conjugate eigensolution pairs, each of them corresponding to a non-overdamped mode.

In Figure 4.15 the numerical efficiency of MSILM is compared to that of the SILM algorithm. In the left hand side plot, the number of Lanczos vectors computed until

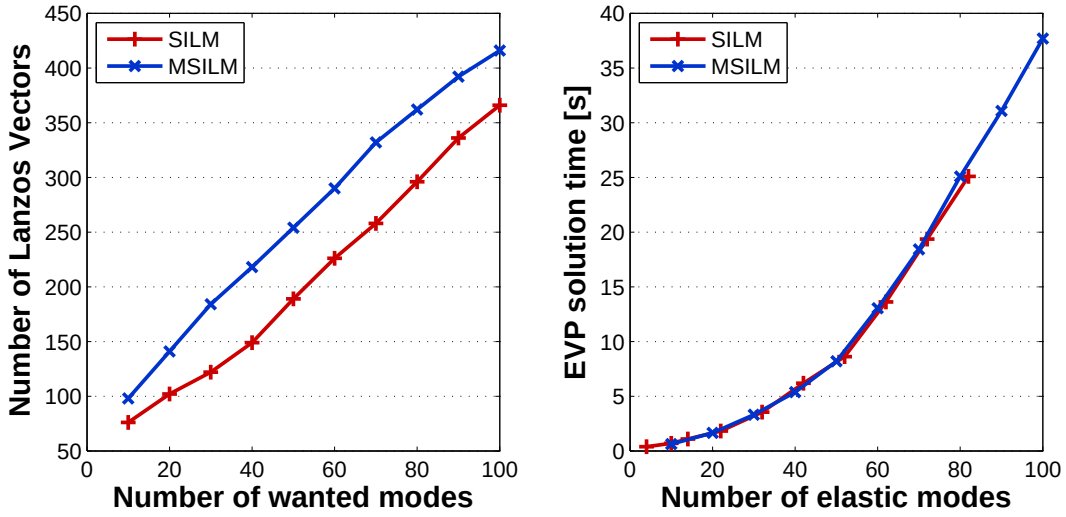

Figure 4.15: Comparison of the computational complexity of SILM and MSILM. Left: Number of Lanczos vectors as a function of the number of wanted modes. Right: EVP solution time as a function of resonant modes obtained.

convergence for SILM and MSILM is compared. For the same number of wanted modes (i.e. requested eigensolution pairs) MSILM has computed an average of 50 more Lanczos vectors. In other words, the algorithm has executed about 50 more iterations, which means that the solution time is increased. Yet, for the same number of computed modes, SILM obtains many overdamped modes. In the right hand side plot of Figure 4.15 the solution time as function of the number of non-overdamped modes obtained is represented. It is clear that, when the overdamped modes are discarded, equivalent computational cost to that of MSILM is effectively needed for computing resonant modes through SILM.

The advantage with the modified version of the Symmetric Indefinite Lanczos Method is that overdamped solutions are intrinsically dismissed. This circumvents the problem of having to track the number of overdamped eigensolutions. In turn, the implementation of state-space based CMS methods is simplified, since no memory must be allocated for an excess number of eigensolutions, which in addition is an uncertain number. Therefore, the issue with overdamped solutions can be overlooked through the use of MSILM.

Yet, this strategy has only been applied for the computation of state-space component modes through the Symmetric Indefinite Lanczos Method. Since the global eigenvalue problem in coupled-modal coordinates is here solved through the IRA algorithm, i.e. `eigs` MATLAB function, similar modifications on the algorithm have not been introduced.

Nevertheless, the number of overdamped eigensolutions obtained from the EVP in coupled-modal coordinates is very reduced due to the fact that most of the potential overdamped solutions have been already filtered out at a component modal level. Therefore, the total number of requested eigensolutions must be increased by a small quantity in order to obtain the wanted number of full system (resonant) modal solutions. This does not cause a significant rise in computation time since the coupled-modal EVP is of reduced order. If any overdamped global modal solutions are obtained, these may be easily filtered out through a simple check on the corresponding eigenvalues.

4.6.4 Computational efficiency of the state-space based CMS methods

The accuracy of Component Mode Synthesis for damped system has been validated through numerical examples in sections 4.6.1 and 4.6.2. It has been shown that state-space based CMS methods show much enhanced accuracy than the classical Craig-Bampton and Craig-Chang CMS methods. However, working in the state-space formulation presents some numerical setbacks which have been subsequently evaluated in section 4.6.3. Overall, these are overcome through the use of a Modified Symmetric Indefinite Lanczos Method (MSILM) algorithm. This section completes the Component Mode Synthesis validation by numerically evaluating the computational complexity of the state-space based CMS methods.

Continuing with the coupled plates example, the computational cost for computing the system modes through the Morgan-Craig-Bampton method and the Craig-Ni method will be compared to that of the cost for computing the system modes from the full system equations of motion in the state-space. In section 4.6.2, only the first 80 out 100 system modes were highly accurately computed through the MCB and CN methods with 50 normal modes (100 state-space eigenvectors) per component. Consequently, the efficiency of CMS methods is here evaluated for the computation of the first 80 system modes.

For each of the 6 meshes defined for the 4 coupled plates system, 160 eigensolutions corresponding to the 80 first vibrating modes have been computed directly for the full system, and also through the MCB and CN methods with 100 eigensolutions per component. The direct modal solution involves computing 160 eigensolutions on the state-space system matrices, whereas the CMS solutions involve computing 400 eigensolutions on state-space component matrices and then 160 eigensolutions

on the coupled-modal matrices.

In Table 4.5 the number of physical and state-space degrees of freedom for each of the meshes is summarised together with the corresponding number of degrees of freedom of the coupled-modal models obtained through the MCB and CN methods. Notice that the number of coupled-modal DOFs for the CN method is constant and corresponds to the number of overall component eigensolutions. Contrarily, the number of coupled-modal DOFs for the MCB method increases for larger meshes since the coupling interface (state-space) DOFs are retained.

	Full System DOFs		Coupled-Modal DOFs	
	Physical	State-Space	MCB method	CN method
Mesh 1	627	1254	574	400
Mesh 2	2331	4662	742	400
Mesh 3	5115	10230	910	400
Mesh 4	8979	17958	1078	400
Mesh 5	13923	27846	1246	400
Mesh 6	19947	39894	1414	400

Table 4.5: Number degrees of freedom comparison between the MCB and CN coupled-modal coordinates and the physical and state-space coordinates for the 6 different meshes in the coupled plates example.

Component matrices have roughly a quarter the number of DOFs compared with the full system matrices, so that the cost for computing a component mode should be much smaller than the cost for computing a full system mode. For the smaller meshes (1 and 2), the number of DOFs of the coupled-modal models is of comparable magnitude to the number of DOFs of the full system, which means that CMS is not very efficient in terms of model order reduction nor in terms of computational complexity reduction. On the contrary, for the larger meshes (3 to 6) the coupled-modal models are of much reduced size with respect to the full system models. It is in these latter cases that CMS may give significant computational savings.

Before evaluating the results a couple of things should be made clear. First, the absolute solution time values are just indicative figures since they depend on the specific processor and operating system that has been used, as well as on the MATLAB coding of the MSILM algortihm. Yet, absolute solution time values are not relevant here since the analysis aim is of comparative nature. Second, the efficiency evaluation is targeted for the solution of large systems. Here, meshes 1 and 2 may be regarded as *small* system models, so that focus will be mainly placed on evaluation of the results obtained for the other four meshes.

The actual solution times for computing the first 80 damped full system modes are presented in Figure 4.16. The results for the direct solution of the full system state-space eigenvalue problem through MSILM are plotted in black, the MCB method results in blue and the CN method results in red.

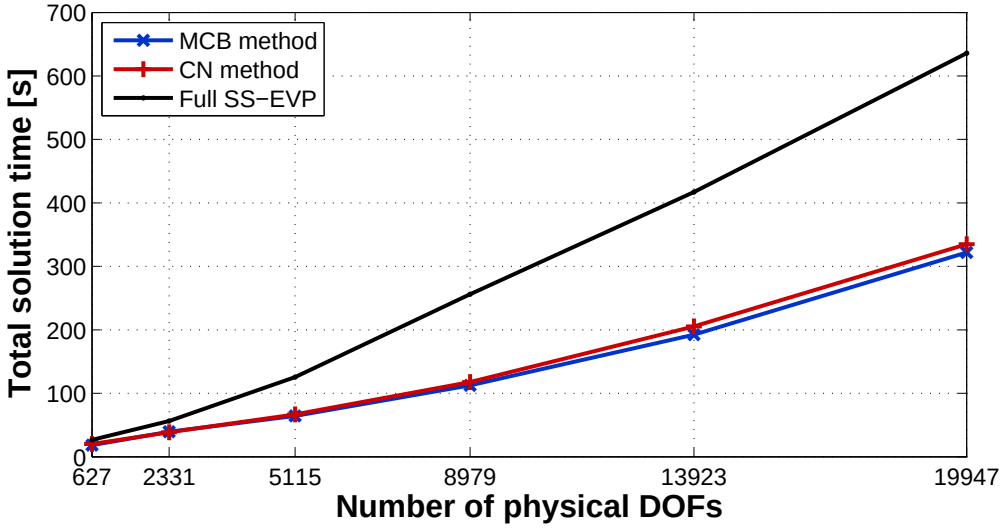

Figure 4.16: Computational time for solving the first 80 damped full system modes of the four coupled plates example as a function of the number of degrees of freedom of the mesh.

Now, the first thing that may be observed in Figure 4.16 is that, for any solution method, the time for computing the first 80 modes increases as the number of DOFs increases. However, if the full state-space EVP solution time curve is observed for meshes 3 to 6, the increase in solution time appears to be almost linear with respect to the number of DOFs. This seems contradictory with the theoretical computational cost of Lanczos algortihms, which in Chapter 2 was estimated proportional to the square of the number of DOFs.

In fact, the solution cost is not actually proportional to the number of DOFs but to a certain power p of the number of DOFs N, i.e. $\mathcal{O}(N^p)$. The exponent p may be estimated from the registered times through a simple calculation

$$p_i = \frac{\log(\frac{t_i}{t_{\text{ref}}})}{\log(\frac{N_i}{N_{\text{ref}}})} \tag{4.125}$$

with N_i and t_i the number of DOFs and solution time corresponding to the i'th mesh, and N_{ref} and t_{ref} the number of DOFs and solution time of one of the meshes which is taken as reference. Taking Mesh 3 as reference, the p_i average for $i = 4, 5, 6$ results

in an exponent estimate of $p = 1.2$. This result is concurrent with the sparsity relation of the coupled plates system matrices. If the number of non-zero elements N_{NZ} in the system matrices is expressed as $N_{NZ} = N^q$, with N the number of state-space DOFs, the resulting q exponent for meshes 3 to 6 range from 1.23 to 1.2 values[9].

Thus, the solution computational cost through MSILM grows at a much smaller rate than the $\mathcal{O}(N^2)$ conservative upper bound claimed in Chapter 2 for Lanczos algorithms. Instead it grows at a rate of $\mathcal{O}(N^{1.2})$ for the present example which, in turn, has a clear relation to the sparsity characteristic of the system matrices.

Looking back again into Figure 4.16 one may observe that the MCB and the CN methods have very similar performance with solution times well below the direct solution of the full system eigenvalue problem. For meshes 3 to 6, the CMS methods take about half the time to obtain the same 80 full system modes, with the MCB method showing slighlty better performance than the CN method. In order to evaluate the performace of the state-space based CMS methods in higher detail, partial solution times for each of the EVPs (the four component EVPs and the couped-modal EVP) have been also recorded. Figure 4.17 shows the computational cost of each of the proceses in the CMS solution in a stacked bar plot.

In Figure 4.17, the CMS computational cost is expressed in relative units with respect to the total cost of the corresponding direct solution, i.e. as the percentage of the full system state-space EVP solution time (black line in Figure 4.16). For each of the meshes two stacked bars are shown, one for the MCB method (in blue) and one for the CN method (in red). Each bar is divided into 6 sections. The blue/red sections indicate the computational cost for solving the four component state-space EVPs for the MCB/CN method respectively, the yellow sections correspond to the computational cost for solving the global EVP in coupled-modal coordinates, and the white sections involve all other CMS associated computation cost (e.g. constraint/attachment modes computation, reduction of the component matrices into the component modal basis, assembly/synthesis of reduced components, etc.). The total height of the stacked bars correspond to the MCB/CN methods total solution time (blue and red lines in Figure 4.16).

Some conclusions may be extracted from the results presented in Figure 4.17. It can be observed that the solution of the 4 component EVPs takes much less time

[9]The number of non-zero elements in state-space system matrices is at least two times N_{NZ} of the system marices. Yet, since the matrices are symmetric, the actual computation cost is halved back. Thence, it makes sense relating N_{NZ} to the number of state-space DOFs

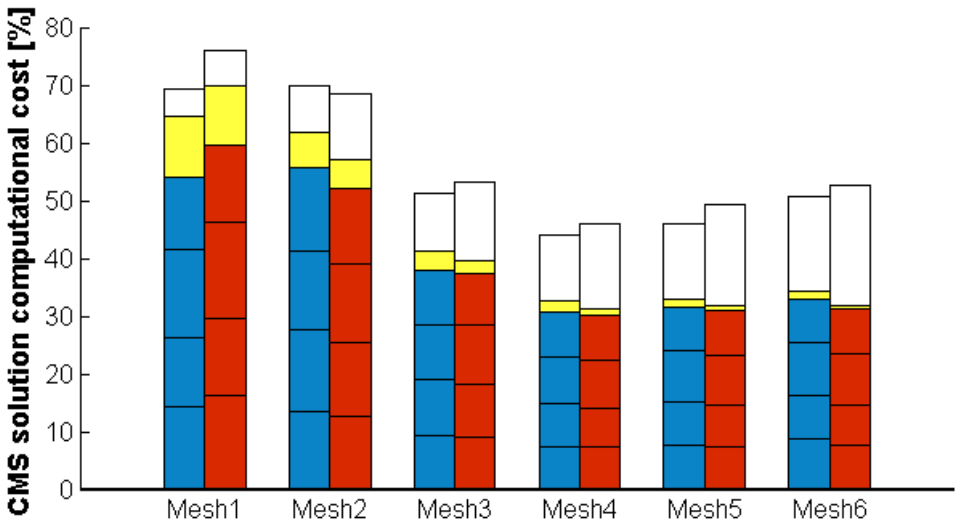

Figure 4.17: Computational time for solving each of the EVPs in the MCB and CN methods relative to the computational time for solving the full order state-space EVP. Blue: MCB components; Red: CN components; Yellow: Coupled-modal; White: Other computations.

than the solution of the full system EVP. As the mesh grows the difference becomes larger, with the solution for the 4 components accounting for just 30% of the time needed for directly solving the full system (meshes 4 to 6).

The overhead cost associated with the CMS processes other than the solution of EVPs is also small in comparison to the solution time required for solving the full system EVP. Yet, this cost is not negligible at all, and it gains prominence for larger systems (up to 20% of the solution cost for the full system EVP). Most of the overhead cost comes from the reduction of the component matrices into modal basis, i.e. $\mathbf{A}_s^y = \boldsymbol{\Upsilon}_s^T \mathbf{A}_s \boldsymbol{\Upsilon}_s$ and $\mathbf{B}_s^y = \boldsymbol{\Upsilon}_s^T \mathbf{B}_s \boldsymbol{\Upsilon}_s$, due to the modal transformation matrices $\boldsymbol{\Upsilon}_s$ being large and fully populated.

The solution of the coupled-modal EVPs involves a very small fraction of the computation cost. For mesh 1 it only supposes about 10% of the full solution cost, and for larger meshes this percentage diminishes even further. However, these figures seem controversial if one looks back into Table 4.5 and compares the number of DOFs of the full system with the number of DOFs of the coupled-modal models. For the smaller meshes the number of coupled-modal DOFs is of comparable magnitude to the total number of system DOFs, so that one might expect much less difference in solution time. On the contrary, this circumstance is cleared up if one recalls that the coupled-modal EVP is solved through the IRA algorithm, i.e. with

the efficiently coded `eigs` MATLAB function.

It has been seen in section 4.6.3 that the `eigs` function is much more efficient than the current SILM implementation as long as the matrices are small. In such a situation, SILM was shown to be 5 times more time demanding (c.f. Figure 4.14). Consequently, comparing the solution time results for the coupled-modal EVPs with the component state-space EVPs ones may be misleading in this case.

Ideally, in order to correctly evaluate the efficiency of the CMS methods, the comparison between the CMS and the full system solution computational cost should be free of the bias introduced by uneven implementations of the algorithms. However, equally efficient implementations of the IRA and SILM algorithms were not available. Therefore, a correction is here introduced consisting on multiplying by a factor of 5 the coupled-modal EVPs solution time. In this way, the solution times can be impartially compared as if a commercial implementation of SILM were available. The computational cost for the MCB and the CN methods is presented again in Figure 4.18 with corrected values for the coupled-modal EVPs.

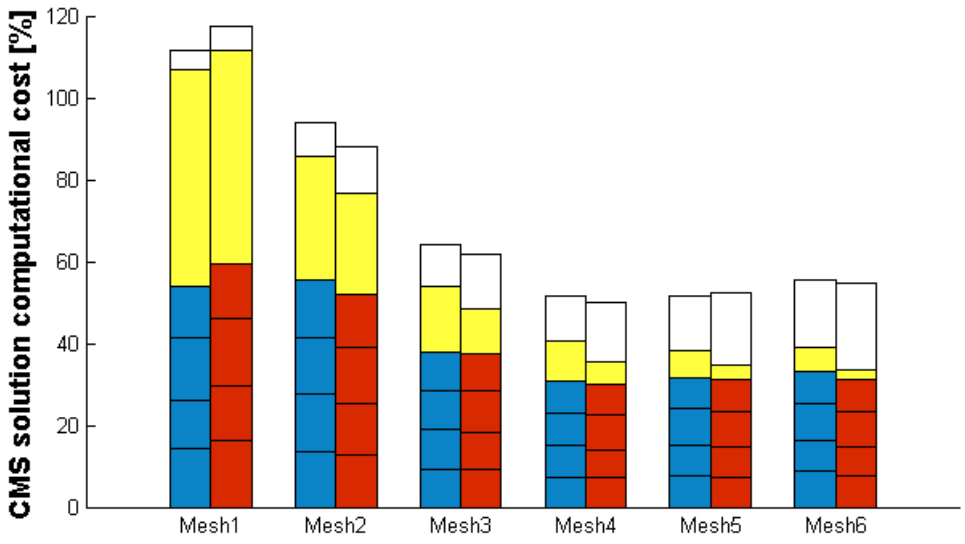

Figure 4.18: Computational time for solving each of the EVPs in the MCB and CN methods relative to the computational time for solving the full order state-space EVP. Blue: MCB components; Red: CN components; Yellow: Coupled-modal (Weighted); White: Other computations.

Here, it can be seen that the MCB and the CN overall *corrected* computational costs increase with respect to the uncorrected ones in Figure 4.17. For Mesh 1, the projected solution times exceed that of the corresponding full system EVP solution

time, so that no computational advantage is achieved by using CMS for such small system models. On the contrary, the relative cost for solving the global modes in coupled-modal coordinates decreases as the mesh grows. For meshes 4 to 6 the cost for solving the coupled-modal EVP is already below 10% of the full EVP solution cost, yielding an overall relative costs for the MCB and CN methods below 60% of the full EVP solution cost.

The MCB and CN methods show similar computation cost but, this time, with the CN method showing slightly better performance. Although the synthesis of components is more straightforwardly addressed in the MCB method, where the coupled-modal matrices are obtained by simple assembly of the component matrices, the increased computational cost of the component synthesis in the CN method is balanced out by the less-demanding solution of a significantly smaller coupled-modal EVP.

4.7 Conclusions

In this chapter the generic Component Mode Synthesis method has been explained on the grounds of the model order reduction methods presented in section 4.1 and the substructuring and coupling processes presented in section 4.2.

In Component Mode Synthesis, each of the components is reduced by means of a coordinate transformation in terms of the component modes. According to the distinct model order reduction methods, different kinds of component modes are defined. Fixed and free-interface component modes correspond to the modal truncation reduction method under specific boundary conditions. Constraint modes correspond to Guyan's condensation method, and the residual attachment modes correspond to the residual flexibility correction for the modal reduction method.

In turn, the synthesis of components is performed by applying the substructure coupling process to the modal reduced components. This leads to the CMS coupled-modal model, which is a dynamic equivalent reduced model for the original system. Finally, the dynamics of the system are solved by performing modal analysis on this reduced model (i.e. solving the corresponding eigenvalue problem).

In the context of structural design, Component Mode Synthesis presents various advantages. First of all, the FE solution of the full system is speeded up because it is more efficient to solve several smaller EVPs for the subsystems than the combined EVP of the full system. Therefore, the use of CMS reduces the time for performing

the modal analysis. Conversely, this means that the frequency limit at which it is bearable to perform FEA is pushed up. In addition to faster modal solutions, once the FE model is solved using CMS, the reduced CMS model can be readily used for solution reanalysis.

Furthermore, CMS is very well suited for modelling a structure under design that is built up of several substructures. When a structural model needs to be recurrently updated, only those components involved in design modifications need to be reanalysed. Therefore, for the reanalysis of the full structure only the solution of the modified components needs to be updated and coupled to the previous solution of the rest of the unchanged components. In a similar way, when designing a structure that may be subject to uncertainty, only the uncertain components need to be reanalysed to perform uncertainty analysis of the full system. Thus, it is somehow a natural choice to tackle the dynamic design of large built-up structures using Component Mode Synthesis.

Different CMS methods exist depending on which component modes are used for the components reduction. The most common (and successful) component modes combinations are fixed-interface modes together with constraint modes, and free-interface modes together with residual attachment modes. These combinations correspond respectively to the Craig-Bampton (CB) and Craig-Chang (CCH) classic CMS methods for undamped modal analysis, which have been described in this chapter. The former method provides a very easy and systematic modal component coupling procedure, but it does not optimally reduce the model order. Furthermore, the fixed-interface modes are more difficult to be verified against measurements than free-interface modes. The latter method offers optimal reduction of the model order at the price of a more complicated synthesis of components, giving rise to system specific coupled-modal model formulations.

However, in this work, Component Mode Synthesis is aimed at being used for the approximate reanalysis of generally damped systems (e.g. locally damped built-up systems). Therefore, the objective in this chapter has been to reclaim CMS methods for damped modal analysis. Explitcly the development of CMS methods based on the state-space formulation.

Here, a generic reformulation in state-space coordinates of the Component Mode Synthesis method has been proposed. Accordingly, two already existing state-space based CMS methods have been revisited, and exposed in detail matching this generic formulation. Namely, the Morgan-Craig-Bampton (MCB) method and the Craig-Ni (CN) method which are state-space analogous to the CB method and CCH

methods respectively. These methods have been studied through two numerical test examples.

The solution of the component state-space eigenvalue problems has proved to be troublesome. On one hand, as it has been already explained in chapter 2, an indefinite GEVP (as it is the case for the component state-space EVP) may not be solved through the standard Lanczos algorithm. Instead, the Symmetric Indefinite Lanczos Method (SILM) shall be used.

On the other hand, overdamped component eigensolutions arise when solving the component state-space EVP. These overdamped solutions are unwanted, since they should not be included in the component modes basis for the modal reduction of the component. For this reason a modified version of the Symmetric Indefinite Lanczos Method (MSILM) has been devised, so that the overdamped solutions are intrinsically filtered out.

With these adopted computational solutions, the performance of the CMS methods for the modal analysis of damped systems has been evaluated. It has been demonstrated how, for generally damped systems, the state-space CMS methods are significantly more accurate than the classical CMS methods, especially for heavily damped systems. Moreover, the computational efficiency of state-space based CMS methods has been tested against the full order state-space modal analysis solution, showing that significant computational savings are obtained for large FE models.

Chapter 5

Perturbation methods for locally damped built-up systems

The perturbation method presented in Chapter 3 is a way for approximating the variations in the modal parameters of a dynamic system when its defining physical parameters vary. The perturbation approximation consists in expressing the system modal parameters as a Taylor series expansion truncated after the linear term, so that the modal variations may be related to physical parameter variations by means of first order sensitivity functions.

For the modal parameters, the sensitivity functions are generically expressed in terms of the system matrix sensitivities, so that when multiplied by the corresponding physical parameter perturbation one may directly consider the perturbation in the modal parameter as a function of system matrix perturbations (c.f. section 3.2.2). This gives rise to the modal perturbation propagation functions $P_{\lambda_m}(\Delta\mathbf{M}, \Delta\mathbf{C}, \Delta\mathbf{K})$ and $P_{\phi_m}(\Delta\mathbf{M}, \Delta\mathbf{C}, \Delta\mathbf{K})$. As proved earlier in Chapter 3, the computational complexity of modal perturbation method (and in general of any linear approximation) is determined by the number of degrees of freedom of the baseband model, i.e. on the size of the system matrices.

The order of the matrices for large built up systems may be conveniently reduced through the Component Mode Synthesis (CMS) methods. Specifically, for locally (or generally) damped built-up systems the state-space based CMS methods described in Chapter 4 may be used. In this chapter, the use of perturbation methods on (state-space) CMS reduced models is proposed for the efficient reanalysis of locally damped built-up systems.

5.1 Perturbation propagation functions in state-space based CMS models

In this section, an original perturbation propagation scheme is proposed for the state-space based Component Mode Synthesis methods[1]. The idea is that for any variation in the physical parameters, the corresponding perturbation in the component matrices may be computed. Then, the perturbation in component matrices is propagated into the component modes through modal perturbation propagation functions and, finally, the perturbation in component modes may be propagated into the global modes of the full system. A block diagram representation of the perturbation propagation across a CMS model is shown in Figure 5.1.

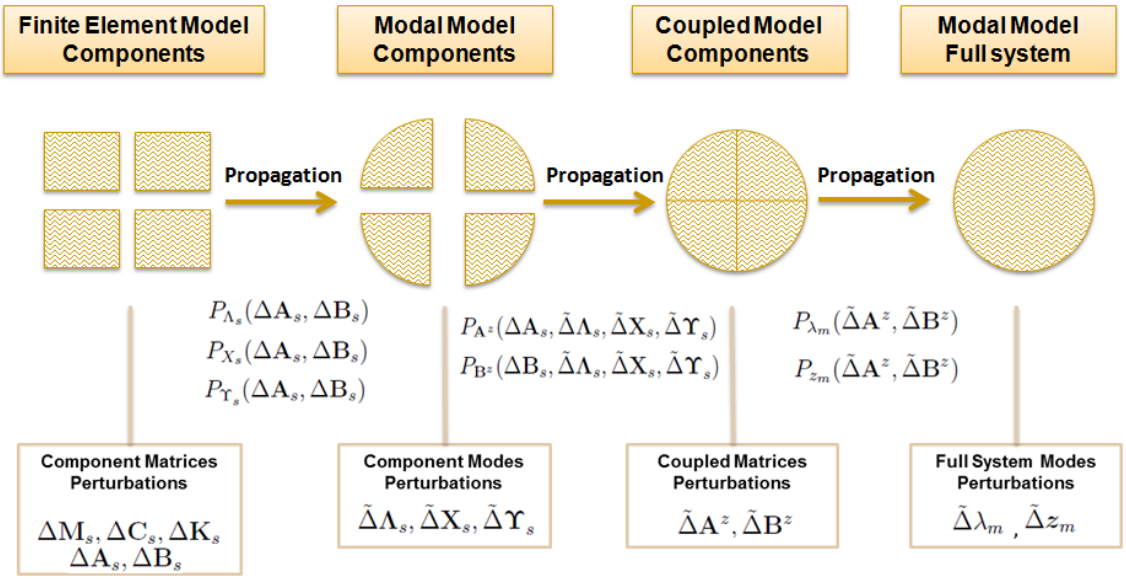

Figure 5.1: Perturbation propagation scheme in state-space based Component Mode Synthesis models.

Modal perturbation propagation functions (PPFs) are used for approximating component mode variations with respect to the component matrix variations. These include PPFs for eigenvalues P_{Λ_s}, state eigenvectors P_{X_s}, state constraint modes $P_{\Upsilon_s^C}$ and state residual attachment modes $P_{\Upsilon_s^R}$. Similar modal PPFs are used for approximating the global mode variations with respect to variations in the coupled-modal matrices, P_{λ_m} for the eigenvalues and P_{z_m} for the eigenvectors. In between, the variation in component modes is propagated into variation in the coupled-modal

[1]The perturbation propagation scheme for the state-space based Component Mode Synthesis methods was presented in [95]

matrices through a third group of perturbation propagation functions $P_{\mathbf{A}^z}$ and $P_{\mathbf{B}^z}$. These latter PPFs are specific to each of the CMS methods since they depend on the structure of the coupled-modal matrices, i.e. on the specific synthesis formulation.

With this scheme, the perturbation propagation from physical parameters to component modes is made independent of the perturbation propagation from component modes to global modes. This may be very convenient in the context of structural design, since design modifications do not usually involve the full built up structure but just one or a few of its constituent substructures.

The supposed scalability of the perturbation propagation in CMS models makes it possible to address variations in a single subsystem independently from the rest of subsystems. Hence, only the perturbations in the corresponding component modes need to be computed. Thereafter, the perturbation propagation from component modes to full system modes can be computed at a very little computational cost by virtue of the CMS coupled-modal models being of much reduced order.

Specifically, local damping variations may be conveniently addressed in state-space based CMS models. Damping treatments in vibrating structures are expensive and, consequently, they are typically applied locally where they are most efficient. The fact that damped component modes are obtained in state-space based CMS methods makes it possible to treat damping variations at a component level, which would not be the case in classical undamped CMS methods. Thus, the perturbation propagation scheme in state-space based CMS models should be well suited for tackling damping modification/optimization, or uncertainty analysis in locally damped structures.

In the following, the state-space based CMS perturbation propagation functions are derived. First, the PPFs for the component modes are presented, next, the PPFs for the global modes and, finally, the PPFs for the matrices in the MCB and the CN methods.

5.1.1 Perturbation of state-space component modes

In this section, perturbation propagation functions for component modes in state-space coordinates are presented. Normal modes, which may result from free-interface or fixed-interface conditions, are defined by the λ_k—$\boldsymbol{x}_k$ eigenpairs and depend on the s'th component matrices $\mathbf{A}_s$ and $\mathbf{B}_s$. Hence, the PPFs for the com-

ponent eigenvalues and eigenvectors sets $\mathbf{\Lambda}_s$ and $\mathbf{X}_s$ are of the form

$$\tilde{\Delta}\mathbf{\Lambda}_s = P_{\Lambda_s}(\Delta\mathbf{A}_s, \Delta\mathbf{B}_s) \tag{5.1}$$

$$\tilde{\Delta}\mathbf{X}_s = P_{X_s}(\Delta\mathbf{A}_s, \Delta\mathbf{B}_s) \tag{5.2}$$

In turn, state constraint modes as defined in the MCB method are only dependent on the stiffness matrix so that the corresponding PPF is of the form

$$\tilde{\Delta}\mathbf{\Upsilon}_s^C = P_{\Upsilon_s^C}(\Delta\mathbf{K}_s) \tag{5.3}$$

State attachment modes are a partition of the state flexibility matrix and, therefore, a function of the $\mathbf{B}_s$ matrix. Accordingly, a PPF for state attachment modes is of the following fashion

$$\tilde{\Delta}\mathbf{\Upsilon}_s^A = P_{\Upsilon_s^A}(\Delta\mathbf{B}_s) \tag{5.4}$$

Last, in order to obtain the state residual attachment modes as defined in the CN method, the residual effects of the kept component modes must be subtracted from the attachment modes. Therefore, the PPF for the state residual attachment modes shall be function of the perturbation in the normal and attachment modes and, consequently, a function of the perturbation in component matrices, i.e.

$$\tilde{\Delta}\mathbf{\Upsilon}_s^R = P_{\Upsilon_s^R}(\tilde{\Delta}\mathbf{\Upsilon}_s^A, \tilde{\Delta}\mathbf{\Lambda}_s, \tilde{\Delta}\mathbf{X}_s) = P_{\Upsilon_s^R}(\Delta\mathbf{A}_s, \Delta\mathbf{B}_s) \tag{5.5}$$

The specific expressions for these perturbation propagation functions are briefly derived next. For clarity, the component subindex s is dropped in the derivations.

Normal modes

The sensitivity functions for damped modes may be either formulated in physical coordinates or in state-space coordinates (see Appendix D). In Chapter 3 sensitivity functions in physical coordinates have been used giving rise to perturbation propagation functions for damped eigenpairs λ—$\boldsymbol{\phi}$ which are expressed in physical coordinates. However, in damped Component Mode Synthesis, state component modes are required for reducing the component matrices in state-space coordinates.

Modal sensitivity functions in the state-space may be used for obtaining the corresponding perturbation approximations. Using the state-space sensitivity functions for the damped eigenvalues (equation D.6) and state eigenvectors (equation D.9) one may find the perurbation propagation functions for the normal state component modes, i.e.

$$\tilde{\Delta}\lambda_k = \boldsymbol{x}_k^T \left[\Delta\mathbf{B} - \lambda_k\Delta\mathbf{A}\right]\boldsymbol{x}_k \tag{5.6}$$

$$\tilde{\Delta}\boldsymbol{x}_k = -\frac{1}{2}\left(\boldsymbol{x}_k^T \Delta\mathbf{A}\boldsymbol{x}_k\right) - \sum_{i\neq k} \frac{\boldsymbol{x}_i^T\left[\Delta\mathbf{B} - \lambda_k\Delta\mathbf{A}\right]\boldsymbol{x}_k}{\lambda_i - \lambda_k}\boldsymbol{x}_i \tag{5.7}$$

with the state eigenvectors being **A**-normalised.

Alternatively the $P_{\lambda_{k,s}}(\Delta\mathbf{M}_s, \Delta\mathbf{C}_s, \Delta\mathbf{K}_s)$ and $P_{\phi_{k,s}}(\Delta\mathbf{M}_s, \Delta\mathbf{C}_s, \Delta\mathbf{K}_s)$ functions in physical coordinates may be used instead. The resulting eigenvalue perturbations are exactly the same, and the state eigenvectors perturbations may be obtained from the physical eigenvector perturbations $\tilde{\Delta}\boldsymbol{\phi}_k$. Since the state eigenvectors can be expressed in terms of the corresponding eigenvalue and physical eigenvector, the perturbation in state eigenvectors can be approximated to first order as

$$\tilde{\Delta}\boldsymbol{x}_k = \begin{bmatrix} \left(\lambda_k\tilde{\Delta}\boldsymbol{\phi}_k + \tilde{\Delta}\lambda_k\boldsymbol{\phi}_k\right) \\ \tilde{\Delta}\boldsymbol{\phi}_k \end{bmatrix} \tag{5.8}$$

Constraint modes

The sensitivity function for the constraint modes in terms of the stiffness matrix may be easily obtained. The interior DOFs of the constraint modes matrix are computed from the stiffness matrix as $\boldsymbol{\Psi}_{ic}^C = -\mathbf{K}_{ii}^{-1}\mathbf{K}_{ic}$. Hence, the corresponding partial derivation with respect to a physical parameter θ reads

$$\frac{\partial\boldsymbol{\Psi}_{ic}^C}{\partial\theta} = \frac{\partial(-\mathbf{K}_{ii}^{-1}\mathbf{K}_{ic})}{\partial\theta} = \left(\mathbf{K}_{ii}^{-1}\frac{\partial\mathbf{K}_{ii}}{\partial\theta}\mathbf{K}_{ii}^{-1}\right)\mathbf{K}_{ic} - \mathbf{K}_{ii}^{-1}\frac{\partial\mathbf{K}_{ic}}{\partial\theta} \tag{5.9}$$

where the derivative of an inverse matrix and the derivation chain rule have been used. In turn, the coupling DOFs of the constraint modes matrix is just an identity matrix, i.e. $\boldsymbol{\Psi}_{cc}^C = \mathbf{I}$, so that its partial derivation is just a zero matrix.

Thence, by using the sensitivity expression in equation 5.9, the perturbation propagation function for the constraint modes matrix is obtained

$$\tilde{\Delta}\boldsymbol{\Psi}^C = \begin{bmatrix} -\mathbf{K}_{ii}^{-1}(\Delta\mathbf{K}_{ii}\boldsymbol{\Psi}_{ic}^C + \Delta\mathbf{K}_{ic}) \\ \mathbf{0}_{cc} \end{bmatrix} \tag{5.10}$$

Finally, since the state constraint modes are defined from the constraint modes in physical coordinates as $\boldsymbol{\Upsilon}^C = \mathrm{diag}(\boldsymbol{\Psi}^C, \boldsymbol{\Psi}^C)$, the perturbation propagation function for state constraint modes is simply obtained as

$$\tilde{\Delta}\boldsymbol{\Upsilon}^C = \begin{bmatrix} \tilde{\Delta}\boldsymbol{\Psi}^C & \mathbf{0} \\ \mathbf{0} & \tilde{\Delta}\boldsymbol{\Psi}^C \end{bmatrix} \tag{5.11}$$

Attachment modes

State attachment modes are defined as the attachment DOFs partition of the state flexibility matrix, i.e. $\boldsymbol{\Upsilon}^A = \mathbf{G}^x_a$. Since the state flexibility matrix is the inverse of the $\mathbf{B}$ matrix, its partial derivative with respect to a physical parameter θ is just the derivative of an inverse matrix. The sensitivity function for the state flexibility matrix is therefore

$$\frac{\partial \mathbf{G}^x}{\partial \theta} = -\mathbf{G}^x \frac{\partial \mathbf{B}}{\partial \theta} \mathbf{G}^x \tag{5.12}$$

A perturbation approximation for the state flexibility matrix may be directly formulated from the sensitivity function in equation 5.12. The corresponding perturbation propagation function for the attachment modes is then achieved by selecting just the attachment DOFs of the state flexibility matrix perturbation approximation, that is

$$\tilde{\Delta}\boldsymbol{\Upsilon}^A = -\mathbf{G}^x \Delta\mathbf{B} \boldsymbol{\Upsilon}^A \tag{5.13}$$

Residual attachment modes

The residual state attachment modes correspond to the attachment DOFs of the residual state flexibility matrix. In other words, attachment modes from which the residual static effects of the kept normal modes have been removed, i.e.

$$\boldsymbol{\Upsilon}^R = \mathbf{G}^{x,h}_a = [\mathbf{G}^x - \mathbf{G}^{x,k}]_a = \boldsymbol{\Upsilon}^A - \mathbf{X}\boldsymbol{\Lambda}^{-1}\mathbf{X}^T_a \tag{5.14}$$

where $\mathbf{G}^{x,k} = \mathbf{X}\boldsymbol{\Lambda}^{-1}\mathbf{X}^T$ is the residual matrix corresponding to the kept modes, and the a subscripts indicate attachment DOFs partitions. A sensitivity function for the $\mathbf{G}^{x,k}$ matrix in terms of the normal eigenvalues and eigenvectors is again easily obtained by partial derivation using the derivative of inverse matrix and the derivation chain rule.

$$\frac{\partial \mathbf{G}^{x,k}}{\partial \theta} = \frac{\partial(\mathbf{X}\boldsymbol{\Lambda}^{-1}\mathbf{X}^T)}{\partial \theta} = \frac{\partial \mathbf{X}}{\partial \theta}\boldsymbol{\Lambda}^{-1}\mathbf{X}^T - \mathbf{X}\boldsymbol{\Lambda}^{-1}\frac{\partial \boldsymbol{\Lambda}}{\partial \theta}\boldsymbol{\Lambda}^{-1}\mathbf{X}^T + \mathbf{X}\boldsymbol{\Lambda}^{-1}\frac{\partial \mathbf{X}^T}{\partial \theta} \tag{5.15}$$

The perturbation propagation function for the residual state attachment modes is then obtained by combining the PPF for the state attachment modes in equation 5.13 and a first order perturbation approximation using the sensitivity function in equation 5.15 for the residual effects of the kept modes

$$\tilde{\Delta}\boldsymbol{\Upsilon}^R = \tilde{\Delta}\boldsymbol{\Upsilon}^A - (\tilde{\Delta}\mathbf{X}\boldsymbol{V}^T_a - \boldsymbol{V}\tilde{\Delta}\boldsymbol{\Lambda}\boldsymbol{V}^T_a + \boldsymbol{V}\tilde{\Delta}\mathbf{X}^T_a) \tag{5.16}$$

where the matrix $\boldsymbol{V} = \mathbf{X}\boldsymbol{\Lambda}^{-1}$ has been introduced for a shorter notation.

5.1.2 Perturbation of global modes

The perturbation propagation from the coupled-modal matrices to global modes is described in this section. Global modes are defined by the λ_m—$\boldsymbol{z}_m$ eigenpairs resulting from the solution of the global eigenvalue problem in coupled-modal coordinates. Therefore, perturbation propagation functions of the following form are sought.

$$\tilde{\Delta}\lambda_m = P_{\lambda_m}(\tilde{\Delta}\mathbf{A}^z, \tilde{\Delta}\mathbf{B}^z) \tag{5.17}$$

$$\tilde{\Delta}\boldsymbol{z}_m = P_{z_m}(\tilde{\Delta}\mathbf{A}^z, \tilde{\Delta}\mathbf{B}^z) \tag{5.18}$$

Regardless of the structure of the coupled-modal matrices $\mathbf{A}^z$ and $\mathbf{B}^z$, the variations in global modes with respect to the coupled-modal matrices follow the same sensitivity relation as in any generic GEVP. Thus, analogous sensitivity functions to those of the undamped EVP (c.f. equations D.2 and D.3) shall be obtained for the global modes in coupled-modal coordinates, i.e.

$$\frac{\partial\lambda_m}{\partial\theta} = \boldsymbol{z}_m^T\left[\frac{\partial\mathbf{B}^z}{\partial\theta} - \lambda_m\frac{\partial\mathbf{A}^z}{\partial\theta}\right]\boldsymbol{z}_m \tag{5.19}$$

$$\frac{\partial\boldsymbol{z}_m}{\partial\theta} = -\frac{1}{2}\left(\boldsymbol{z}_m^T\frac{\partial\mathbf{A}^z}{\partial\theta}\boldsymbol{z}_m\right)\boldsymbol{z}_m - \sum_{i\neq m}\frac{\boldsymbol{z}_i^T\left[\frac{\partial\mathbf{B}^z}{\partial\theta} - \lambda_m\frac{\partial\mathbf{A}^z}{\partial\theta}\right]\boldsymbol{z}_m}{\lambda_i - \lambda_m}\boldsymbol{z}_i \tag{5.20}$$

where the $\boldsymbol{z}_m$ eigenvectors are assumed to be A-normalised. This means that the perturbation propagation functions for the global modes have exactly the same mathematical formulation as the modal perturbation propagation functions for undamped modes in section 3.2.3, i.e.

$$\tilde{\Delta}\lambda_m = \boldsymbol{z}_m^T\left[\tilde{\Delta}\mathbf{B}^z - \lambda_m\tilde{\Delta}\mathbf{A}^z\right]\boldsymbol{z}_m \tag{5.21}$$

$$\tilde{\Delta}\boldsymbol{z}_m = -\frac{1}{2}\left(\boldsymbol{z}_m^T\tilde{\Delta}\mathbf{A}^z\boldsymbol{z}_m\right)\boldsymbol{z}_m - \sum_{i\neq m}\frac{\boldsymbol{z}_i^T\left[\tilde{\Delta}\mathbf{B}^z - \lambda_m\tilde{\Delta}\mathbf{A}^z\right]\boldsymbol{z}_m}{\lambda_i - \lambda_m}\boldsymbol{z}_i \tag{5.22}$$

where $\tilde{\Delta}\mathbf{A}^z = \frac{\partial\mathbf{A}^z}{\partial\theta}\Delta\theta$ and $\tilde{\Delta}\mathbf{B}^z = \frac{\partial\mathbf{B}^z}{\partial\theta}\Delta\theta$ are first order perturbation approximations of the variation in the coupled-modal matrices with respect to a generic varying parameter θ.

If the mode shape vectors $\boldsymbol{x}_m$ in physical or state-space coordinates are to be recovered, then the perturbed $\tilde{\boldsymbol{z}}_m$ eigenvectors need to be transformed back by means of the $\mathbf{T}^z$ transformation matrix. However, the transformation matrix is also a function of the component modes, which means that it is also perturbed by a quantity $\Delta\mathbf{T}^z$ when the system is subject to variations. Hence, approximate perturbed

eigenvectors in full order coordinates may be recovered through the coordinate transformation

$$\tilde{\boldsymbol{x}}_m = (\mathbf{T}^z + \tilde{\Delta}\mathbf{T}^z)(\boldsymbol{z}_m + \tilde{\Delta}\boldsymbol{z}_m) \tag{5.23}$$

Clearly, the first order perturbation approximations for the coupled-modal matrices perturbations, $\tilde{\Delta}\mathbf{A}^z$, $\tilde{\Delta}\mathbf{B}^z$ and $\tilde{\Delta}\mathbf{T}^z$ need to be computed in order to use the global modes perturbation propagation functions in equations 5.21, 5.22 and 5.23. In the context of perturbation propagation in CMS models, the variations with respect to the component modes perturbations are specifically regarded.

In the following sections, the perturbation propagation functions for propagating perturbations from the component modes to the coupled-modal matrices in state-space based CMS methods are subsequently presented. Since the structure of these matrices is specific to each CMS method, different perturbation propagation functions are obtained for the MCB method and the CN method.

5.1.3 Perturbation of Morgan-Craig-Bampton matrices

In this section, perturbation propagation functions for the MCB coupled-modal matrices $\mathbf{A}^z$ and $\mathbf{B}^z$ in terms of the component modes are derived. The coupled-modal matrices in the MCB method are obtained by assembly of the reduced modal component matrices $\mathbf{A}_s^y$ and $\mathbf{B}_s^y$, where the modal component matrices are reduced through pre and post-multiplication with the modal transformation matrix $\boldsymbol{\Upsilon}_s$ consisting of the fixed-interface eigenvectors $\mathbf{X}_s^F$ and the constraint modes $\boldsymbol{\Upsilon}_s^C$ in state-space coordinates.

Accordingly, the pursued coupled-modal matrices perturbation expressions will be functions of the perturbation in component modes and also in the full order component matrices, i.e.

$$\tilde{\Delta}\mathbf{A}^z = P_{\mathbf{A}^z}(\Delta\mathbf{A}_s, \tilde{\Delta}\mathbf{X}_s^F, \tilde{\Delta}\boldsymbol{\Upsilon}_s^C) \tag{5.24}$$

$$\tilde{\Delta}\mathbf{B}^z = P_{\mathbf{B}^z}(\Delta\mathbf{B}_s, \tilde{\Delta}\boldsymbol{\Lambda}_s^F, \tilde{\Delta}\mathbf{X}_s^F, \tilde{\Delta}\boldsymbol{\Upsilon}_s^C) \tag{5.25}$$

where the approximate perturbations in component modes correspond to the ones derived in section 5.1.1. Here, it is assumed that the eigenvectors are $\mathbf{A}$-normalised, so that only matrix $\mathbf{B}^z$ is dependent on the fixed-interface eigenvalues matrix $\boldsymbol{\Lambda}_s^F$.

Component matrices

First, it is convenient to derive perturbation approximation expression for the MCB component matrices. Sensitivity function for the component matrices can be straightforwardly derived using partial differentiation. For instance, the sensitivity function for the MCB reduced component matrix $\mathbf{A}_s^y$ is

$$\frac{\partial \mathbf{A}_s^y}{\partial \theta} = \frac{\partial(\boldsymbol{\Upsilon}_s^T \mathbf{A}_s \boldsymbol{\Upsilon}_s)}{\partial \theta} = \frac{\partial \boldsymbol{\Upsilon}_s^T}{\partial \theta}\mathbf{A}_s\boldsymbol{\Upsilon}_s + \boldsymbol{\Upsilon}_s^T\frac{\partial \mathbf{A}_s}{\partial \theta}\boldsymbol{\Upsilon}_s + \boldsymbol{\Upsilon}_s^T\mathbf{A}_s\frac{\partial \boldsymbol{\Upsilon}_s}{\partial \theta} \tag{5.26}$$

Thence, a first order perturbation approximation for $\mathbf{A}_s^y$ follows as

$$\tilde{\Delta}\mathbf{A}_s^y = \tilde{\Delta}\boldsymbol{\Upsilon}_s^T\mathbf{A}_s\boldsymbol{\Upsilon}_s + \boldsymbol{\Upsilon}_s^T\tilde{\Delta}\mathbf{A}_s\boldsymbol{\Upsilon}_s + \boldsymbol{\Upsilon}_s^T\mathbf{A}_s\tilde{\Delta}\boldsymbol{\Upsilon}_s \equiv \tilde{\Delta}(\boldsymbol{\Upsilon}^T\mathbf{A}\boldsymbol{\Upsilon})_s \tag{5.27}$$

where the short notation $\tilde{\Delta}(\boldsymbol{\Upsilon}^T\mathbf{A}\boldsymbol{\Upsilon})_s$ is introduced. An analogous expression is obtained for the $\mathbf{B}_s^y$ matrix, i.e. $\tilde{\Delta}\mathbf{B}_s^y = \tilde{\Delta}(\boldsymbol{\Upsilon}^T\mathbf{B}\boldsymbol{\Upsilon})_s$.

Now, the expressions for $\tilde{\Delta}\mathbf{A}_s^y$ and $\tilde{\Delta}\mathbf{B}_s^y$ shall be better expressed in terms of the component modal and constraint DOFs partitions. According to the MCB component modal matrices in terms of modal and constraint partitions, i.e.

$$\mathbf{A}_s^y = \begin{bmatrix} \mathbf{I} & \mathbf{X}^{F^T}\mathbf{A}\boldsymbol{\Upsilon}^C \\ \boldsymbol{\Upsilon}^{C^T}\mathbf{A}\mathbf{X}^F & \boldsymbol{\Upsilon}^{C^T}\mathbf{A}\boldsymbol{\Upsilon}^C \end{bmatrix}_s \qquad \mathbf{B}_s^y = \begin{bmatrix} \boldsymbol{\Lambda}^F & \mathbf{X}^{F^T}\mathbf{B}\boldsymbol{\Upsilon}^C \\ \boldsymbol{\Upsilon}^{C^T}\mathbf{B}\mathbf{X}^F & \boldsymbol{\Upsilon}^{C^T}\mathbf{B}\boldsymbol{\Upsilon}^C \end{bmatrix}_s$$

equation 5.27 may be expanded as

$$\tilde{\Delta}\mathbf{A}_s^y = \begin{bmatrix} \mathbf{0} & \tilde{\Delta}(\mathbf{X}^{F^T}\mathbf{A}\boldsymbol{\Upsilon}^C) \\ \tilde{\Delta}(\boldsymbol{\Upsilon}^{C^T}\mathbf{A}\mathbf{X}^F) & \tilde{\Delta}(\boldsymbol{\Upsilon}^{C^T}\mathbf{A}\boldsymbol{\Upsilon}^C) \end{bmatrix}_s \tag{5.28}$$

and a similar expression is found for $\tilde{\Delta}\mathbf{B}_s^y$, that is

$$\tilde{\Delta}\mathbf{B}_s^y = \begin{bmatrix} \tilde{\Delta}\boldsymbol{\Lambda}^F & \tilde{\Delta}(\mathbf{X}^{F^T}\mathbf{B}\boldsymbol{\Upsilon}^C) \\ \tilde{\Delta}(\boldsymbol{\Upsilon}^{C^T}\mathbf{B}\mathbf{X}^F) & \tilde{\Delta}(\boldsymbol{\Upsilon}^{C^T}\mathbf{B}\boldsymbol{\Upsilon}^C) \end{bmatrix}_s \tag{5.29}$$

Perturbation propagation functions for the MCB coupled-modal matrices can now be easily derived from the component matrices perturbation approximations in equations 5.28 and 5.29.

Coupled-modal matrices

Since the MCB coupled-modal matrices are obtained by simple assembly of the reduced component matrices, their corresponding perturbation propagation function can be directly obtained through the adequate assembly of the perturbation approximations in equations 5.28 and 5.29 for each of the reduced components matrices.

Hence, the PPFs for the $\mathbf{A}^z$ and $\mathbf{B}^z$ coupled-modal matrices have the following structure

$$\tilde{\Delta}\mathbf{A}^z = \begin{bmatrix} \mathbf{0} & \mathbf{0} & \cdots & \tilde{\Delta}\left(\mathbf{X}^{F^T}\mathbf{A}\boldsymbol{\Upsilon}^C\right)_1 \\ \mathbf{0} & \mathbf{0} & \cdots & \tilde{\Delta}\left(\mathbf{X}^{F^T}\mathbf{A}\boldsymbol{\Upsilon}^C\right)_2 \\ \vdots & \vdots & \ddots & \vdots \\ \tilde{\Delta}\left(\boldsymbol{\Upsilon}^{C^T}\mathbf{A}\mathbf{X}^F\right)_1 & \tilde{\Delta}\left(\boldsymbol{\Upsilon}^{C^T}\mathbf{A}\mathbf{X}^F\right)_2 & \cdots & \sum_s \tilde{\Delta}\left(\boldsymbol{\Upsilon}^{C^T}\mathbf{A}\boldsymbol{\Upsilon}^C\right)_s \end{bmatrix} \tag{5.30}$$

$$\tilde{\Delta}\mathbf{B}^z = \begin{bmatrix} \tilde{\Delta}\boldsymbol{\Lambda}_1^F & \mathbf{0} & \cdots & \tilde{\Delta}\left(\mathbf{X}^{F^T}\mathbf{B}\boldsymbol{\Upsilon}^C\right)_1 \\ \mathbf{0} & \tilde{\Delta}\boldsymbol{\Lambda}_2^F & \cdots & \tilde{\Delta}\left(\mathbf{X}^{F^T}\mathbf{B}\boldsymbol{\Upsilon}^C\right)_2 \\ \vdots & \vdots & \ddots & \vdots \\ \tilde{\Delta}\left(\boldsymbol{\Upsilon}^{C^T}\mathbf{B}\mathbf{X}^F\right)_1 & \tilde{\Delta}\left(\boldsymbol{\Upsilon}^{C^T}\mathbf{B}\mathbf{X}^F\right)_2 & \cdots & \sum_s \tilde{\Delta}\left(\boldsymbol{\Upsilon}^{C^T}\mathbf{B}\boldsymbol{\Upsilon}^C\right)_s \end{bmatrix} \tag{5.31}$$

Here, it can be observed that the PPF for the $\mathbf{B}^z$ coupled-modal matrix is posed as function of the $\tilde{\Delta}\boldsymbol{\Lambda}_s^F$, $\tilde{\Delta}\mathbf{X}_s^F$ $\tilde{\Delta}\boldsymbol{\Upsilon}_s^C$ and $\tilde{\Delta}\mathbf{B}_s$ (approximate) perturbations in each of the components, whereas the PPF for the $\mathbf{A}^z$ matrix is function of the $\tilde{\Delta}\mathbf{X}_s^F$ $\tilde{\Delta}\boldsymbol{\Upsilon}_s^C$ and $\tilde{\Delta}\mathbf{A}_s$ perturbations, but not of the $\tilde{\Delta}\boldsymbol{\Lambda}_s^F$ perturbations.

Global modes transformation matrix

Similarly, in the MCB method, the transformation matrix $\mathbf{T}^z$ for recovering the global modes in physical coordinates is obtained by assembly of the component modal transformation matrices $\boldsymbol{\Upsilon}_s = [\mathbf{X}^F\boldsymbol{\Upsilon}^C]_s$. Thence, the perturbation expression for $\mathbf{T}^z$ can also be obtained by adequate assembly of the component modes perturbation approximated through the corresponding PPFs, yielding the following expression

$$\tilde{\Delta}\mathbf{T}^z = \begin{bmatrix} \tilde{\Delta}\mathbf{X}_{ik,1}^F & \mathbf{0} & \cdots & \tilde{\Delta}\boldsymbol{\Upsilon}_{ic,1}^C \\ \mathbf{0} & \tilde{\Delta}\mathbf{X}_{ik,2}^F & \cdots & \tilde{\Delta}\boldsymbol{\Upsilon}_{ic,2}^C \\ \vdots & \vdots & \ddots & \vdots \\ \mathbf{0} & \mathbf{0} & \cdots & \mathbf{0}_{cc} \end{bmatrix} \tag{5.32}$$

In conclusion, when a FE model is reduced into a MCB model, any perturbation in a system parameter can be effectively propagated into the full system modes through perturbation propagation functions. A perturbation in any of the defined elements is propagated into the MCB coupled modal matrices following equations 5.30 and 5.31 together with the PPFs for the fixed-interface and the constraint modes in state-space coordinates defined in section 5.1.1. Then, the perturbation in the MCB reduced matrices is propagated into the global modes at a small computational cost

(equations 5.21 and 5.22). Finally, the perturbed transformation matrix, as has just been defined, may be used to recover the mode shapes in physical coordinates.

5.1.4 Perturbation of Craig-Ni matrices

The perturbation propagation functions for the CN coupled-modal matrices $\mathbf{A}^z$ and $\mathbf{B}^z$ in terms of the component modes are derived in this section. In this case, the PPFs will be function of the perturbation in the full order component matrices and in CN component modes, that is

$$\tilde{\Delta}\mathbf{A}^z = P_{\mathbf{A}^z}(\Delta\mathbf{A}_s, \tilde{\Delta}\mathbf{\Lambda}_s, \tilde{\Delta}\mathbf{X}_s, \tilde{\Delta}\mathbf{\Upsilon}_s^R) \tag{5.33}$$

$$\tilde{\Delta}\mathbf{B}^z = P_{\mathbf{B}^z}(\Delta\mathbf{B}_s, \tilde{\Delta}\mathbf{\Lambda}_s, \tilde{\Delta}\mathbf{X}_s, \tilde{\Delta}\mathbf{\Upsilon}_s^R) \tag{5.34}$$

where, this time, $\mathbf{A}^z$ is also function of the component eigenvalues matrix $\mathbf{\Lambda}_s$ by reason of the use of residual attachment modes.

Component matrices

As for the MCB method, it is convenient to first derive the perturbation expressions for the reduced component matrices. Component matrices reduction is performed analogously to the MCB method, i.e. $\mathbf{A}_s^y = \mathbf{\Upsilon}_s^T\mathbf{A}_s\mathbf{\Upsilon}_s$ and $\mathbf{B}_s^y = \mathbf{\Upsilon}_s^T\mathbf{B}_s\mathbf{\Upsilon}_s$, but this time with the modal reduction matrix consisting of free-interface normal modes and residual attachment modes in state-space coordinates, i.e. $\mathbf{\Upsilon}_s = [\mathbf{X}\ \mathbf{\Upsilon}^R]_s$. This results in the CN reduced component matrices having the following structure

$$\mathbf{A}_s^y = \begin{bmatrix} \bar{\mathbf{A}}_{kk} & \mathbf{0}_{ka} \\ \mathbf{0}_{ak} & \mathbf{A}_{aa}^y \end{bmatrix}_s = \begin{bmatrix} \mathbf{I} & \mathbf{0} \\ \mathbf{0} & \mathbf{\Upsilon}^{R^T}\mathbf{A}\mathbf{\Upsilon}^R \end{bmatrix}_s \tag{5.35}$$

$$\mathbf{B}_s^y = \begin{bmatrix} \bar{\mathbf{B}}_{kk} & \mathbf{0}_{ka} \\ \mathbf{0}_{ak} & \mathbf{B}_{aa}^y \end{bmatrix}_s = \begin{bmatrix} \mathbf{\Lambda} & \mathbf{0} \\ \mathbf{0} & -\mathbf{\Upsilon}_a^R \end{bmatrix}_s \tag{5.36}$$

where the free-interface modes are assumed $\mathbf{A}$-normalised. Equations 5.35 and 5.36 show simple expressions where the reduced component matrices depend basically on the residual attachment modes $\mathbf{\Upsilon}^R$.

This very simple structure of the CN component matrices yield equally simple expressions for the CN component matrices perturbations. The perturbation expression for matrix $\mathbf{A}_s^y$ reads

$$\tilde{\Delta}\mathbf{A}_s^y = \begin{bmatrix} \mathbf{0} & \mathbf{0} \\ \mathbf{0} & \tilde{\Delta}(\mathbf{\Upsilon}^{R^T}\mathbf{A}\mathbf{\Upsilon}^R) \end{bmatrix}_s \tag{5.37}$$

where the short notation $\tilde{\Delta}(\boldsymbol{\Upsilon}^{R^T}\mathbf{A}\boldsymbol{\Upsilon}^R)$ is introduced again as in equation 5.27. Hence, $\tilde{\Delta}\mathbf{A}_s^y$ depends only on the full order component matrix perturbation $\tilde{\Delta}\mathbf{A}_s$ and the residual attachment modes perturbation $\tilde{\Delta}\boldsymbol{\Upsilon}_s^R$. In turn, the perturbation expression for matrix $\mathbf{B}_s^y$ is even simpler

$$\tilde{\Delta}\mathbf{B}_s^y = \begin{bmatrix} \tilde{\Delta}\boldsymbol{\Lambda} & \mathbf{0} \\ \mathbf{0} & -\tilde{\Delta}\boldsymbol{\Upsilon}_a^R \end{bmatrix}_s \tag{5.38}$$

being just a function of the eigenvalues perturbation $\tilde{\Delta}\boldsymbol{\Lambda}$ and the residual attachment modes perturbation $\tilde{\Delta}\boldsymbol{\Upsilon}_a^R$ at the attachment DOFs. However, recall that the residual attachment modes perturbation involves the perturbation of the free-interface modes as well (both eigenvalues and eigenvectors). Thus, both component matrices are functions of the perturbation in all of the component modes.

Coupled-modal matrices

Once the perturbation expressions for the CN component matrices have been derived, the perturbation propagation functions for the coupled-modal matrices may be derived. Yet, the synthesis of components in the CN method is more complicated than the simple superelement assembly process resulting in the MCB method. In consequence, the PPFs for the CN coupled-modal matrices are not so straightforward in this case.

The synthesis of CN components is enforced by pre- and post-multiplying the $\mathbf{A}^y$ and $\mathbf{B}^y$ component-modal matrices[2] with the modal condensation matrix $\mathbf{S}^z$. Given the structure of $\mathbf{S}^z$ for the CN coupling process, the CN coupled-modal matrices may be expressed as a sum of modal and residual matrices[3], i.e.

$$\mathbf{A}^z = \bar{\mathbf{A}}_{kk} + {\mathbf{S}_{ak}^z}^T\mathbf{A}_{aa}^y\mathbf{S}_{ak}^z = \mathbf{I} + \mathbf{A}^R \tag{5.39}$$

$$\mathbf{B}^z = \bar{\mathbf{B}}_{kk} + {\mathbf{S}_{ak}^z}^T\mathbf{B}_{aa}^y\mathbf{S}_{ak}^z = \boldsymbol{\Lambda} + \mathbf{B}^R \tag{5.40}$$

Sensitivity functions for the coupled modal matrices are easily obtained by partial differentiation of equations 5.39 and 5.40 using the chain rule. Accordingly, first order perturbation approximation for the coupled-modal matrices read

$$\tilde{\Delta}\mathbf{A}^z = \tilde{\Delta}\mathbf{A}^R = \tilde{\Delta}({\mathbf{S}_{ak}^z}^T\mathbf{A}_{aa}^y\mathbf{S}_{ak}^z) \tag{5.41}$$

[2]Here $\mathbf{A}^y$ and $\mathbf{B}^y$ are block diagonal matrices in generalised component-modal coordinates, that is, containing all of the CN component matrices $\mathbf{A}_s^y$ and $\mathbf{B}_s^y$.

[3]Here $\bar{\mathbf{A}}_{kk} = \mathbf{I}$ and $\bar{\mathbf{B}}_{kk} = \boldsymbol{\Lambda}$ are block diagonal matrices containing all of the components modal matrices, and the residual matrices $\mathbf{A}^R$ and $\mathbf{B}^R$ contain all the residual effects of the truncated high order component modes.

$$\tilde{\Delta}\mathbf{B}^z = \tilde{\Delta}\mathbf{\Lambda} + \tilde{\Delta}(\mathbf{S}_{ak}^{z\,T}\mathbf{B}_{aa}^y\mathbf{S}_{ak}^z) \tag{5.42}$$

where the $\tilde{\Delta}(\ )$ compact notation is introduced again for clarity. The $\tilde{\Delta}\mathbf{A}_{aa}^y$ and $\tilde{\Delta}\mathbf{B}_{aa}^y$ perturbations are directly obtained from equations 5.37 and 5.38. The $\tilde{\Delta}\mathbf{S}_{ak}^z$ perturbation shall be further derived.

The attachment partition of the modal condensation matrix $\mathbf{S}_{ak}^z$ is obtained from the modal coupling matrix $\boldsymbol{\mathcal{C}}^y$. Its mathematical expression, i.e. $\mathbf{S}_{ak}^z = -\boldsymbol{\mathcal{C}}_{ca}^{y\,-1}\boldsymbol{\mathcal{C}}_{ck}^y$, is analogous to the expression for computing the constraint modes. Hence, the perturbation aproximation for $\mathbf{S}_{ak}^z$ is exactly of the same form as the perturbation approximation for $\mathbf{\Psi}_{ic}^C$ in equation 5.10, that is

$$\tilde{\Delta}\mathbf{S}_{ak}^z = -\boldsymbol{\mathcal{C}}_{ca}^{y\,-1}\left(\tilde{\Delta}\boldsymbol{\mathcal{C}}_{ca}^y\mathbf{S}_{ak}^z + \tilde{\Delta}\boldsymbol{\mathcal{C}}_{ck}^y\right) \tag{5.43}$$

Equation 5.43 propagates the perturbation in modal coupling matrix into the modal condensation matrix. A perturbation expression for $\tilde{\Delta}\boldsymbol{\mathcal{C}}^y$ in terms of the component modes is therefore needed. However, there is no generic expression for the modal coupling matrix since its structure is system specific (e.g. how many couplings has a component, how many components are involved at each coupling DOF, etc.).

Therefore, explicit expressions for the coupled-modal matrices perturbation may not be given for a generic case. Nevertheless, the modal coupling matrix is always composed of component modes matrices $\mathbf{X}_s$ and $\mathbf{\Upsilon}_s^R$. For instance, in Chapter 4 the modal coupling matrix for a simple system consisting of just two coupled components was given in equation 4.118. Accordingly, the corresponding perturbation expression is simply

$$\tilde{\Delta}\boldsymbol{\mathcal{C}}^y = [\tilde{\Delta}\boldsymbol{\mathcal{C}}_{ck}^y\ \tilde{\Delta}\boldsymbol{\mathcal{C}}_{ca}^y] = \begin{bmatrix} \mathbf{0}_{ck} & \mathbf{0}_{ck} & \mathbf{0}_{ca} & \mathbf{0}_{ca} \\ \tilde{\Delta}\mathbf{X}_{ck,1}^D & -\tilde{\Delta}\mathbf{X}_{ck,2}^D & \tilde{\Delta}\mathbf{\Upsilon}_{ca,1}^{D,R} & -\tilde{\Delta}\mathbf{\Upsilon}_{ca,2}^{D,R} \end{bmatrix} \tag{5.44}$$

Hence, a perturbation expression for $\boldsymbol{\mathcal{C}}^y$ may be always found in terms of the $\tilde{\Delta}\mathbf{X}_s$ and $\tilde{\Delta}\mathbf{\Upsilon}_s^R$ perturbations, but this will always be system specific.

In any case, considering that a perturbation approximation $\tilde{\Delta}\boldsymbol{\mathcal{C}}^y$ may be obtained, PPFs for the CN coupled-modal matrices in terms of the component modes perturbations are derived by inserting the specific $\tilde{\Delta}\boldsymbol{\mathcal{C}}^y$ perturbation expression into equation 5.43, and this latter equation into equations 5.41 and 5.42.

Global modes transformation matrix

Once the perturbations in component modes are propagated into the CN coupled-modal matrices, these can be further propagated into the global modes through

equations 5.21 and 5.22. In order to recover global modes in physical coordinates, the global modes in CN coupled-modal coordinates must be transformed back. Yet, CN transformation matrix $\mathbf{T}^z$ is a function of the component modes, so that it also gets perturbed by a quantity $\Delta\mathbf{T}^z$. A first order perturbation approximation $\tilde{\Delta}\mathbf{T}^z$ may be computed.

The CN transformation matrix is obtained by post-multiplication of the $\boldsymbol{\Upsilon}$ component modes matrix[4] with the modal condensation matrix $\mathbf{S}^z$, i.e. $\mathbf{T}^z = \boldsymbol{\Upsilon}\mathbf{S}^z$. Both matrices, $\boldsymbol{\Upsilon}$ and $\mathbf{S}^z$ are functions of the component modes for all the components, but the exact structure of these matrices is dependent on the coupling constraint equations, which are system specific. Thus no explicit form for $\mathbf{T}^z$ in the CN method may be given.

At best, the CN transformation matrix may be expressed as a sum of two matrices, i.e. $\mathbf{T}^z = \mathbf{X} + \boldsymbol{\Upsilon}^R\mathbf{S}^z_{ak} = \mathbf{X} + \mathbf{T}^R$, from which a $\tilde{\Delta}\mathbf{T}^z$ perturbation approximation can be derived

$$\tilde{\Delta}\mathbf{T}^z = \tilde{\Delta}\mathbf{X} + \tilde{\Delta}\boldsymbol{\Upsilon}^R\mathbf{S}^z_{ak} + \boldsymbol{\Upsilon}^R\tilde{\Delta}\mathbf{S}^z_{ak} \tag{5.45}$$

where $\tilde{\Delta}\mathbf{S}^z_{ak}$ is given by equation 5.43 and the $\tilde{\Delta}\mathbf{X}$, $\tilde{\Delta}\boldsymbol{\Upsilon}^R$ and $\tilde{\Delta}\boldsymbol{\mathcal{C}}^y$ perturbations are system specific, but simple expressions in terms of the component modes perturbations.

In conclusion, perturbation approximation expressions $\tilde{\Delta}\mathbf{A}^z$, $\tilde{\Delta}\mathbf{B}^z$ and $\tilde{\Delta}\mathbf{T}^z$ exist for the Craig-Ni matrices, however, their mathematical formulation is system specific. Moreover, although the perturbation approximation for the CN component matrices is very simple, intermediate perturbation approximations (e.g. $\tilde{\Delta}\mathbf{S}^z$, $\tilde{\Delta}\boldsymbol{\mathcal{C}}^y$ ...) are needed in order to get the linear perturbation propagation function for the the CN coupled modal-matrices.

This makes the use of the perturbation propagation scheme with CN reduced models less amenable than its use with MCB reduced models. This does not mean that efficient perturbation methods may not be derived for CN reduced models, but their mathematical derivations would be very tedious. Accordingly, in the remaining parts of this chapter the MCB method will be considered throughout for the derivation of efficient perturbation methods in state-space based CMS models.

[4]Here the component modes matrix $\boldsymbol{\Upsilon}$ is a matrix constructed by the adequate assembly of all of the component modes transformation matrices $\boldsymbol{\Upsilon}_s$ into a generalised coordinates matrix $\boldsymbol{\Upsilon}^y$ and further transformation into (state-space) physical coordinates through condensation of the redundant coupling DOFs between components, i.e. $\boldsymbol{\Upsilon} = \mathbf{S}^{-1}\boldsymbol{\Upsilon}^y$.

5.1.5 Numerical validation

The locally damped cantilever example is here used again in order to test the performance of the damped CMS perturbation propagation approximation. The description of the beam is exactly the same as in section 4.6.1 for the heavily damped case, with elements 5 and 8 in Figure 5.2 having ten times higher damping than the rest of the elements. The beam is divided into two components and the ten first modes are computed through the MCB method.

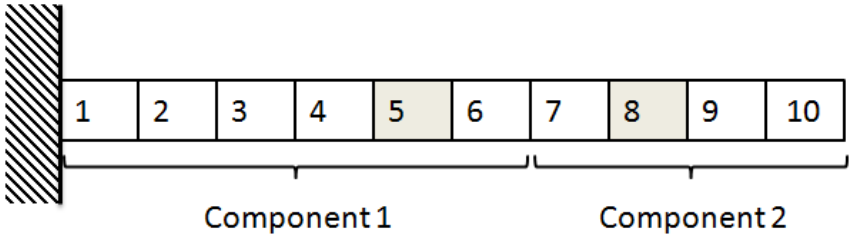

Figure 5.2: Locally damped cantilever beam example.

Damping variation

First, variation of the localised damping in component 2 is considered. The damping in element 8 is described by the corresponding element damping matrix $\mathbf{C}_{E8}$. A variation $\Delta\mathbf{C}_{E8}$ from -50% to +50% of the original $\mathbf{C}_{E8}$ value is defined in steps of 10%. The modal solution for each variation is sought.

For each of the first ten damped modes, Figure 5.3 shows the exact eigenvalue variation curves in a modal frequency versus modal damping complex plane when the $\mathbf{C}_{E8}$ matrix is perturbed from -50% to +50% of its original value. Here, these modal solutions will be computed through perturbation approximations for each of the 10% perturbation steps.

From the baseline solution the full system modes of the system are approximated in two ways. First, they are computed through the CMS perturbation propagation functions defined for the MCB method. The perturbation approximations are subsequently compared to the exact modal solutions by means of relative error and MAC values. Then, the same modes are directly computed through full system modes perturbation approximation (as defined in section 3.2.3), and compared to the exact solutions. In this way, the state-space CMS perturbation propagation scheme can be assessed against the full order modal perturbation approximation.

Figure 5.4 shows the relative errors in the perturbed modal frequencies of the first

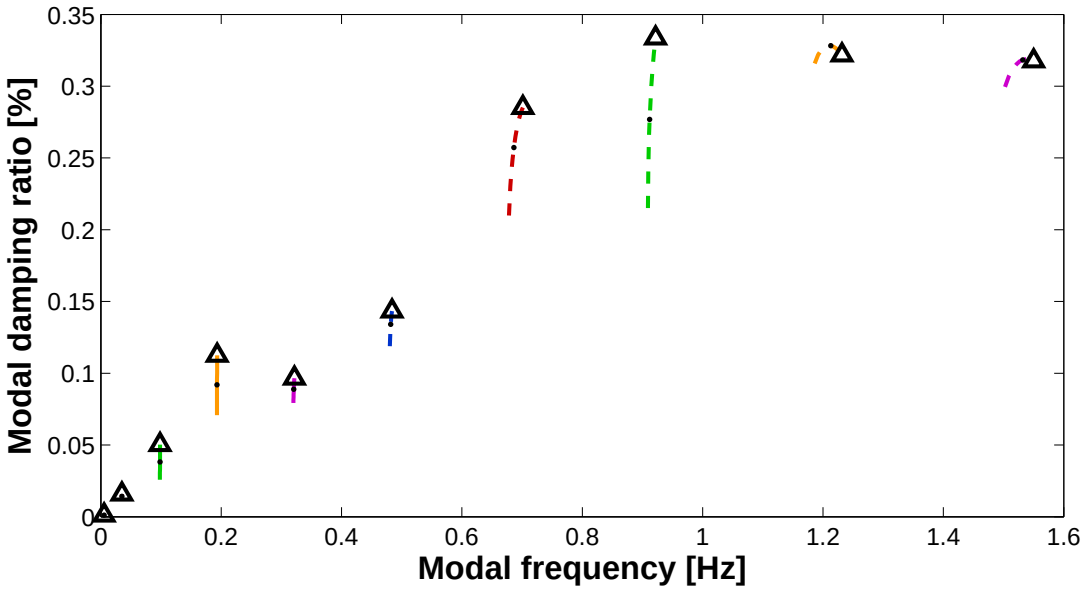

Figure 5.3: Exact variation for the first 10 eigenvalues of the cantilever example when $\mathbf{C}_{\mathrm{E8}}$ is perturbed by -50% to +50%. Black dots and black triangles indicate eigenvalues at 0% and +50% perturbations respectively.

ten modes. The error curves for the CMS perturbation propagation scheme are presented in the left hand side plot, and the error curves for the full order perturbation approximation are presented in the right hand side plot. It can be seen that, in both cases, the approximation error in the six lowest modes is below 0.1% of the modal frequency value for all of the damping variation range. In fact, in Figure 5.3 the modes 1 to 6 show modal damping values below 15%, so that they can be considered lightly damped. Hence, damping variations imply almost no perturbation in modal frequency, and the perturbation approximation error is consequently very small. On the contrary, modes 7 to 10 show modal damping values well over 20%, i.e. they are heavily damped. Therefore, noticeable perturbations in modal frequencies occur for variation in the system damping. Nevertheless, the perturbation approximation error in these latter modes is still below 1% error in modal frequency, which is a rather small error for engineering purposes.

If the left and right hand plots in Figure 5.4 are compared it can be seen that the error curves for the four largest frequency modes show significant differences. For the full order modal perturbation solutions, the exact solution is obtained at 0% damping perturbation, and maximum approximation errors are encountered almost symmetrically at both extremes of the damping variation interval, all of them in the range of 0.3% to 0.5% error. On the contrary, for the CMS perturbation propagation solutions, significant modal frequency errors are already present at

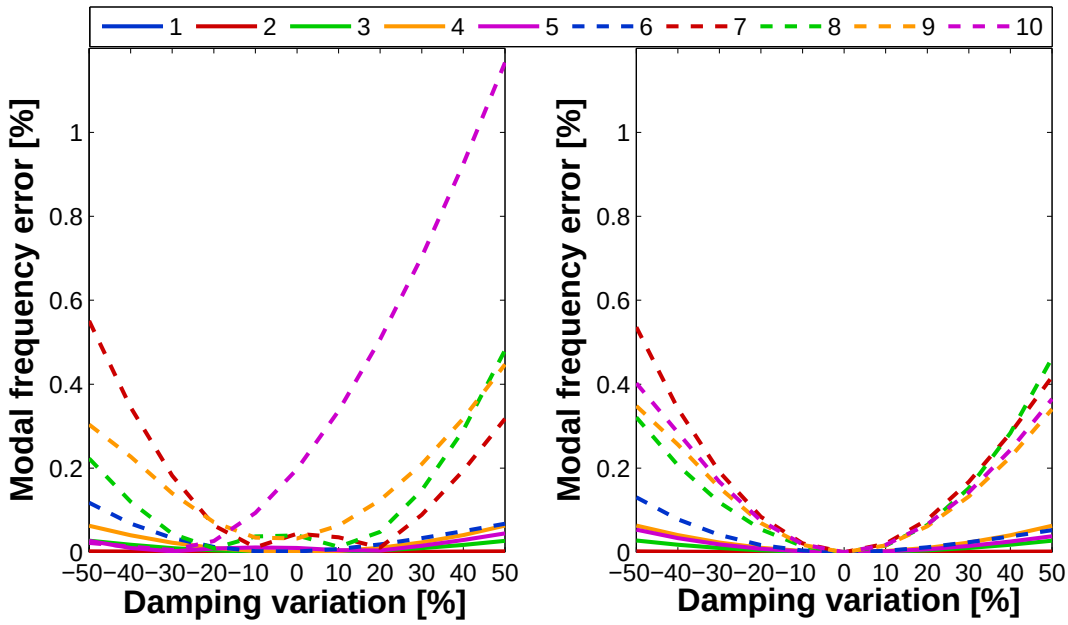

Figure 5.4: Modal frequency error values for the first 10 eigenvalues of the cantilever example when $\mathbf{C}_{\mathrm{E8}}$ is perturbed from -50% to +50%. Left: CMS perturbation propagation. Right: Full order modal perturbation.

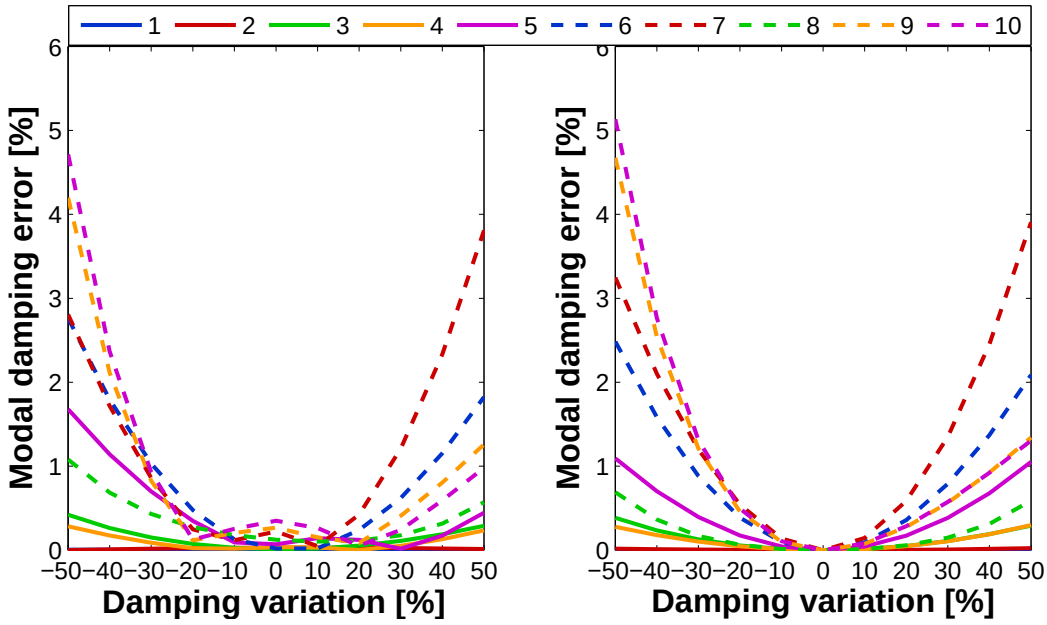

Figure 5.5: Modal damping error values for the first 10 eigenvalues of the cantilever example when $\mathbf{C}_{\mathrm{E8}}$ is perturbed by -50% to +50%. Left: CMS perturbation propagation. Right: Full order modal perturbation.

0% damping perturbation[5] (e.g. 0.2% error in mode 10). Thence, in the highest

[5]These errors are not due to the perturbation propagation scheme but to the fact that the CMS

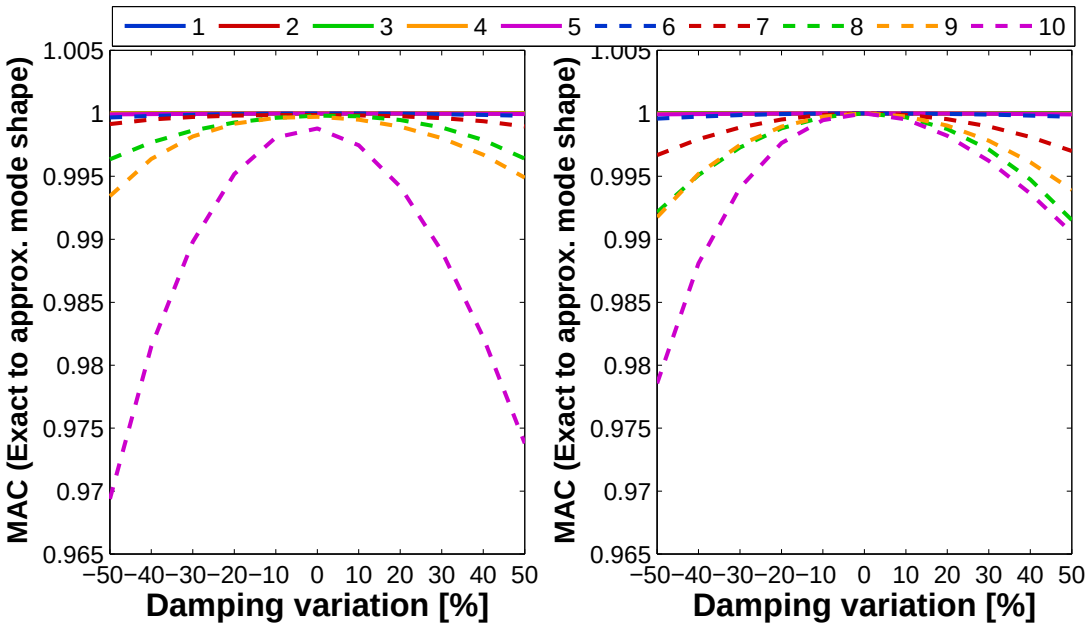

Figure 5.6: Modal Assurance Criterion values for the first 10 eigenvectors of the cantilever example when $\mathbf{C}_{\mathrm{E8}}$ is perturbed by -50% to +50%. Left: CMS perturbation propagation. Right: Full order modal perturbation.

modes, slightly bigger maximum errors result from CMS perturbation propagation approximation (up to 1% error), and these are not symmetrical with respect to the damping variation interval. In both cases, it can be said that the approximation errors in the modal frequencies are of similar magnitude.

Figure 5.5 shows the relative errors in the perturbed modal damping ratios of the first ten modes. It can be seen that modal damping errors are of larger magnitude than modal frequency errors. For the 4 highest modes (heavily damped) maximum approximation errors up to 5% of the damping value are encountered at the extremes of the variation interval. Moreover, modal damping errors for the 6 lowest modes (lightly damped) increase up to 2% error, which are not negligible errors as were the case for the modal frequency error. This happens because significant modal damping perturbations occur even for the lightly damped modes, as can be seen in Figure 5.3. This time, the perturbation approximation error dominates over the CMS modal solution error so that, besides not obtaining the exact solution at 0% damping variation, the CMS perturbation propagation approximation obtains roughly the same error curves as the full order modal perturbation approximation.

Finally, the mode shape vectors obtained through perturbation approximations were

baseline solution already presents some approximation error for the highest modes. The reference case CMS solution errors might be minimised by increasing the number of component modes.

evaluated by computing the Modal Assurance Criterion between the approximate eigenvectors and their corresponding exact eigenvector solution. The resulting MAC values are shown in Figure 5.6. MAC values over 0.97 are obtained for all modes throughout all the variation range, with slightly worse performance for the CMS perturbation approximation as a result of non-exact baseline solution obtained in the MCB method. This means that eigenvectors are very well approximated through perturbation approximation, probably because the actual eigenvector perturbations are very small when system damping varies.

Stiffness variation

Next, a second variation scenario is considered. The elastic modulus in Component 2 is assumed to vary from -50% to +50% of its nominal value (with damping held fixed). That is, the assembled stiffness matrix for Component 2 $\mathbf{K}_{C2}$ is subject to elastic modulus proportional variations $\Delta\mathbf{K}_{C2}$. The same modal solutions as in the damping variation case have been computed in steps of 10% variations.

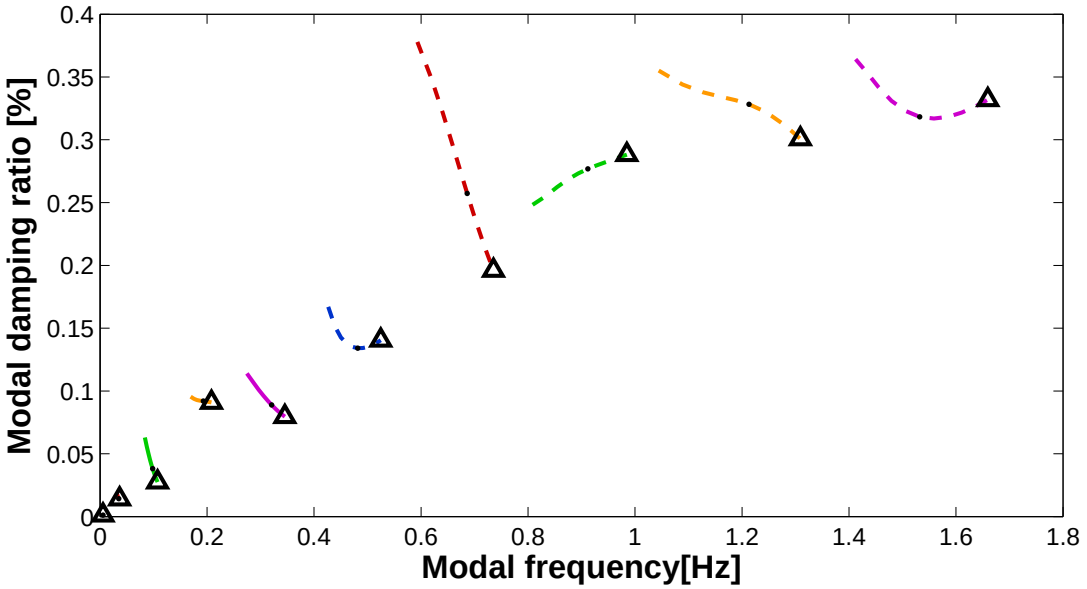

Figure 5.7: Exact variation for the first 10 eigenvalues of the cantilever example when $\mathbf{K}_{C2}$ is perturbed by -50% to +50%. Black dots and black triangles indicate eigenvalues at 0% and +50% perturbations respectively.

Figure 5.7 shows the exact variation of the eigenvalues for -50% to +50% $\mathbf{K}_{C2}$ variations for which perturbation approximations are computed. Notice that the eigenvalue variations are much more pronounced for $\Delta\mathbf{K}_{C2}$ variations than for $\Delta\mathbf{C}_{E2}$

variations in Figure 5.3. For increasing $\mathbf{K}_{C2}$ values the modal frequencies increase monotonically, whereas the modal damping values do not all vary increasingly nor monotonically. Thence, it is clear that modal damping values are strongly sensitive to system stiffness variations in a non-linear way.

The perturbation approximations for the first ten modes are evaluated in the following. Approximation errors for the modal frequencies and modal damping values are presented in Figures 5.8 and 5.9 respectively, and the MAC values for the corresponding mode shape vectors are shown in Figure 5.10.

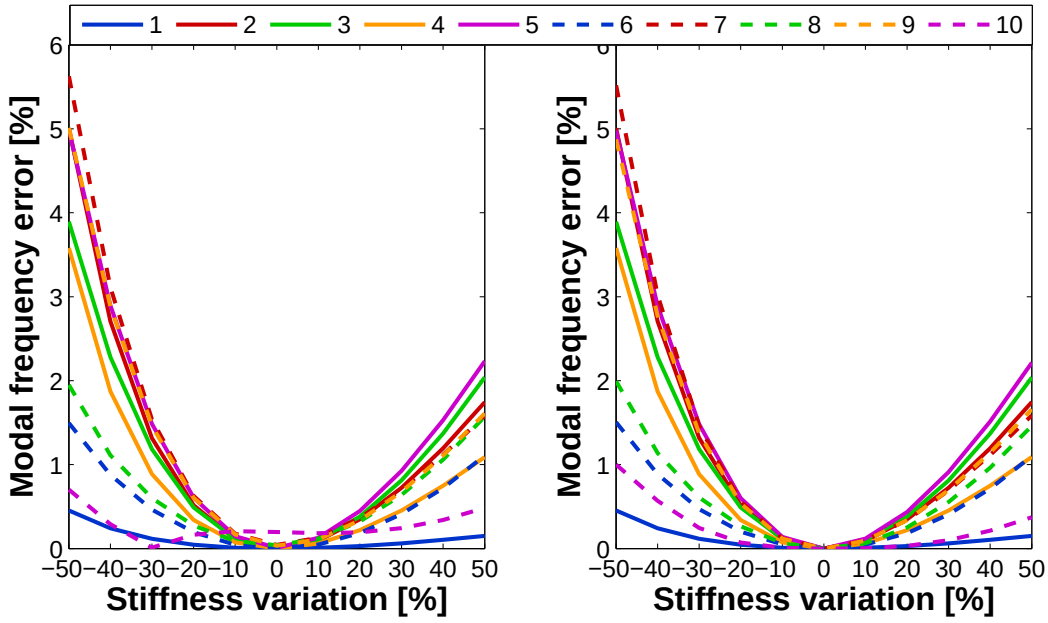

Figure 5.8: Modal frequency error values for the first 10 eigenvalues of the cantilever example when $\mathbf{K}_{C2}$ is perturbed by -50% to +50%. Left: CMS perturbation propagation. Right: Full order modal perturbation.

Modal frequency errors show maximum values of 5% to 6% relative error at the variation interval lower extreme. These are significantly bigger figures than in the previous example case, most likely due to larger modal frequency variations. Similarly, modal damping errors are bigger than in the system damping variation example. Maximum modal damping errors rise up to 18% at the variation interval lower extreme for certain modes (those that have the least linear damping variation). MAC values show also worse performance, decreasing down to 0.84 for the largest modes at the variation interval lower extreme.

In this case, the error curves and the MAC values for the CMS perturbation propagation (left plots) and the full order perturbation approximation (right plots) are very similar, since the perturbation approximation errors dominate over the base-

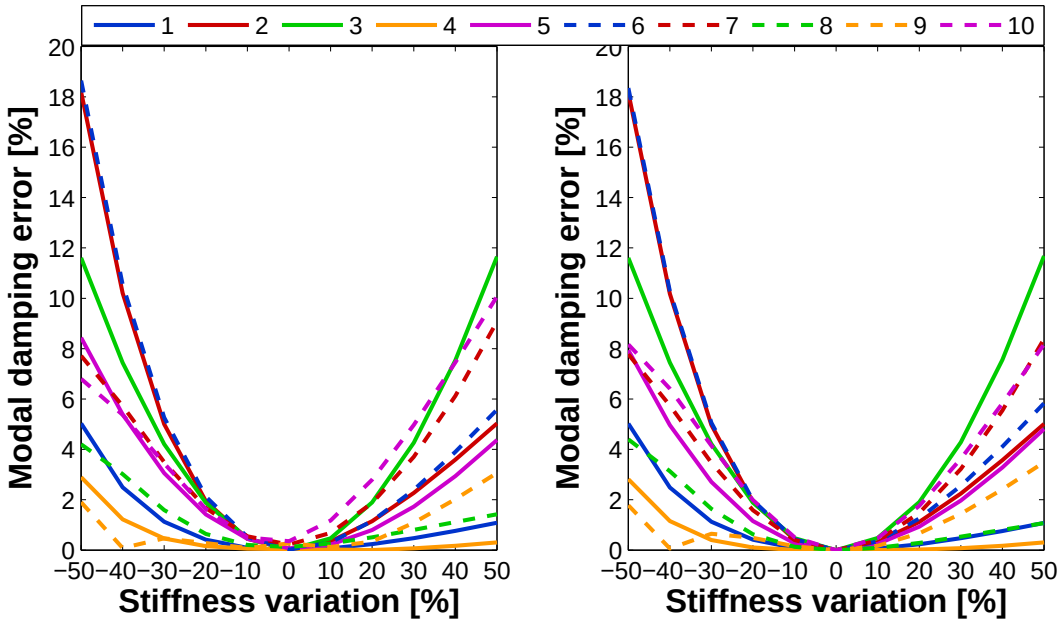

Figure 5.9: Modal damping error values for the first 10 eigenvalues of the cantilever example when $\mathbf{K}_{C2}$ is perturbed by -50% to +50%. Left: CMS perturbation propagation. Right: Full order modal perturbation.

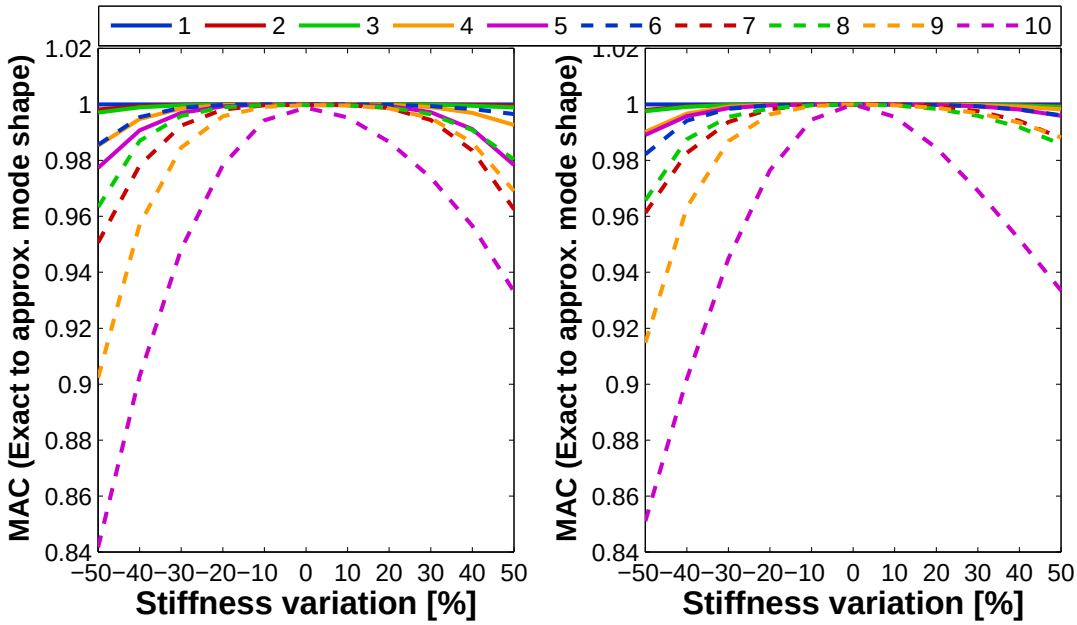

Figure 5.10: Modal Assurance Criterion values for the first 10 eigenvectors of the cantilever example when $\mathbf{K}_{C2}$ is perturbed by -50% to +50%. Left: CMS perturbation propagation. Right: Full order modal perturbation.

band CMS solution errors.

Stiffness variation in all of the elements of Component 2 has shown much larger

perturbation of the modal frequencies and a much more non-linear variation in the modal damping than damping variation in element 8. Consequently, the perturbation approximation errors are bigger for the same range of variation. In this case, perturbation methods should be restricted to a narrower variation interval. For example, if a ±20% variation interval is considered for $\mathbf{K}_{C2}$ similar errors in the modal parameters are obtained in comparison to those for the ±50% variations in $\mathbf{C}_{E8}$.

Mass variation

A third perturbation test may be conducted considering variation in component mass values. Analogous to the stiffness perturbation test, the mass density in Component 2 is assumed to vary from -50% to +50% of its nominal value, implying that the assembled mass matrix for Component 2 $\mathbf{M}_{C2}$ is subject to proportional variations $\Delta\mathbf{M}_{C2}$. For the same 10% variation steps modal solutions have been computed.

The resulting frequency and damping errors as well as MAC values are very similar to those of the stiffness perturbation test, with almost identical figures regarding maximum error at the interval extremes. It would be redundant to show almost repeated error results to those presented in Figures 5.8, 5.9 and 5.10, so that error figures for the mass variation results will be omitted here. In any case, it can be said that the perturbation propagation scheme in CMS models shows equivalent accuracy for mass variations as for stiffness variations. Thus, the same conclusions as found for the stiffness perturbation test apply in this case.

5.2 Local modal perturbation method

The perturbation propagation scheme presented in the previous section obtained modal perturbation approximations with equal accuracy as the perturbation method in full coordinates. Reanalysis flexibility is gained by performing perturbation approximations in a substructured model, since any variation may be addressed at a component level and then propagated into the reduced model of the full system. Yet, several perturbation propagation functions have been defined for the CMS parameters (e.g. for component constraint and attachment modes, for the reduced order and transformation matrices) so that all of the computational efficiency gain that has been reached by virtue of the substructuring may be lost again due to the

need for computing the approximation for so many intermediate variables.

However, not all of the PPFs in the CMS scheme necessarily contribute significantly to the perturbation in the full system modes. Some CMS parameters may experience variations of very little magnitude or, perhaps, the full system modes may be more sensitive to variations in some parameters than others. Hence, the propagation of perturbations in a CMS model might be made more efficient if some of the PPFs in section 5.1 can be neglected at the price of a small increase in the approximation errors.

Following this idea, Mace and Shorter [23] first proposed a perturbation method for propagating uncertainties from component modes to global modes in Craig-Bampton CMS models at very little computational cost. Firstly, they considered that system uncertainties may be better quantified at a component modal level, since the variability in modal parameters is more easily measured than the randomness in spatially distributed physical parameters. This assumption implies that the perturbations are directly defined in the component modes so that the perturbation propagation from component matrices to component modes can be bypassed.

Secondly, they assumed that the natural frequencies of the component modes are the only CMS parameters that vary significantly. Then, since the component (undamped) eigenvalues appear as $\mathbf{\Lambda}$ submatrices in the Craig-Bampton matrices (c.f. equation 4.55), it is trivial to obtain global mode sensitivities with respect to component eigenvalue variations. Accordingly, very simple perturbation propagation functions can be derived for the global undamped modes.

The *local modal perturbation* (LMP) method achieves in this way a very cost-efficient approximation of the global modes variation once the perturbation in component modes is available. However, since it is based on the Craig-Bampton method, this approach is only applicable for approximating undamped modes. Therefore, its use is restricted to lightly damped systems.

In this thesis, the local modal perturbation method is extended using a novel approach of the method based on state-space CMS models[6]. The aim of this new approach is to perform approximate vibration analyses on large built-up systems which typically have localised damping treatments.

In this case, the LMP method is developed based on the Morgan-Craig-Bampton CMS method. Consider the coupled-modal matrices in the MCB method which

[6]The Local modal perturbation method in state-space CMS models was presented in [96]

have the following structure

$$\mathbf{A}^y = \begin{bmatrix} \mathbf{I}_{kk} & \mathbf{A}^y_{kc} \\ \mathbf{A}^y_{ck} & \mathbf{A}^y_{cc} \end{bmatrix} \qquad \mathbf{B}^y = \begin{bmatrix} \mathbf{\Lambda}_{kk} & \mathbf{B}^y_{kc} \\ \mathbf{B}^y_{ck} & \mathbf{B}^y_{cc} \end{bmatrix}$$

where the $\mathbf{\Lambda}_{kk}$ submatrix contains all of the components (fixed-interface) damped eigenvalues $\lambda_k = -\sigma_k \pm i\omega_{d,k}$ in its diagonal.

Now, assume as in the original LMP method that the component eigenvalues are the only CMS parameters that may vary, with the particularity that damped eigenvalues involve both the modal frequency and the modal damping parameters. Thence, the resulting sensitivity functions for the coupled-modal matrices with respect to a component eigenvalue λ_j are

$$\frac{\partial \mathbf{A}^y}{\partial \lambda_j} = \begin{bmatrix} \mathbf{0}_{kk} & \mathbf{0}_{kc} \\ \mathbf{0}_{ck} & \mathbf{0}_{cc} \end{bmatrix} \qquad \frac{\partial \mathbf{B}^y}{\partial \lambda_j} = \begin{bmatrix} \frac{\partial \mathbf{\Lambda}_{kk}}{\partial \lambda_j} & \mathbf{0}_{kc} \\ \mathbf{0}_{ck} & \mathbf{0}_{cc} \end{bmatrix} \tag{5.46}$$

That is, the $\mathbf{A}^y$ matrix in MCB coordinates is invariant, and only the $\mathbf{\Lambda}_{kk}$ submatrix in $\mathbf{B}^y$ is sensitive to variations in component eigenvalues.

In fact, since the component eigenvalues are independent variables, the partial derivation of a component eigenvalue λ_k with respect to another component eigenvalue λ_j equals zero unless both eigenvalues are the same one, i.e.

$$\frac{\partial \lambda_k}{\partial \lambda_j} = \delta_{kj} \tag{5.47}$$

with δ_{kj} the Kronecker delta. Notice that complex conjugate eigenvalue pairs in $\mathbf{\Lambda}_{kk}$ are also independent since for any complex number $z \in \mathbb{C}$ the partial derivative of the complex conjugate is zero, i.e. $\frac{\partial z^*}{\partial z} = 0$.

Consequently, the $\mathbf{B}^y$ sensitivity in equation 5.46 is a $\mathbf{J}^{jj}$ single-entry matrix[7] with $\mathbf{J}_{jj} = \frac{\partial \lambda_j}{\partial \lambda_j} = 1$. Therefore, in the LMP method, first order perturbation approximations for the MCB coupled modal matrices simply read

$$\tilde{\Delta}\mathbf{A}^y = \mathbf{0} \qquad \tilde{\Delta}\mathbf{B}^y = \mathbf{J}^{jj}\Delta\lambda_j \tag{5.48}$$

Then, by inserting these simple perturbation approximations for $\Delta\mathbf{A}^y$ and $\Delta\mathbf{B}^y$ in the PPFs for damped global modes (equations 5.21 and 5.22) the following expressions are obtained for the global modes eigenvalues λ_m and eigenvectors $\boldsymbol{z}_m$ perturbations with respect to component eigenvalues λ_j perturbations

$$\tilde{\Delta}\lambda_m = (\boldsymbol{z}_{jm})^2 \, \Delta\lambda_j \tag{5.49}$$

[7] A single-entry matrix $\mathbf{J}^{ij}$ is a binary matrix with all zero-valued elements except for element $\mathbf{J}_{ij}$ which is unity-valued.

$$\tilde{\Delta}\boldsymbol{z}_m = \sum_{i \neq m} -\frac{\boldsymbol{z}_{ji}^T \boldsymbol{z}_{jm}}{\lambda_i - \lambda_m} \boldsymbol{z}_i \Delta\lambda_j \tag{5.50}$$

where the $\boldsymbol{z}_i$ global eigenvectors are expressed in coupled-modal coordinates.

Thus, a perturbation in a component eigenvalue λ_j is propagated into the global eigenvalues λ_m at a trivial cost, just by multiplying $\Delta\lambda_j$ with a squared scalar value $\boldsymbol{z}_{jm}$ corresponding to j'th coupled-modal DOF of the m'th global eigenvector.

In turn, the propagation into the global eigenvectors $\boldsymbol{z}_m$ is not so straightforward, but it is significantly more cost-efficient than the full order perturbation approximation. Although a weighted sum over all of the $i \neq m$ global modes needs to be computed, all of the weighting quantities in equation 5.50 are scalar values, and the $\boldsymbol{z}_i$ global eigenvectors are of reduced order since they are in coupled-modal coordinates. Moreover, since the component eigenvectors are assumed invariant, the full order eigenvectors perturbation are simply recovered by multiplication with the deterministic back-transformation matrix, i.e.

$$\tilde{\Delta}\boldsymbol{x}_m = \mathbf{T}^z \tilde{\Delta}\boldsymbol{z}_m \tag{5.51}$$

The LMP perturbation propagation functions in equations 5.49, 5.50 and 5.51 are the direct extension to MCB reduced models of the original LMP method PPFs in Craig-Bampton coordinates (see [23]). Hence, these might be used for modal uncertainty analysis in the same way as proposed by Mace and Shorter. That is, the uncertainty may be introduced in the MCB model at a component modal-level by assuming some random distribution for the component eigenvalue perturbations. Then, the damped component eigenvalue perturbations may be propagated into the global modes.

5.2.1 Numerical validation

The LMP method for the MCB models is evaluated in the following using the cantilever example in section 5.1.5. The same two tests are performed, namely, the -50% to 50% $\mathbf{C}_{\text{E8}}$ and $\mathbf{K}_{\text{C2}}$ variations in 10% steps. First, the corresponding component eigenvalues perturbations are computed using the state-space normal modes perturbation propagation function in equation 5.6. Then, these are propagated into the global modes through the LMP perturbation propagation functions.

The error in the first 10 LMP approximated cantilever modes with respect to the exact solution is presented in Figures 5.11, 5.12 and 5.13 for the modal frequencies,

modal damping and mode shape vectors respectively. The results for $\mathbf{C}_{E8}$ damping variations are shown in the left hand side plots, and the the results for the $\mathbf{K}_{C2}$ stiffness perturbations are shown in the right hand side plots.

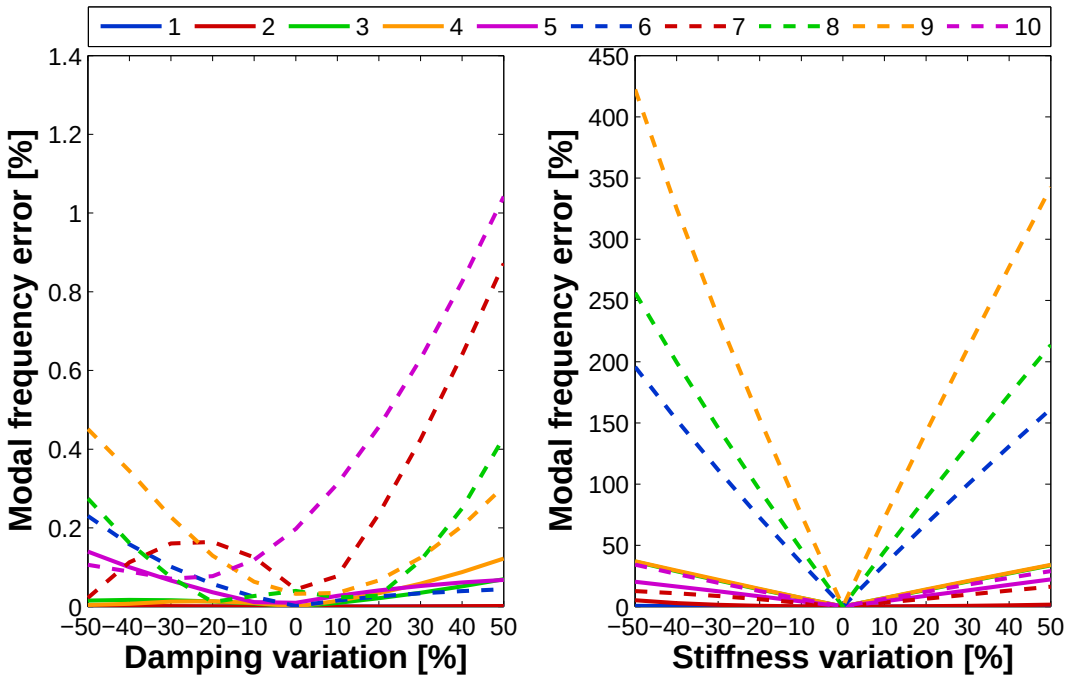

Figure 5.11: Modal frequency error in the first 10 cantilever modes computed through the LMP method with perturbed $\mathbf{C}_{E8}$ (left) / $\mathbf{K}_{C2}$ (right).

Looking first at the results for system damping variation, it can be observed that the error in modal frequencies (Figure 5.11) and the MAC values for the mode shapes (Figure 5.13) are almost the same as the ones obtained in Figures 5.4 and 5.6 for the full CMS perturbation propagation scheme. In other words, the accuracy in modal frequencies and mode shapes is as good as it can be for a first order perturbation approximation. On the contrary, the modal damping approximation is significantly worse in the LMP case. In Figure 5.12, the damping error rises steeply even for the central part of the variation interval, and maximum errors up to 20% of the modal damping value are obtained at the extremes of the interval.

A completely different situation is observed when looking at the LMP results for stiffness variation in the right hand plots of Figures 5.11, 5.12 and 5.13. The LMP results for the global modes are completely wrong, they cannot even be considered *approximations*: Modal frequency errors of up to 400%, modal damping errors of up to 1400% and MAC values falling to zero even for the 10% $\mathbf{K}_{C2}$ perturbations. Similar completely inaccurate results would be obtained for mass variations.

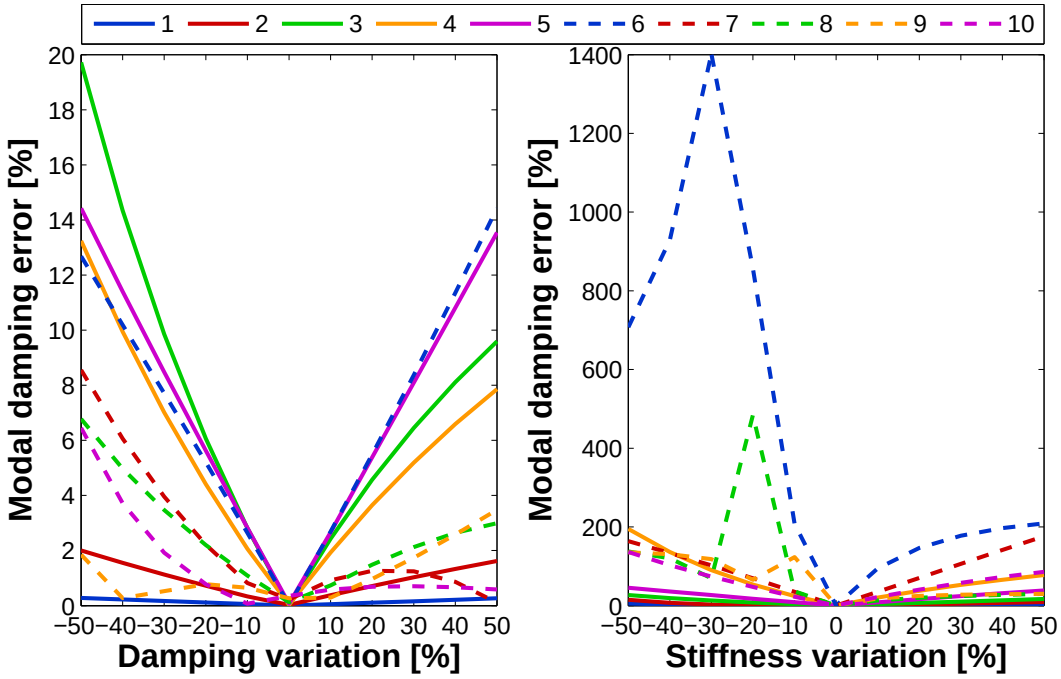

Figure 5.12: Modal damping error in the first 10 cantilever modes computed through the LMP method with perturbed $\mathbf{C}_{\mathrm{E8}}$ (left) / $\mathbf{K}_{\mathrm{C2}}$ (right).

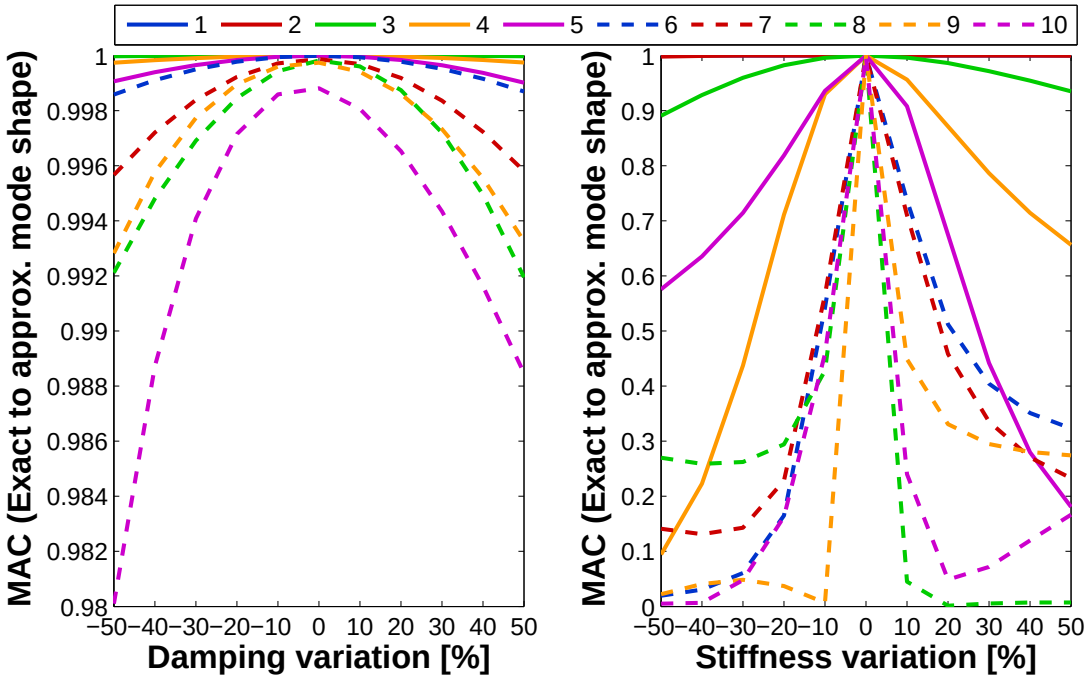

Figure 5.13: Modal Assurance Criterion for the first 10 cantilever eigenvectors computed through the LMP method with perturbed $\mathbf{C}_{\mathrm{E8}}$ (left) / $\mathbf{K}_{\mathrm{C2}}$ (right).

5.2.2 Validity of the LMP method

The LMP method when applied to MCB reduced models does not appear to work at all for variations in the system stiffness. However, the LMP method provides

fairly accurate undamped modes estimations when applied to CB reduced models as demonstrated by Mace and Shorter in [23]. What is then the reason why inaccurate results are attained when applied to state-space based CMS models?

The answer to this question lies in the fact that the component state-eigenvectors $\boldsymbol{x}_k$ used for the component model reduction may not be considered by any means unperturbed. On one hand, when the system is heavily damped, variations in any of the three component matrices $\mathbf{M}$, $\mathbf{C}$ or $\mathbf{K}$ produce significant variations in modal frequencies and also in modal damping (c.f. section 3.1). Consequently, the damped mode shapes of the components show variation in their complexity at the very least.

On the other hand, and more determining, the velocity DOFs of state-eigenvectors involve the corresponding damped mode shape and damped eigenvalue, i.e. $\boldsymbol{x}_k^V = \lambda_k \boldsymbol{\phi}_k$. Therefore, as is evident if one inspects the $\tilde{\Delta}\boldsymbol{x}_k$ alternative perturbation approximation in equation 5.8, a perturbation in a component eigenvalue λ_k necessarily implies a perturbation in the corresponding state-eigenvector $\boldsymbol{x}_k$. It is inconsistent to assume perturbation in the component eigenvalues but not in their corresponding state-eigenvectors.

Thus, variation in component state-eigenvectors may not be neglected for an accurate analysis of the global modes perturbation coming from an state-space based CMS solution. However, although it is possible to reformulate the LMP method in order to include the sensitivities of the global modes with respect to component mode shape variations, a local modal perturbation approach involving the component mode shapes would make the LMP method much less appealing for propagating uncertainties. Since mode shapes are spatially distributed variables, defining uncertainties at a component modal level would involve defining a mode shape random field for each of the considered component modes. Hence, consistently quantifying uncertainty in the local mode shapes may be even more difficult than the quantification over the primary physical parameters.

Nevertheless, the LMP method may still be used for propagating system damping perturbations only. In the $\mathbf{C}_{\text{E8}}$ perturbation test good accuracy in modal frequencies and mode shapes was obtained. Actually, the relatively accurate results are rather a consequence of the perturbation in modal frequencies and mode shapes being small in comparison with the baseline values, as has been already pointed out in section 5.1.5. On the contrary, the accuracy in modal damping of the global modes was not as good due to component mode shape perturbation being neglected. Yet, for a sufficiently narrow range of variation modal damping errors fall below an acceptable tolerance (e.g. 5% maximum error value for $\pm 20\%$ $\mathbf{C}_{\text{E8}}$ perturbation).

Accordingly, the use of the LMP method for damping uncertainty propagation has been proposed in [97] for locally damped systems. The LMP method proved very cost-efficient and reasonably accurate for a system with uncertain localised damping, where Gaussian random variations of just the component modal damping were assumed with relative standard deviation of 5% times its nominal value.

5.3 Component modal-propagation method

In locally damped built-up systems, perturbations in the physical properties of the constituent subsystems may be propagated into the full system modes by means of the perturbation propagation functions defined in section 5.1.1. However, efficient propagation of stiffness/mass perturbations in state-space based CMS models has not yet been resolved.

Even though the LMP method may be used for damping variability analyses, it has been shown in the previous section that stiffness/mass variations may not be addressed at a component modal level through the LMP method. This happens because component mode shapes play an important role in the propagation of perturbations into the global modes. Therefore, a state-space based CMS perturbation method which addresses stiffness/mass variability in locally damped systems must necessarily involve component mode shape perturbations.

In this section, following the idea that global modes might be more sensitive to variation in certain CMS parameters than in others, a new perturbation method is presented for state-space based CMS models. In this case it is assumed that only the normal component modes vary for any variation in the physical parameters of a component. In other words, that the perturbation propagation goes from component matrices to the component eigensolutions, and from the component eigensolutions directly to the global modes.

The perturbation approximations for component eigensolutions have already been described [8]. Thence, what is looked for here are perturbation propagation functions that directly relate the perturbation in component eigensolutions to perturbation

[8]For state-eigensolutions the modal perturbation propagation functions $P_{\lambda_{k,s}}(\Delta\mathbf{A}_s, \Delta\mathbf{B}_s)$ and $P_{x_{k,s}}(\Delta\mathbf{A}_s, \Delta\mathbf{B}_s)$ in equations 5.6 and 5.7 may be used. Alternatively, perturbation propagation functions in physical coordinates may be used, i.e. $P_{\lambda_{k,s}}(\Delta\mathbf{M}_s, \Delta\mathbf{C}_s, \Delta\mathbf{K}_s)$ and $P_{\phi_{k,s}}(\Delta\mathbf{M}_s, \Delta\mathbf{C}_s, \Delta\mathbf{K}_s)$ in equations 3.18 and 3.19.

in the global eigensolutions, that is

$$\tilde{\Delta}\lambda_m = P_{\lambda_m}(\tilde{\Delta}\boldsymbol{\Lambda}_s, \tilde{\Delta}\boldsymbol{\Phi}_s) \tag{5.52}$$

$$\tilde{\Delta}\boldsymbol{z}_m = P_{\boldsymbol{z}_m}(\tilde{\Delta}\boldsymbol{\Lambda}_s, \tilde{\Delta}\boldsymbol{\Phi}_s) \tag{5.53}$$

These PPFs will be derived in the following for the Morgan-Craig-Bampton CMS method.

5.3.1 Component modal to global modal perturbation propagation in state-space coordinates

Consider the perturbation approximations for the MCB reduced component matrices in equations 5.28 and 5.29. There, the approximate perturbation in component-modal matrices $\tilde{\Delta}\mathbf{A}_s^y$ and $\tilde{\Delta}\mathbf{B}_s^y$ is a function of the perturbation in the component eigensolutions, constraint modes and component matrices.

Now, assume that any perturbation in a physical parameter of a component is fully described by the $\tilde{\Delta}\boldsymbol{\Lambda}_s^F$ and $\tilde{\Delta}\mathbf{X}_s^F$ fixed-interface state-eigensolutions perturbation approximations. That is, that the perturbation in constraint modes can be neglected, i.e. $\Delta\boldsymbol{\Upsilon}_s^C = \mathbf{0}$, and that the perturbations in component matrices $\Delta\mathbf{A}_s$ and $\Delta\mathbf{B}_s$ need not to be considered since they are already included in $\tilde{\Delta}\boldsymbol{\Lambda}_s^F$ and $\tilde{\Delta}\mathbf{X}_s^F$. Then, the perturbation expressions for the MCB component-modal matrices get simplified into

$$\tilde{\Delta}\mathbf{A}_s^y = \begin{bmatrix} \mathbf{0} & \tilde{\Delta}\mathbf{X}^{F^T}\mathbf{A}\boldsymbol{\Upsilon}^C \\ \boldsymbol{\Upsilon}^{C^T}\mathbf{A}\tilde{\Delta}\mathbf{X}^F & \mathbf{0} \end{bmatrix}_s \tag{5.54}$$

$$\tilde{\Delta}\mathbf{B}_s^y = \begin{bmatrix} \tilde{\Delta}\boldsymbol{\Lambda}^F & \tilde{\Delta}\mathbf{X}^{F^T}\mathbf{B}\boldsymbol{\Upsilon}^C \\ \boldsymbol{\Upsilon}^{C^T}\mathbf{B}\tilde{\Delta}\mathbf{X}^F & \mathbf{0} \end{bmatrix}_s \tag{5.55}$$

These may be easily assembled for all components in order to obtain the perturbation approximation for the MCB coupled-modal matrices. Yet, when variability is contemplated in built-up systems (e.g. design modifications, uncertainty, etc.), independent variations are typically assumed from one component to another. Therefore, perturbation in global modes shall be computed considering perturbation in a single component at a time.

Accordingly, if only one component s is assumed to be perturbed, the corresponding perturbations in MCB coupled-modal matrices will be matrices with most of their entries zero valued, except for those entries corresponding to the s'th component.

For instance, for a two-component system where only the second component is perturbed, the coupled-modal matrices would read

$$\tilde{\Delta}\mathbf{A}^z = \begin{bmatrix} \mathbf{0} & \mathbf{0} & \mathbf{0} \\ \mathbf{0} & \mathbf{0} & \tilde{\Delta}\mathbf{A}^y_{2c} \\ \mathbf{0} & \tilde{\Delta}\mathbf{A}^{y\,T}_{2c} & \mathbf{0} \end{bmatrix} \qquad \tilde{\Delta}\mathbf{B}^z = \begin{bmatrix} \mathbf{0} & \mathbf{0} & \mathbf{0} \\ \mathbf{0} & \tilde{\Delta}\mathbf{\Lambda}^F_2 & \tilde{\Delta}\mathbf{B}^y_{2c} \\ \mathbf{0} & \tilde{\Delta}\mathbf{B}^{y\,T}_{2c} & \mathbf{0} \end{bmatrix} \tag{5.56}$$

with $\tilde{\Delta}\mathbf{A}^y_{sc} = \tilde{\Delta}\mathbf{X}^{F\,T}_s \mathbf{A}_s \mathbf{\Upsilon}^C_s$ and $\tilde{\Delta}\mathbf{B}^y_{sc} = \tilde{\Delta}\mathbf{X}^{F\,T}_s \mathbf{B}_s \mathbf{\Upsilon}^C_s$.

Then, the perturbation in global modes can be approximated by introducing $\tilde{\Delta}\mathbf{A}^z$ and $\tilde{\Delta}\mathbf{B}^z$ into the global-modal PPFs in equations 5.21 and 5.22. However, notice that the global-modal PPFs involve bilinear forms of the kind $\boldsymbol{z}_i^T \tilde{\Delta}\mathbf{A}^z \boldsymbol{z}_m$ and $\boldsymbol{z}_i^T \tilde{\Delta}\mathbf{B}^z \boldsymbol{z}_m$. Accordingly, since most of the $\tilde{\Delta}\mathbf{A}^z$ and $\tilde{\Delta}\mathbf{B}^z$ entries are zero valued, these bilinear forms may be rewritten just for the entries corresponding to the s'th component.

The global eigenvectors in MCB coupled-modal coordinates $\boldsymbol{z}_m$ are composed of the modal degrees of freedom corresponding to each of the N_c components, and of the state-space coupling degrees of freedom, i.e.

$$\boldsymbol{z}_m = \left\{ \begin{array}{c} \boldsymbol{z}_1 \\ \vdots \\ \boldsymbol{z}_{N_c} \\ \boldsymbol{x}_c \end{array} \right\}_m \tag{5.57}$$

From these, only the modal DOFs $\boldsymbol{z}_{sm}$ and the coupling DOFs $\boldsymbol{x}_{cm}$ corresponding to the s'th component multiply with non-zero entries. Thus, the bilinear forms can be rewritten as

$$a^z_{im} = \boldsymbol{z}_i^T \tilde{\Delta}\mathbf{A}^z \boldsymbol{z}_m = \boldsymbol{z}_{si}^T \tilde{\Delta}\mathbf{A}^y_{sc} \boldsymbol{x}_{cm} + \boldsymbol{x}_{ci}^T \tilde{\Delta}\mathbf{A}^{y\,T}_{sc} \boldsymbol{z}_{sm} \tag{5.58}$$

$$b^z_{im} = \boldsymbol{z}_i^T \tilde{\Delta}\mathbf{B}^z \boldsymbol{z}_m = \boldsymbol{z}_{si}^T \tilde{\Delta}\mathbf{B}^y_{sc} \boldsymbol{x}_{cm} + \boldsymbol{x}_{ci}^T \tilde{\Delta}\mathbf{B}^{y\,T}_{sc} \boldsymbol{z}_{sm} + \boldsymbol{z}_{si}^T \tilde{\Delta}\mathbf{\Lambda}^F_s \boldsymbol{z}_{sm} \tag{5.59}$$

where $\tilde{\Delta}\mathbf{A}^y_{sc}$ and $\tilde{\Delta}\mathbf{B}^y_{sc}$ are function of the state-eigenvalues perturbation $\tilde{\Delta}\mathbf{X}^F_s$ only.

Finally, the perturbation in global modes can be posed in terms of the weighting factors defined in equations 5.58 and 5.59, i.e.

$$\tilde{\Delta}\lambda_m = b^z_{mm} - \lambda_m a^z_{mm} \tag{5.60}$$

$$\tilde{\Delta}\boldsymbol{z}_m = -\frac{1}{2} a^z_{mm} \boldsymbol{z}_m - \sum_{i \neq m} \frac{b^z_{im} - \lambda_m a^z_{im}}{\lambda_i - \lambda_m} \boldsymbol{z}_i \tag{5.61}$$

Note that these are the direct PPFs from component modes to global modes since a^z_{im} and b^z_{im} are function of just the perturbation in component eigenvalues $\tilde{\Delta}\mathbf{\Lambda}^F_s$

and eigenvectors $\tilde{\Delta}\mathbf{X}_s^F$ of the s'th component. Notice as well that the last term in equation 5.59, i.e.

$$l_{im}^z = \boldsymbol{z}_{si}^T \tilde{\Delta}\boldsymbol{\Lambda}_s^F \boldsymbol{z}_{sm} \tag{5.62}$$

is the only one dependent on the component eigenvalues. If component eigenvectors were assumed unperturbed, all other terms in a_{im}^z and b_{im}^z would vanish except for l_{im}^z. In such case, the global-modal perturbation propagation functions would be simply

$$\tilde{\Delta}\lambda_m = l_{mm}^z \tag{5.63}$$

$$\tilde{\Delta}\boldsymbol{z}_m = -\sum_{i \neq m} \frac{l_{im}^z}{\lambda_i - \lambda_m} \boldsymbol{z}_i \tag{5.64}$$

which are, in fact, the generic expressions for the Local Modal Perturbation method.

Eventually, the perturbed global mode shape vectors in physical (or state-space) coordinates may be recovered by multiplication with the back-transformation matrix (c.f. equation 5.23). In this case, since component eigenvectors perturbation has been considered, the back transformation matrix will be perturbed accordingly. For example, for a two-component system where only the second component is perturbed the back-transformation matrix would simply read

$$\tilde{\Delta}\mathbf{T}^z = \begin{bmatrix} \mathbf{0} & \mathbf{0} & \mathbf{0} \\ \mathbf{0} & \tilde{\Delta}\mathbf{X}_{ik,2}^F & \mathbf{0} \\ \mathbf{0} & \mathbf{0} & \mathbf{0} \end{bmatrix} \tag{5.65}$$

5.3.2 Component modal to global modal perturbation propagation in physical coordinates

The efficiency of the Component Modal-Propagation (CMP) perturbation method can be improved if the global modes perturbation approximations are computed directly from the component matrices in physical coordinates. Equivalent perturbation expressions to those in equations 5.60 and 5.61 may be derived by decomposing the state-space coordinates into the velocity and displacement physical coordinates. The explicit derivations may be consulted in Appendix G.

On one hand, the $\mathbf{A}_s$ and $\mathbf{B}_s$ state-space component matrices are block matrices consisting of the $\mathbf{M}_s$, $\mathbf{C}_s$ and $\mathbf{K}_s$ component matrices in their displacement/velocity DOFs. Likewise, the state-constraint modes $\boldsymbol{\Upsilon}_s^C$ are a composition of the baseband constraint modes $\boldsymbol{\Psi}_s^C$, and the component state-eigenvectors perturbations $\tilde{\Delta}\mathbf{X}_s^F$

may be also split into velocity V and displacement D DOFs as

$$\tilde{\Delta}\mathbf{X}_s^F = \begin{bmatrix} \tilde{\Delta}\mathbf{X}^{V,F} \\ \tilde{\Delta}\mathbf{X}^{D,F} \end{bmatrix}_s = \begin{bmatrix} \tilde{\Delta}\boldsymbol{\Phi}^F\boldsymbol{\Lambda}^F + \boldsymbol{\Phi}^F\tilde{\Delta}\boldsymbol{\Lambda}^F \\ \tilde{\Delta}\boldsymbol{\Phi}^F \end{bmatrix}_s \tag{5.66}$$

Hence, the $\tilde{\Delta}\mathbf{A}_{sc}^y$ and $\tilde{\Delta}\mathbf{B}_{sc}^y$ submatrices may be expressed in terms of the $\mathbf{M}_s$, $\mathbf{C}_s$, $\mathbf{K}_s$, $\boldsymbol{\Psi}_s^C$ and $\boldsymbol{\Phi}_s^F$ component matrices and their corresponding eigensolutions perturbation approximations $\tilde{\Delta}\boldsymbol{\Lambda}_s^F$ and $\tilde{\Delta}\boldsymbol{\Phi}_s^F$.

On the other hand, the global eigenvectors in coupled-modal MCB coordinates involve the state-space DOFs for the coupling interface between components, which may be also split into velocity and displacement DOFs as

$$\boldsymbol{x}_{cm} = \begin{Bmatrix} \boldsymbol{x}_{cm}^V \\ \boldsymbol{x}_{cm}^D \end{Bmatrix} = \begin{Bmatrix} \lambda_m\boldsymbol{\phi}_{cm} \\ \boldsymbol{\phi}_{cm} \end{Bmatrix} \tag{5.67}$$

Accordingly, the a_{im}^z and b_{im}^z weighting factors in equations 5.58 and 5.59 may be decomposed into several terms so that each of them is computed from component matrices in physical coordinates.

Simplified formulation

Proceeding in this way, the CMP perturbation propagation functions for the global modes may be reformulated as

$$\tilde{\Delta}\lambda_m = l_{mm}^z - \left(\lambda_m^2 m_{mm}^z + \lambda_m c_{mm}^z + k_{mm}^z\right) \tag{5.68}$$

$$\tilde{\Delta}\boldsymbol{z}_m = -\frac{1}{2}\left(2\lambda_m m_{mm}^z + c_{mm}^z\right)\boldsymbol{z}_m - \sum_{i\neq m}\frac{l_{im}^z - \left(\lambda_m^2 m_{im}^z + \lambda_m c_{im}^z + k_{im}^z\right)}{\lambda_i - \lambda_m}\boldsymbol{z}_i \tag{5.69}$$

where new weighting factors in physical coordinates analogous to a_{im}^z and b_{im}^z are defined for the mass, damping and stiffness matrices, i.e.

$$m_{im}^z = \boldsymbol{z}_{si}^T\tilde{\Delta}\mathbf{M}_{sc}^y\boldsymbol{\phi}_{cm} + \boldsymbol{\phi}_{ci}^T\tilde{\Delta}\mathbf{M}_{sc}^{y\,T}\boldsymbol{z}_{sm} \tag{5.70}$$

$$c_{im}^z = \boldsymbol{z}_{si}^T\tilde{\Delta}\mathbf{C}_{sc}^y\boldsymbol{\phi}_{cm} + \boldsymbol{\phi}_{ci}^T\tilde{\Delta}\mathbf{C}_{sc}^{y\,T}\boldsymbol{z}_{sm} \tag{5.71}$$

$$k_{im}^z = \boldsymbol{z}_{si}^T\tilde{\Delta}\mathbf{K}_{sc}^y\boldsymbol{\phi}_{cm} + \boldsymbol{\phi}_{ci}^T\tilde{\Delta}\mathbf{K}_{sc}^{y\,T}\boldsymbol{z}_{sm} \tag{5.72}$$

with $\tilde{\Delta}\mathbf{M}_{sc}^y = \tilde{\Delta}\boldsymbol{\Phi}_s^{F\,T}\mathbf{M}_s\boldsymbol{\Psi}_s^C$, $\tilde{\Delta}\mathbf{C}_{sc}^y = \tilde{\Delta}\boldsymbol{\Phi}_s^{F\,T}\mathbf{C}_s\boldsymbol{\Psi}_s^C$ and $\tilde{\Delta}\mathbf{K}_{sc}^y = \tilde{\Delta}\boldsymbol{\Phi}_s^{F\,T}\mathbf{K}_s\boldsymbol{\Psi}_s^C$.

Notice that in the CMP perturbation approximations for MCB global modes in equations 5.68 and 5.69, the l_{im}^z factors account for the dependency on component

eigenvalues perturbations (as in the LMP method) and the m^z_{im}, c^z_{im} and k^z_{im} factors account for the dependency on component eigenvectors perturbations.

Yet, the validity of the CMP perturbation propagation functions above relies on the fact that *exact* solutions for the global modes are available. Otherwise it cannot be guaranteed that equation 5.67 holds.

However, exact solutions are rarely achieved through CMS methods. When damped global modes are computed through the MCB method, an exact solution is obtained if and only if all of the component fixed-interface eigensolutions are used for the component modal transformation. That is, when there is no modal truncation. That would mean no model order reduction of the components.

On the contrary, when modal truncation is applied the global modes are the solution of a reduced global EVP in MCB coordinates which is just an approximation to the full order EVP. Accordingly, coupling velocity-DOFs of the global MCB eigenvectors may well deviate from showing a constant relation to the coupling displacement-DOFs, i.e.

$$\boldsymbol{x}^V_{cm} \neq \lambda_m \boldsymbol{x}^D_{cm} \tag{5.73}$$

Thus, serious approximation errors shall occur when using equations 5.68 and 5.69 on MCB reduced models.

Generic formulation

Alternatively, independent $\boldsymbol{x}^V_{cm}$ and $\boldsymbol{x}^D_{cm}$ values shall be assumed yielding generic perturbation expressions (see Appendix G), i.e.

$$\tilde{\Delta}\lambda_m = l^z_{mm} - (\lambda_m \hat{m}^z_{mm} + \lambda_m c^z_{mm} + k^z_{mm}) + (\hat{\mu}^z_{mm} - \lambda_m \mu^z_{mm}) \tag{5.74}$$

$$\begin{aligned}\tilde{\Delta}\boldsymbol{z}_m = &-\frac{1}{2}(\hat{m}^z_{mm} + \mu^z_{mm} + c^z_{mm})\boldsymbol{z}_m \\ &- \sum_{i\neq m} \frac{l^z_{im} - (\lambda_m \hat{m}^z_{im} + \lambda_m c^z_{im} + k^z_{im}) + (\hat{\mu}^z_{im} - \lambda_m \mu^z_{im})}{\lambda_i - \lambda_m}\boldsymbol{z}_i\end{aligned} \tag{5.75}$$

where additional weighting factors have been defined as

$$\hat{m}^z_{im} = \boldsymbol{z}^T_{si}\tilde{\Delta}\mathbf{M}^y_{sc}\boldsymbol{x}^V_{cm} + \boldsymbol{x}^{V^T}_{ci}\tilde{\Delta}\mathbf{M}^{y\ T}_{sc}\boldsymbol{z}_{sm} \tag{5.76}$$

$$\mu^z_{im} = \boldsymbol{z}^T_{si}\tilde{\Delta}\check{\mathbf{M}}^y_{sc}\boldsymbol{x}^D_{cm} + \boldsymbol{x}^{D^T}_{ci}\tilde{\Delta}\check{\mathbf{M}}^{y\ T}_{sc}\boldsymbol{z}_{sm} \tag{5.77}$$

$$\hat{\mu}^z_{im} = \boldsymbol{z}^T_{si}\tilde{\Delta}\check{\mathbf{M}}^y_{sc}\boldsymbol{x}^V_{cm} + \boldsymbol{x}^{V^T}_{ci}\tilde{\Delta}\check{\mathbf{M}}^{y\ T}_{sc}\boldsymbol{z}_{sm} \tag{5.78}$$

with $\tilde{\Delta}\check{\mathbf{M}}^y_{sc} = [\boldsymbol{\Phi}^F_s\tilde{\Delta}\boldsymbol{\Lambda}^F_s + \tilde{\Delta}\boldsymbol{\Phi}^F_s\boldsymbol{\Lambda}^F_s]^T\mathbf{M}_s\boldsymbol{\Psi}^C_s$.

Notice that the $\hat{m}^z_{im}$ weighting factor equals $\lambda_m m^z_{im}$ if the assumption in equation 5.67 is fulfilled. Furthermore, the $(\hat{\mu}^z_{im} - \lambda_m \mu^z_{im})$ terms in equations 5.74 and 5.75 cancel out when $\boldsymbol{x}^V_{cm} = \lambda_m \boldsymbol{x}^D_{cm}$, but they don't otherwise. Therefore, equations 5.68 and 5.69 are just simplifications of the generic PPFs where the $(\hat{\mu}^z_{im} - \lambda_m \mu^z_{im})$ contribution is neglected, which may yield a significant amount of error in the approximation.

Although being also posed in terms of weighting factors in physical coordinates, the generic PPFs in equations 5.74 and 5.75 do not show such a clear distinction between the contributions of the component eigenvalues and eigenvectors perturbations. Moreover, they do not resemble the damped modes perturbation approximations for a full order model (c.f. equations 3.18 and 3.19) as much as the simplified PPFs in equations 5.68 and 5.69 did.

On the contrary, the CMP generic PPFs shall obtain identical results to those of the state-space based expressions presented in the previous section, while proving a more efficient computation of the global modes perturbation. Furthermore, some simplification is still possible. Notice how, by the definition of the fixed-interface and constraint modes, it holds that

$$\tilde{\Delta}\mathbf{K}^y_{sc} = \tilde{\Delta}\boldsymbol{\Phi}^{F^T}\mathbf{K}\boldsymbol{\Psi}^C = \begin{bmatrix}\tilde{\Delta}\boldsymbol{\Phi}^{F^T}_{ic} & \mathbf{0}_{cc}\end{bmatrix}\begin{bmatrix}\mathbf{K}_{ii} & \mathbf{K}_{ic}\\ \mathbf{K}_{ci} & \mathbf{K}_{cc}\end{bmatrix}\begin{bmatrix}-\mathbf{K}^{-1}_{ii}\mathbf{K}_{ic}\\ \mathbf{I}_{cc}\end{bmatrix} = \mathbf{0} \tag{5.79}$$

Therefore, the k^z_{im} weighting factor is invariably zero valued, which means that its computation is not necessary.

In the following the accuracy of the CMP method is evaluated, and the performance of equations 5.74 and 5.75 (which are exactly equivalent to equations 5.61 and 5.61) is compared with that of equations 5.68 and 5.69.

5.3.3 Numerical Validation

The CMP method for MCB models is evaluated using the cantilever example again. The same two tests are performed, namely, the -50% to 50% $\mathbf{C}_{\mathrm{E8}}$ and $\mathbf{K}_{\mathrm{C2}}$ variations in 10% steps.

First, the corresponding component eigenvalue and eigenvector perturbations are computed using the modal perturbation propagation functions in physical coordinates. Then, these are propagated into the global modes through the CMP perturbation propagation functions. Specifically, the component-modal to global-modal perturbation propagation is computed two times: first using the simplified PPFs in

equations 5.68 and 5.69, and second using the generic PPFs in equations 5.74 and 5.75.

For the $\mathbf{C}_{E8}$ variation test, the error in the first 10 CMP approximated cantilever modes with respect to the exact solution is presented in Figures 5.14, 5.15 and 5.16 for the modal frequencies, modal damping and mode shape vectors respectively. The left hand side plots correspond to simplified PPFs approximations and the right hand side plots correspond to generic PPFs approximations.

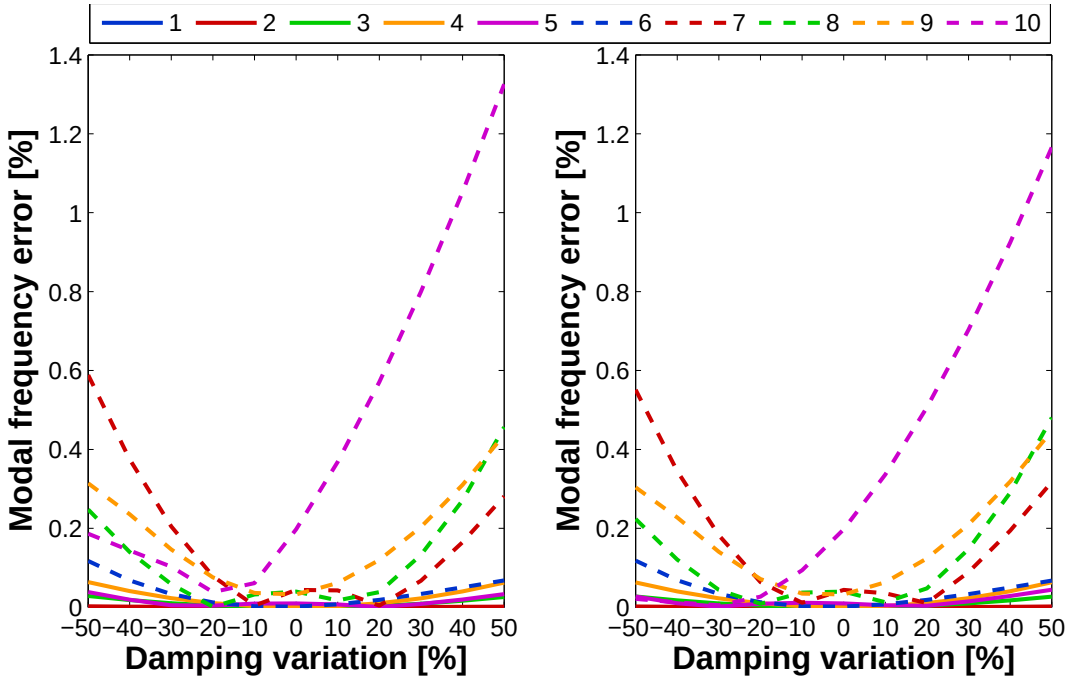

Figure 5.14: Modal frequency error in the first 10 cantilever modes computed through the CMP method with respect to $\mathbf{C}_{E8}$ damping perturbations. Left: Simplified PPFs Right: Generic PPFs.

It can be observed in Figures 5.14, 5.15 and 5.16 how the error values for the global mode approximations are very similar for both CMP formulations. This means that, in this case, the simplified PPFs give almost identical results to that of the generic PPFs.

Moreover, if one revisits the numerical test for the full perturbation propagation scheme in section 5.1.5, it can be observed that the error plots fully coincide with those of the current CMP method. Therefore, all of the assumptions of the CMP perturbation method are valid for system damping variations.

Next, the error in the first 10 CMP approximated cantilever modes with respect to $\mathbf{K}_{C2}$ variations is presented subsequently in Figures 5.17, 5.18 and 5.19 for the

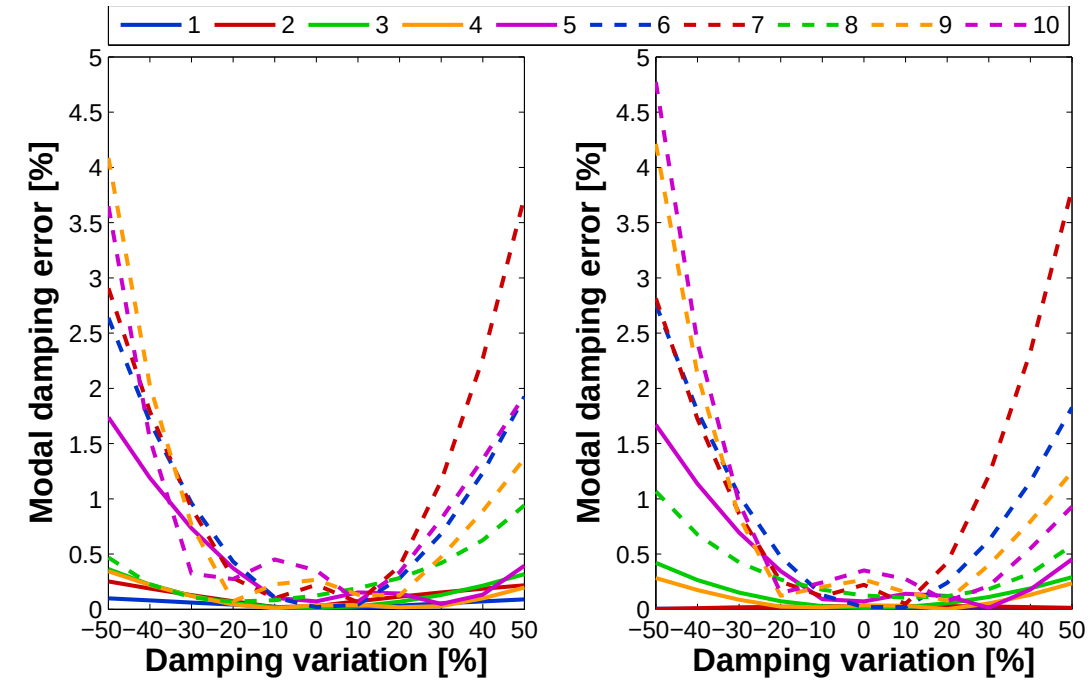

Figure 5.15: Modal damping error in the first 10 cantilever modes computed through the CMP method with respect to $\mathbf{C}_{\mathrm{E8}}$ damping perturbations. Left: Simplified PPFs Right: Generic PPFs.

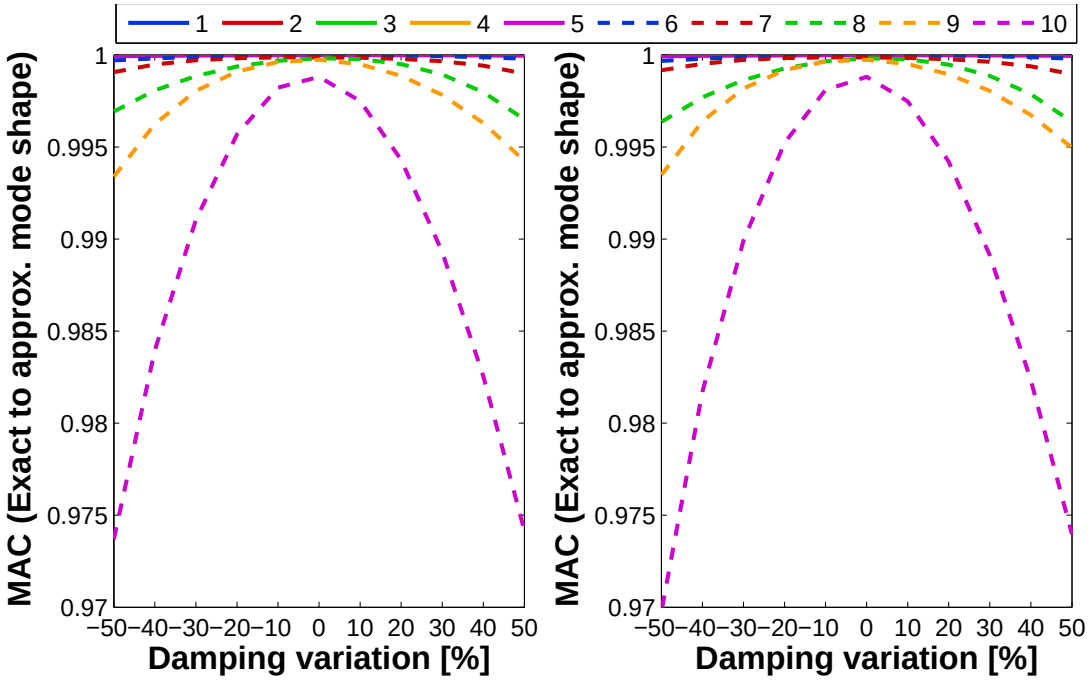

Figure 5.16: Modal Assurance Criterion for the first 10 cantilever modes computed through the CMP method with respect to $\mathbf{C}_{\mathrm{E8}}$ damping perturbations. Left: Simplified PPFs Right: Generic PPFs.

modal frequencies, modal damping and mode shape vectors respectively.

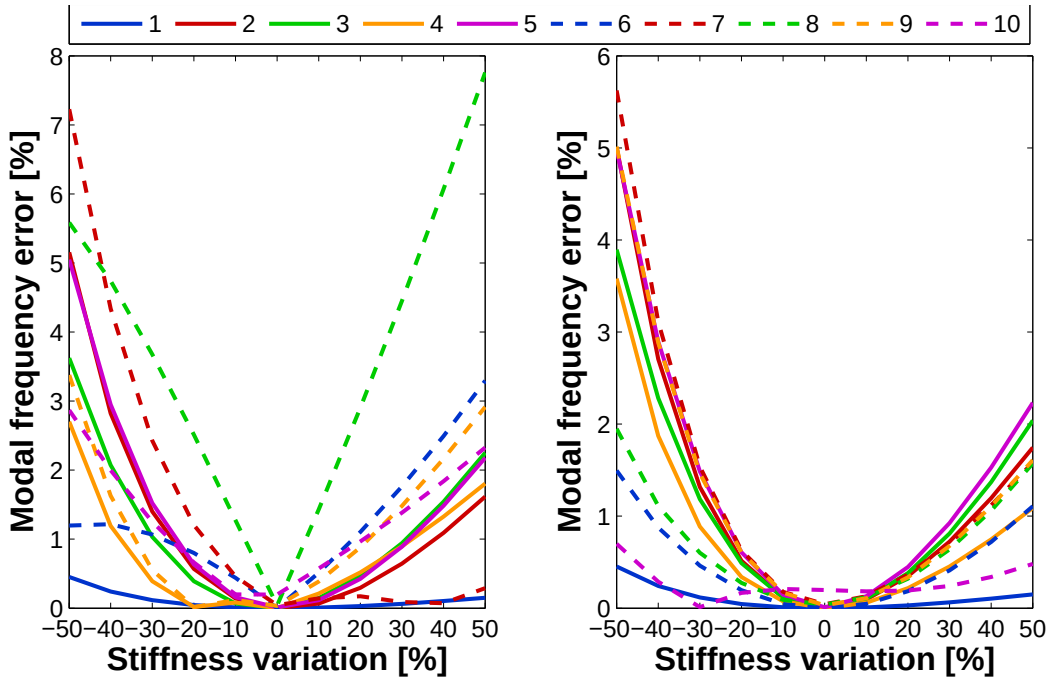

Figure 5.17: Modal frequency error in the first 10 cantilever modes computed through the CMP method with respect to $\mathbf{K}_{C2}$ damping perturbations. Left: Simplified PPFs Right: Generic PPFs.

In this case very different results are obtained whether the simplified or the generic PPFs are used. Acceptable approximation errors are obtained through the generic CMP formulation which actually match those of full perturbation propagation scheme. On the contrary, the simplified CMP formulation gives rise to approximate modal results with large errors.

In the left hand side plots (corresponding to the simplified PPFs in equations 5.68 and 5.69) the error in modal frequencies stays at an acceptable maximum error of 8% at the interval extremes. However, modal damping errors rise up over 100% for some of the modes, and the mode shape vector accuracy rapidly falls towards zero MAC values for the majority of the modes. That is, the global mode perturbation approximation is largely inaccurate.

It has been previously stated that the reason why the simplified formulation may not work is due to the assumption expressed in equation 5.67 not being fulfilled, i.e. $\boldsymbol{x}_{cm}^{V} \neq \lambda_m \boldsymbol{x}_{cm}^{D}$. However, it is surprising that the simplified approximation does not work for stiffness variations while it does work for damping variations, considering that in both cases the same $\boldsymbol{x}_{cm}^{V}$ and $\boldsymbol{x}_{cm}^{D}$ vectors apply.

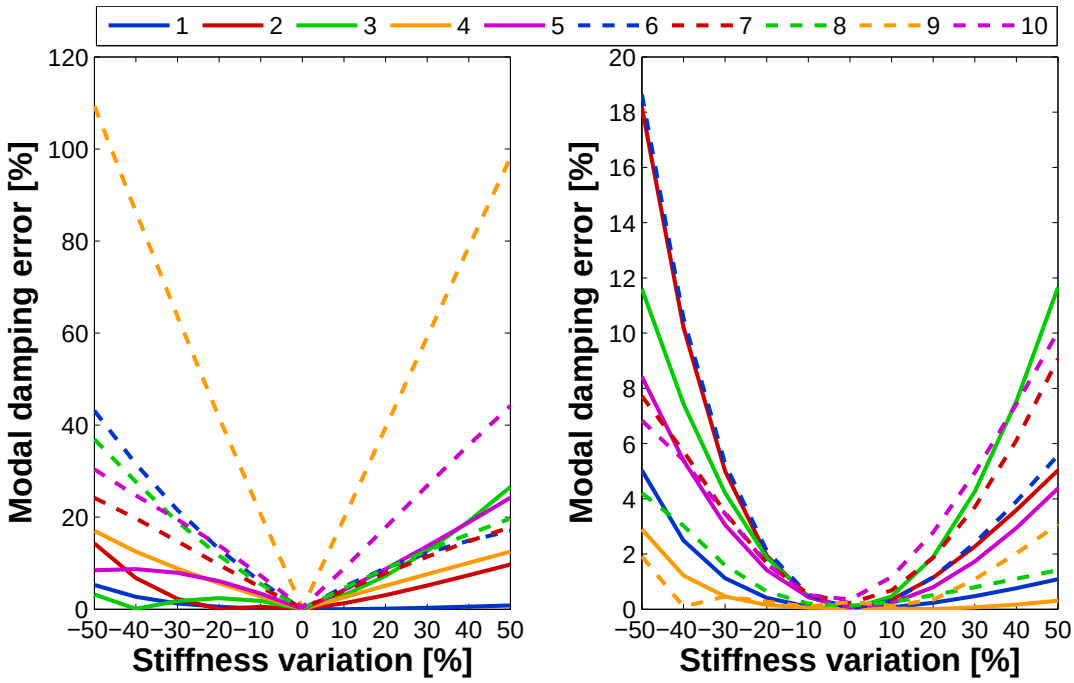

Figure 5.18: Modal damping error in the first 10 cantilever modes computed through the CMP method with respect to $\mathbf{K}_{C2}$ damping perturbations. Left: Simplified PPFs Right: Generic PPFs.

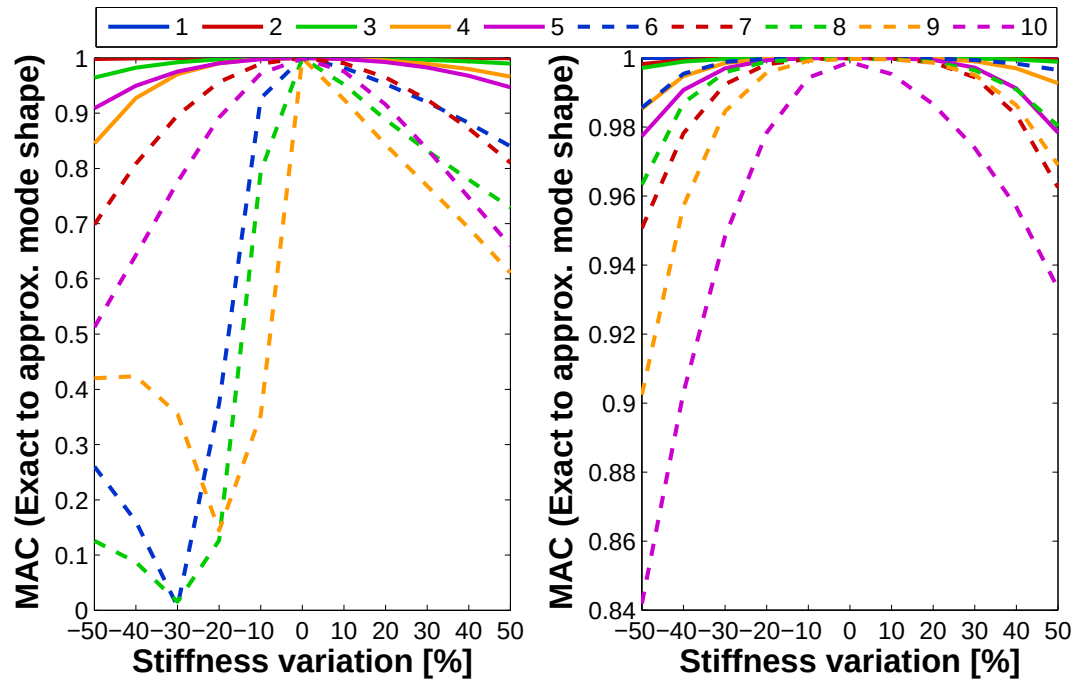

Figure 5.19: Modal Assurance Criterion for the first 10 cantilever modes computed through the CMP method with respect to $\mathbf{K}_{C2}$ damping perturbations. Left: Simplified PPFs Right: Generic PPFs.

What actually happens is that the $\hat{\mu}_{im}^{z}$ and μ_{im}^{z} weighting factors, which are neglected in the simplified formulation, have much larger values for stiffness variations than for damping variations. Accordingly, for damping variations, the non-zero contribution of the $(\hat{\mu}_{im}^{z} - \lambda_m \mu_{im}^{z})$ terms is much smaller than the other weighting factors in the generalised PPFs, so that little error is made by neglecting them. On the contrary, the value of $(\hat{\mu}_{im}^{z} - \lambda_m \mu_{im}^{z})$ is of significant magnitude for stiffness variations. Therefore, large approximation errors are made by using the simplified formulation.

5.3.4 Validity of the CMP method

For the cantilever example, the CMP perturbation method has proved to work in its generic formulation for stiffness and damping variations with equal accuracy to the full perturbation propagation scheme. Moreover, its simplified formulation also works with similar accuracy for damping variations.

One would expect that the CMP method works for mass variations as well, at least in its generic formulation. However, this is not the case. Considering a mass variation test analogous to the stiffness variation test, the CMP results give perturbations in global modes with large approximation errors, similar to those of the LMP method for stiffness variations.

This means that the initial assumption of the CMP method, i.e. that only the perturbation in component eigensolutions need to be considered in order to propagate perturbations into the global modes, is valid only in certain circumstances.

For mass variations, neglecting the component mass perturbations $\tilde{\Delta}\mathbf{M}_s$ introduces large errors in the component MCB matrices perturbation approximation. In particular, this happens because the component mass matrices are multiplied with the velocity DOFs of the component modes in the MCB component reduction process. Hence, component mass matrix perturbations are somehow *weighted* by larger factors (i.e. by velocity mode shapes) than damping or stiffness component matrices (i.e. by displacement mode shapes).

On the contrary, for damping and stiffness variations, efficient perturbation approximations are obtained by neglecting the component damping/stiffness matrices perturbations $\tilde{\Delta}\mathbf{C}_s$ and $\tilde{\Delta}\mathbf{K}_s$ in the global modes perturbation propagation without loss in accuracy for the cantilever example. Therefore, the CMP method is only applicable to damping and stiffness variation scenarios.

5.3.5 Low-frequency modes correction

In general, structures having line/surface coupling interfaces between components result in a much larger number of coupling DOFs than in the cantilever example. Since the MCB reduction method is based on fixed-interface component modes, the lowest global modes of such structures are mostly characterised by the constraint modes relating the interior and the coupling partitions of the MCB reduced component matrices, rather than by the fixed-interface component modes. Therefore, the CMP method may fail to correctly propagate perturbation in the lowest global modes of vibration.

A correction for the low-frequency modes can be easily introduced in the CMP formulation. The c^z_{im} and k^z_{im} weighting factors in equations 5.74 and 5.75 may be conveniently redefined as

$$\hat{c}^z_{im} = c^z_{im} + \boldsymbol{\phi}^T_{ci}\tilde{\Delta}\mathbf{C}^y_{cc}\boldsymbol{\phi}_{cm} \tag{5.80}$$

$$\hat{k}^z_{im} = k^z_{im} + \boldsymbol{\phi}^T_{ci}\tilde{\Delta}\mathbf{K}^y_{cc,s}\boldsymbol{\phi}_{cm} \tag{5.81}$$

with $\tilde{\Delta}\mathbf{C}^y_{cc,s} = \boldsymbol{\Psi}^{C^T}_s\tilde{\Delta}\mathbf{C}_s\boldsymbol{\Psi}^C_s$ and $\tilde{\Delta}\mathbf{K}^y_{cc,s} = \boldsymbol{\Psi}^{C^T}_s\tilde{\Delta}\mathbf{K}_s\boldsymbol{\Psi}^C_s$. In this way the perturbation in the coupling partitions of the damping/stiffness matrices is introduced at a little cost and without altering the formulation of the CMP method.

5.4 Interdependency of the perturbation propagation functions

So far in this chapter, perturbation methods for damped built-up systems have been developed on the basis that the system model is reduced using state-space based CMS methods. Specifically, the LMP and CMP methods have been derived from the generic perturbation propagation scheme applied to MCB reduced models.

In section 5.1, the propagation scheme has been presented as a sequence of perturbation propagations, each of them defined by its corresponding perturbation propagation functions (PPFs). Accordingly, perturbations in subsystem physical parameters may be propagated into the component modes which, in turn, may be propagated into the coupled-modal matrices and, eventually, into the global modes of the system. Hence, the propagation scheme could be understood as if the variation in the system modal solutions with respect to a variation in physical parameters is the result of the concatenation of independent propagation processes.

However, this abstract conception may be misleading since all of the perturbation propagation functions defined in section 5.1 are implicitly interdependent. Essentially, they are just parts of one single linear perturbation approximation expression. For instance, for the global eigenvalues the full-end perturbation propagation function would be

$$\tilde{\Delta}\lambda_m = P_{\lambda_m}\left(P_{A^z}(P_{A_s}, P_{\Lambda_s}, P_{X_s}, P_{\Upsilon_s}), P_{B^z}(P_{B_s}, P_{\Lambda_s}, P_{X_s}, P_{\Upsilon_s})\right) \tag{5.82}$$

where P_{Λ_s}, P_{X_s} and P_{Υ_s} are also function of the component matrices perturbations.

This single perturbation propagation expression obtained from the perturbation propagation scheme in CMS models shall be equivalent to the generic definition of a linear perturbation approximation, i.e.

$$\tilde{\Delta}\lambda_m = S_{\lambda_m}(\theta)\Delta\theta = \frac{\partial\lambda_m}{\partial\theta}\Delta\theta \tag{5.83}$$

where $S_{\lambda_m}(\theta)$ is the first order sensitivity function for damped eigenvalues. For a full order FE model, the sensitivity functions expressions correspond to those defined in Appendix D (c.f. equation D.7 for the damped eigenvalues). Yet, for a state-space CMS model, the overall sensitivities for the global modes result in extremely long mathematical expressions, which are more conveniently expressed in terms of the sensitivities between intermediate CMS quantities, i.e.

$$S_{\lambda_m}(\theta) = S_{\lambda_m}\left(S_{A^z}(S_{A_s}, S_{\Lambda_s}, S_{X_s}, S_{\Upsilon_s}), S_{B^z}(S_{B_s}, S_{\Lambda_s}, S_{X_s}, S_{\Upsilon_s})\right) \tag{5.84}$$

This is exactly what the perturbation propagation scheme proposes.

In a mathematical sense, what it is actually done is rewriting the overall sensitivities for the global modes in terms of the partial derivatives between intermediate CMS parameters (e.g. the partial derivative of the component modes with respect to the component matrices, etc.). Then, since all the sensitivities are of first order, the $\Delta\theta$ perturbation can be introduced inside the sensitivity expression in equation 5.84 giving rise to the corresponding perturbation propagation functions in equation 5.82.

Notice how, the fact that the PPFs for the CMS model global modes are obtained using the partial derivative chain rule, implies that definition of each of the PPFs is dependent on the other intermediate PPFs definitions (i.e. P_{B_s}, P_{A_s}, P_{Λ_s}, P_{X_s}, P_{Υ_s}, P_{A^z}, and P_{B^z}). This means that the PPFs in the CMS perturbation propagation scheme shall not be though as being a set of independent approximations.

5.4.1 Consequences of the perturbation propagation functions' interdependence

The consequences of the interdependence between the PPFs in the CMS perturbation propagation scheme may be illustrated through a simple numerical demonstration.

Consider the perturbation propagation functions in equations 5.21 and 5.22, which propagate the perturbation from the coupled-modal matrices into the global modes. These correspond to a sensitivity derivation through the partial derivative chain rule as exposed above.

Now, returning to the cantilever example, presume that for each 10% damping or stiffness perturbation the exact coupled modal matrices are computed through the MCB method. Thence, the exact coupled-modal matrices perturbations $\Delta\mathbf{A}^z$ and $\Delta\mathbf{B}^z$ may be computed, so that they can be introduced into the global modes PPFs, i.e.

$$\tilde{\Delta}\lambda_m = P_{\lambda_m}(\Delta\mathbf{A}^z, \Delta\mathbf{B}^z) \tag{5.85}$$

$$\tilde{\Delta}\boldsymbol{z}_m = P_{z_m}(\Delta\mathbf{A}^z, \Delta\mathbf{B}^z) \tag{5.86}$$

One may expect that, by using the exact perturbations $\Delta\mathbf{A}^z$ and $\Delta\mathbf{B}^z$ instead of their approximate counterparts $\tilde{\Delta}\mathbf{A}^z$ and $\tilde{\Delta}\mathbf{B}^z$, the approximation in the global modes should be more accurate. However, performing this simple exercise one realises that, in fact, completely erroneous results are attained.

In Figures 5.20 and 5.21 the relative error in the global eigenvalues computed as in equation 5.85 is presented. Figure 5.20 shows the modal frequency error in logarithmic scale for the damping variation test (left) and the stiffness variation test (right). Similarly, Figure 5.21 shows the modal damping error in logarithmic scale for the damping variation test (left) and the stiffness variation test (right).

It can be observed how for both tests the error in modal damping and modal frequencies reach maximum values far above 1000% values. In fact, values of 100% error are obtained already for the minimum considered perturbation (10%), except for the lowest two modes which show little sensitivity to any perturbation. This shows that introducing exact perturbations in the perturbation propagation scheme does not lead to more accurate results in the global modes approximations. However, does this mean that the cause for such failing results is the propagation functions interdependence?

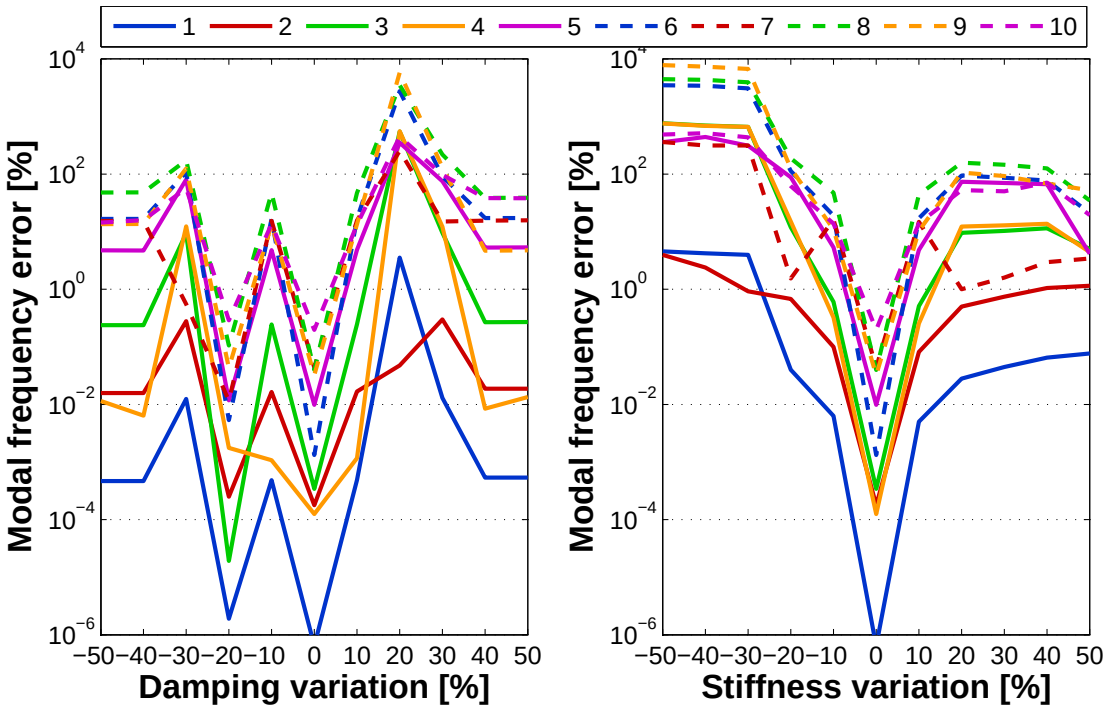

Figure 5.20: Modal frequency error in the first 10 cantilever modes with perturbed $\mathbf{C}_{\mathrm{E8}}$ (left) / $\mathbf{K}_{\mathrm{C2}}$ (right) propagated from exact $\Delta\mathbf{A}^z$ and $\Delta\mathbf{B}^z$.

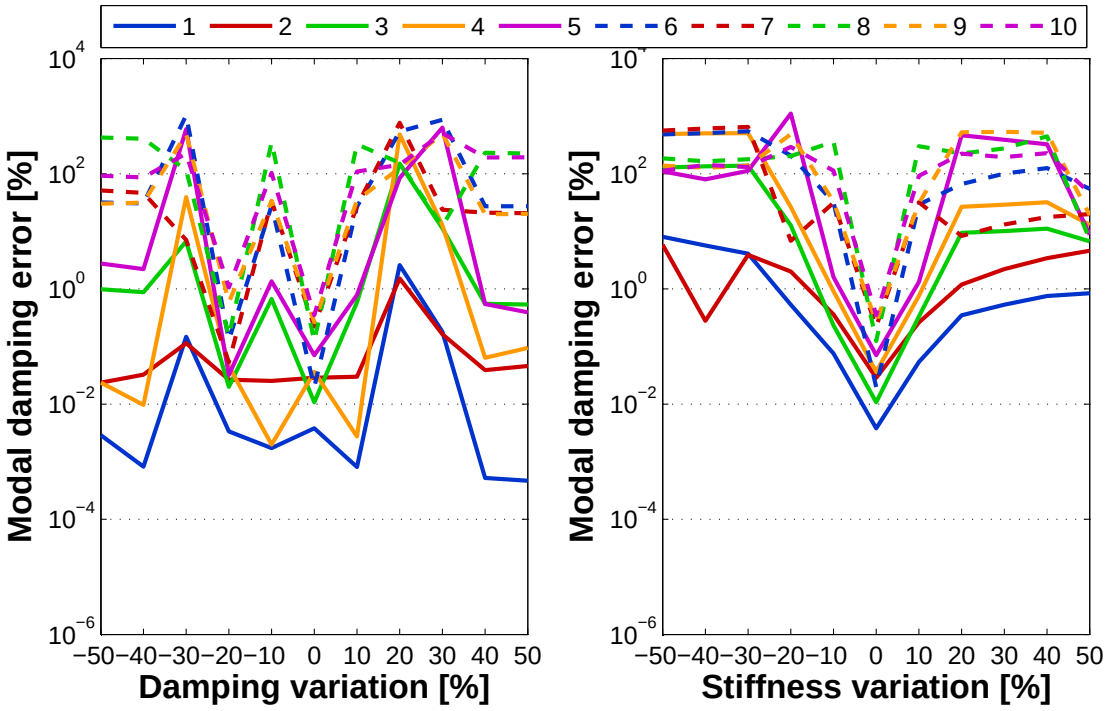

Figure 5.21: Modal damping error in the first 10 cantilever modes with perturbed $\mathbf{C}_{\mathrm{E8}}$ (left) / $\mathbf{K}_{\mathrm{C2}}$ (right) propagated from exact $\Delta\mathbf{A}^z$ and $\Delta\mathbf{B}^z$.

One may argue that the component eigenvectors may be obtained with different arbitrary phase for each exact solution corresponding to a physical parameter perturbation. Therefore, computing exact coupled-modal matrices perturbations from component eigenvectors with non-matching absolute phases might not be coherent. This could explain why the error values in Figures 5.20 and 5.21 vary non-monotonically as the perturbation grows. In fact, this is partially true, but it is not the whole explanation.

Consider now that instead of using the exact MCB coupled-modal matrices perturbations $\Delta\mathbf{A}^z$ and $\Delta\mathbf{B}^z$ in equations 5.85 and 5.86, their linear perturbations approximations are used, i.e.

$$\tilde{\Delta}\mathbf{A}^z = P_{\mathbf{A}^z}(\Delta\mathbf{A}_s, \tilde{\Delta}\mathbf{X}_s^F, \tilde{\Delta}\boldsymbol{\Upsilon}_s^C) \tag{5.87}$$

$$\tilde{\Delta}\mathbf{B}^z = P_{\mathbf{B}^z}(\Delta\mathbf{B}_s, \Delta\boldsymbol{\Lambda}_s^F, \tilde{\Delta}\mathbf{X}_s^F, \tilde{\Delta}\boldsymbol{\Upsilon}_s^C) \tag{5.88}$$

with the particularity that the exact component eigenvalues perturbations $\Delta\boldsymbol{\Lambda}_s^F$ are introduced. Component eigenvalues experience significant variations for system stiffness variations. Thence, there is a sensible difference between using their exact perturbation value or the corresponding linear perturbation approximation. Moreover, no component eigenvectors arbitrary phase influence may be claimed in this case.

Performing the stiffness variation test again (using the exact component eigenvalues perturbations) leads to the results presented in Figure 5.22. This time, the error curves grow monotonically as they depart from the unperturbed position. Yet, the maximum error values obtained are as high as 70% modal frequency error and 170% modal damping error. Even though more accurate component perturbations are used, the accuracy in global modes decays drastically.

The results obtained in the numerical examples in this section show that the CMS parameters (component modes, component modal matrices, coupled-modal matrices and global modes) are intimately related. This is equivalent to saying that the distinct perturbation propagation functions are interdependent. In consequence, the independent perturbation of one CMS parameter (say for instance the component eigenvalues) supposes that the accuracy of the perturbation propagation scheme and its derived perturbation methods (the LMP and the CMP methods) gets jeopardised.

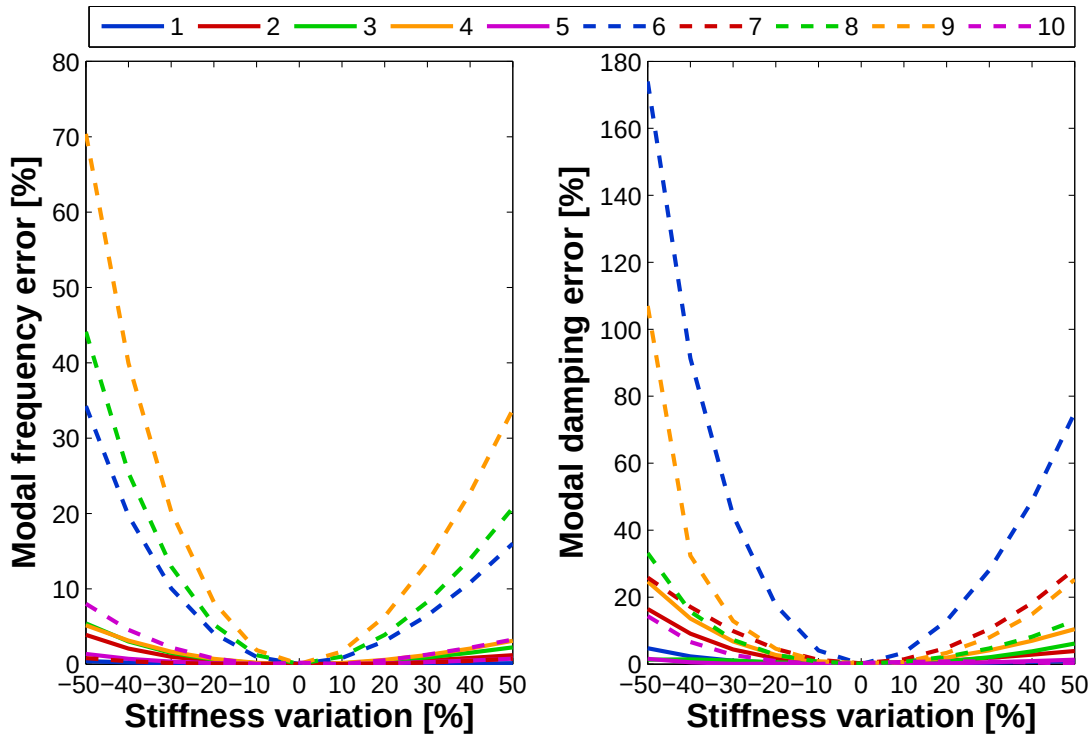

Figure 5.22: Modal frequency and damping error in the first 10 cantilever modes with perturbed $\mathbf{K}_{C2}$ propagated from exact $\Delta\mathbf{\Lambda}_s^F$.

5.5 Computational efficiency of the perturbation methods

This section will discuss whether the perturbation methods presented in this chapter are cost-efficient. This will be done through a numerical example where the perturbation methods' solution cost is compared to the cost for computing the exact solution of a perturbed system.

The *four locally damped coupled plates* test example presented in the previous chapter is used here again for evaluating the computational efficiency of the perturbation methods in state-space CMS models. Three of the meshes defined in section 4.6.2 are considered, namely mesh 1 having 627 physical DOFs, mesh 2 having 2331 physical DOFs, and mesh 3 having 5115 DOFs. For each of the meshes the first 80 damped modes of the full structure are to be computed.

First, the exact modal solution of the baseline system may be computed either by solving the full order state-space eigenvalue problem or through state-space based CMS methods. Then, assume that only plate number 2 out of the 4 coupled plates is subject to variations. For any variation in a physical parameter, the corresponding

variation in the global modal solution is examined.

The computational cost for obtaining exact solutions is taken here as a reference for evaluating the efficiency of the perturbation methods. In figure 5.23 the computational time for obtaining the exact solutions for the baseline and the perturbed system are presented. The computation time for the full order *undamped* EVP so-

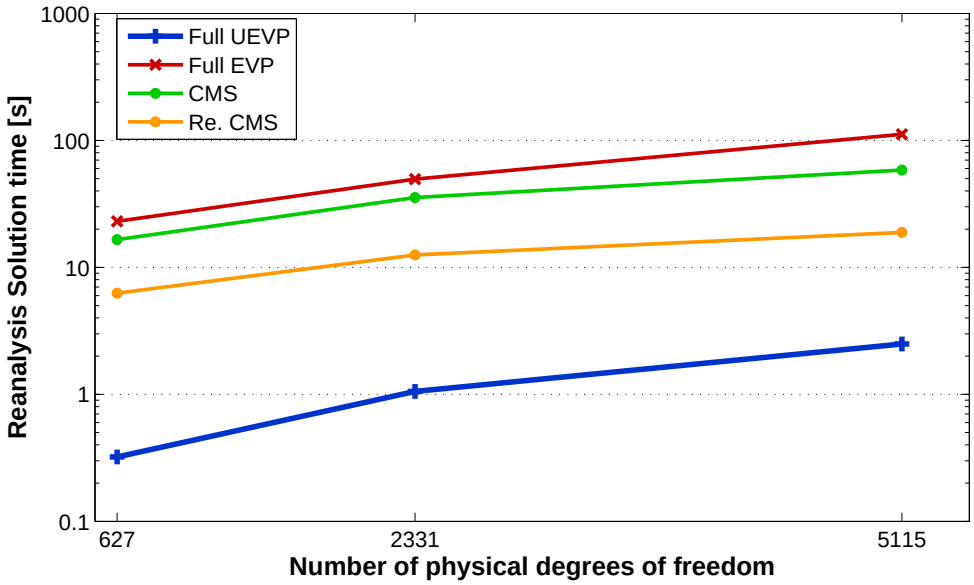

Figure 5.23: Global modes exact reanalysis solution time as a function of the number of physical degrees of freedom of the full system.

lution is plotted in blue. Likewise, the modal analysis computation time through the full order state-space EVP solution is plotted in red. The solution time for an equivalent modal analysis performed through the MCB method with 50 damped modes (100 eigensolutions) per component is plotted in green. Last, for a given perturbation in component 2 (only), the solution time for CMS reanalysis[9] is plotted in yellow.

The exact solutions are only obtained from the modal analysis in state-space coordinates. Hence, the undamped EVP solution does not provide the exact solution since the system is heavily and locally damped. Yet, the undamped solution time is indicated here as a reference for efficiency evaluation.

As has been explained in the previous chapter, the solution time for solving the

[9]The modal reanalysis involves only the solution of the state-space EVP of component 2 and the coupled-modal EVP. Accordingly, the CMS solution cost for the reanalyses is lower than for the baseline system.

state-space eigenvalue problem through the the SILM eigenvalue algorithm may not be directly compared to other solution times since the available SILM MATLAB implementation is not coded in an efficient low-level programming language. Accordingly, an efficient implementation of SILM may give rise to solution times an order of magnitude below the ones presented in Figure 5.23. As can be observed, the undamped EVP solution time is approximately an order of magnitude lower than the CMS reanalysis solution time, which is the most efficient way for obtaining exact reanalyses. Therefore, it is assumed here that comparison with the full order undamped EVP solution time is a fair measure of the perturbation methods efficiency.

A similar perturbation test to those applied to the cantilever example throughout this chapter is applied to the four coupled-plates system. In particular, stiffness perturbations $\Delta\mathbf{K}_{C2}$ in all of the component 2 domain are considered from -20% to +20% of the $\mathbf{K}_{C2}$ value in steps of 5% perturbations.

For each $\Delta\mathbf{K}_{C2}$ perturbation the approximate perturbations in the modal solutions are computed through perturbation methods. Specifically, they are computed using four methods: the full order perturbation approximation for damped modes (c.f. section 3.2.3), the full state-space based CMS perturbation propagation scheme for the MCB method (c.f. section 5.1), the Component modal-propagation (CMP) method in its generic formulation (c.f. section 5.3) and the Local-modal perturbation (LMP) method (c.f. section 5.2). This is done for the three meshes described above.

This time it is not the approximation error with respect to the exact solution that is to be evaluated, but the perturbation approximation computation time with respect to the exact solution computation time. Hence, for each perturbation method and every mesh size, the time for propagating each $\Delta\mathbf{K}_{C2}$ perturbation into the global modes has been recorded. The average computation times have been subsequently calculated.

In Figure 5.24 the average computation time values for the approximate reanalyses in each of the defined meshes are presented in a logarithmic scale. The blue line serves as a reference and it indicates the computational time needed for solving the full order undamped eigenvalue problem. The computation time for the full order damped modes perturbation approximation is plotted in red, the computation time for the full CMS perturbation scheme is plotted in green, the computation time for the CMP method in yellow and for the LMP method in purple.

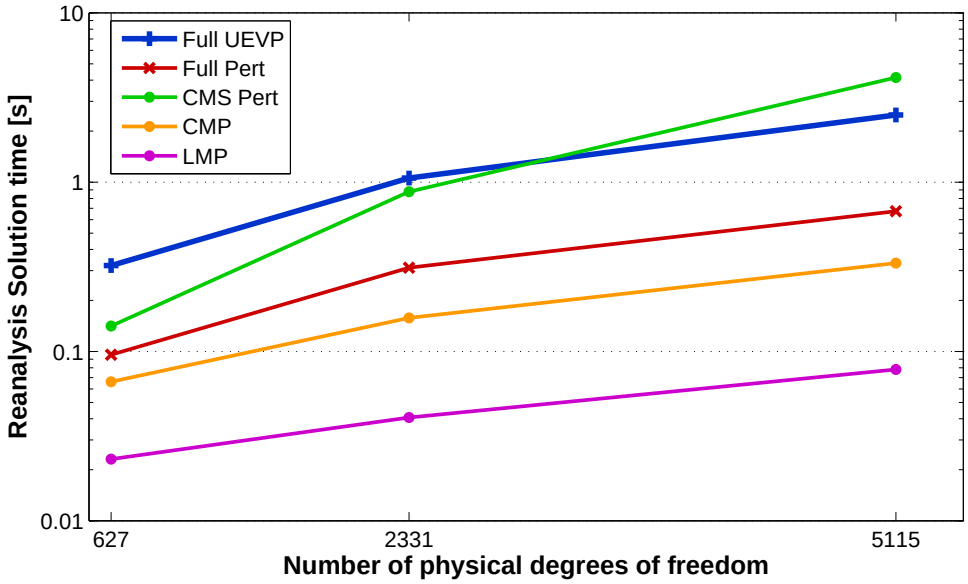

Figure 5.24: Global modes approximate reanalysis solution time as a function of the number of physical degrees of freedom of the full system.

Here, it is of interest to compare the computational efficiency of the CMS based perturbation methods with respect to the exact solution cost and also with respect to the computational cost for full order damped modes perturbation method. First it may be observed that, as expected, the full order perturbation method (red line) is more efficient than obtaining exact EVP solutions (blue line). This is true for all of the mesh sizes considered, which have a relatively small number of degrees of freedom. According to the asymptotic computational costs discussed in section 3.2.4, the efficiency of the perturbation methods with respect to the EVP solution cost shall further increase for larger models.

However, for the full perturbation propagation scheme (green line), the computational cost asymptotic behaviour is completely the opposite. Although the reanalysis solution time is lower for the smaller mesh (2×627 state-space DOFs), the computation time as a function of number of DOFs increases at a greater rate than the solution time through eigenvalue algorithms. The reason for such an increased computational cost may be found in the calculation of the constraint mode perturbation (c.f. equation 5.10), where a matrix inversion operation is required.

In fact, the inverse matrix $\mathbf{K}_{ii}^{-1}$ in the constraint modes perturbation propagation function may be computed just once, so that it can be used at each perturbation propagation with no extra cost. This would reduce the average computation time shown in Figure 5.24 (green line). Nevertheless, the full CMS perturbation prop-

agation scheme computation cost is in any case higher than the cost for full order damped modes perturbation. Thus, the full perturbation propagation scheme shows no computational advantage with respect to the existing methods.

On the contrary, the CMP (yellow line) and the LMP (purple line) methods invariably show computation times below that of the full order damped modes perturbation and, of course, lower than the full order EVP solution. The efficiency of these latter two methods may be better evaluated by expressing the reanalysis solution time of the perturbation methods as the computation cost relative to the undamped EVP (UEVP) solution time.

In figure 5.25, the UEVP relative computation cost for the full order damped modes, the CMP and the LMP perturbation methods is shown on a linear scale. As the number of degrees of freedom increases, the relative computation times decrease. This is concordant with the perturbation methods cost asymptotic behaviour.

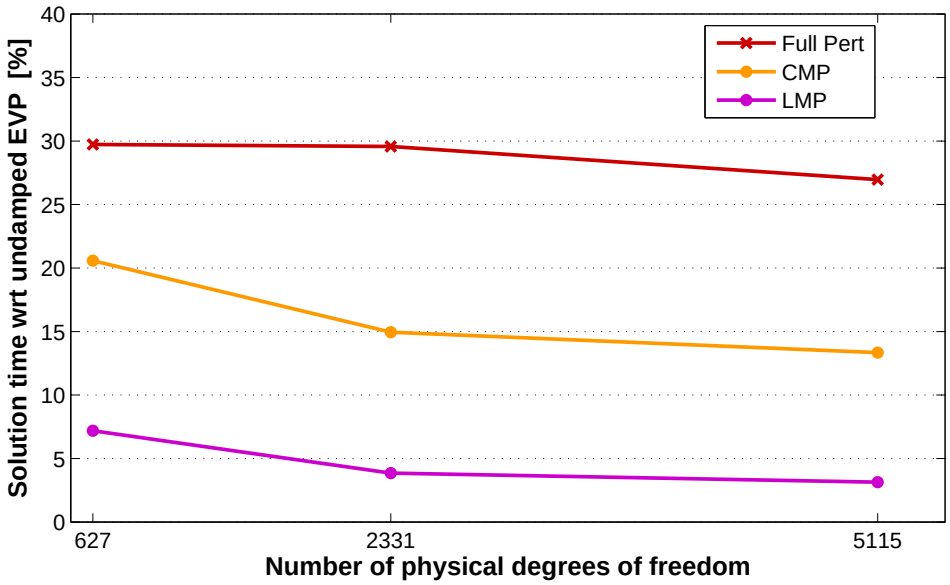

Figure 5.25: Global modes approximate reanalysis solution cost relative to the reanalysis solution time for the undamped eigenvalue problem of the full system.

The CMP method appears to converge to a value between 10% and 15% the UEVP computational cost, i.e. the CMP method is an order of magnitude more efficient. At the same time, the CMP computational cost is approximately half of the full order perturbation cost for all three meshes. In turn, the LMP method is even more cost-efficient (although less accurate). Compared to the CMP method, the LMP method is about 3 to 4 times more efficient, showing times relative to UEVP below 5%.

These relative time values are specific to the test example that is being evaluated, that is, a system composed of four similar-sized components where just one component is subject to variation. The efficiency figures may vary depending on the amount and size of varying components with respect to the total number of components of the system.

In a system composed of many components, a small number of component modes in each component are needed relative to the number of global modes required. On the contrary, for a system with few components the number of component modes in each component needs to be of the same order as the number of global modes. Moreover, in the context of structural design, variations in the physical model parameters are typically considered in a few subsystems at a time.

Hence, for large built-up systems, relatively few component modes need to be perturbed. Notice that component mode perturbation propagation functions are the ones that contribute the most to the overall computation cost in the CMP and LMP methods, since the full order component matrices and shape vectors are involved. Thus, it can be stated that for large built-up systems the CMP and LMP methods are significantly more efficient than full order perturbation methods.

5.6 Conclusions

In this chapter original perturbation methods have been devised using CMS reduced order models for damped systems. The novelty in these methods consists in the use of damped component modes for the model reduction, which allows one to tackle damping variations as well as any other parameter variations showing covariance relation with damping (e.g. stiffness variations in heavily damped systems).

The main idea is that if, in a substructured model, one reduces each component model by means of damped component modes, variations in the full system dynamics may be efficiently computed from the variations in the damped component modes. Thence, by considering parameter perturbations in the varying components only, the perturbed dynamic response of the full system is linearly approximated from the corresponding damped component mode perturbation approximations.

On the perturbation approximation in damped CMS models

Here, a linear perturbation approximation for the global modes of the system with respect to a perturbation in component parameters has been proposed in terms of the linear approximations for the perturbation in intermediate CMS parameters.

However, not all of the CMS parameters perturbations necessarily contribute to the perturbation in global modes for small perturbations in the physical parameters. Therefore, any intermediate perturbation approximation which does not contribute significantly to the global modes perturbation may be conveniently ignored in order to make the computation more efficient without loss in the approximation accuracy.

With this regard, one very important feature is that damped modes of vibration correspond to complex conjugate pairs of eigensolutions, that is, to complex valued eigenvalues and eigenvectors. In practice, this implies that CMS methods based on state-space formulation shall be used. These facts have serious implications regarding the efficiency that may be achieved by computing damped dynamics variations through CMS perturbation approximations.

On one hand, the components' model order is doubled, meaning that the number of degrees of freedom of the state-eigenvectors used in the component reduction is also doubled. Besides, highly damped modes present a broader bandwidth, which means that the number of component modes required for a correct dynamic modelling within a frequency range of interest grows as the system becomes heavily damped.

On the other hand it has been demonstrated that, due to the complexity of the damped eigensolutions, any variation in mass, damping or stiffness of a component produces significant variations in both the eigenvalues and the eigenvectors, as opposed to undamped eigenvectors which show very little dependency on small perturbations in mass or stiffness. This implies that component damped eigenvectors perturbations may not be neglected or, otherwise, the dynamics of the perturbed system would be very poorly estimated by the perturbed CMS model. Thus, perturbation methods based on damped CMS methods must involve component eigenvectors perturbation approximations in order to obtain fairly accurate results.

It should be further mentioned that, as it has been proved in section 5.4, the CMS parameters perturbation approximations are interdependent, so that these approximations may not be used independently, but as constituent parts of a whole perturbation approximation expression.

Proposed methods

In particular, perturbation methods based on the MCB method for Component Mode Synthesis have been explored in this chapter. It has been observed that when a system is reduced using the MCB component modes (i.e. fixed-interface state-eigenvectors and state-space constraint modes), the perturbation in constraint modes is insignificant for small perturbations in either mass, damping or stiffness component parameters. Consequently, there is no need for computing the perturbation approximation for the state constraint modes defined in section 5.1.1, which involves a costly matrix inversion operation.

Furthermore, it has also been observed that for variations in component damping or stiffness (but not mass), the variation in the component dynamics is mainly described by the variation in the fixed-interface damped component modes. Therefore, once the component modes perturbation approximations are computed, the $\Delta\mathbf{A}_s$ and $\Delta\mathbf{B}_s$ state component matrices are not required anymore for the computation of the MCB coupled-modal matrices perturbation approximation presented in section 5.1.3. Thus, by neglecting the constraint modes and the component matrices perturbations, the perturbation approximation for the global modes of the system may be greatly simplified. This is the basis of the proposed methods.

The Component Modal-Propagation (CMP) perturbation method has been devised on these grounds, yielding perturbation propagation functions which directly approximate variations in global modes from perturbations in component eigenvalues and eigenvectors. The required damped component modes perturbations may well be computed using the baseband perturbation method on the component FE model.

The CMP method shows identical approximation error as the damped modes perturbation method presented in Chapter 3. In turn, it offers enhanced computational efficiency by virtue of the use of substructuring and model reduction in CMS models. Since variations may be restricted to one or few components, and since these variations are independent from the rest of subsystems, any non-varying component model is just kept in its reduced order modal basis. Thence, only the perturbations in the damped modes of the varying components have to be computed, and these are then propagated to the global modes at a little cost. This can be done at a fraction of the time for computing the modes perturbation in the full order system, as it has been illustrated through a numerical example in section 5.5.

Notice, that the Component Modal-Propagation is valid for damping and stiffness variations. This fact makes the CMP method suitable for applications where damp-

ing treatments are incorporated in built-up systems. First, because those are situations where small-damping models may give poor estimation of the modal damping. Second, because uncertainty in the damping values should be commonly assumed, given that the modelling and estimation of damping in conventional industry scenarios is not as certain as for other physical quantities.

A much simplified perturbation method has also been proposed for damped built-up systems, the Local Modal Perturbation (LMP) method. This second method is an extension to locally damped systems of the homonymous method for undamped systems (see [23]). In the LMP method, only the component eigenvalues are considered to vary. In this way, very simple perturbation expressions for the global modes are encountered in terms of perturbations in the component eigenvalues. Moreover, it is assumed that perturbations are directly defined at a component-modal level, avoiding in this way the computation of component eigenvalue perturbations from the corresponding component matrices. The LMP method thus achieves a very cost-efficient approximation of the global modes perturbation.

However, neglecting the component eigenvector perturbations is clearly in contradiction with the statement above saying that component eigenvectors perturbations should be included in the damped case. Consequently, the LMP method is significantly less accurate than the CMP method. In fact, the LMP method works with a fair accuracy for only small component damping perturbations.

For this reason, its usage for uncertainty modelling purposes is restricted to cases where very localised additional damping is placed in a structure. Alternatively, it may also be used in scenarios in which a very general result is sought. For example, when deciding where to put more damping in a structure, several attempts can be executed at a low cost through the LMP method. It may not give very accurate results, but it may help the decision making for a trivial solution time.

Discarded methods

Due to the interdependent property of the perturbation expressions in state-space based CMS models, the methods proposed here may not be further improved by a combination with other linear approximation methods.

For example, one might intend to use the Q quotient (c.f section 3.4.3) for damped systems in order to improve the accuracy of the component eigenvalues perturbation approximation. However, doing that would be worthless since it has been proved in section 5.4 that the error in the global modes would then grow. Using the Q

quotient on the approximate perturbation for the coupled-modal matrices would be equally worthless, since the Q quotient value would converge to the eigenvalues of the approximately perturbed coupled-modal matrices.

Likewise, one could also try to approximate the perturbed component modes through interpolation methods. This would be advantageous because interpolation methods are more cost-efficient than perturbation methods, specially when the eigenvectors are required as it is the case for component eigenvectors in Component Mode Synthesis. Furthermore, interpolation methods are suitable for wider variation intervals. Yet, as has been proved also in section 5.4, the use of interpolated component modes within the perturbation propagation scheme would lead to completely erroneous results. In fact, this was initially attempted numerically in this work yielding very unsatisfactory results. Thus, the perturbation methods presented in this chapter shall always be used without violating the perturbed parameters interdependence.

Besides, efficient perturbation methods based on CMS models in Craig-Ni coordinates (i.e. free-interface and residual attachment component modes) have not been further developed in this work for good reasons. Foremost, the difficulty in improving the efficiency of a CN perturbation method is due to the fact that residual attachment modes may not be neglected, opposite to constraint modes perturbation in MCB models.

By their very definition, residual attachment modes are dependent on the component eigenvalues and eigenvectors. Hence, since it has been resolved that both eigenvalues and eigenvectors perturbations are to be included in perturbation methods, residual attachment modes perturbation should also be included for a correct perturbation approximation in the global modes through perturbation methods.

Accordingly, the inclusion of residual attachment modes perturbation supposes a significant computation effort in any would-be CN perturbation method. First, because the perturbation approximation for the residual attachment modes involve several matrix products. Second, because by not neglecting them one cannot simplify any of the perturbation propagation functions for the CN coupled-modal matrices. Thus, no computational saving for approximating the global modes would be obtained.

Chapter 6

Application of the perturbation methods to uncertainty analysis: A numerical case study.

In this chapter a numerical case study is presented where the CMS perturbation methods devised in the previous chapter are applied for the uncertainty analysis of a locally damped benchmark example. Perturbation methods are often applied for the analysis of uncertainties because they offer efficient computation of the variation in the dynamics of a system model, given that the variations are not too large. Thus, the performance of the CMS perturbation methods is evaluated here in a realistic application. The system dynamic response uncertainty is estimated through CMS perturbation methods and compared to uncertainty estimates obtained from the exact CMS reanalysis of the system. The computational cost for the perturbation uncertainty analyses is also evaluated.

6.1 Description of the benchmark example

A ribbed plate structure is used as a test example. Here the ribbed plate in Figure 6.1 is considered. The ribbed plate structure in the example consists of four consecutive aluminium plate sections which are stiffened by means of three intermediate steel ribs. A damping treatment is assumed on all of the surface of the aluminium plates. Ribbed plates are often found in mechanical structures, such as airplane fuselages. More complex curved ribbed plate structures may be used, but a small

flat ribbed plate is chosen here for simplicity without loss of generality.

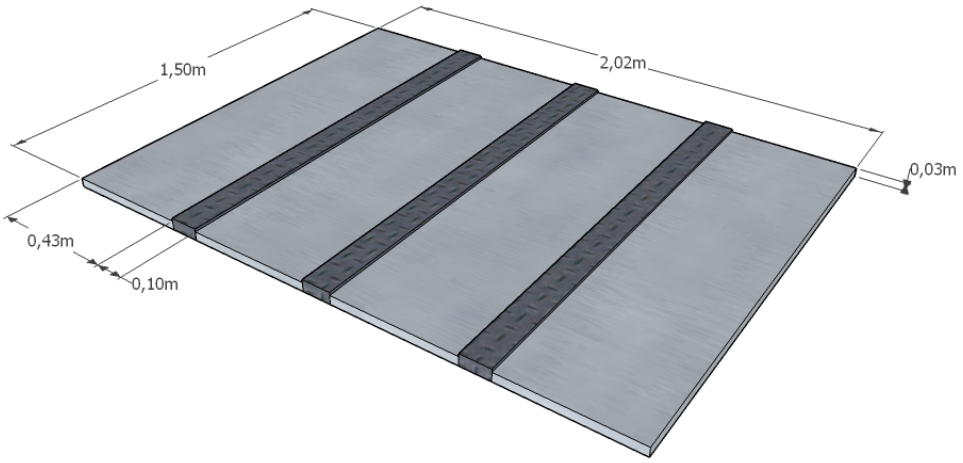

Figure 6.1: Description of the locally damped coupled plates example and its dimensions.

The dimensions of each aluminium plate and steel rib are $0.43 \times 1.50 \times 0.03$ metres and $0.10 \times 1.50 \times 0.04$ metres respectively. Their physical properties are summarised in Table 6.1. In this example, the vibration behaviour of the structure is to be analysed in a frequency range up to 1.5 kHz.

	Elastic Modulus	Mass Density	Poisson's Ratio	Thickness	Proportional Damping Factor
Aluminium Plates	70 GPa	2700 kg/m^3	0.31	3 cm	4×10^{-5}
Steel Ribs	210 GPa	7800 kg/m^3	0.34	4 cm	10^{-7}

Table 6.1: Material properties for the damped ribbed plates example.

A finite element model for the ribbed plate structure has been produced, using 4-noded thin plate elements for the modelling of both the aluminium plates and the steel ribs. Each aluminium plate is partitioned into 180 rectangular elements, and the steel ribs are subdivided into 60 elements each. The resulting mesh, shown in Figure 6.2, consists of 966 nodes. Since the thin plate elements have three degrees of freedom per node (i.e. one transverse displacement, and two in-plane rotation DOFs), the finite element model order is of 2898 DOFs. The ribbed plate is assumed to be simply supported at its four corners, so that according boundary conditions are applied to the model.

Seven components are defined, one for each of the four aluminium plates and one for each of the three steel ribs. The damping in each components is modelled as being proportional to stiffness by a proportional viscous damping factor. Steel

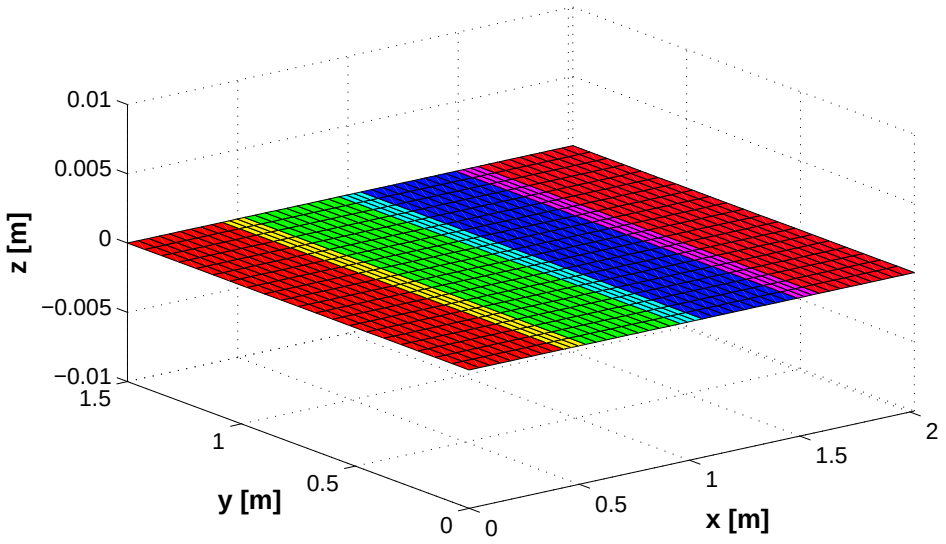

Figure 6.2: Description of the locally damped coupled plates example and its dimensions.

beams and plates are typically very lightly damped with modal damping ratios of 0.1%-0.2% [98]. This is here characterised with a proportional damping factor of 10^{-7}, which yields realistic modal damping values for the steel ribs in the target frequency range of analysis. Likewise, aluminium parts are also very lightly damped with modal damping of the order of 0.01% [99]. Also, they are assumed to have some added damping, which could be the addition of a thin layer of rubber material, and some extra dissipation may be assumed at the plate-rib joints. For simplicity of the numerical example, the overall dissipation effects in the aluminium plates are then characterised with an overall proportional damping factor, which is chosen to be 4×10^{-5}. Despite each of the components being proportionally damped, the full structure model is non-proportionally damped.

6.2 Deterministic solution

The ribbed plate is considered to be heavily damped. Hence, the solution of the system dynamics is addressed through state-space modal analysis. The exact modal solution may be computed by solving the global system state-space EVP through the MSILM algorithm presented in Chapter 4. The maximum frequency of the analysis is set to 1.5 kHz. Accordingly, 60 global modes (120 state eigensolutions) of the ribbed plate are needed to cover the target frequency range.

The 60th mode has a modal frequency of 1.53 kHz and 36% modal damping ratio, confirming that the target frequency range is covered and that the system is heavily damped. In addition, the mode shape of the 60th mode is shown in Figure 6.3 (only displacement DOFs), where it can be observed that the current mesh is fine enough for modelling vibrations up to 1.5 kHz (i.e. there are ~10 elements per wavelength in both directions x and y).

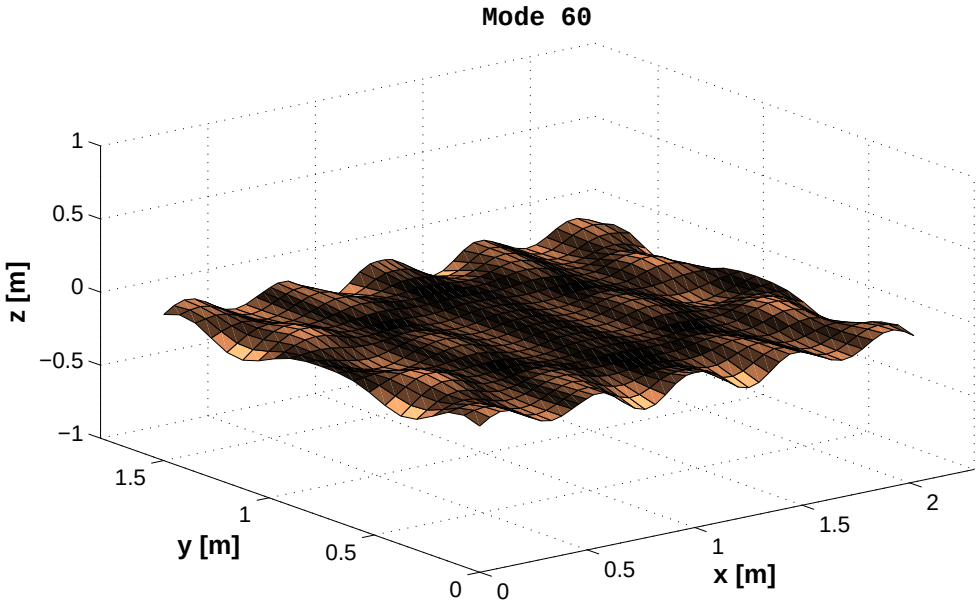

Figure 6.3: Mode shape of the 60th ribbed plate mode of vibration.

Computing all of the 60 global modes takes 16.91 seconds. The corresponding dynamic response of the ribbed plate can then be evaluated. In Figure 6.4, the dynamic behaviour of the ribbed plate is shown from two points of view, frequency response and modal views. In the top plot, the input mobility of the ribbed plate at a loading position is presented. This has been computed at the 100th node of the mesh, which corresponds to position (x,y,z)=(0.191,1.125,0.0) in the leftmost aluminium plate. In the bottom plot the positive-frequency eigenvalues corresponding to each of the 60 modes are presented in a modal frequency-damping ratio complex plane. In both plots the frequency axis is logarithmic, and in the second plot the 16 Hz to 1 kHz octave bands are indicated.

The low-frequency, mid-frequency and high-frequency vibrating behaviour of the ribbed plate can be observed in Figure 6.4. In fact, the modal density of the plates is almost constant. For the ribbed plate the average density is of 0.041 modes/Hz or, conversely, an average spacing of 24.4 Hz between modes. However, this constant spacing implies increasing modal overlap in the different frequency ranges since high

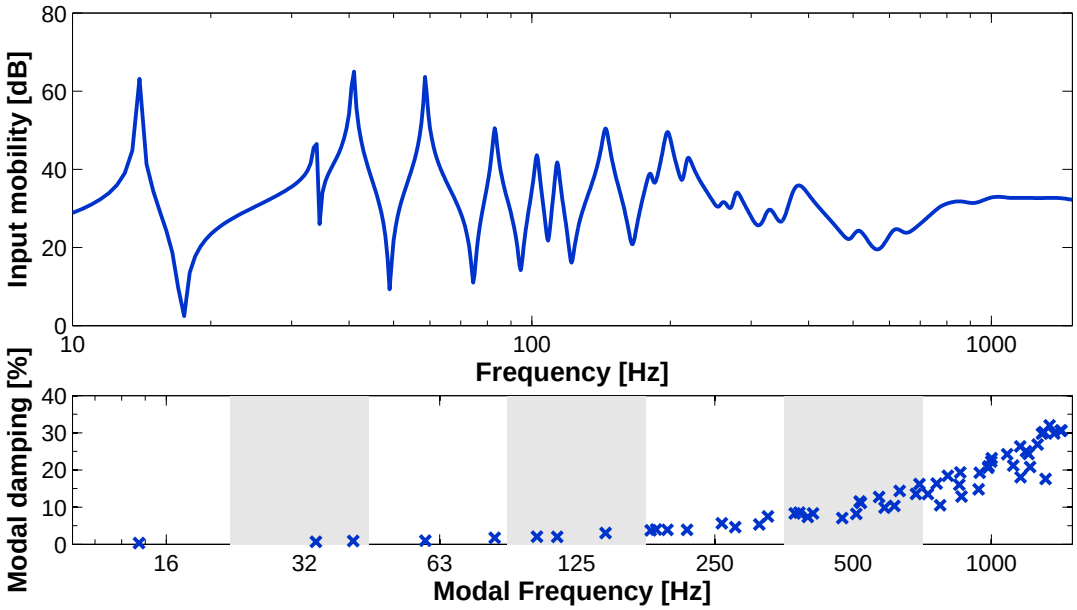

Figure 6.4: Dynamic response of the ribbed plate. Top plot: Input mobility in dB ref. $10^{-6}\mathrm{ms}^{-1}/\mathrm{N}$ at the 100th node displacement DOF. Bottom plot: modal frequency and damping for the 60 computed modes.

frequency modes have larger modal bandwidth than low frequency modes.

A low-frequency regime is observed in the first four octave bands, namely the 16 Hz, 31.5 Hz, 63 Hz and 125 Hz bands. In the eigenvalues plot it can be seen how there are just 8 modes in the frequency range covering the first four octave bands, that is an average of two modes per band. Since, maximum modal damping values of 3% are found in this range (i.e. the modes are lightly damped), the modal bandwidth of the modes is much smaller than the modal spacing, so that there is hardly any modal overlap in the low frequencies. Accordingly, in the mobility plot resonance peaks corresponding to each of the vibration modes can be clearly distinguished.

A high frequency regime is observed for the 1 kHz band. With a large number of modes (27) in the band and modal damping values between 10% and 32%, many modes overlap at each frequency, yielding the flat spectrum characteristic observed in the mobility plot.

Lastly, mid-frequency characteristics are observed in the intermediate frequencies. Average modal damping ratios of 5% and 10% are obtained in the 250 Hz and 500 Hz bands respectively. These modes are moderately to highly damped so that their modal bandwidth is of comparable magnitude to the modal spacing. In fact, a modal overlap equal to one is obtained at 313 Hz, which is close to the border

between the two bands. In the mobility plot this gets translated into an irregular frequency response which does not show isolated modal resonances as in the low-frequencies nor the flat spectrum characteristic of the high frequencies. This is in principle the frequency range in which uncertainty analysis is most necessary.

	Physical description	State-Space DOFs	State Eigenvectors	Max. Modal Frequency
Comp. 1 and 7	Outer Aluminium Plates	1260	50	2949 Hz
Comp. 2, 4 and 6	Steel "rib" plates	504	10	24379 Hz
Comp. 3 and 5	Inner Aluminium Plates	1260	30	2692 Hz

Table 6.2: Description of the ribbed plate components substructuring and reduction.

Alternatively, the same modal analysis can be conducted through state-space based CMS methods. In this way, the modal solution computation time is reduced while providing almost identical results. Furthermore, a reduced order model in terms of the system modal components is obtained and can be used for any required reanalysis of the modelled structure.

The Morgan-Craig-Bampton (MCB) method is used here for the CMS solution. A reduced number of component modes were computed for each component: 25 modes for the outer aluminium plates, 15 modes for the inner aluminium plates and 5 modes for the steel ribs. These numbers of modes were chosen so that each component has fixed-interface modes with frequencies over one and a half times the maximum frequency of analysis (as a rule of thumb), which is explicitly given in Table 6.2. The MCB solution for the global modes takes 12.79 seconds, which is a smaller time than the full model direct solution even though the model considered is not very large. The resulting MCB coupled-modal model has 906 DOFs, as opposed to the 5796 DOFs of the full model in state-space coordinates.

6.3 Uncertainty modelling

In this case study example a damping treatment has been added to the ribbed plate, specifically on the aluminium components. As it has been pointed out throughout the thesis, the modelling of damping remains a challenging matter, since mechanical structures usually present many dissipation mechanisms at the same time. Thus, the modelling of damping is often addressed through simple damping models (such as viscous damping) which approximately describe the overall damping introduced by the different dissipation mechanisms. It is therefore natural to assume uncertainty in the modelling of damping. It may further be assumed that not only the modelled damping is uncertain due to the applied damping treatment. The damping layer

may be glued to the surface of the plates, so that it could alter other physical properties like, for example, the stiffness properties of the aluminium plates.

The parameters in the ribbed plate physical model (e.g. damping factor, Young modulus, etc.) have been assumed to be homogeneous values for all of the spatial domain of each component. That is, all elements of, say, an aluminium plate have the same physical parameter values. However, when uncertainty is considered, the physical parameters typically show spatially varying properties. In other words, the variation in one physical parameter may differ from one position to another.

6.3.1 Random fields

The spatial distribution of the varying parameters may be represented by means of random fields [17]. A random field is a set of correlated random variables which are spatially distributed. For varying parameter θ, a corresponding random field $\theta(x, y, z)$ may be defined.

Random fields are described by the correlation between the variation of random variables at different spatial positions. Homogeneous isotropic Gaussian random fields are usually used to represent the spatial variation of uncertain physical parameters. Given an uncertain physical parameter θ with mean value $\bar{\theta}$ and standard deviation σ_θ, the correlation r between its variation at two positions separated by a distance d is modelled through a decaying exponential function

$$r(d, L_c, \sigma_\theta) = \sigma_\theta^2 \exp\left(-\left|\frac{d}{L_c}\right|\right) \tag{6.1}$$

with L_c the *correlation length*, which characterises the spatial rate of the variation in the random field. In the asymptotical extremes, $L_c = 0$ indicates independent variation at all positions, and $L_c = \infty$ fully correlated variation in all of the field domain.

For applying spatial variations in a Finite Element model, the continuous random field $\theta(x, y, z)$ must be discretised. One possible discretisation is to consider the variation inside each finite element to be fully correlated. The random field takes then one single value in each of the N_e elements. Thence, a corresponding *covariance matrix* $\mathbf{Cov}(\theta)$ can be computed, with each covariance matrix element $\mathrm{cov}_{kl}(\theta)$ being the correlation function between the centroids of the (k,l) finite elements, i.e.

$$\mathrm{cov}_{kl}(\theta) = r(d_{kl}, L_c, \sigma_\theta) \tag{6.2}$$

Thus, a discretised random field $\boldsymbol{\theta}$ is a set N_e interdependent Gaussian random variables ϑ_e whose correlation is characterised by the covariance matrix $\mathbf{Cov}(\theta)$. In order to produce a random field sample, a random number for each of the field variables must be generated. Since the random field variables are correlated, these random numbers must be generated according to the covariance matrix. By finding an orthogonal basis for the covariance matrix one may express the set of correlated random variables ϑ_e in terms of a set of uncorrelated random variables ξ_i. Consequently, a random field can be produced by generating a random sample for each of the independent random variables ξ_i.

The Karhunen-Loève (KL) expansion [18] is usually used for efficiently generating a random field with a minimum number of independent random variables ξ_i. It uses the eigenvalues μ_i and eigenvectors $\boldsymbol{\psi}_i$ of the covariance matrix for its orthogonal decomposition. Thereupon, the random field may be posed in terms of the KL expansion as

$$\boldsymbol{\theta}(\boldsymbol{\xi}) = \bar{\theta} + \sum_i \sqrt{\mu}_i \boldsymbol{\psi}_i \xi_i \tag{6.3}$$

where $\bar{\theta}$ is the mean value of the field which typically corresponds to the nominal value of θ. In general, the correlation length is high enough so that a very small number of covariance matrix eigenvalues dominate. Therefore, the KL expansion may just be truncated after the first few dominant eigensolutions, which implies that a very small number of independent random variables ξ_i are needed for modelling the random field.

6.3.2 Quantification of uncertainty at a component level

The uncertainty in the ribbed plate components is modelled here through random fields and KL expansions. Each component's uncertainty is assumed uncorrelated from the uncertainty in the other components, so that a random field is generated for each aluminium plate. In fact, since the 4 aluminium plates have the same nominal properties, the same random field is valid for all of them in this case. Therefore, a normalised random field $\boldsymbol{\theta}_0$ with zero mean and unit variance is generated with an assumed correlation length $L_c = 0.5$ m. Then, a KL expansion for $\boldsymbol{\theta}_0$ is defined using just 3 covariance eigensolutions, i.e.

$$\boldsymbol{\theta}_0(\boldsymbol{\xi}) = \sum_{i=1}^{3} \sqrt{\mu}_i \boldsymbol{\psi}_i \xi_i \tag{6.4}$$

since the 4th eigenvalue $\mu_4 = 7.9167$ is already an order of magnitude below the first eigenvalue $\mu_1 = 59.7802$ which is the most dominant one.

The damping and stiffness properties of the aluminium plate components are considered uncertain. A 20% *coefficient of variation*[1] (CV) is assumed in the viscous damping proportionality factor α, while a 10% CV is assumed for the damped aluminium plates' Young's modulus E. For each component s, a damping random field $\boldsymbol{\alpha}_s$ and a stiffness random field $\boldsymbol{E}_s$ are then defined using KL expansion for the $\boldsymbol{\theta}_0$ random field, that is

$$\boldsymbol{\alpha}_s = \alpha + \sigma_\alpha \boldsymbol{\theta}_0 = \alpha(1 + \mathrm{CV}_\alpha \boldsymbol{\theta}_0) \tag{6.5}$$

$$\boldsymbol{E}_s = E + \sigma_E \boldsymbol{\theta}_0 = E(1 + \mathrm{CV}_E \boldsymbol{\theta}_0) \tag{6.6}$$

Thus, 6 independent random parameters ξ_i are used for describing the uncertainty in each component (3 for the damping and 3 for the stiffness random fields). Hence, a component damping perturbation $\Delta\boldsymbol{\alpha}_s = \sigma_\alpha \boldsymbol{\theta}_0$ is produced by generating 3 ξ_i independent random numbers. Likewise, a component stiffness perturbation $\Delta\boldsymbol{E}_s = \sigma_E \boldsymbol{\theta}_0$ is produced by generating 3 other ξ_i independent random numbers. Each ξ_i random variable has a normal Gaussian probability distribution function.

Yet, when a perturbation method is used for approximating the variation in the dynamic response, each of the ξ_i random variables must be regarded as an independently perturbed parameter. Therefore, a damping perturbation $\Delta\boldsymbol{\alpha}_s^i = \sigma_\alpha \sqrt{\mu}_i \boldsymbol{\psi}_i \xi_i$ or stiffness perturbation $\Delta\boldsymbol{E}_s^i = \sigma_E \sqrt{\mu}_i \boldsymbol{\psi}_i \xi_i$ for each ξ_i must be considered.

For a damping perturbation, the corresponding component damping matrix perturbation $\Delta\mathbf{C}_s^i$ is subsequently calculated element by element. If the damping matrix of element e in component s is $\mathbf{C}_{e,s}$, the damping element matrix is perturbed according to its corresponding damping factor perturbation, i.e.

$$\Delta\mathbf{C}_{e,s}^i = \mathrm{CV}_\alpha \sqrt{\mu}_i \psi_{ei} \xi_i \mathbf{C}_{e,s} \tag{6.7}$$

For a stiffness perturbation, stiffness as well as damping component matrix perturbations $\Delta\mathbf{K}_s^i$ and $\Delta\mathbf{C}_s^i$ follow. These are also computed by perturbing each element matrix according to the Young's modulus perturbation, i.e.

$$\Delta\mathbf{K}_{e,s}^i = \mathrm{CV}_E \sqrt{\mu}_i \psi_{ei} \xi_i \mathbf{K}_{e,s} \tag{6.8}$$

$$\Delta\mathbf{C}_{e,s}^i = \mathrm{CV}_E \sqrt{\mu}_i \psi_{ei} \xi_i \mathbf{C}_{e,s} \tag{6.9}$$

Then, 6 independent perturbation approximations are calculated, one for each ξ_i, in order to propagate the component total uncertainty into the dynamic response parameters. Each perturbation approximation uses the corresponding $\Delta\mathbf{K}_s^i$ and/or $\Delta\mathbf{C}_s^i$ component matrices perturbations.

[1] For a random variable x the coefficient of variation is the standard deviation σ_x normalised by the corresponding mean value μ_x, i.e. $CV = \sigma_x/\mu_x$.

6.3.3 Component-modal quantification of uncertainty

Given that a CMS model in MCB coordinates has been created, one may attempt to quantify the components' uncertainty directly on the component modes, rather than describing the uncertainty at a physical level. This was originally proposed by Mace and Shorter in [23]. Quantifying uncertainty at a component-modal level implies that it is not necessary to propagate component matrix perturbations into component modes, in order to resolve the uncertainty in the full system dynamics. This will certainly reduce the computational cost of the uncertainty analysis.

As for the uncertainty in physical parameters, there is the need to coherently model the uncertainty in the component modes. However, this is not an easy task. Each of the component modes is described by its three modal parameters, namely modal frequency, modal damping and mode shape. In a heavily damped system, such as the ribbed plate example, the uncertainty in the three modal parameters is necessarily correlated. Hence, each of them should be considered as a correlated random variable (or random field in the case of the mode shapes). Thus, the uncertainty in a component mode may be quantified by means of a mode covariance matrix. Moreover, there may exist correlation between the uncertainty in the different modes. Therefore, the component uncertainty may not be modelled for each mode independently. Instead, a component modal covariance matrix for the modal parameters of all component modes should be considered.

Quantifying the modal covariance matrix may be very difficult, especially if the mode shapes are considered uncertain. One way of obtaining the covariance matrix is to perform repeated modal testing measurements of a physical structure. However, the cost for performing modal testing may exceed by far the cost reduction obtained by component-modal uncertainty quantification. Alternatively, the covariance matrix may be computed from repeated simulations in a Monte Carlo scheme.

Besides, if only the component eigenvalues are assumed uncertain (as would be the case for the LMP method), the eigenvalue covariance matrix may be efficiently computed using sensitivity relations. Hasselman and Hart [100] demonstrated that the eigenvalue covariance matrix $\mathbf{Cov}(\boldsymbol{\lambda})$ can be related to the physical parameters covariance matrix $\mathbf{Cov}(\boldsymbol{\theta})$, by means of the sensitivity functions $S_{\lambda_m}(\theta_n)$ for the eigenvalues λ_m with respect to an uncertain physical parameter θ_n, i.e.

$$\mathbf{Cov}(\boldsymbol{\lambda}) = \mathbf{S}_{\boldsymbol{\lambda}}(\boldsymbol{\theta})\mathbf{Cov}(\boldsymbol{\theta})\mathbf{S}_{\boldsymbol{\lambda}}^{T}(\boldsymbol{\theta}) \tag{6.10}$$

Thereupon, equation 6.10 may be reformulated for each component in terms of the KL parameters of the random fields defined in the previous section. Consider a component damped eigenvalue sensitivity function (c.f. equation D.7 in Appendix D) with respect to a KL random field parameter ξ_i

$$S_{\lambda_k}(\xi_i) = \frac{\partial \lambda_k}{\partial \xi_i} = S_{\lambda_k}\left(\frac{\partial \mathbf{M}_s}{\partial \xi_i}, \frac{\partial \mathbf{C}_s}{\partial \xi_i}, \frac{\partial \mathbf{K}_s}{\partial \xi_i}\right) \tag{6.11}$$

which is posed in terms of the component matrix sensitivities. The matrix sensitivities with respect to ξ_i are easily derived by virtue of the KL expansion. By inspection of equations 6.7, 6.8 and 6.9 one realises that, for the $\boldsymbol{\alpha}_s$ random field, the element damping matrix sensitivity functions are simply

$$\frac{\partial \mathbf{C}_{e,s}}{\partial \xi_i} = \mathrm{CV}_\alpha \sqrt{\mu}_i \psi_{ei} \mathbf{C}_{e,s} \tag{6.12}$$

and the mass and stiffness sensitivities are zero valued. Likewise, for the $\boldsymbol{E}_s$ random field, the element damping and stiffness matrices sensitivities are

$$\frac{\partial \mathbf{K}_{e,s}}{\partial \xi_i} = \mathrm{CV}_E \sqrt{\mu}_i \psi_{ei} \mathbf{K}_{e,s} \tag{6.13}$$

$$\frac{\partial \mathbf{C}_{e,s}}{\partial \xi_i} = \mathrm{CV}_E \sqrt{\mu}_i \psi_{ei} \mathbf{C}_{e,s} \tag{6.14}$$

and the mass sensitivities are zero valued. Thence, the full component matrix sensitivities are obtained by assembly of the element matrix sensitivities. This implies that a closed form expression for the $S_{\lambda_k}(\xi_i)$ sensitivities is available.

Since ξ_i are independent random variables with unit variance, their corresponding covariance matrix is just an identity matrix i.e. $\mathbf{Cov}(\boldsymbol{\xi}) = \mathbf{I}$. Consequently, the component eigenvalue covariance matrix is simply

$$\mathbf{Cov}(\boldsymbol{\lambda}_s) = \mathbf{S}_{\boldsymbol{\lambda}}(\boldsymbol{\xi})\mathbf{S}_{\boldsymbol{\lambda}}^T(\boldsymbol{\xi}) \tag{6.15}$$

whose computation is trivial given that a closed form exists for the $S_{\lambda_k}(\xi_i)$ sensitivity functions.

Now, considering the quantification of uncertainty in the aluminium plates, i.e. 20% CV for the damping factor and 10% CV for the Young's modulus, a corresponding modal covariance matrix is computed here for each aluminium component, assuming that only the eigenvalues of each component are uncertain, but not the eigenvectors. Consequently, if N_k is the number of kept state-eigensolutions in a MCB reduced component, the uncertainty in each component is modelled through a modal random field $\boldsymbol{\lambda}_s$ consisting of N_k correlated random variables.

This supposes that the uncertainty is modelled through 50 and 30 correlated modal random variables for the outer and the inner aluminium plates respectively. Again, the component modes uncertainty is more efficiently expressed using a KL expansion. By taking an eigendecomposition of the modal covariance matrix $\mathbf{Cov}(\boldsymbol{\lambda}_s)$, i.e.

$$\mathbf{Cov}(\boldsymbol{\lambda}_s)\boldsymbol{\psi}_j = \mu_j \boldsymbol{\psi}_j \tag{6.16}$$

the $\boldsymbol{\lambda}_s$ random field may be expanded into a modal KL expansion:

$$\boldsymbol{\lambda}_s(\boldsymbol{\xi}) = \bar{\boldsymbol{\lambda}}_s + \sum_{i=1}^{2} \sqrt{\mu}_j \boldsymbol{\psi}_j \xi_j \tag{6.17}$$

In this case, the modal random field may be correctly characterised using just 2 modal covariance eigensolutions.

Thus, with the uncertainty quantification at a component-modal level, the whole randomness in the damping proportionality factor throughout an aluminium plate is modelled with just two uncorrelated random variables ξ_j per component. The same applies for the Young's modulus uncertainty. A component modal perturbation is then created by simply sampling the ξ_j independent random variables, which are assumed to have a normal Gaussian probability distribution function. This modal perturbation is consistent with the physical uncertainty described for the components.

6.4 Uncertainty Analysis

Once the uncertainty in the ribbed plate has been characterised, the effects of uncertainty in the dynamic behaviour of the ribbed plate are analysed in this section. The Monte Carlo (MC) method [101] is used here for estimating the statistics of the dynamic outputs.

The ribbed plate uncertainty is analysed through 100 MC samples. For each MC sample, a ribbed plate model realisation is produced by perturbing the model parameters according to the uncertainty defined in each of the aluminium plates, and the dynamics of the system are then solved. Finally, from the results for all of the MC samples the first and second order statistics (i.e. mean and variance) of the dynamic outputs are computed.

In order to evaluate the performance of the CMP and LMP methods presented in the previous chapter, the Monte Carlo uncertainty analysis is executed three times as summarised in Table 6.3.

Analysis	MC samples	Uncertainty modeling	Reanalysis method	Uncertainty propagation	Total computation time
1st	100	Component-Physical	MCB	1 MCB solution	1428.8 s
2nd	100	Component-Physical	CMP	24 CMP approximations	722.3 s
3rd	100	Component-Modal	LMP	8 LMP approximations	76.4 s

Table 6.3: Description of the Monte Carlo uncertainty analyses.

In the first analysis the uncertainty is quantified at a component-physical level, and the perturbed system dynamics are solved exactly at each MC sample through the Morgan-Craig-Bampton CMS method. Since only the aluminium plates are uncertain, the component modal solutions for the steel ribs are not recomputed. The total time for the MCB reanalysis of the 100 MC samples is 1428.8 seconds. This exact solution is used as a reference for assessing the accuracy of the LMP and CMP approximations.

In the second analysis the same component-physical uncertainty quantification is used for each MC sample, and the uncertainty is propagated into the global modes through the CMP method. In this case, the low-frequency correction for the CMP method is included (c.f. section 5.3.4). Notice that for each uncertain component six independent parameters ξ_i are perturbed. This means that an overall number of 24 CMP perturbation propagations per MC sample are required.

The total analysis time through CMP perturbation approximations is 722.3 seconds, which is roughly half the time for an exact solution. The computation cost with respect to the exact solution may vary for other models than the one considered here. For example, for larger models the component EVP solution cost grows exponentially with the number of DOFs, whereas the CMP approximation cost rises linearly. Conversely, a simpler description of uncertainty (e.g. an uncertain scalar parameter) would need much less CMP perturbation propagations. Thus, it is remarkable that, in this case (small model and random field uncertainty modelling), the CMP method is already significally more efficient than the CMS reanalysis.

Last, for the third analysis the modal covariance matrices for the aluminium plates component modes are computed, so that the uncertainty is quantified at a component-modal level. Then, for each MC sample the component-modal uncertainty is propagated into the global modes through the LMP method. Since two independent parameters ξ_i are used for describing the uncertainty in each component, 8 LMP perturbation propagations are performed at each MC sample. By virtue of the modal quantification of the uncertainty, the total MC analysis time is reduced to just 76.4 seconds. This is a much more efficient method (an order of magnitude) than the CMP method.

Next, the uncertainty analysis results are presented and the accuracy of the CMP and LMP methods are evaluated by comparison to the exact solution.

6.4.1 Component modes uncertainty

First, the uncertainty in the component modes is assessed by comparing the component eigenvalue statistics for the three Monte Carlo simulations. Recall that the exact component modes are computed at each MC iteration in the MCB uncertainty analysis by solving the state-EVP of the perturbed component. On the contrary, in the CMP uncertainty analysis these are obtained through damped mode perturbation approximation (c.f. equation 5.6). In turn, in the LMP uncertainty analysis the component eigenvalue perturbations are obtained by sampling the component modal covariance matrix.

Figure 6.5 shows the resulting coefficient of variation[2] for each of the 25 fixed-interface component modes of the first component (i.e. the left-most outer damped aluminium plate). The damped modal frequency CVs and the modal damping ratio CVs in percentage units are presented in the left hand plot and right hand plot respectively. Similar plots result for the other three aluminium plates.

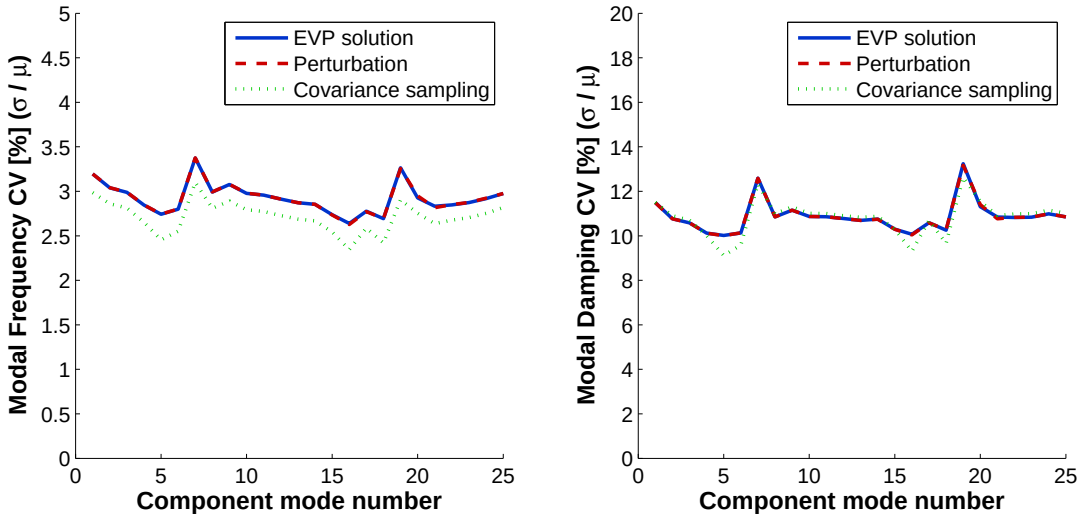

Figure 6.5: Coefficient of variation for the first component eigenvalues.

[2]It must be pointed out that hardly any differences in the mean values for the modal frequencies and modal damping of the component modes have been obtained for the MCB, CMP and LMP results. Therefore, Figure 6.5 merely shows the differences in the variance results, since the coefficient of variation is the standard deviation normalised by the mean value.

The results for the three methods are very close and show basically the same component mode variability characteristics. All component modes show standard deviations around 3% of their damped modal frequency value, and around 11% of their modal damping value.

Notice that these CV values are much smaller than the CV values assumed for the physical parameters (i.e. 20% CV for damping proportionality factor and 10% CV for Young's modulus). Clearly, this is due to the fact that the uncertainty is modelled through random fields, since the physical parameter variation at different elements may average out. It can also be observed that the 8th and 19th component modes show slightly higher variability than the rest of the component modes. This is also a consequence of the use of random field uncertainty modelling since the damping is no longer proportional when a random field perturbation is applied to the damping/stiffness matrices, and this may have a higher effect in certain modes due to uneven damping distribution.

For the MCB and CMP analyses, the uncertainty has been modelled at a component physical level. Furthermore, the same quantification has been used for the MC samples. Therefore, any difference in the component mode uncertainty estimation is due to the approximation error in the modal perturbation propagation. Yet, it can be observed that the exact CV results and the perturbation results practically match each other for both modal frequencies and modal damping, which indicates that the damped modal perturbation approximation has very good accuracy for such levels of uncertainty.

For the LMP analysis, the MC samples are generated by independent modal covariance sampling. This explains the slightly biased results for the component eigenvalues CVs. Nevertheless, this bias is a result of having just 100 Monte Carlo samples. With a much higher number of Monte Carlo iterations the CV results would converge to the exact ones. Furthermore, differences observed in the modal damping CV (such as for the 5th component mode) may diminish by taking more terms in the KL expansion for the modal covariance matrix.

Lastly, although the component eigenvector variability is not explicitly addressed in this section, it is worth to mention that, in the CMP analyses, component eigenvectors perturbations are obtained with very little error with respect to exact perturbations. On the contrary, no eigenvector variability is considered in the LMP case.

6.4.2 Global modes uncertainty

The uncertainty in the full ribbed plate system is evaluated next at a modal level. The 60 first global modes of the system are considered, and their uncertainty is again studied by evaluation of their corresponding eigenvalue coefficient of variation for the MCB, CMP and LMP analyses.

The first 60 modes for the deterministic FE model have been examined previously in Figure 6.4. There, it may be observed that the modal damping does not increase monotonically with respect to modal frequency, which implies that their modal damping values correspond to a general distribution of physical damping. This means that the physical damping has uneven influence in the global modes. Therefore, the uncertainty in the global modes will presumably be unevenly distributed as well.

In Figure 6.6 the global eigenvalue uncertainty is presented in terms of the coefficients of variation for the damped modal frequencies (left) and the modal damping ratios (right). The results shown correspond to the three Monte Carlo simulations through MCB, CMP and LMP reanalyses respectively.

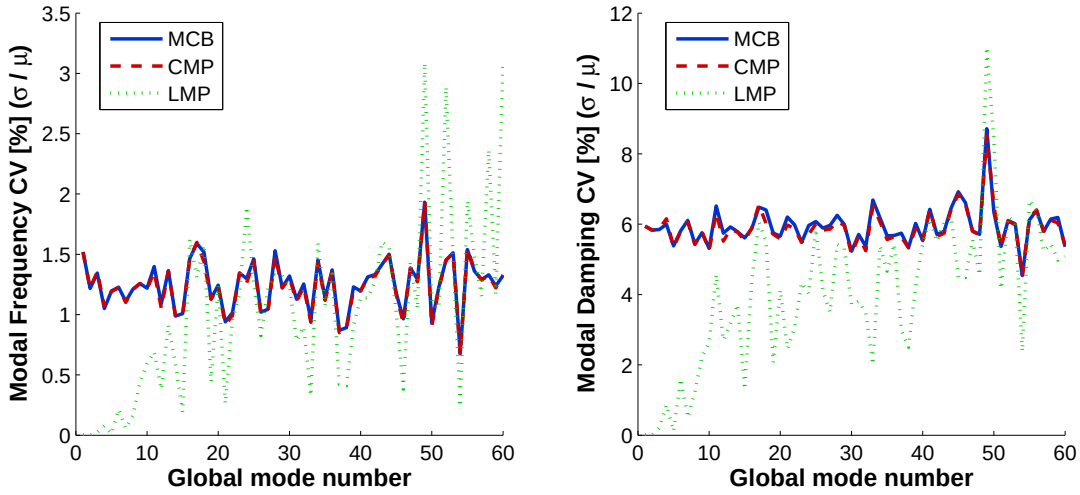

Figure 6.6: Coefficient of variation for the ribbed plate global eigenvalues.

The MCB results (in blue) are considered to be exact solutions. It is readily observable how the global modes present fluctuating values for their variance (i.e. the CV plots are very peaky). Global modes show standard deviations from 0.5% to 2% of their modal frequency values and standard deviations from 4% to 9% of their modal damping values.

CMP results (in red) show very good agreement with the exact results. The coef-

ficients of variation for the modal frequencies are almost coincident with the MCB ones. Slightly larger differences are observed in the modal damping coefficient of variations. These results are in agreement with the perturbation errors observed in the CMP validation example in section 5.3.3, that is, very good accuracy for small perturbations (<20%) with slightly bigger error for modal damping than for modal frequencies.

On the contrary, LMP results (in green) show very poor estimation of the uncertainty in global modes. The estimation variation for the lower 10-15 modes is clearly below the exact values. The LMP estimated CV values tend to zero as the modal frequencies approach zero, meaning that the variability information is lost for the low-frequencies. Conversely, for modes in the mid and high frequencies the LMP results tend to converge to a range of variation for the global modes similar to the exact variation range (i.e. $CV_{f_m} = 0.5\%$ to $CV_{f_m} = 2\%$, and $CV_{\zeta_m} = 4\%$ to $CV_{\zeta_m} = 4\%$). Nevertheless, for each individual mode the CV values for the LMP method show large errors with respect to the exact ones, specially for the modal frequencies.

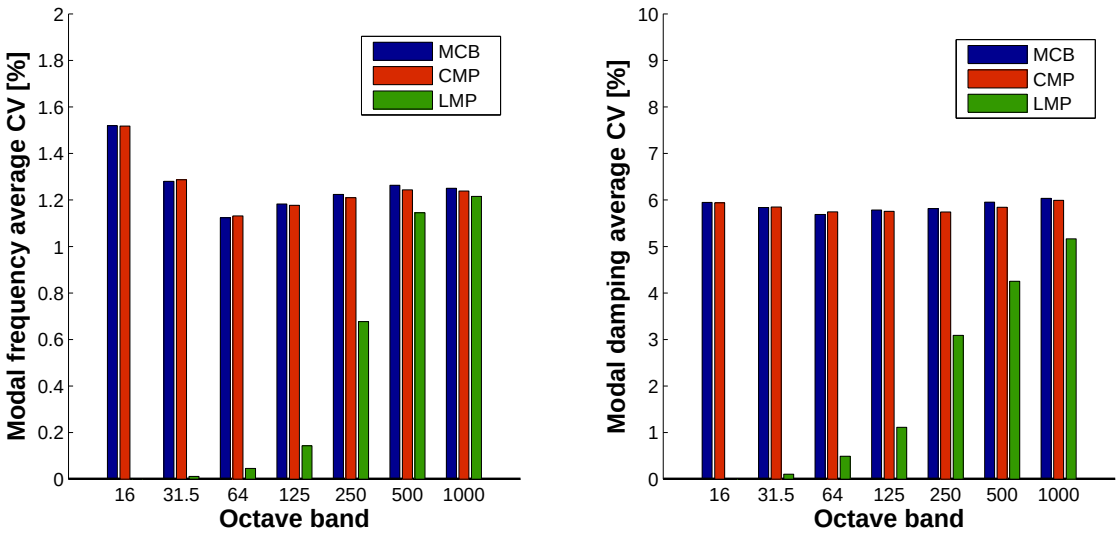

Figure 6.7: Band average coefficient of variation for the ribbed plate global eigenvalues.

The variability in each global mode is not correctly estimated through the LMP method because the uncertainty in component eigenvectors has been ignored. Neglecting the component eigenvector variability has been shown to be the major source of error in perturbation methods on state-space based CMS models. However, if one regards the ensemble eigenvalue variability in frequency band averages (see Figure 6.7), one identifies that the ensemble average CV values for the LMP

method tend to converge to the exact average CV values as frequency increases. In fact, the global modes ensemble variability is fairly well approximated for the 500 Hz and 1 kHz bands due to high number of modes per band. This implies that, in a statistical sense, the LMP method provides valid variability results for these high frequency bands. Moreover, there is high modal overlap in these bands since the system is heavily damped, so that even if the individual mode variability is not accurately resolved, the corresponding frequency response statistical moments will be quite accurate.

It is worth noting that, in this example, there are many coupling interface DOFs between the plates and the ribs. Hence, the constraint modes used in the MCB reduced model highly contribute to the description of the ribbed plate low frequency behaviour. Hence, the CMP method accuracy for the lowest modes changes drastically depending on whether the CMP low-frequency correction is used (c.f. section 5.3.4). The mode variability results shown here correspond to CMP method with low-frequency correction. Otherwise, if a low-frequency correction is not applied, the variance of the lower modes is greatly underestimated, which is what actually happens for the LMP method as can be observed in Figures 6.6 and 6.7.

6.4.3 Forced response uncertainty

Finally, the dynamic response of the uncertain ribbed plate is evaluated when a set of forces is applied to the system. For this purpose, a set of four uncorrelated point input forces are considered, each of them having unit amplitude in Newtons. Then, the power spectral density of the velocity response is computed at a single DOF corresponding to the vertical displacement in node 100 (i.e. the same position in which the input mobility has been computed for the deterministic solution). Figure 6.8 sketches the placement of the four point forces and the point response. The exact location of the point forces and response are resumed in Table 6.4.

	Node	Position (x,y,z) [m]	Degree of freedom
Response	100	(0.191,1.125,0.000)	vertical displacement
Force	463	(0.993,0.000,0.000)	vertical displacement
Force	471	(0.993,0.600,0.000)	vertical displacement
Force	694	(1.490,0.000,0.000)	vertical displacement
Force	702	(1.490,0.600,0.000)	vertical displacement

Table 6.4: Ribbed plate example: Forces and response positions.

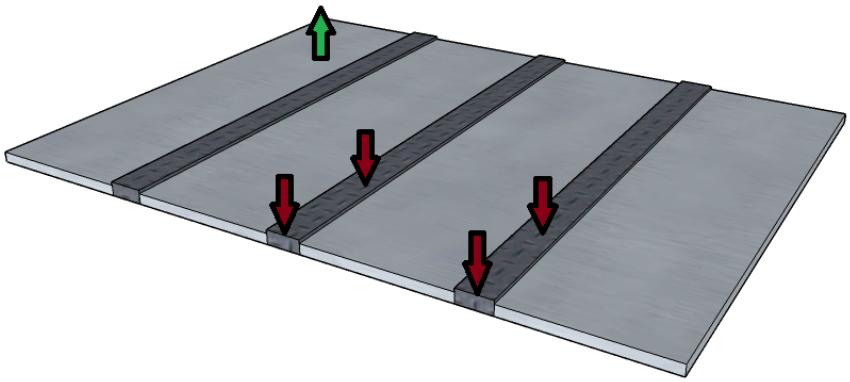

Figure 6.8: Sketch of the point forces and response in the ribbed plate example.

The velocity spectrum at node 100 has been computed for each Monte Carlo sample. Accordingly, the mean as well as the extreme values of the ensemble velocity spectra have been computed at each analysis frequency.

The velocity spectrum for each MC sample together with the mean and extreme estimates are presented in Figures 6.9, 6.10 and 6.11 for the MCB, CMP and LMP methods respectively. Each of the 100 velocity responses (in grey) overlay with each other, creating in this way a grey area which illustrates the range of variation of the response due to the uncertainty in the system. The minimum and maximum curves can therefore be taken as safety margins for design purposes.

For the low-frequency bands, individual modes are recognisable with small variation around them accounting for the uncertainty in modal frequency and modal damping. Mid-frequency bands present a wider variation envelope because the modal variation areas overlap. Moreover, great variability is observed around the mid-frequency spectra antiresonances, which are a consequence of the cancelation of the overlapping modes at the response location. At high frequencies the mid-frequency variability characteristics are exacerbated so that the ensemble resonances and antiresonances add up into a flat mean spectrum and uncertainty envelope.

Comparing Figures 6.9 and 6.10 it can be observed that the mean velocity spectra for the MCB and CMP analyses are almost identical. In turn, very similar envelopes for the uncertain area of variation are obtained. Differences between the two plots are not observed for the low-frequency bands. At mid-frequencies there are some differences in the antiresonance variation which may happen due to small perturbation errors in the the global eigenvectors. In the high frequency band, the CMP analysis provides a wider envelope than the exact one. This may happen due

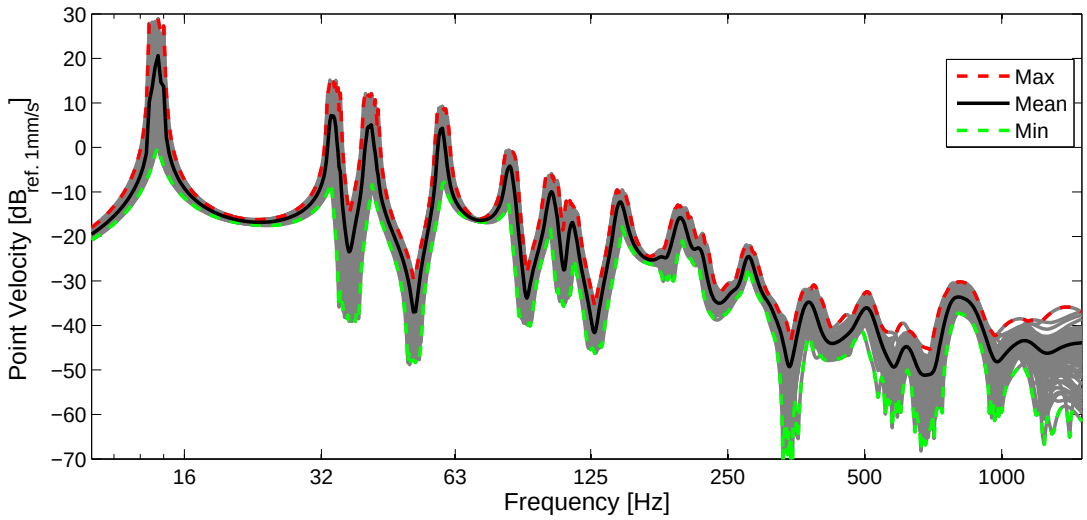

Figure 6.9: Point velocity power spectral density statistics at node 100. Exact solution through CMS reanalysis.

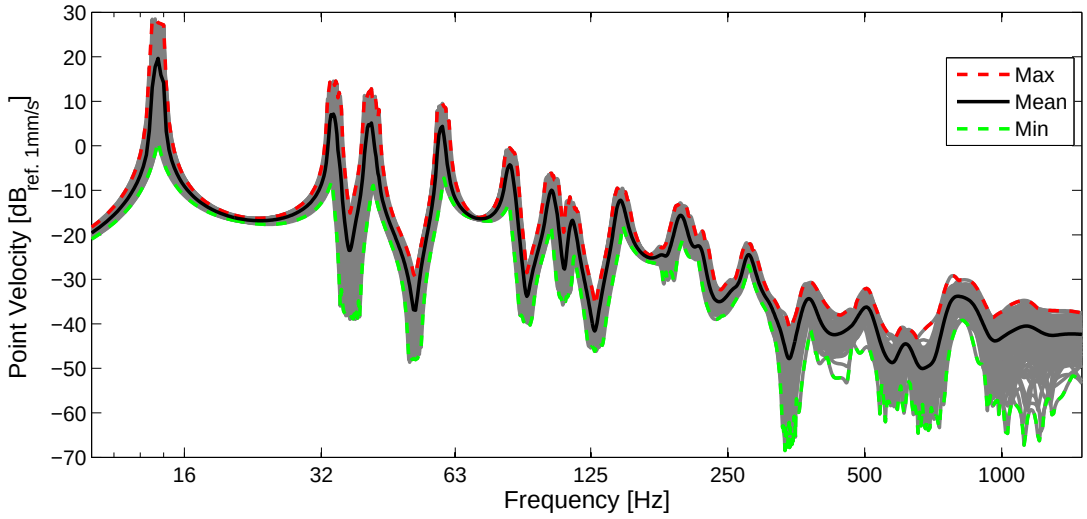

Figure 6.10: Point velocity power spectral density statistics at node 100. Approximate solution through CMP perturbation propagation.

to larger perturbation approximation errors in the CMP estimates as the frequency increases (as happened for the cantilever example in section 5.3.3).

On the contrary, Figure 6.11 shows a very distinct estimation of the velocity response uncertainty. For the low frequency bands almost no variability is observed. Just in the vicinity of the modal resonances a small variation in the peak amplitude is observed, which corresponds to modal damping variability. Accordingly, the LMP mean low-frequency spectrum basically matches that of the deterministic

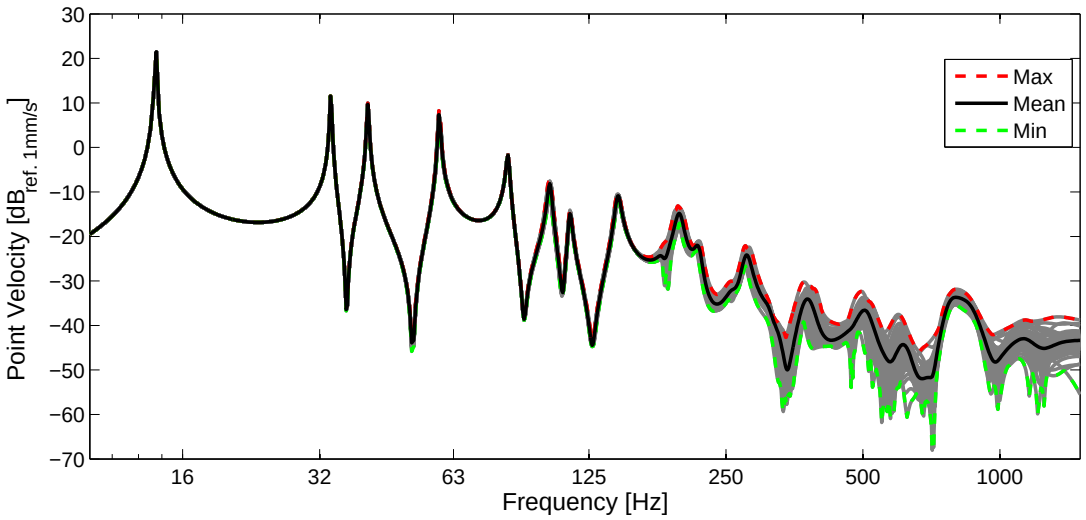

Figure 6.11: Point velocity power spectral density statistics at node 100. Approximate solution through LMP perturbation propagation.

solution. This erroneous estimate for the low-frequency behaviour is in agreement with the underestimation of the low-frequency global mode uncertainty discussed in the previous section, corroborating in this way the inadequacy of the LMP method for low-frequency response uncertainty analysis.

Nevertheless, for higher frequencies of analysis, the LMP method does propagate the system uncertainty into the global modes. It can be observed in Figure 6.11 how for the mid-frequency and the high-frequency bands there is variation in the velocity spectra. For these bands the mean curve matches the exact one, and the variation envelope converges to that of the exact solution as well.

6.5 Conclusions

In this chapter the CMP and the LMP methods have been applied for the uncertainty analysis of the ribbed plate example. The ribbed plate structure has been analysed for a wide frequency range, so that low-frequency, mid-frequency and high-frequency dynamic response behaviours have been covered. Since the benchmark example is locally and heavily damped, the analysis of uncertainty has been conducted on the grounds of a CMS reduction of the finite element model in state-space coordinates, specifically through the MCB method.

The CMS reduction of the ribbed plate model facilitates the modelling of the uncer-

tainty at a component level. In this numerical study, the heavily damped components have been considered to have uncertain damping and stiffness properties. Two alternatives for the modelling of the uncertainty have been used. In first place, the uncertainties in the component physical parameters have been modelled through random fields. Also, a second approach has been proposed in which the component uncertainties are quantified directly on the component modal basis.

In both cases, the component uncertainties are described by means of a large set of correlated uncertain parameters. This represents a challenging scenario with regard to the efficiency for the application of CMS perturbation methods, since an independent perturbation approximation is required for each varying parameter. Yet, the sets of correlated uncertain parameters may be conveniently projected into a much reduced set of independent random variables through the Karhunen-Loève expansion. Thus, the component uncertainties are eventually quantified through a reduced number of uncorrelated KL parameters: six parameters for component-physical uncertainty modelling and just two parameters for the component-modal uncertainty modelling.

A reference uncertainty analysis has been conducted through exact CMS reanalysis of the uncertain components. Then, the same analysis has been conducted through the CMP method with component-physical uncertainty quantification and through the LMP method with component-modal uncertainty quantification.

It has been seen how the CMP method obtains practically equal uncertainty estimates for the dynamic solution of the ribbed plates (i.e. for the damped system modes and the forced frequency response), while half the computation effort with respect to the reference analysis has been required. In this example, the CMP correction for the low-frequency modes has been indispensable for an accurate estimation of the modes variability. Nevertheless, its inclusion supposes a minor increase in the total computation time. In fact, it has also been argued that for larger finite element models the gain in efficiency of the CMP method with respect to CMS reanalysis would be even more substantial. Thus, the CMP method has shown very good performance for all of the analysis frequency range.

On the other hand, LMP reanalysis method has proved to be much more efficient than the CMP method. The overall computation time is reduced by an order of magnitude through the LMP method together with the component-modal uncertainty quantification. However, its application is restricted to the analysis of medium to high frequencies. The low frequency uncertainty is largely underestimated because the physical uncertainty is not propagated through the constraint

modes. Additionally, the uncertainty in individual modes is inadequately estimated because uncertainty in the component eigenvectors is neglected. Nevertheless, at the mid-frequencies and high frequencies, the uncertainty estimates for the ensemble of modes is sufficiently accurate by virtue of a high modal overlap, which produces fair statistical averages for the first and second moments of variation. Accordingly, the LMP method can be used as a fast estimation method of the uncertainty at mid/high frequencies.

Chapter 7

Conclusions

7.1 Conclusions

This thesis concerned the efficient numerical analysis of vibrations of heavily damped dynamic systems. In the development of mechanical structures repeated vibration analyses of numerical models are required for their robust design, be it for adjusting the model to the actual system response measurements, for optimising the system performance, or estimating the inherent response variability due to system uncertainty. In most of the cases the vibration analyses are conducted on finite element models, and their numerical solution supposes a very high computational cost, specially for increasing frequencies of analysis. In particular, heavily damped dynamics may be correctly estimated through state-space modal analysis. However, the state-space formulation introduces additional difficulties to the numerical solution computation since the number of equations of motion to solve is doubled, and due to the corresponding matrices not being positive-definite. Therefore, the high computational cost for the numerical solution is exacerbated for the analysis of heavily damped systems. In this work various approximate methods for reducing the cost of repeated vibration analysis of generally damped systems have been proposed.

Although the solution of the state-space equations of motion presents some numerical challenges, it has been demonstrated that the corresponding eigenvalue problem may be solved using an appropriate eigenvalue algorithm. Even for large finite element models, the damped complex modes of vibration are properly estimated through the Symmetric Indefinite Lanczos Method algorithm. Accordingly,

approximate modal solution methods for the state-space equations of motion have been derived given that an initial (state-space) damped modal solution is available.

First, linear approximations for the damped modal solutions have been considered because the modal parameters of generally damped system show smooth variations with respect to physical parameters variations (as opposed to frequency responses).

The modal perturbation approximation and the modal interpolation approximation for damped modes have been explored. For heavily damped systems, perturbation and interpolation methods for damped modes show much improved accuracy in comparison to analogous methods based on undamped eigensolutions and classical small damping approximation. Yet, their range of applicability is restricted to small variations in the physical parameters of the system due to non-linear variation of the modal parameters.

The computational cost for the linear approximations depends on two main factors. On one hand it depends linearly on the number of degrees of freedom of the system model. A linear approximation is therefore less costly than the eigensolution computation which depends quadratically on the number of degrees of freedom. On the other hand, the computation cost grows with the number of varying physical parameters. Therefore the perturbation and interpolation methods are significantly advantageous just when only a few parameters vary.

Thus, the applicability of the approximate analysis methods is limited in terms of accuracy by the approximately linear range of modal variation, and in terms of efficiency by the number of degrees of freedom and the number of varying physical parameters. Accordingly, their applicability may be improved in three ways, that is, by use of enhanced non-linear approximations, by reduction of the number of degrees of freedom and by reduction of the number of varying parameters.

In this work, these three aspects have been investigated to a greater or lesser extent for state-space models. Non-linear eigenvalue approximation has been proposed through a Rayleigh quotient for damped equations of motion. The reduction of the number of degrees of freedom has been accomplished through the Component Mode Synthesis methods in state-space coordinates. The reduction of the number of varying parameters has been addressed in the uncertainty analysis case example through the Karhunen-Loève expansion for random fields.

There is certain trade-off between how accurate and how efficient an approximation method can be. For example, non-linear approximations may improve the accuracy in the approximation but they also increase the approximation computational

cost. Therefore, one shall evaluate how necessary is to enhance the accuracy of the approximation for the analysis purposes and whether the associated increase in computation cost yields benefits. Conversely, it has to be ensured that an efficient approximate method provides sufficient accuracy for the analysis purposes.

For instance, frequency and spatial averaged quantities are regarded in vibration analysis at high frequencies. Since high frequency damped modes largely overlap, average quantities are generally well estimated regardless of the error in individual modes approximations. Consequently, the accuracy requirements for the approximate damped modes may be relaxed at high frequencies. Hence, for high frequency analysis, the linear perturbation an interpolation methods can be applied for larger variation ranges.

It has also been discussed that among the modal parameters mode shape vectors are the ones that show less sensitivity to physical parameters variations. Variation in mode shapes are small and in consequence variation approximation errors are very small with respect to the absolute mode shape values. Moreover, vibration analyses often focus on the spectral position and amplitude of the response resonances, i.e. on the modal frequencies and modal damping. Thus, one may require accurate methods for the estimation of the damped eigenvalues but not necessarily as much accuracy for the damped eigenvectors.

The Rayleigh quotient eigenvalue approximation precisely provides enhanced estimates for the eigenvalues. The application of the proposed Q quotient for damped equations of motion broadens the potential range of variation of the physical parameters that can be analysed with sufficient accuracy. Opposite to the classical Rayleigh quotient, a posteriori error bounds for the Q quotient may not be formulated due to non-positive definiteness of the state-space matrices. Nevertheless, it has been proved numerically that the Q quotient approximation reduces the approximation error by an order of magnitude with respect to the linear approximations, while its computation cost is of the same order as for linearly approximating a single eigenvector. Since the eigenvectors linear approximation cost is much reduced in interpolation methods, the use of the quotient approximation is most efficient in conjunction with interpolated estimates. All together, the quotient approximation allows one to tackle the analysis of gross modifications in the design at a low computational cost while preserving good accuracy in the modal estimates.

In the research of more efficient methods for the analysis of large models, reduction of the state-space equations of motion through Component Mode Synthesis has been investigated. For heavily damped systems, state-space based CMS methods largely

improve the accuracy of the damped modes estimates with respect to conventional CMS methods based on undamped component modes. In turn, the computation cost for the initial state-space solution is greatly reduced. CMS models are not only of reduced order, but they also provide a substructured description of the system. Therefore, they are a suitable framework in which approximate analyses become scalable since variations in each component may be addressed independently, and more efficient because of the model order reduction. Two CMS perturbation methods for the approximate analysis of heavily damped systems have been devised, specifically on models reduced through the Morgan-Craig-Bampton method.

The Component Modal-Propagation (CMP) method approximates the damped modal solution variations by propagating the components perturbations through the component modes. Including a correction for the correct estimation of low-frequency variability, the CMP method provides equivalent accuracy to the perturbation method applied to the full order model. Moreover, it provides a moderate gain in efficiency since only the perturbed components need to be taken into account. The efficiency gain depends on the number and size of the perturbed components. Therefore, its use is very beneficial for analysing small to modest localised variations (e.g. parameter modifications, parameter uncertainty, design optimisation) in large system models. Specifically, damping treatments are usually applied locally. Thus, the CMP method is very well suited for the analysis of dynamic response variation in locally damped systems.

The Local Modal Perturbation (LMP) method defines perturbations at a component-modal level and propagates them into the global system modes. Hence, the CMP method performs the perturbation approximation directly on the reduced CMS model. Consequently, a very notable gain in efficiency is obtained, reaching over an order of magnitude lower computational cost with respect to the full order perturbation method. However, the state-space component eigenvectors variations have proved to be crucial for the correct perturbation propagation in CMS models, and these are not included in the LMP method. Only the eigenvalue perturbations are considered in the damped component modes, and this makes the global modes approximation highly imprecise. Nevertheless, the high efficiency of the LMP method can be exploited for vibration analysis at high frequencies where average estimates are regarded. This has been illustrated in the uncertainty analysis numerical case example. In conclusion, the LMP method is applicable for obtaining computationally cheap estimates of medium to high-frequency dynamics variability of heavily damped systems.

7.2 Future work suggestions

Research at a fundamental level has been undertaken in this thesis based on the viscous modelling of damping, which is the simplest and more conventionally used damping model. The approximate methods proposed here follow from the state-space formulation for generally damped systems, under the assumption that the damping is of the viscous kind. Many times, however, damping materials such as rubbers and polymers show viscoelastic behaviour, which does not correspond to the viscous damping model. The modelling of viscoelastic damping corresponds to a frequency dependent damping matrix which may be linear or not. Therefore, it would be worthwhile to further the research on approximate methods for the analysis of heavily damped systems by taking into account other damping models.

Nevertheless, for a frequency domain vibration analysis viscoelastic damping is typically assumed linear, and a usual approach is to perform independent analyses for limited frequency bands in which the damping matrix is assumed constant. Thus, the approximate methods based on state-space formulation may be used for each of the frequency bands. The use of the proposed methods in a viscoelastic damping scenario could also be a future research line.

In a more applied research, the approximate analysis methods for damped systems that have been developed throughout this work may be used in optimisation and model updating processes. These, together with uncertainty analysis, were processes which have been motivation for their development, in fact. Specifically, one may suspect that a suitable application might be for the optimisation of damping treatment in a design.

Furthermore, the Component Mode Synthesis methods for damped systems might be exploited for the modelling of damped joints and couplings. Perhaps, a hybrid CMS modelling would then be necessary combining simultaneously large components with free interface modes and the joint components with fixed interface modes. The CMS perturbation scheme could then be adapted to this hypothetical hybrid CMS method. Joint uncertainty, updating or optimisation problems might be tackled in this way.

Perturbation methods based on the Craig-Ni method for Component Mode Synthesis have been discarded because residual attachment mode perturbations were not negligible, and the coupled-modal matrices were costly to compute. Yet, an LMP method on Craig-Ni coordinates might be formulated having a similar efficiency to the LMP method in Morgan-Craig-Bampton coordinates. Although it would

not provide good accuracy (presumably) it may be the case that it would be valid for high-frequency average estimates. The use of perturbation methods based on free interface modes may be beneficial whenever the numerical estimates are to be matched with actual measurements.

Finally, the use of the LMP method could be combined with other approximate methods. For instance, use of the CMP method for low to mid frequencies and the LMP method for the high frequencies could be combined in one analysis. Also, the LMP method may be used for the derivation of energy models for heavily damped systems. Since the energy coupling factors are ensemble average quantities, the LMP method may be used for obtaining these at a low computational cost from a nominal FE model containing an uncertainty description. Such energy models would be valid at high frequencies.

Bibliography

[1] M. Petyt, *Introduction to Finite Element Vibration Analysis*. Cambridge University Press, Aug. 2010.

[2] R. C. Aster, B. Borchers, and C. H. Thurber, *Parameter Estimation and Inverse Problems*. Academic Press, 2005.

[3] W. Desmet, B. Pluymbers, and O. Atak, *"Mid-Frequency" CAE Methodologies for Mid-Frequency Analysis in Vibration and Acoustics*. Katholieke Universiteit Leuven, 2012.

[4] W. C. Hurty, "Dynamic analysis of structural systems using component modes," *AIAA Journal*, vol. 3, pp. 678–685, Apr. 1965.

[5] R. R. Craig, Jr. and M. C. C. Bampton, "Coupling of substructures for dynamic analyses.," *AIAA Journal*, vol. 6, pp. 1313–1319, July 1968.

[6] R. L. Goldman, "Vibration analysis by dynamic partitioning.," *AIAA Journal*, vol. 7, pp. 1152–1154, June 1969.

[7] R. Craig and C.-J. Chang, "Free-interface methods of substructure coupling for dynamic analysis," *AIAA Journal*, vol. 14, pp. 1633–1635, Nov. 1976.

[8] J. Craig, "Substructure Methods in Vibration," *Journal of Vibration and Acoustics*, vol. 117, pp. 207–213, June 1995.

[9] T. K. Hasselman and A. Kaplan, "Dynamic Analysis of Large Systems by Complex Mode Synthesis," *Journal of Dynamic Systems, Measurement, and Control*, vol. 96, pp. 327–333, Sept. 1974.

[10] R. R. Craig Jr and Y. Yung-Tseng, "Generalized Substructure Coupling Procedure for Damped Systems," *Aiaa Journal - AIAA J*, vol. 20, no. 3, pp. 442–444, 1982.

[11] L. Wu and R. Greif, "Substructuring and modal synthesis for damped systems," *Journal of Sound and Vibration*, vol. 90, pp. 407–422, Oct. 1983.

[12] K. F. Martin and K. H. Ghlaim, "System Prediction Using Damped Component Modes," *Proceedings of the Institution of Mechanical Engineers, Part C: Journal of Mechanical Engineering Science*, vol. 198, pp. 261–268, Oct. 1984.

[13] R. R. Craig and Z. Ni, "Component mode synthesis for model order reduction of nonclassicallydamped systems," *Journal of Guidance, Control, and Dynamics*, vol. 12, pp. 577–584, July 1989.

[14] J. A. Morgan, C. Pierre, and G. M. Hulbert, "Component Mode Synthesis Methods for Non-proportionally Damped Systems," in *Procedings of IMAC XVII - 17th International Modal Analysis Conference*, pp. 1472–1480, 1999.

[15] J. Morgan and R. Craig, Jr., "Comparison of three Component Mode Synthesis methods for non-proportionally damped systems," in *41st Structures, Structural Dynamics, And Materials Conference And Exhibit*, American Institute of Aeronautics and Astronautics, Apr. 2000.

[16] H. Benaroya and M. Rehak, "Finite Element Methods in Probabilistic Structural Analysis: A Selective Review," *Applied Mechanics Reviews*, vol. 41, pp. 201–213, May 1988.

[17] W. K. Liu, T. Belytschko, and A. Mani, "Random field finite elements," *International Journal for Numerical Methods in Engineering*, vol. 23, no. 10, pp. 1831–1845, 1986.

[18] R. G. Ghanem and P. D. Spanos, *Stochastic Finite Elements: A Spectral Approach*. Courier Dover Publications, 2003.

[19] G. Stefanou, "The stochastic finite element method: Past, present and future," *Computer Methods in Applied Mechanics and Engineering*, vol. 198, pp. 1031–1051, Feb. 2009.

[20] D. Moens and D. Vandepitte, "Recent advances in non-probabilistic approaches for non-deterministic dynamic finite element analysis," *Archives of Computational Methods in Engineering*, vol. 13, pp. 389–464, Sept. 2006.

[21] M. Beer, S. Ferson, and V. Kreinovich, "Imprecise probabilities in engineering analyses," *Mechanical Systems and Signal Processing*, vol. 37, pp. 4–29, May 2013.

[22] A. M. Brown and A. A. Ferri, "Probabilistic component mode synthesis of nondeterministic substructures," *AIAA Journal*, vol. 34, pp. 830–834, Apr. 1996.

[23] B. Mace and P. Shorter, "A local modal/perturbational method for estimating frequency response statistics of built-up structures with uncertain properties," *Journal of Sound and Vibration*, vol. 242, pp. 793–811, May 2001.

[24] L. Hinke, F. Dohnal, B. Mace, T. Waters, and N. Ferguson, "Component mode synthesis as a framework for uncertainty analysis," *Journal of Sound and Vibration*, vol. 324, pp. 161–178, July 2009.

[25] L. Hinke, *Modelling approaches for the low-frequency analysis of built-up structures with non-deterministic properties*. phd, University of Southampton, Apr. 2008.

[26] D. C. Kammer and D. Krattiger, "Propagation of Uncertainty in Substructured Spacecraft Using Frequency Response," *AIAA Journal*, vol. 51, pp. 353–361, Feb. 2013.

[27] J.-M. Mencik, "Model reduction and perturbation analysis of wave finite element formulations for computing the forced response of coupled elastic systems involving junctions with uncertain eigenfrequencies," *Computer Methods in Applied Mechanics and Engineering*, vol. 200, pp. 3051–3065, Oct. 2011.

[28] D. Sarsri, L. Azrar, A. Jebbouri, and A. El Hami, "Component mode synthesis and polynomial chaos expansions for stochastic frequency functions of large linear FE models," *Computers & Structures*, vol. 89, pp. 346–356, Feb. 2011.

[29] O. Giannini and M. Hanss, "The component mode transformation method: A fast implementation of fuzzy arithmetic for uncertainty management in structural dynamics," *Journal of Sound and Vibration*, vol. 311, pp. 1340–1357, Apr. 2008.

[30] H. De Gersem, D. Moens, W. Desmet, and D. Vandepitte, "Interval and fuzzy dynamic analysis of finite element models with superelements," *Computers & Structures*, vol. 85, pp. 304–319, Mar. 2007.

[31] P. B. Nair and A. J. Keane, "Stochastic reduced basis methods," *American Institute Aeronautics and Astronautics Journal*, vol. 40, no. 8, pp. 1653–1664, 2002.

[32] M. Bah, P. Nair, A. Bhaskar, and A. Keane, "Stochastic Component Mode Synthesis," in *44th AIAA Structures, Structural Dynamics, and Materials Confernence*, American Institute of Aeronautics and Astronautics, Apr. 2003.

[33] M. Guedri, N. Bouhaddi, and R. Majed, "Reduction of the stochastic finite element models using a robust dynamic condensation method," *Journal of Sound and Vibration*, vol. 297, pp. 123–145, Oct. 2006.

[34] Q. H. Tran, M. Ouisse, and N. Bouhaddi, "A robust component mode synthesis method for stochastic damped vibroacoustics," *Mechanical Systems and Signal Processing*, vol. 24, pp. 164–181, Jan. 2010.

[35] F. Dohnal, B. R. Mace, and N. S. Ferguson, "Joint Uncertainty Propagation in Linear Structural Dynamics Using Stochastic Reduced Basis Methods," *AIAA Journal*, vol. 47, pp. 961–969, Apr. 2009.

[36] M. I. Friswell, "Candidate Reduced Order Models for Structural Parameter Estimation," *Journal of Vibration and Acoustics*, vol. 112, pp. 93–97, Jan. 1990.

[37] J. Mottershead and M. Friswell, "Model Updating In Structural Dynamics: A Survey," *Journal of Sound and Vibration*, vol. 167, pp. 347–375, Oct. 1993.

[38] M. Friswell and J. Penny, "Updating model parameters from frequency domain data via reduced order models," *Mechanical Systems and Signal Processing*, vol. 4, pp. 377–391, Sept. 1990.

[39] A. A. Huckelbridge and C. Lawrence, "Identification of Structural Interface Characteristics Using Component Mode Synthesis," *Journal of Vibration, Acoustics Stress and Reliability in Design*, vol. 111, pp. 140–147, Apr. 1989.

[40] M. Link, "Updating analytical models by using local and global parameters and relaxed optimisation requirements," *Mechanical Systems and Signal Processing*, vol. 12, pp. 7–22, Jan. 1998.

[41] H. Grafe, *Model updating of large structural dynamics models using measured response functions.* PhD thesis, Imperial College of Science, Technology and Medicine University of London, Oct. 1998.

[42] J. A. Morgan, C. Pierre, and G. M. Hulbert, "Calculation of Component Mode Synthesis Matrices From Measured Frequency Response Functions, Part 1: Theory," *Journal of Vibration and Acoustics*, vol. 120, pp. 503–508, Apr. 1998.

[43] J. A. Morgan, C. Pierre, and G. M. Hulbert, "Calculation of Component Mode Synthesis Matrices From Measured Frequency Response Functions, Part 2: Application," *Journal of Vibration and Acoustics*, vol. 120, pp. 509–516, Apr. 1998.

[44] J. A. Morgan, C. Pierre, and G. M. Hulbert, "Baseband methods of Component Mode Synthesis for non-proportionally damped systems," *Mechanical Systems and Signal Processing*, vol. 17, pp. 589–598, May 2003.

[45] I. Takewaki and K. Uetani, "Inverse component-mode synthesis method for damped large structural systems," *Computers & Structures*, vol. 78, pp. 415–423, Nov. 2000.

[46] J. W. S. Rayleigh, *The Theory of Sound*. New York: Dover Editions, 2 ed., 1945.

[47] J. Woodhouse, "Linear damping models for structural vibration," *Journal of Sound and Vibration*, vol. 215, pp. 547–569, Aug. 1998.

[48] D. J. Ewins, *Modal testing: Theory and practice*. Baldock, England: Research Studies Press, 2000.

[49] S. Crandall, "The role of damping in vibration theory," *Journal of Sound and Vibration*, vol. 11, pp. 3–IN1, Jan. 1970.

[50] S. Adhikari, *Damping Models for Structural Vibrations*. PhD thesis, Cambridge University Engineering Department, Cambridge, UK, Sept. 2000.

[51] F. Tisseur and K. Meerbergen, "The Quadratic Eigenvalue Problem," *SIAM Review*, vol. 43, pp. 235–286, Jan. 2001.

[52] L. Meirovitch, *Fundamentals of vibrations*. Boston: McGraw-Hill, 2001.

[53] J. H. Wilkinson, *The Algebraic Eigenvalue Problem*. Clarendon Press, 1988.

[54] Z. Bai, J. Demmel, J. Dongarra, A. Ruhe, and H. v. d. Vorst, *Templates for the Solution of Algebraic Eigenvalue Problems: A Practical Guide*. Philadelphia, PA: Society for Industrial and Applied Mathematics, 1 edition ed., Jan. 2000.

[55] Y. Saad, *Numerical Methods for Large Eigenvalue Problems*. Classics in Applied Mathematics, Society for Industrial and Applied Mathematics, Jan. 2011.

[56] C. Lanczos, *An iterative method for the solution of the eigenvalue problem of linear differential and integral*. 1950.

[57] J. Gilbert, C. Moler, and R. Schreiber, "Sparse Matrices in MATLAB: Design and Implementation," *SIAM Journal on Matrix Analysis and Applications*, vol. 13, pp. 333–356, Jan. 1992.

[58] C. C. Paige and M. A. Saunders, "LSQR: An Algorithm for Sparse Linear Equations and Sparse Least Squares," *ACM Trans. Math. Softw.*, vol. 8, pp. 43–71, Mar. 1982.

[59] R. Lehoucq and D. Sorensen, "Deflation Techniques for an Implicitly Restarted Arnoldi Iteration," *SIAM Journal on Matrix Analysis and Applications*, vol. 17, pp. 789–821, Oct. 1996.

[60] H. C. Chen and R. L. Taylor, "Solution of eigenproblems for damped structural systems by the Lanczos algorithm," *Computers & Structures*, vol. 30, no. 1-2, pp. 151–161, 1988.

[61] B. N. Parlett and H. C. Chen, "Use of indefinite pencils for computing damped natural modes," *Linear Algebra and Its Applications*, vol. 140, pp. 53–88, 1990.

[62] M. Kim, H. Jung, and I. Lee, "Solution of eigenvalue problems for non-classically damped systems with multiple frequencies," *Journal of Sound and Vibration*, vol. 219, pp. 207–222, Jan. 1999.

[63] K. Yosida, *Functional Analysis*. Springer, Feb. 1995.

[64] T. Kato, "On the Upper and Lower Bounds of Eigenvalues," *Journal of the Physical Society of Japan*, vol. 4, no. 4, pp. 334–339, 1949.

[65] F. L. Bauer and C. T. Fike, "Norms and exclusion theorems.," *Numerische Mathematik*, vol. 2, pp. 137–141, 1960.

[66] W. K. Liu, T. Belytschko, and A. Mani, "Probabilistic finite elements for nonlinear structural dynamics," *Computer Methods in Applied Mechanics and Engineering*, vol. 56, pp. 61–81, May 1986.

[67] A. Bhaskar, S. Sahu, and B. Nakra, "Approximations and reanalysis over a parameter interval for dynamic design," *Journal of Sound and Vibration*, vol. 248, pp. 178–186, Nov. 2001.

[68] A. Bhaskar, "Rayliegh quotient for non-conservative discrete systems," in *RASD 2010 - 10th International Conference on Recent Advances in Structural Dynamics*, 2010.

[69] R. L. Fox and M. P. Kapoor, "Rates of change of eigenvalues and eigenvectors.," *AIAA Journal*, vol. 6, pp. 2426–2429, Dec. 1968.

[70] R. B. Nelson, "Simplified calculation of eigenvector derivatives," *AIAA Journal*, vol. 14, pp. 1201–1205, Sept. 1976.

[71] A. Bhaskar, "Rayleigh's classical sensitivity analysis extended to damped and gyroscopic systems," in *IUTAM-IITD International Einter School on Optimum Dynamic Design using Modal Testing and Structural Dynamic Modification*, Dec. 1997.

[72] S. Adhikari, "Rates of Change of Eigenvalues and Eigenvectors in Damped Dynamic System," *AIAA Journal*, vol. 37, pp. 1452–1458, Nov. 1999.

[73] S. Adhikari, "Derivative of Eigensolutions of Nonviscously Damped Linear Systems," *AIAA Journal*, vol. 40, pp. 2061–2069, Oct. 2002.

[74] S. Adhikari and M. I. Friswell, "The Calculation of Eigensolution derivatives for Nonviscously damped systems using Nelson's method," *AIAA Journal*, vol. 44(8), pp. 1799–1806, 2006.

[75] S. Adhikari and B. Pascual, "Eigenvalues of linear viscoelastic systems," *Journal of Sound and Vibration*, vol. 325, pp. 1000–1011, Sept. 2009.

[76] A. Bhaskar, "Gross modifications in structural dynamics via interpolated modes," in *Proceeding of the 7th International Conference on Recent Advances in Structural Dynamics*, pp. 61–73, Institute of Sound and Vibration Research, University of Southampton, 2000.

[77] N. R. Maddox, "On the Number of Modes Necessary for Accurate Response and Resulting Forces in Dynamic Analyses," *Journal of Applied Mechanics*, vol. 42, pp. 516–517, June 1975.

[78] O. E. Hansteen and K. Bell, "On the accuracy of mode superposition analysis in structural dynamics," *Earthquake Engineering & Structural Dynamics*, vol. 7, no. 5, pp. 405–411, 1979.

[79] R. E. Cornwell, R. R. Craig, and C. P. Johnson, "On the application of the mode-acceleration method to structural engineering problems," *Earthquake Engineering & Structural Dynamics*, vol. 11, no. 5, pp. 679–688, 1983.

[80] R. J. Guyan, "Reduction of stiffness and mass matrices," *AIAA Journal*, vol. 3, pp. 380–380, Feb. 1965.

[81] M. Paz, "Dynamic Condensation," *AIAA Journal*, vol. 22, pp. 724–727, May 1984.

[82] J. C. O'Callahan, "A procedure for an improved reduced system (IRS) model," in *Proceedings of the 6 th International Modal Analysis Conference*, (Las Vegas), pp. 17–21, Jan. 1989.

[83] J. C. O'Callahan, P. Avitabile, and R. Riemer, "System equivalent reduction expansion process (SEREP)," in *Proceedings of the 6 th International Modal Analysis Conference*, (Las Vegas), pp. 29–37, Jan. 1989.

[84] Z. Bai, "Krylov subspace techniques for reduced-order modeling of large-scale dynamical systems," *Applied Numerical Mathematics*, vol. 43, pp. 9–44, Oct. 2002.

[85] G. A. Baker and P. R. Graves-Morris, *Pade Approximants*. Cambridge University Press, Jan. 1996.

[86] Y. Shamash, "Stable reduced-order models using PadÃ©-type approximations," *IEEE Transactions on Automatic Control*, vol. 19, no. 5, pp. 615–616, 1974.

[87] S. Gugercin and A. C. Antoulas, "A Survey of Model Reduction by Balanced Truncation and Some New Results," *International Journal of Control*, vol. 77, no. 8, pp. 748–766, 2004.

[88] L. Meirovitch, *Computational Methods in Structural Dynamics*. Alphen aan den Rijn, The Netherlands ; Rockville, Md., U.S.A: Springer, 1980 edition ed., Oct. 1980.

[89] H. Soriano and F. Filho, "On the modal acceleration method in structural dynamics. Mode truncation and static correction," *Computers & Structures*, vol. 29, no. 5, pp. 777–782, 1988.

[90] R. M. Hintz, "Analytical Methods in Component Modal Synthesis," *AIAA Journal*, vol. 13, pp. 1007–1016, Aug. 1975.

[91] M. P. Castanier, Y.-C. Tan, and C. Pierre, "Characteristic Constraint Modes for Component Mode Synthesis," *AIAA Journal*, vol. 39, no. 6, pp. 1182–1187, 2001.

[92] R. R. Craig, Jr., T. Si, and Z. Ni, "State-variable models of structures having rigid-body modes," *Journal of Guidance, Control, and Dynamics*, vol. 13, no. 6, pp. 1157–1160, 1990.

[93] T. Howsman, T. and R. R. Craig, "A substructure coupling procedure applicable to general linear time-invariant dynamic systems," *25th AIAA Structures, Structural Dynamics, and Materials Confernence*, 1984.

[94] W. Wang and J. Kirkhope, "Component Mode Synthesis For Damped Rotor Systems With Hybrid Interfaces," *Journal of Sound and Vibration*, vol. 177, pp. 393–410, Oct. 1994.

[95] L. Cortes, N. S. Ferguson, and A. Bhaskar, "Uncertainty propagation in complex modes based Component Mode Synthesis," in *RASD 2013 11th International Conference on Recent Advances in Structural Dynamics 1st - 3rd July 2013*, May 2013.

[96] L. Cortes, N. S. Ferguson, and A. Bhaskar, "A perturbation method for locally damped dynamic systems," in *19th International Congress on Sound and Vibration*, July 2012.

[97] L. Cortes, N. S. Ferguson, and A. Bhaskar, "Uncertainty propagation in locally damped dynamic systems," in *ISMA 2012 - Conference on Noise and Vibration Engineering*, Sept. 2012.

[98] H. Bachmann, *Vibration Problems in Structures: Practical Guidelines*. Basel, Switz. ; Boston, Mass: Springer-Verlag, Jan. 1995.

[99] L. Cremer and M. Heckl, *Structure-Borne Sound: Structural Vibrations and Sound Radiation at Audio Frequencies*. Springer Science & Business Media, Mar. 2013.

[100] T. K. Hasselman and G. C. Hart, "Modal Analysis of Random Structural Systems," *Journal of the Engineering Mechanics Division*, vol. 98, pp. 561–579, June 1972.

[101] R. Y. Rubinstein and D. P. Kroese, *Simulation and the Monte Carlo Method*. John Wiley & Sons, Sept. 2011.

[102] G. Temple, "The Theory of Rayleigh's Principle as Applied to Continuous Systems," *Proceedings of the Royal Society of London. Series A*, vol. 119, pp. 276–293, June 1928.

[103] E. M. Harrell, "Generalizations of Temple's Inequality," *Proceedings of The American Mathematical Society*, vol. 69, no. 2, 1978.

[104] R. R. Craig and A. L. Hale, "Block-Krylov component synthesis method for structural model reduction," *Journal of Guidance, Control, and Dynamics*, vol. 11, pp. 562–570, Nov. 1988.

Appendix A

Norms and normalisation of eigenvectors

In modal analysis (c.f. section 2.2), eigenvectors are typically chosen to be normalised with respect to the mass (or $\mathbf{A}$) matrix. In this section, the concept of norm is revisited in order to formalise the way eigenvectors are normalised.

For the undamped case, a so called M-norm is defined. The M-norm is used for the mass normalisation of eigenvectors. For the state-space case, the eigenvectors normalisation is done using an A-normalisation factor, which is not a norm.

Additionally, the norms defined in this section are also of application for the establishment of eigenvalues error bounds. The error bounds are presented in section 2.4.2 and their derivations can be found in appendix B.

A.1 Vector norm

The norm of a vector $\mathbf{v}$ is a functional that gives a real-positive number indicating the size of the vector. The vector norm is therefore positive-definite. The most common norm is the euclidian norm $\|\mathbf{v}\|$, which is defined as the square root of the inner product of a vector with itself.

$$\|\mathbf{v}\| = \langle \mathbf{v}, \mathbf{v} \rangle^{\frac{1}{2}} \tag{A.1}$$

The inner product between any two complex vectors $\mathbf{v}$ and $\mathbf{w}$ is defined as

$$\langle \mathbf{v}, \mathbf{w} \rangle = \mathbf{w}^H \mathbf{v} \tag{A.2}$$

where H stands for the complex conjugate transpose. When the inner product of two distinct vectors $\mathbf{v}$ and $\mathbf{w}$ equals zero, this vectors are said to be orthogonal. If $\mathbf{v}$ and $\mathbf{w}$ are real vectors, then the conjugate transpose operation H simply becomes the vector transpose T, i.e. $\langle \mathbf{v}, \mathbf{w} \rangle = \mathbf{w}^T \mathbf{v}$.

The inner product has three important mathematical properties, namely:

- linearity: $\langle a\mathbf{v}, \mathbf{w} \rangle = a \langle \mathbf{v}, \mathbf{w} \rangle$ and $\langle \mathbf{v}_1 + \mathbf{v}_2, \mathbf{w} \rangle = \langle \mathbf{v}_1, \mathbf{w} \rangle + \langle \mathbf{v}_2, \mathbf{w} \rangle$
- conjugate symmetry: $\langle \mathbf{v}, \mathbf{w} \rangle = \langle \mathbf{w}, \mathbf{v} \rangle^*$, and
- positive-definiteness: $\langle \mathbf{v}, \mathbf{v} \rangle \geq \mathbf{0}$ and $\langle \mathbf{v}, \mathbf{v} \rangle = \mathbf{0} \Rightarrow \mathbf{v} = \mathbf{0}$

On the contrary, the norm of a vector does not hold the linearity property; although it satisfies homogeneity ($\|a\mathbf{v}\| = a \|\mathbf{v}\|$), it does not necessarily satisfy additivity ($\|\mathbf{v} + \mathbf{w}\| = \|\mathbf{v}\| + \|\mathbf{w}\|$).

Nonetheless, the euclidian vector norm fulfils the triangle inequality

$$\|\mathbf{v} + \mathbf{w}\| \leq \|\mathbf{v}\| + \|\mathbf{w}\| \tag{A.3}$$

which is, in turn, a consequence of the Cauchy-Schwarz inequality.

$$|\langle \mathbf{v}, \mathbf{w} \rangle| \leq \|\mathbf{v}\| \, \|\mathbf{w}\| \tag{A.4}$$

A.2 Matrix norm

The notion of vector norms may be extended to matrices. The norm of a matrix $\mathbf{V}$ assigns a real-positive number indicating the size of the matrix. Matrix norms hold all the properties of vector norms. Again, the most common matrix norm is the euclidian norm $\|\mathbf{V}\|$ defined as a matrix norm induced by the euclidian vector norm. The euclidian matrix norm is defined as the maximum ratio of two vector norms, that is

$$\|\mathbf{V}\| = \max_{\mathbf{v} \neq \mathbf{0}} \frac{\|\mathbf{V}\mathbf{v}\|}{\|\mathbf{v}\|} \tag{A.5}$$

with $\mathbf{v}$ the vector that maximises the ratio.

For square matrices, the euclidian matrix norm corresponds to the maximum singular value σ of the matrix, with the singular values of a matrix $\mathbf{V}$ being the square rooted eigenvalues of the matrix $\mathbf{V}^H \mathbf{V}$.

$$\sigma(\mathbf{V}) = \sqrt{\lambda(\mathbf{V}^H \mathbf{V})} \tag{A.6}$$

A fundamental property (sub-multiplicativity) that arises as a consequence of the way the induced matrix norm is defined is that the inequality

$$\|\mathbf{V}\mathbf{v}\| \leq \|\mathbf{V}\| \cdot \|\mathbf{v}\| \tag{A.7}$$

is always fulfilled for any vector $\mathbf{v}$. Analogously, this is also true for the norm of the product of any two square matrices $\mathbf{V}$ and $\mathbf{W}$.

$$\|\mathbf{V}\mathbf{W}\| \leq \|\mathbf{V}\| \cdot \|\mathbf{W}\| \tag{A.8}$$

A.3 Mass normalisation

The undamped eigenvectors are usually considered to be mass normalised. This means that the undamped eigenvectors $\boldsymbol{u}$ are scaled so that the quadratic form $\boldsymbol{u}^T\mathbf{M}\boldsymbol{u}$ equals unity. Here, the mass normalisation is described in terms of the *M-norm*, which is defined next.

First, the M-product is introduced. For two real vectors $\mathbf{v}$ and $\mathbf{w}$ an inner product with respect to the mass matrix $\mathbf{M}$ may be defined.

$$\langle \mathbf{v}, \mathbf{w} \rangle_M = \langle \mathbf{M}\mathbf{v}, \mathbf{w} \rangle = \mathbf{w}^T\mathbf{M}\mathbf{v} \tag{A.9}$$

When the M-product equals zero, the two vectors are said to be orthogonal with respect to the mass matrix. This is the case for the two vectors being eigenvectors of an undamped system with distinct associated eigenvalue.

Then, the M-norm can be defined as the square rooted M-product of a vector with itself, that is

$$\|\mathbf{v}\|_M = \langle \mathbf{v}, \mathbf{v} \rangle_M^{\frac{1}{2}} \tag{A.10}$$

The M-norm may be related to the euclidian norm in the following way. Considering that the mass matrix is tipically a positive-definite real-symmetric matrix, it can be decomposed using the Cholesky decomposition. The Cholesky decomposition decomposes the mass matrix in terms of a lower triangular matrix $\mathbf{L}$, i.e. $\mathbf{M} = \mathbf{L}\mathbf{L}^T$. Hence, the relation between the euclidian and the M-norm may be expressed in the following way

$$\|\mathbf{v}\|_M = \left\langle \mathbf{L}^T\mathbf{v}, \mathbf{L}^T\mathbf{v} \right\rangle^{\frac{1}{2}} = \left\| \mathbf{L}^T\mathbf{v} \right\| \tag{A.11}$$

An eigenvector is said to be mass-normalised when it is scaled by division with its M-norm. Notice that the M-norm in equation A.10 is indeed the square root of

the $\mathbf{v}^T\mathbf{M}\mathbf{v}$ quadratic form. Thence, for any mass-normalised eigenvector $\bar{\boldsymbol{u}}$ it holds that

$$\bar{\boldsymbol{u}}^T\mathbf{M}\bar{\boldsymbol{u}} = \frac{\boldsymbol{u}^T\mathbf{M}\boldsymbol{u}}{\|\boldsymbol{u}\|_M \|\boldsymbol{u}\|_M} = 1 \tag{A.12}$$

A.4 The A-normalisation

In analogy with the undamped eigenvalue problem, the state eigenvectors $\boldsymbol{x}$ resulting from the solution of the state-space eigenvalue problem may be normalised with respect to the $\mathbf{A}$ matrix. This is done so that the modal matrix $\bar{\mathbf{A}}$ equals the identity matrix. An A-normalised state eigenvector $\bar{\boldsymbol{x}}$ is such that $\bar{\boldsymbol{x}}^T\mathbf{A}\bar{\boldsymbol{x}} = 1$.

In this case, however, the A-normalisation presents some mathematical differences with respect to the mass normalisation that do not allow it to be defined in terms of an *A-norm*. Unlike the undamped pencil $(\mathbf{M}, \mathbf{K})$, the state-space pencil $(\mathbf{A}, \mathbf{B})$ is not positive-definite and, therefore, the state eigenvectors are complex valued. Thence, the $\boldsymbol{x}^T\mathbf{A}\boldsymbol{x}$ form is not a quadratic form but a bilinear form.

For any two complex vectors $\mathbf{v}$ and $\mathbf{w}$ a bilinear form B_A with respect to the $\mathbf{A}$ matrix may be defined as

$$B_A(\mathbf{v}, \mathbf{w}) = \mathbf{w}^T\mathbf{A}\mathbf{v} \tag{A.13}$$

Then, a normalisation factor $A(\boldsymbol{x})$ can be defined as the square root of the B_A form of a state eigenvector with itself, i.e.

$$A(\boldsymbol{x}) = B_A^{\frac{1}{2}}(\boldsymbol{x}, \boldsymbol{x}) = \sqrt{\boldsymbol{x}^T\mathbf{A}\boldsymbol{x}} \tag{A.14}$$

A state eigenvector is said to be A-normalised when it is scaled by division with its *A-normalisation factor*, so that

$$\bar{\boldsymbol{x}}^T\mathbf{A}\bar{\boldsymbol{x}} = \frac{\boldsymbol{x}^T\mathbf{A}\boldsymbol{x}}{A(\boldsymbol{x})\,A(\boldsymbol{x})} = 1 \tag{A.15}$$

Notice that in this case the normalisation factor $A(\boldsymbol{x})$ is not a vector norm. Since the state-vectors are complex valued, the B_A form has the property of linearity, but not conjugate-symmetry nor positive-definiteness. Hence, it does not candidate as an inner product. An A-product analogous to the M-product in equation A.9 would involve the hermitian transpose of the second vector, that is

$$\langle \mathbf{v}, \mathbf{w} \rangle_A = \langle \mathbf{A}\mathbf{v}, \mathbf{w} \rangle = \mathbf{w}^H\mathbf{A}\mathbf{v} \tag{A.16}$$

from which an A-norm might be defined as

$$\|\mathbf{v}\|_A = \langle \mathbf{v}, \mathbf{v} \rangle_A^{\frac{1}{2}} \tag{A.17}$$

However, the A-norm is of little benefit when applied to state eigenvectors. Due to the fact that the complex conjugate of a state eigenvector is another state eigenvector with distinct eigenvalue, they are orthogonal with respect to B_A. So since the A-norm of a state eigenvector may be expressed as $\|\boldsymbol{x}\|_A = B_A^{\frac{1}{2}}(\boldsymbol{x}, \boldsymbol{x}^*)$, it will always equal zero.

Appendix B

Error bounds for the generalised eigenvalue problem

The computation of the eigensolutions of a system is always subject to a certain degree of error. It is therefore of interest to determine the amount of error present. Error bounds for the eigenvalues can be found in the literature, typically in publications about the computational aspects of the eigenvalue problem, e.g. [53–55]. Most of the time, however, these error bounds are solely formulated for the standard eigenvalue problem of a matrix, and no explicit derivation is given for the generalised eigenvalue problem encountered in structural dynamics.

More general or tighter bounds can be derived depending on the properties of the matrices defining the eigenvalue problem. Three well known error bounds are the Bauer-Fike [65], the Krylov-Weinstein [63], and the Kato-Temple [64] bounds. Here, the formulations of these error bounds are derived for the generalised eigenvalue problem. Specifically, the undamped equations of motion are used for the derivations.

All three error bounds are valid for the undamped eigenvalues whereas only the most general one (the Bauer-Fike bound) is valid for the complex eigenvalues arising from the state-space formulation. This is because the matrix pencils defining the undamped EVP and the state-space EVP have important differences in their mathematical properties.

The undamped pencil ($\mathbf{M}$,$\mathbf{K}$) is a positive (semi)definite pencil, which means that it has positive (or zero) valued eigenvalues. In turn the $\mathbf{M}$ and $\mathbf{K}$ matrices are real, symmetric and positive (semi)definite as well. On the contrary, the state-space

pencil (**A**,**B**) is an indefinite pencil with complex eigenvalues. Although the **A** and **B** matrices are real and symmetric, they are not positive definite (they have in fact positive as well as negative valued eigenvalues). The indefiniteness of **A**, **B** and the (**A**,**B**) pencil makes impossible to define the Krylov-Weinstein and the Kato-Temple eigenvalue bounds for the state-space EVP [54, 61].

B.1 Bauer-Fike

A general bound (Bauer-Fike) for the error in the eigenvalue approximation may be derived in terms of the norm of the residual vector. Consider an approximate solution eigenpair $\tilde{\lambda} - \tilde{\boldsymbol{u}}$ corresponding to an exact eigenpair $\lambda - \boldsymbol{u}$ of a vibration mode. The corresponding residual vector $\mathbf{r}$ reads

$$\mathbf{r} = \left(\mathbf{K} - \tilde{\lambda}\mathbf{M}\right)\tilde{\boldsymbol{u}} \tag{B.1}$$

Equation B.1 can be rewritten to get an expression for the approximate eigenvector as a function of the residual vector.

$$\tilde{\boldsymbol{u}} = \left(\mathbf{K} - \tilde{\lambda}\mathbf{M}\right)^{-1}\mathbf{r} \tag{B.2}$$

Now two identities are introduced. The stiffness matrix $\mathbf{K}$ may be substituted with an equivalent expression making use of the spectral decomposition of the of a matrix $\mathbf{M}^{-1}\mathbf{K}$, whose solutions equal those of the undamped EVP, i.e. $\mathbf{K} = \mathbf{M}\mathbf{U}\boldsymbol{\Lambda}\mathbf{U}^{-1}$, with $\mathbf{U}$ a matrix containing all the eigenvectors and $\boldsymbol{\Lambda}$ a diagonal matrix containing all the eigenvalues. In turn the mass matrix $\mathbf{M}$ may be post-multiplied with the identity $\mathbf{U}\mathbf{U}^{-1} = \mathbf{I}$. This gives

$$\tilde{\boldsymbol{u}} = \left(\mathbf{M}\mathbf{U}\boldsymbol{\Lambda}\mathbf{U}^{-1} - \tilde{\lambda}\mathbf{M}\mathbf{U}\mathbf{U}^{-1}\right)^{-1}\mathbf{r} \tag{B.3}$$

and, with some algebraic rearrangement

$$\tilde{\boldsymbol{u}} = \mathbf{U}\left(\boldsymbol{\Lambda} - \tilde{\lambda}\mathbf{I}\right)^{-1}\mathbf{U}^{-1}\mathbf{M}^{-1}\mathbf{r} \tag{B.4}$$

Notice that in Equation B.4 a diagonal matrix $\left(\boldsymbol{\Lambda} - \tilde{\lambda}\mathbf{I}\right)$ appears, which contains in its i'th diagonal elements the difference between the exact eigenvalues λ_i and the approximate eigenvalue $\tilde{\lambda}$ corresponding to one of the exact eigenvalues λ. Hence, the bound for the eigenvalue error $\lambda - \tilde{\lambda}$ may be estimated from equation B.4.

Taking the euclidian norm on both sides of equation B.4 and applying the sub-multiplicative property of matrix norms one obtains the following inequality

$$\|\tilde{\boldsymbol{u}}\| \leq \|\mathbf{U}\| \left\|\mathbf{U}^{-1}\right\| \left\|(\boldsymbol{\Lambda} - \tilde{\lambda}\mathbf{I})^{-1}\right\| \left\|\mathbf{M}^{-1}\right\| \|\mathbf{r}\| \tag{B.5}$$

where the norm of the $(\mathbf{\Lambda}-\tilde{\lambda}\mathbf{I})^{-1}$ diagonal matrix is is the maximum of the absolute values of its diagonal entries, i.e.

$$\left\|(\mathbf{\Lambda}-\tilde{\lambda}\mathbf{I})^{-1}\right\| = \max_i\left(\left|\lambda_i-\tilde{\lambda}\right|^{-1}\right) = \left|\lambda-\tilde{\lambda}\right|^{-1} \tag{B.6}$$

which is in fact the inverse of the smallest absolute error, that is, the $\lambda-\tilde{\lambda}$ error we are looking to determine. Notice as well that the norms product $\|\mathbf{U}\|\|\mathbf{U}^{-1}\|$ is by definition the condition number of matrix $\mathbf{U}$. Therefore, solving the inequality in equation B.5 for the term $\left|\lambda-\tilde{\lambda}\right|$ encountered in equation B.6 one reaches the definition of the Bauer-Fike bound for the generalised eigenvalue problem.

$$\left|\lambda-\tilde{\lambda}\right| \leq \mathrm{Cond}(\mathbf{U})\left\|\mathbf{M}^{-1}\right\|\frac{\|\mathbf{r}\|}{\|\tilde{\boldsymbol{u}}\|} \tag{B.7}$$

B.2 Krylov-Weinstein

From the Bauer-Fike bound, a narrower and more practical bound can be derived given that the system matrices fulfil some properties.

Since the mass matrix is real-symmetric and positive definite it can be decomposed using the Cholesky decomposition, i.e. $\mathbf{M}=\mathbf{L}\mathbf{L}^T$, with $\mathbf{L}$ a lower-triangular real matrix. Pre-multiplying both sides in equation B.4 with $\mathbf{L}^T$ and introducing the notation $\mathbf{V}=\mathbf{L}^T\mathbf{U}$, an equivalent equation is obtained.

$$\mathbf{L}^T\tilde{\boldsymbol{u}} = \mathbf{V}\left(\mathbf{\Lambda}-\tilde{\lambda}\mathbf{I}\right)^{-1}\mathbf{V}^{-1}\mathbf{L}^{-1}\mathbf{r} \tag{B.8}$$

Again, if the euclidian norm is taken on both sides of equation B.8 the following inequality arises

$$\|\tilde{\boldsymbol{u}}\|_M \leq \|\mathbf{V}\|\left\|\mathbf{V}^{-1}\right\|\left\|(\mathbf{\Lambda}-\tilde{\lambda}\mathbf{I})^{-1}\right\|\|\mathbf{r}\|_{M^{-1}} \tag{B.9}$$

where the M-norm of the approximate eigenvalue $\|\tilde{\boldsymbol{u}}\|_M = \left\|\mathbf{L}^T\tilde{\boldsymbol{u}}\right\|$ (c.f. section A.3), and the analogous M-inverse norm of the residual vector $\|\mathbf{r}\|_{M^{-1}} = \|\mathbf{L}^{-1}\boldsymbol{r}\|$ have been introduced. A modified version of the Bauer-Fike bound follows.

$$\left|\lambda-\tilde{\lambda}\right| \leq \mathrm{Cond}(\mathbf{V})\frac{\|\mathbf{r}\|_{M^{-1}}}{\|\tilde{\boldsymbol{u}}\|_M} \tag{B.10}$$

Equation B.10 may be further simplified by assuming that the eigenvectors in $\mathbf{U}$ and $\tilde{\boldsymbol{u}}$ are mass normalised. In such case, $\|\tilde{\boldsymbol{u}}\|_M = 1$ by definition of the M-norm, and $\mathrm{Cond}(\mathbf{V})=1$ because the $\mathbf{V}$ matrix becomes an orthogonal matrix (i.e. $\mathbf{V}^T\mathbf{V}=\mathbf{U}^T\mathbf{L}\mathbf{L}^T\mathbf{U}=\mathbf{U}^T\mathbf{M}\mathbf{U}=\mathbf{I}$). Hence, the eigenvalue error bound simplifies to

$$\left|\lambda-\tilde{\lambda}\right| \leq \|\mathbf{r}\|_{M^{-1}} \tag{B.11}$$

which is the generalised Krylov-Weinstein error bound for the eigenvalues of the (**M**,**K**) pencil. This error bound is much more useful than the Bauer-Fike bound since it does not depend on the full set of exact eigenvectors **U** which in general is not computable.

For large systems, however, the computation of the inverse of the mass matrix in the M-inverse norm might be very computationally expensive. If that cost is unbearable a more relaxed bound may be utilised instead. An upper bound for the M-inverse norm is given by the inequality

$$\|\mathbf{r}\|_{M^{-1}} \leq \lambda_{\min}(\mathbf{M}) \|\mathbf{r}\| \tag{B.12}$$

so that a less exact error bound can be obtained at the expense of computing the lowest eigenvalue of matrix **M**, i.e.

$$\left|\lambda - \tilde{\lambda}\right| \leq \lambda_{\min}(\mathbf{M}) \|\mathbf{r}\| \tag{B.13}$$

so that computing the inverse of the mass matrix is avoided.

B.3 Kato-Temple

A tighter error bound in terms of the residual vector norm may be defined following the Kato-Temple theorem. The Kato-Temple bound only holds when the approximate eigenvalues are computed using the Rayleigh Quotient (c.f. section 3.4.1), i.e. $\tilde{\lambda} = R(\tilde{\boldsymbol{u}})$. Here, this bound is derived for the generalised eigenvalue problem.

The Kato-Temple error bound originates from Temple's inequality [102]. Consider an interval (α, β) that contains the approximate eigenvalue $\tilde{\lambda} = R(\tilde{\boldsymbol{u}})$ but it does not contain any exact eigenvalue λ. Then, it holds that

$$\|\mathbf{r}\|^2_{M^{-1}} \leq \left(\tilde{\lambda} - \alpha\right)\left(\beta - \tilde{\lambda}\right) \tag{B.14}$$

which is the generalisation of Temple's inequality to the (**M**,**K**) EVP, assuming $\tilde{\boldsymbol{u}}$ is mass normalised (This is proved in the following section B.4).

Then, Kato [64] extended Temple's inequality showing that it does still hold when the closest exact eigenvalue λ is contained in the (α, β) interval (see [103] for proof). Hence, for the extreme case $\lambda = \alpha$ we have

$$0 \leq \tilde{\lambda} - \lambda \leq \frac{\|\mathbf{r}\|^2_{M^{-1}}}{\beta - \tilde{\lambda}} \tag{B.15}$$

and, conversely, for the case $\beta = \lambda$

$$0 \leq \lambda - \tilde{\lambda} \leq \frac{\|\mathbf{r}\|^2_{M^{-1}}}{\tilde{\lambda} - \alpha} \tag{B.16}$$

Thus, for any position of the exact eigenvalue λ inside the interval it can be assured that

$$\frac{\|\mathbf{r}\|^2_{M^{-1}}}{\alpha - \tilde{\lambda}} \leq \tilde{\lambda} - \lambda \leq \frac{\|\mathbf{r}\|^2_{M^{-1}}}{\beta - \tilde{\lambda}} \tag{B.17}$$

The Kato-Temple error bound is finally obtained by considering the interval to be centered at $\tilde{\lambda}$. In this way, if a distance d is defined so that $\alpha = \tilde{\lambda} - d$ and $\beta = \tilde{\lambda} + d$, then the eigenvalue error bound reads

$$\left|\tilde{\lambda} - \lambda\right| \leq \frac{\|\mathbf{r}\|^2_{M^{-1}}}{d} \tag{B.18}$$

where distance d can be as large as the distance form $\tilde{\lambda}$ to the next closer eigenvalue (not counting with λ). Therefore, when the spacing between eigenvalues is wide enough, Kato-Temple gives a much narrower bound than the Krylov-Weinstein one.

B.4 Generalisation of Temple's inequality

The Temple's inequality presented in equation B.14 is derived here for the generalised eigenvalue problem encountered for undamped vibrating systems. This is done on the grounds that the residual vector $\mathbf{r}$ is orthogonal to the approximate eigenvector $\tilde{\boldsymbol{u}}$ when the Rayleigh Quotient is used for eigenvalue approximation, i.e. $\tilde{\lambda} = R(\tilde{\boldsymbol{u}})$.

First, recall the interval (α, β) containing $\tilde{\lambda}$ but none of the exact eigenvalues. Let $\mathbf{r}_\alpha$ and $\mathbf{r}_\beta$ be two residual vectors with α and β eigenvalue respectively. They can be expressed in terms of $\mathbf{r}$ and $\tilde{\lambda}$ as shown in equations B.19 and B.20.

$$\mathbf{r}_\alpha = (\mathbf{K} - \alpha\mathbf{M})\,\tilde{\boldsymbol{u}} = \mathbf{r} + \left(\tilde{\lambda} - \alpha\right)\mathbf{M}\tilde{\boldsymbol{u}} \tag{B.19}$$

$$\mathbf{r}_\beta = (\mathbf{K} - \beta\mathbf{M})\,\tilde{\boldsymbol{u}} = \mathbf{r} + \left(\tilde{\lambda} - \beta\right)\mathbf{M}\tilde{\boldsymbol{u}} \tag{B.20}$$

Then, the M-inverse product of the two residual vectors, i.e. $\langle \mathbf{r}_\alpha, \mathbf{r}_\beta \rangle_{M^{-1}} = \mathbf{r}_\beta^T \mathbf{M}^{-1} \mathbf{r}_\alpha$, may be expanded as follows.

$$\begin{aligned} \langle \mathbf{r}_\alpha, \mathbf{r}_\beta \rangle_{M^{-1}} &= \left\langle \mathbf{r} + \left(\tilde{\lambda} - \alpha\right)\mathbf{M}\tilde{\boldsymbol{u}}\,,\, \mathbf{r} + \left(\tilde{\lambda} - \beta\right)\mathbf{M}\tilde{\boldsymbol{u}} \right\rangle_{M^{-1}} \\ &= \|\mathbf{r}\|^2_{M^{-1}} + \left(2\tilde{\lambda} - \alpha - \beta\right)\langle \mathbf{r}, \tilde{\boldsymbol{u}} \rangle + \left(\tilde{\lambda} - \alpha\right)\left(\tilde{\lambda} - \beta\right)\|\tilde{\boldsymbol{u}}\|^2_M \\ &= \|\mathbf{r}\|^2_{M^{-1}} + \left(\tilde{\lambda} - \alpha\right)\left(\tilde{\lambda} - \beta\right) \end{aligned} \tag{B.21}$$

Notice that here the product $\langle \mathbf{r}, \tilde{\boldsymbol{u}} \rangle = 0$ because Rayleigh Quotient is assumed for eigenvalue approximation. Temple's inequality is achieved by verifying that the product in equation B.21 is positive, that is

$$\|\mathbf{r}\|^2_{M^{-1}} + \left(\tilde{\lambda} - \alpha\right)\left(\tilde{\lambda} - \beta\right) \geq 0 \tag{B.22}$$

This can be proved by using the spectral theorem. The approximate eigenvector can be expanded as a weighted sum of the exact eigenvectors $\boldsymbol{u}_m$, i.e.

$$\tilde{\boldsymbol{u}} = \sum_m c_m \boldsymbol{u}_m \tag{B.23}$$

Accordingly, the $\mathbf{r}_\alpha$ and $\mathbf{r}_\beta$ vectors can be also expanded in terms of the exact eigensolutions.

$$\begin{aligned} \boldsymbol{r}_\alpha &= (\mathbf{K} - \alpha\mathbf{M}) \sum_m c_m \boldsymbol{u}_m = \sum_m c_m \left(\mathbf{K} - \alpha\mathbf{M}\right) \boldsymbol{u}_m \\ &= \sum_m c_m \left(\mathbf{K} - \lambda_m\mathbf{M}\right) \boldsymbol{u}_m + \left(\lambda_m - \alpha\right) \mathbf{M}\boldsymbol{u}_m \\ &= \sum_m c_m \left(\lambda_m - \alpha\right) \mathbf{M}\boldsymbol{u}_m \end{aligned} \tag{B.24}$$

Using the last expression in equation B.24, the $\langle \mathbf{r}_\alpha, \mathbf{r}_\beta \rangle_{M^{-1}}$ product may be expanded as

$$\begin{aligned} \langle \mathbf{r}_\alpha, \mathbf{r}_\beta \rangle_{M^{-1}} &= \left\langle \sum_i c_i \left(\lambda_i - \alpha\right) \mathbf{M}\boldsymbol{u}_i, \sum_j c_j \left(\lambda_j - \beta\right) \mathbf{M}\boldsymbol{u}_j \right\rangle_{M^{-1}} \\ &= \sum_i \sum_j c_i c_j \left(\lambda_i - \alpha\right)\left(\lambda_j - \beta\right) \langle \boldsymbol{u}_i, \boldsymbol{u}_j \rangle_M \\ &= \sum_m |c_m|^2 \left(\lambda_m - \alpha\right)\left(\lambda_m - \beta\right) \end{aligned} \tag{B.25}$$

Given that it has been assumed that no exact eigenvalue belongs to the (α, β) interval, then either $(\lambda_m - \alpha)$ and $(\lambda_m - \beta)$ are both positive, or they are both negative. Therefore, in equation B.25 all terms in the sum are positive valued. This result corroborates with the statement in equation B.22, thus Temple's inequality is as expressed in equation B.14.

Appendix C

Modal parameters variation in a single degree of freedom system

The dynamics of a vibrating systems are typically analysed through modal analysis, where the system vibration is described in terms of vibration modes. The vibration modes are linearly independent one another and, consequently, they behave analogously to a single degree of freedom (SDOF) oscillator.

A SDOF system is defined by its mass m, stiffness k and damping constant c (see figure C.1). If a SDOF system is undamped, i.e. $c = 0$, its free (non-forced) vibration does not decay, and is characterised by the natural resonance frequency ω_n. On the contrary, a damped SDOF shows a decaying free vibration characterised by the damped resonance frequency ω_d and the decay rate damping ratio ζ.

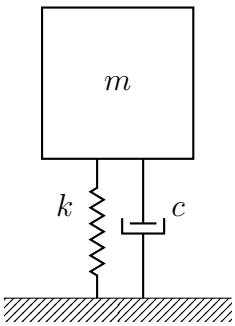

Figure C.1: A damped single degree of freedom system.

In this appendix, the rates of change of ω_n, ω_d and ζ with respect to m, k and c are analysed for a SDOF system. For a generic vibrating system, the analogous modal parameters (i.e. modal frequencies and modal damping) will show similar rates

of change with respect to physical parameters (i.e. mass, stiffness and damping). Therefore, by analysing the SDOF system, a qualitative notion of the rate of change of modal parameters can be extracted. This information is used in chapter 3 when determining the convenience of modal approximate reanalysis methods.

C.1 Variation in natural resonance frequency

For an undamped SDOF system with stiffness k and mass m the natural resonance frequency is found as

$$\omega_n = \sqrt{\frac{k}{m}} \tag{C.1}$$

This means that the natural resonance frequency is proportional to the square root of the stiffness, and inversely proportional to the square root of the mass. Thence, undamped modal frequencies of a generic vibrating system will show the same proportionality relation with respect to mass and stiffness.

In other words, variations in stiffness may be related linearly to variations in squared modal frequencies, that is, to variation in undamped eigenvalues since for the undamped EVP $\lambda_m = \omega_m^2$. Conversely, undamped eigenvalues vary according to a function of the kind of $f(x) = x^{-1}$ with respect to mass variations.

In order to qualitatively illustrate the rate of change of undamped frequencies and eigenvalues with respect to mass and stiffness, consider a variable $x = \frac{k}{m}$ and some arbitrary scaling constants a, b, c and d. The modal frequencies shall vary following a $ax^{\frac{1}{2}}$ function for stiffness variations and following a $bx^{-\frac{1}{2}}$ function for mass variations. Analogously, the undamped eigenvalues vary according to functions cx and dx^{-1} for stiffness and mass variations respectively.

In figure C.2 the shape of functions x, x^{-1}, $x^{\frac{1}{2}}$, and $x^{-\frac{1}{2}}$ are shown for $x \in [0, 10]$. Notice that all four functions present very smooth variation for $x > 1$. Inverse functions are particulary flat after the knee-point at $x = 1$. Therefore, variations in the $x > 1$ range induce much smaller $f(x)$ variations when the mass varies (x^{-1} and $x^{-\frac{1}{2}}$ curves) than when the stiffness vaires (x and $x^{\frac{1}{2}}$ curves).

In fact, a value of $x = 1$ would correspond to a $f_n = \frac{1}{2\pi} \approx 0.16$ Hz resonance frequency. Modal frequencies as low as tenths of Hertz are rarely found in dynamics (perhaps only the first few modes in very large structures such as bridges). In general cases (e.g. cars, airplanes, machinery...), modal frequencies are located above tens of Hertz, which means that the stiffness magnitude is much larger than the mass,

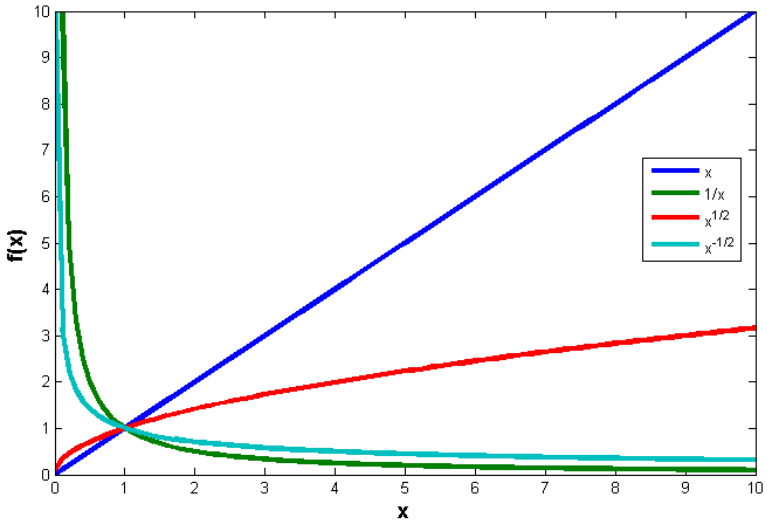

Figure C.2: Function shapes for functions x, x^{-1}, $x^{\frac{1}{2}}$, and $x^{-\frac{1}{2}}$.

i.e. $k > m$. Therefore, $x > 1$ is precisely the range of variation corresponding to modal frequencies in dynamics.

In conclusion, undamped modal frequencies show a non-linear rate of change with respect to mass and stiffness, yet the rate of variation is rather smooth. On the contrary, undamped eigenvalues show a linear rate of change with respect to stiffness variations and a flat quasi-linear rate of change with respect to mass variations. In any case, variations in stiffness imply larger variations in modal frequencies / eigenvalues than mass variations.

C.2 Variation in damping ratio

As for the undamped modes, the variation of the modal parameters for a damped system may be analysed. For a damped SDOF system with mass m, stiffness k and viscous damping constant c, the damping ratio ζ is found as

$$\zeta = \frac{c}{2\sqrt{km}} \tag{C.2}$$

Here, the range of variation of the damping ratio is assumed to be inside the interval $\zeta \in [0, 1]$ since the system would be overdamped (i.e. non-vibrating) otherwise.

From equation C.2 it can be stated that variations in the damping ratio relate linearly to variations in the damping constant. Analogously, modal damping variations will vary at a rate proportional to variations damping constants.

For variations in mass or stiffness consider a variable $x = 4km/c^2$ so that $\zeta = x^{\frac{1}{2}}$. Thence, the damping ratio varies as of $ax^{\frac{1}{2}}$ when mass or stiffness vary. Notice that x is greater than 1 for any underdamped (i.e. $\zeta < 1$) vibrating system. Therefore, the variations will take place in the $x > 1$ region of function $x^{\frac{1}{2}}$ (c.f. figure C.2). These variations will be very small above $x = 5$ (i.e. 20% damping ratio) where the curve becomes almost a horizontal line. On the contrary, mass- or stiffness-induced damping ratio variations will be significant in the $1 < x < 5$ range ((i.e. above 20% damping ratio)).

In conclusion, modal damping varies proportionally to damping constants variations. For high modal damping values the variation of mass or stiffness induces non-linear significant variations in modal damping. Otherwise, modal damping incurs very small quasi-linear variations due to mass or stiffness variations.

C.3 Variation in damped resonance frequency

The damped resonance frequency of a damped SDOF system is found as

$$\omega_d = \omega_n \sqrt{1 - \zeta^2} \tag{C.3}$$

with ω_n the undamped resonance frequency introduced in equation C.1, and ζ the damping ratio introduced in equation C.2. The variations in undamped resonance frequency and damping ratio have been already analysed in the previous section. The overall variation will be a combination of the variation in ω_n and the function $f(\zeta) = \sqrt{1 - \zeta^2}$ which depends on the variation in ζ. Therefore, focus will be taken on the variation of function $f(\zeta)$ initally.

In figure C.3 the shape of function $f(\zeta)$ is illustrated for the damping range $\zeta \in [0, 1]$ corresponding to underdamped vibrating systems. This function is clearly non-linear and it ranges from a maximum value $f(\zeta) = 1$ when the system is undamped ($\zeta = 0$) to a minimum value $f(\zeta) = 0$ when the system is critically damped ($\zeta = 1$). When the system is critically damped it stops resonating, i.e. $\omega_d(\zeta = 1) = 0$.

Function $f(\zeta)$ multiplies with ω_n in equation C.3, which means that the damped resonance frequency is necessarily smaller than the natural resonance frequency, and that the damped natural frequency will be decrease as modal damping increases.

In between the undamped and the critically damped case two regions may be distinguished. One region in which the $f(\zeta)$ function is very flat (below $\zeta = 0.15$), and the complementary region (above $\zeta = 0.15$) where the value of $f(\zeta)$ varies strongly.

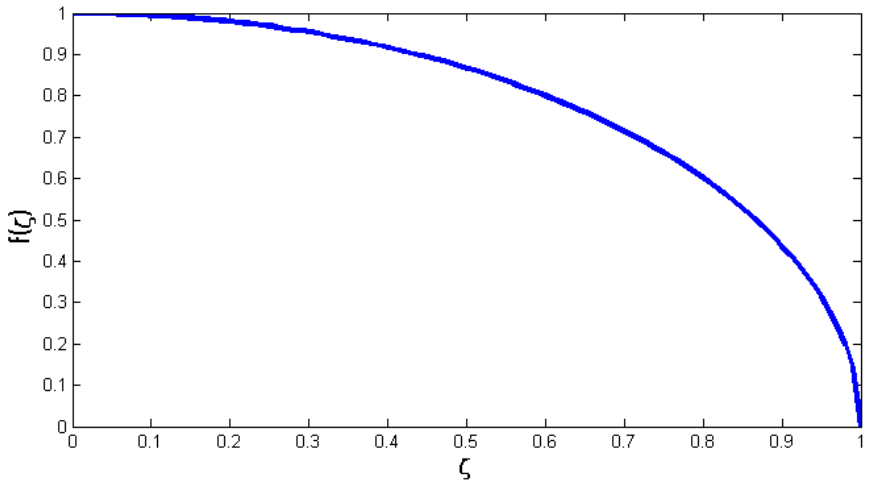

Figure C.3: Shape of function $f(\zeta) = \sqrt{1-\zeta^2}$ for $\zeta \in [0, 1]$.

If the damping lies in the former region the system is said to be lightly damped or having low damping. Otherwise, if the damping lies in the latter region the system is said to be heavily damped or having high damping. Sometimes, the system is said to be moderately damped when damping is in the limit of the two regions (say $0.1 < \zeta < 0.2$).

The division between low and high damping matches with the variation behaviour of the damping ratio with respect to mass and stiffness variations described in the previous section. Hence, the variation in damped modal frequencies is described separately for low or high damping conditions.

For a lightly damped SDOF system, damping variations produce hardly no variation in the damped resonance frequency. This is because the $f(\zeta)$ function is almost constant for low damping condition, and the natural resonance frequency is frequency independent. Mass and stiffness variations induce significant variations in the natural resonance frequency and, consequently, in the damped resonance frequency. If the system is lightly damped the damping ratio incurs hardly no variation due to mass or stiffness variations, let alone the $f(\zeta)$ function. Hence, lightly damped modal frequencies vary in the same way as undamped modal frequencies.

On the contrary, for a heavily damped SDOF system, damping variations do shift the damped resonance frequency significantly, since the $f(\zeta)$ value varies strongly under high damping condition. Increasing the damping notably shifts the resonance frequency downwards and vice-versa. Furthermore, mass and stiffness variations induce damping ratio variations. Thence, both ω_n and $f(\zeta)$ vary strongly when mass or stiffness vary, so that describing the damped resonance frequency variation

is not trivial at all [1].

In conclusion, the rate of change of damped modal frequencies show different characteristic whether the system is lightly or heavily damped. Lightly damped modal frequencies incur smoothly non-linear variations for mass and stiffness variations, and are almost invariant for (low) damping variations. Heavily damped modal frequencies vary in a very non-linear way for variations in any of the dynamic systems parameters: mass, stiffness and damping.

[1] Under high damping condition, increasing stiffness involves higher ω_n, lower ζ, and higher $f(\zeta)$; all in all, a non-linear increase in ω_d. In turn, increasing mass involves lower ω_n, lower ζ, and higher $f(\zeta)$; which means that ω_d may decrease or increase depending on which factor ω_n or $f(\zeta)$ dominates.

Appendix D

Analytical sensitivities

In the perturbation method (c.f. section 3.2), first order partial derivatives of the output quantities $\mathbf{z}(\boldsymbol{\theta})$ with respect to the model parameters $\boldsymbol{\theta}$ are used to derive the perturbation expressions. These derivatives express a first order approximation of the rate of change of the outputs when the parameters vary, and they are referred to as *sensitivity functions* or *sensitivities*. In this appendix, sensitivity functions are derived for the modal approach and the frequency responses approach of the perturbation method.

D.1 Sensitivities for undamped modes

The considered output quantities $\mathbf{z}(\boldsymbol{\theta})$ for the modal approach are the eigenvalues λ_m and eigenvectors $\boldsymbol{\phi}_m$ of the system. For an undamped system the eigenvalues correspond to the squared natural frequencies of the system, i.e. $\lambda_m = \omega_m^2$, and the eigenvectors are real valued, i.e. $\boldsymbol{\phi}_m = \boldsymbol{u}_m$.

Analytical expressions for the rate of change of eigenvalues and eigenvectors where first derived by Fox and Kapoor [69]. In their work linear and second order sensitivities are derived for the undamped eigenvalues and eigenvectors, being the linear expression the one that has found the wider use. The sensitivities for eigenvalues and eigenvectors are obtained from the partial derivative of the undamped EVP set of equations with respect to a model parameter θ.

$$\frac{\partial}{\partial \theta}\left[\left(-\lambda_m \mathbf{M} + \mathbf{K}\right)\boldsymbol{u}_m\right] = 0 \tag{D.1}$$

Rearranging terms and with the use of orthogonality properties of the eigenvectors the linear sensitivities for the m'th system mode can be derived. Thence, the m'th eigenvalue sensitivity function $S_{\lambda_m}(\theta) = \frac{\partial \lambda_m}{\partial \theta}$ reads

$$\frac{\partial \lambda_m}{\partial \theta} = \alpha_m \boldsymbol{u}_m^T \left[\frac{\partial \mathbf{K}}{\partial \theta} - \lambda_m \frac{\partial \mathbf{M}}{\partial \theta} \right] \boldsymbol{u}_m \tag{D.2}$$

and the m'th eigenvector sensitivity function $S_{\phi_m}(\theta) = \frac{\partial \boldsymbol{u}_m}{\partial \theta}$ is

$$\frac{\partial \boldsymbol{u}_m}{\partial \theta} = -\frac{\alpha_m}{2} \left(\boldsymbol{u}_m^T \frac{\partial \mathbf{M}}{\partial \theta} \boldsymbol{u}_m \right) \boldsymbol{u}_m - \sum_{i \neq m} \alpha_i \frac{\boldsymbol{u}_i^T \left[\frac{\partial \mathbf{K}}{\partial \theta} - \lambda_m \frac{\partial \mathbf{M}}{\partial \theta} \right] \boldsymbol{u}_m}{\lambda_i - \lambda_m} \boldsymbol{u}_i \tag{D.3}$$

with

$$\alpha_m = \left(\boldsymbol{u}_m^T \mathbf{M} \boldsymbol{u}_m \right)^{-1} \tag{D.4}$$

If the eigenvectors are mass-normalised the α_m factor in equations D.2 and D.3 equals the unity and, therefore, it may be dropped. This expressions are derived under the assumption that the system modes have no multiplicity, i.e. non repeated eigenvalues. For eigenvalues with multiplicity Nelson's method [70] can be used instead.

D.2 Sensitivities for damped modes

If the system is non-classically damped the sensitivity functions for the eigenvalues and eigenvectors must be obtained in an alternative way. For a damped system the eigenvalues are complex valued, i.e. $\lambda_m = -\sigma_m \pm i\omega_{d,m}$, with real and imaginary parts corresponding to modal damping and modal frequency respectively. The damped system eigenvectors $\boldsymbol{\phi}_m$ are complex valued as well.

Similarly to the undamped case, the eigenvalues and eigenvector sensitivities of viscously damped systems may be obtained form the partial differentiation of the state-space EVP with respect to θ.

$$\frac{\partial}{\partial \theta} \left[(\lambda_m \mathbf{A} - \mathbf{B}) \, \boldsymbol{x}_m \right] = 0 \tag{D.5}$$

This was first proposed by Bhaskar [71] for the eigenvalues sensitivities of viscously damped systems, and later Adhikari [72] used the same idea for deriving the eigenvectors sensitivities. Equation D.5 is analogous to D.1 and therefore similar

sensitivity equations to those of Fox and Kapoor are obtained in state-space form. For the eigenvalues, the $S_{\lambda_m}(\theta)$ function reads

$$\frac{\partial \lambda_m}{\partial \theta} = \beta_m \boldsymbol{x}_m^T \left[\frac{\partial \mathbf{B}}{\partial \theta} - \lambda_m \frac{\partial \mathbf{A}}{\partial \theta} \right] \boldsymbol{x}_m \tag{D.6}$$

In [71] however, the sensitivity function for damped eigenvalues is conveniently reformulated so that the expression avoids quantities in state-space form, i.e.

$$\frac{\partial \lambda_m}{\partial \theta} = -\beta_m \boldsymbol{\phi}_m^T \left[\lambda_m^2 \frac{\partial \mathbf{M}}{\partial \theta} + \lambda_m \frac{\partial \mathbf{C}}{\partial \theta} + \frac{\partial \mathbf{K}}{\partial \theta} \right] \boldsymbol{\phi}_m \tag{D.7}$$

with

$$\beta_m = \left(\boldsymbol{x}_m^T \mathbf{A} \boldsymbol{x}_m \right)^{-1} = \left(\boldsymbol{\phi}_m^T \left[2\lambda_m \mathbf{M} + \mathbf{C} \right] \boldsymbol{\phi}_m \right)^{-1} \tag{D.8}$$

Here, the β_m factor is equal to the unity if the state-eigenvectors $\boldsymbol{x}_m$ are $\mathbf{A}$-normalised. The sensitivity function for the state-eigenvectors is analogous the one in equation D.3, that is

$$\frac{\partial \boldsymbol{x}_m}{\partial \theta} = -\frac{\beta_m}{2} \left(\boldsymbol{x}_m^T \frac{\partial \mathbf{A}}{\partial \theta} \boldsymbol{x}_m \right) \boldsymbol{x}_m - \sum_{i \neq m} \beta_i \frac{\boldsymbol{x}_i^T \left[\frac{\partial \mathbf{B}}{\partial \theta} - \lambda_m \frac{\partial \mathbf{A}}{\partial \theta} \right] \boldsymbol{x}_m}{\lambda_i - \lambda_m} \boldsymbol{x}_i \tag{D.9}$$

Reformulating this expression conveniently, the $S_{\phi_m}(\theta)$ function is obtained for the baseline eigenvectors of viscously damped systems.

$$\frac{\partial \boldsymbol{\phi}_m}{\partial \theta} = -\frac{\beta_m}{2} \left(\phi_m^T \left[2\lambda_m \frac{\partial \boldsymbol{M}}{\partial \theta} + \frac{\partial \boldsymbol{C}}{\partial \theta} \right] \phi_m \right) \phi_m + \sum_{i \neq m} \beta_i \frac{\boldsymbol{\phi}_i^T \left[\lambda_m^2 \frac{\partial \boldsymbol{M}}{\partial \theta} + \lambda_m \frac{\partial \boldsymbol{C}}{\partial \theta} + \frac{\partial \boldsymbol{K}}{\partial \theta} \right] \boldsymbol{\phi}_m}{\lambda_i - \lambda_m} \boldsymbol{\phi}_i \tag{D.10}$$

D.3 Sensitivities for frequency responses

In the frequency responses approach, the considered output quantities $\mathbf{z}(\boldsymbol{\theta})$ to be perturbed are the frequency response functions $H_{ij}(\omega)$ and the displacement frequency responses $u_i(\omega)$ of the system.

Analytical expressions for the rate of change of frequency response functions and displacement responses can be found based on the rate of change of the dynamic stiffness matrix $\mathbf{D}(\omega)$. The dynamic stiffness matrix for viscously damped systems is

$$\mathbf{D}(\omega) = \left[-\omega^2 \mathbf{M} + i\omega \mathbf{C} + \mathbf{K} \right] \tag{D.11}$$

In case the system is undamped the $\mathbf{C}(\omega)$ matrix equals zero, so that the $\mathbf{D}(\omega)$ matrix does not contain the complex term $i\omega\mathbf{C}$. The expression for the rate of change of the dynamic stiffness matrix is obtained straightforwardly bt partial derivation with respect to the varying parameter θ.

$$\frac{\partial \mathbf{D}(\omega)}{\partial \theta} = \left[-\omega^2 \frac{\partial \mathbf{M}}{\partial \theta} + i\omega \frac{\partial \mathbf{C}}{\partial \theta} + \frac{\partial \mathbf{K}}{\partial \theta} \right] \tag{D.12}$$

Now, the FRF matrix may be expressed mathematically as the inverse of the dynamic stiffness matrix, i.e. $\mathbf{H}(\omega) = [\mathbf{D}(\omega)]^{-1}$. Therefore, the matrix $\mathbf{S}_{\mathbf{H}}(\theta)$ consisting of the sensitivity functions for the FRFs is obtained as the partial derivative of an inverse matrix.

$$\frac{\partial \mathbf{H}}{\partial \theta} = \frac{\partial \mathbf{D}^{-1}}{\partial \theta} = -\mathbf{D}^{-1} \frac{\partial \mathbf{D}}{\partial \theta} \mathbf{D}^{-1} = -\mathbf{H} \frac{\partial \mathbf{D}}{\partial \theta} \mathbf{H} \tag{D.13}$$

Here, the frequency dependency has been dropped for clarity. The sensitivity function $\mathbf{S}_{\mathbf{u}}(\theta)$ for the displacement frequency responses $\mathbf{u}(\omega)$ follows straightforwardly

$$\frac{\partial \mathbf{u}}{\partial \theta} = \frac{\partial \left(\mathbf{H}\mathbf{f} \right)}{\partial \theta} = \frac{\partial \mathbf{H}}{\partial \theta} \mathbf{f} = -\mathbf{H} \frac{\partial \mathbf{D}}{\partial \theta} \mathbf{u} \tag{D.14}$$

where use of definition of FRFs has been made, i.e. $\mathbf{u} = \mathbf{H}\mathbf{f}$.

Appendix E

Properties of the Rayleigh quotient

The Rayleigh quotient is an important quantity in modal analysis since it is often used in the methods that solve the equations of motion of the system in order to find its modes of vibration. In this work, however, the main interest is in its use as a modes approximant. The classical Rayleigh quotient has been defined for undamped systems in section 3.4.1 as

$$R(\boldsymbol{u}) = R(\boldsymbol{u}; \mathbf{M}, \mathbf{K}) = \frac{\boldsymbol{u}^T \mathbf{K} \boldsymbol{u}}{\boldsymbol{u}^T \mathbf{M} \boldsymbol{u}} \tag{E.1}$$

In this appendix the relevant properties that have been shortly outlined in section 3.4.1 are demonstrated.

E.1 Stationarity of the Rayleigh quotient

The Rayleigh quotient is *stationary* for any trial vector $\boldsymbol{u}$ in the neighbourhood of an eigenvector $\boldsymbol{u}_m$. This means that the rate of change of the Rayleigh quotient is zero at the system eigenvectors.

$$\delta R(\boldsymbol{u})_{|\boldsymbol{u}=\boldsymbol{u}_m} = 0 \tag{E.2}$$

This is demonstrated in the following. The set of undamped eigenvectors $\mathbf{U}$ form an orthogonal basis for the vector space $\mathcal{V}$. Therefore, using the expansion theorem, any shape vector $\boldsymbol{u} \in \mathcal{V}$ may be expressed as a weighted superposition of the undamped eigenvectors $\boldsymbol{u}_m$

$$\boldsymbol{u} = \sum_m c_m \boldsymbol{u}_m = \mathbf{U}\mathbf{c} \tag{E.3}$$

with $\mathbf{c}$ a vector containing the eigenvectors weights c_m. Introducing equation E.3 into the Rayleigh quotient definition (equation 3.31), the Rayleigh quotient is re-written as a function of the eigenvalues and modal weights.

$$R(\boldsymbol{u}) = \frac{\mathbf{c}^T\mathbf{U}^T\mathbf{K}\mathbf{U}\mathbf{c}}{\mathbf{c}^T\mathbf{U}^T\mathbf{M}\mathbf{U}\mathbf{c}} = \frac{\mathbf{c}^T\boldsymbol{\Omega}^2\mathbf{c}}{\mathbf{c}^T\mathbf{I}\mathbf{c}} = \frac{\sum_m c_m^2\omega_m^2}{\sum_m c_m^2} \tag{E.4}$$

Now, if the trial vector $\boldsymbol{u}$ is close to the r'th eigenvector $\boldsymbol{u}_r$, the r'th weight c_r is much larger than any other weight, since $\boldsymbol{u}_r$ is the major contributor to $\boldsymbol{u}$. A normalized weight ϵ_m can be defined with respect to c_r

$$\epsilon_m = \left|\frac{c_m}{c_r}\right| \tag{E.5}$$

so that ϵ_m is a small number for all modes other than the r'th mode, that is $\epsilon_r = 1$, and $\epsilon_m \ll 1$ for $m \neq r$. Dividing the numerator and denominator in equation E.4 by c_r^2 we get an expression of the Rayleigh quotient in terms of the normalised weights.

$$R(\boldsymbol{u}) = \frac{\omega_r^2 + \sum_{m\neq r}\epsilon_m^2\omega_m^2}{1 + \sum_{m\neq r}\epsilon_m^2} = \omega_r^2(1 + \mathcal{O}(\epsilon^2)) \tag{E.6}$$

Equation E.6 proves the stationarity of the Rayleigh quotient. It shows that for a trial vector $\boldsymbol{u}$ that differs from an eigenvector $\boldsymbol{u}_r$ by a small quantity ϵ, the Rayleigh quotient $R(\boldsymbol{u})$ differs from the corresponding eigenvalue ω_r^2 by small quantity of the order of ϵ^2.

E.2 Optimality of the Rayleigh quotient

It has been stated in section 2.4.2 that the eigenvalue approximation error is bounded by the M-inverse norm of the residual vector. Hence, consider the residual vector corresponding to any trial eigenvalue–eigenvector pair $\alpha - \boldsymbol{u}$.

$$\mathbf{r} = (\mathbf{K} - \alpha\mathbf{M})\,\boldsymbol{u} \tag{E.7}$$

The question now is, which is the value of α that minimizes $\|\mathbf{r}\|_{M^{-1}}$ and, thus, gives the optimal eigenvalue approximation. The answer will be the Rayleigh quotient. By expanding the squared M-inverse norm of the residual vector as a function of α

$$\|\mathbf{r}\|_{M^{-1}}^2 = \alpha^2\boldsymbol{u}^T\mathbf{M}\boldsymbol{u} - 2\alpha\boldsymbol{u}^T\mathbf{K}\boldsymbol{u} + \boldsymbol{u}^T\mathbf{K}\mathbf{M}^{-1}\mathbf{K}\boldsymbol{u} = f(\alpha) \tag{E.8}$$

one can find the zeros of its derivative with respect to α

$$f'(\alpha) = 2\alpha\boldsymbol{u}^T\mathbf{M}\boldsymbol{u} - 2\boldsymbol{u}^T\mathbf{K}\boldsymbol{u} = 0 \tag{E.9}$$

and since its second derivative is positive valued, i.e.

$$f''(\alpha) = 2\boldsymbol{u}^T\mathbf{M}\boldsymbol{u} = 2\left\|\boldsymbol{u}\right\|_M^2 > 0 \tag{E.10}$$

one can conclude from equation E.9 that the minimum $\left\|\mathbf{r}\right\|_{M^{-1}}$ value is achieved for $\alpha = R(\boldsymbol{u})$. This completes the prove.

E.3 Orthogonality and the Temple's inequality

Expanding the inner product of the residual to the trial eigenvector as

$$\langle \mathbf{r}, \boldsymbol{u}\rangle = \langle \mathbf{K}\boldsymbol{u} - \alpha\mathbf{M}\boldsymbol{u}, \boldsymbol{u}\rangle = \langle \mathbf{K}\boldsymbol{u}, \boldsymbol{u}\rangle - \alpha\langle \mathbf{M}\boldsymbol{u}, \boldsymbol{u}\rangle \tag{E.11}$$

and regarding that the Rayleigh quotient can be expressed alternatively as the quotient of two inner products, that is

$$R(\boldsymbol{u}) = \frac{\langle \mathbf{K}\boldsymbol{u}, \boldsymbol{u}\rangle}{\langle \mathbf{M}\boldsymbol{u}, \boldsymbol{u}\rangle} \tag{E.12}$$

it is apparent that when $\alpha = R(\boldsymbol{u})$ the residual vector and the trial eigenvector are orthogonal with respect to the euclidian inner-product.

$$\langle \mathbf{r}, \boldsymbol{u}\rangle = 0 \tag{E.13}$$

The orthogonality property implies that for two residual vectors $\mathbf{r}_a$ and $\mathbf{r}_b$ with trial eigenvalues a and b respectively it holds that

$$\langle \mathbf{r}_a, \mathbf{r}_b\rangle_{M^{-1}} = \mathbf{r}_b^T\mathbf{M}^{-1}\mathbf{r}_a = \left\|\mathbf{r}\right\|_{M^{-1}}^2 + \left(R(\boldsymbol{u}) - a\right)\left(R(\boldsymbol{u}) - b\right) \tag{E.14}$$

with $\mathbf{r}$ the residual vector with the Rayleigh quotient as the trial eigenvalue.

Temple's theorem (c.f. Appendix B.4) states that the expression in equation E.14 can be expanded using the spectral theorem (equation E.3) as

$$\langle \mathbf{r}_a, \mathbf{r}_b\rangle_{M^{-1}} = \sum_m \left|c_m\right|^2 \left(\lambda_m - a\right)\left(\lambda_m - b\right) \tag{E.15}$$

and, therefore, it is positive valued for any interval (a, b) containing $R(\boldsymbol{u})$ but no exact eigenvalue λ_m. This conforms Temple's Inequality, i.e.

$$\left\|\mathbf{r}\right\|_{M^{-1}}^2 \leq \left(R(\boldsymbol{u}) - a\right)\left(b - R(\boldsymbol{u})\right) \tag{E.16}$$

which can be extended to (a, b) containing one exact eigenvalue (Kato [64]). Considering a and b to be equidistant to $R(\boldsymbol{u})$ by a distance d the Kato-Temple error bound is attained.

Appendix F

Component Modes Definitions

In Component Mode Synthesis the system is split into N_κ components that are connected to one or more adjacent components by redundant interfaces. For a component $\kappa \in \{1, N_\kappa\}$ the undamped equations of motion in physical coordinates $\mathbf{u}$ read

$$\mathbf{M}_\kappa \ddot{\mathbf{u}}_\kappa + \mathbf{K}_\kappa \mathbf{u}_\kappa = \mathbf{f}_\kappa \tag{F.1}$$

with $\mathbf{u}_\kappa$ the component's physical degrees of freedom, $\mathbf{M}_\kappa$ and $\mathbf{K}_\kappa$ the component's mass and stiffness matrices respectively, and $\mathbf{f}_\kappa$ the vector of external forces. The physical degrees of freedom consist of the FE-nodes' displacements and rotations in the considered motion dimensions, i.e. x, y, z, θ_x, θ_y and/or θ_z.

In each component the degrees of freedom may be split into two subsets. On one hand, those degrees of freedom corresponding to component nodes located at the coupling interface with other components. On the other hand, those degrees of freedom of the component that do not correspond to the coupling interface nodes. The former are termed *coupling* degrees of freedom $\mathbf{u}_{c,\kappa}$ and the later are termed *interior* degrees of freedom $\mathbf{u}_{i,\kappa}$. The equations of motion may be rearranged according to this nomenclature, that is

$$\begin{bmatrix} \mathbf{M}_{ii} & \mathbf{M}_{ic} \\ \mathbf{M}_{ci} & \mathbf{M}_{cc} \end{bmatrix}_\kappa \begin{Bmatrix} \ddot{\mathbf{u}}_i \\ \ddot{\mathbf{u}}_c \end{Bmatrix}_\kappa + \begin{bmatrix} \mathbf{K}_{ii} & \mathbf{K}_{ic} \\ \mathbf{K}_{ci} & \mathbf{K}_{cc} \end{bmatrix}_\kappa \begin{Bmatrix} \mathbf{u}_i \\ \mathbf{u}_c \end{Bmatrix}_\kappa = \begin{Bmatrix} \mathbf{f}_i \\ \mathbf{f}_c \end{Bmatrix}_\kappa \tag{F.2}$$

This partitioned form in Equation F.2 will be useful in the derivation of component modes.

Component modes are used as a basis for a coordinate transformation from com-

ponent physical coordinates $\mathbf{u}_\kappa$ to component modal coordinates $\mathbf{q}_\kappa$

$$\mathbf{u}_\kappa = \mathbf{T}_\kappa \mathbf{q}_\kappa \tag{F.3}$$

with $\mathbf{T}_\kappa$ the coordinate transformation matrix consisting of the component modes.

There exist several kinds of component modes in CMS. Notice that, while the boundary conditions at the interior component nodes may be known a priori, the boundary conditions at its coupling interface will depend on the motion at the adjacent components. For this reason, the component transformation matrix is typically compound of two subsets of component modes.

$$\mathbf{T}_\kappa = \begin{bmatrix} \mathbf{\Phi}_\kappa & \mathbf{\Psi}_\kappa \end{bmatrix} \tag{F.4}$$

The first subset of modes $\mathbf{\Phi}_\kappa$ describes the free vibration of the component when uncoupled from the rest of the system. Typically, the uncoupled component boundary conditions at the interface nodes are assumed to be either free or fixed condition. *Normal modes* of free vibration are the most common kind of modes to use for describing the component's motion, although other kind of modes - e.g. Krylov Vectors [104] - may be used instead. In the case of assuming free boundaries at the interface rigid body modes might arise, and they must be also included in the transformation matrix.

The second subset of modes $\mathbf{\Psi}_\kappa$ approximate the motion of the component nodes due to a set of prescribed boundary conditions at the coupling interface. These boundary conditions may be displacement and/or force conditions, and they must form a basis able to describe whatever boundary condition that the adjacent components might impose on the component. The most common coupling modes used in CMS are the *constraint modes* and the *attachment modes* which enforce displacement and force boundary conditions respectively, and use static approximation of the components' motion.

Normal modes, constraint modes and attachment modes are the component modes that will be used in this thesis and they will be defined next. For simplicity, the component subindex κ will be omitted for the rest of the section.

F.1 Normal Modes

The component normal modes are the natural modes of vibration of the uncoupled component when no external forces are applied. In other words, normal modes

are specific solutions to the homogeneous equations of motion for given boundary conditions. The boundary conditions at the coupling interface may be chosen to be free motion or fixed interface. These give rise to two types of normal modes, namely *Free-Interface Normal Modes* and *Fixed-Interface Normal Modes*.

The component equations of motion (c.f. Equation F.1) are second order partial differential equations (PDEs) whose solution is known to be of harmonic kind. Hence, the displacement of each component normal mode will have the following form

$$\mathbf{u}(t) = \boldsymbol{\phi} e^{i\omega t} \tag{F.5}$$

with ϕ the mode shape vector and ω the angular frequency. In the CMS context, the term *normal mode* is commonly used to refer directly to the mode shape vector.

Normal modes may arranged in a normal modes matrix that contains as many modes as unconstrained degrees of freedom N_u the component possesses.

$$\boldsymbol{\Phi} = \begin{bmatrix} \boldsymbol{\phi}_1 & \cdots & \boldsymbol{\phi}_j & \cdots & \boldsymbol{\phi}_{N_u} \end{bmatrix} = \begin{bmatrix} \boldsymbol{\Phi}_k & \boldsymbol{\Phi}_h \end{bmatrix} \tag{F.6}$$

However, not all modes contribute to the motion in a certain frequency range of interest. Only a reduced set $\boldsymbol{\Phi}_k$ of the normal modes needs to be *kept* - the ones with lower frequency - while the *higher* order modes set $\boldsymbol{\Phi}_h$ can be discarded. This will lead to the model order reduction when transforming from component physical to component modal coordinates (c.f. Equations F.3 and F.4).

F.1.1 Free-Interface Normal Modes

When the coupling interface is assumed to have free boundary conditions, the homogeneous equations of motion with harmonic solution read

$$(-\omega^2 \mathbf{M} + \mathbf{K})\mathbf{u} = 0 \tag{F.7}$$

Then, the normal modes are found as the solution to the generalized eigenvalue problem

$$\mathbf{K}\boldsymbol{\phi}_j = \lambda_j \mathbf{M}\boldsymbol{\phi}_j \tag{F.8}$$

with $\lambda_j = \omega_j^2$ the eigenvalue and $\boldsymbol{\phi}_j = \boldsymbol{u}_j$ the eigenvector of the jth eigensolution pair. The normal modes are fully described by the $\lambda - \boldsymbol{\phi}$ eigenpairs.

The set of normal modes are an orthogonal basis with respect to the mass and stiffness matrix. This means that the equations of motion can be transformed into

a linear independent set of equations, i.e. normal modes diagonalise the mass and the stiffness matrices.

$$\mathbf{\Phi}^T\mathbf{M}\mathbf{\Phi} = \mathbf{I} \tag{F.9}$$

$$\mathbf{\Phi}^T\mathbf{K}\mathbf{\Phi} = \mathbf{\Lambda} \tag{F.10}$$

Typically, the eigenvalues are normalized so that the modal mass matrix equals the identity matrix $\mathbf{I}$ and, consequently, the modal stiffness matrix equals the diagonal matrix $\mathbf{\Lambda}$ which has the eigenvalues at its diagonal.

F.1.2 Fixed-Interface Normal Modes

When the coupling interface is assumed to have fixed boundary conditions, the solution for the coupling interface degrees of freedom is set to zero

$$\left(-\omega^2\begin{bmatrix}\mathbf{M}_{ii} & \mathbf{M}_{ic}\\ \mathbf{M}_{ci} & \mathbf{M}_{cc}\end{bmatrix} + \begin{bmatrix}\mathbf{K}_{ii} & \mathbf{K}_{ic}\\ \mathbf{K}_{ci} & \mathbf{K}_{cc}\end{bmatrix}\right)\begin{Bmatrix}\mathbf{u}_i\\ \mathbf{0}_c\end{Bmatrix} = \begin{Bmatrix}\mathbf{0}_i\\ \mathbf{f}_c\end{Bmatrix} \tag{F.11}$$

Then, the generalized eigenvalue problem needs be solved only for the interior degrees of freedom of the component

$$\mathbf{K}_{ii}\boldsymbol{\phi}_{i,j} = \lambda_j\mathbf{M}_{ii}\boldsymbol{\phi}_{i,j} \tag{F.12}$$

in order to find the fixed-interface normal modes $\boldsymbol{\phi}_j^F = \begin{Bmatrix}\boldsymbol{\phi}_i\\ \mathbf{0}_c\end{Bmatrix}_j$ with associated eigenvalue $\lambda_j = \omega_j^2$. The eigenvalues are mass normalized as for the free interface case. Notice that the eigenvalues in Equation F.10 are different eigenvalues than the ones for the free-interface normal modes.

F.1.3 Rigid Body Modes

Component rigid body modes can be understood as a special case of free-interface normal modes. It may happen that the uncoupled component is not fully constrained when solving free-interface normal modes. In such case, the component stiffness matrix is singular, so that there will exist solutions with eigenvalue equaling zero, i.e.

$$\mathbf{K}\boldsymbol{\phi}_r = 0 \tag{F.13}$$

These modes describe the rigid-body motion of the component. Rigid body modes $\boldsymbol{\phi}_r$ are often regarded as a separate kind of component modes to the *elastic* free-interface normal modes $\boldsymbol{\phi}_e$ with non zero modal frequency. In any case, the full set

of component normal modes for free-interface boundary conditions is a compound of the rigid and the flexible modes.

$$\mathbf{\Phi} = \begin{bmatrix} \mathbf{\Phi}_r & \mathbf{\Phi}_e \end{bmatrix} \tag{F.14}$$

F.2 Constraint Modes

Constraint modes describe the static deformation of the component when a unit displacement is applied to one coupling degree of freedom while all other coupling degrees of freedom are held fixed. There are as many constraint modes as component coupling degrees of freedom. The set of constraint modes $\mathbf{\Psi}^C$ is computed from the static equations of motion with interface boundary conditions as described above, that is

$$\begin{bmatrix} \mathbf{K}_{ii} & \mathbf{K}_{ic} \\ \mathbf{K}_{ci} & \mathbf{K}_c \end{bmatrix} \begin{bmatrix} \mathbf{\Psi}_{ic}^C \\ \mathbf{I}_{cc} \end{bmatrix} = \begin{bmatrix} \mathbf{0}_{ic} \\ \mathbf{F}_{cc} \end{bmatrix} \tag{F.15}$$

with $\mathbf{I}_{cc}$ the identity matrix describing the displacement boundary conditions for all constraint modes and $\mathbf{\Psi}_{ic}^C$ the corresponding static displacement in the interior degrees of freedom. From the first row of Equation F.15 the constraint modes may be derived.

$$\mathbf{\Psi}_{ic}^C = -\mathbf{K}_{ii}^{-1}\mathbf{K}_{ic} \tag{F.16}$$

$$\mathbf{\Psi}^C = \begin{bmatrix} \mathbf{\Psi}_{ic}^C \\ \mathbf{I}_{cc} \end{bmatrix} \tag{F.17}$$

The set of constraint modes spans all possible displacement boundary conditions that any adjacent component might impose to its interface. In CMS, it is common to use the constraint modes together with fixed-interface normal modes, which is known as the Craig-Bampton method [5].

F.3 Attachment Modes

Attachment modes describe the static deformation of the component when a unit force is applied to one coupling degree of freedom while all other coupling degrees of freedom are force free. As for the constraint modes, there exist as many attachment modes as component coupling degrees of freedom. The set of attachment modes $\mathbf{\Psi}^A$ is computed from the static equations of motion with the described force boundary

conditions at the component interface.

$$\begin{bmatrix} \mathbf{K}_{ii} & \mathbf{K}_{ic} \\ \mathbf{K}_{ci} & \mathbf{K}_{cc} \end{bmatrix} \begin{bmatrix} \mathbf{\Psi}_{ic}^{A} \\ \mathbf{\Psi}_{cc}^{A} \end{bmatrix} = \begin{bmatrix} \mathbf{0}_{ic} \\ \mathbf{I}_{cc} \end{bmatrix} \tag{F.18}$$

For a non-singular stiffness matrix $\mathbf{K}$ the component static-flexibility matrix $\mathbf{G}$ is computed as its inverse, i.e. $\mathbf{G} = \mathbf{K}^{-1}$, so that Equation F.18 may be rearranged as follows

$$\begin{bmatrix} \mathbf{\Psi}_{ic}^{A} \\ \mathbf{\Psi}_{cc}^{A} \end{bmatrix} = \begin{bmatrix} \mathbf{K}_{ii} & \mathbf{K}_{ic} \\ \mathbf{K}_{ci} & \mathbf{K}_{cc} \end{bmatrix}^{-1} \begin{bmatrix} \mathbf{0}_{ic} \\ \mathbf{I}_{cc} \end{bmatrix} = \begin{bmatrix} \mathbf{G}_{ii} & \mathbf{G}_{ic} \\ \mathbf{G}_{ci} & \mathbf{G}_{cc} \end{bmatrix} \begin{bmatrix} \mathbf{0}_{ic} \\ \mathbf{I}_{cc} \end{bmatrix} \tag{F.19}$$

from which the expression for the attachment modes matrix is straightforwardly obtained.

$$\mathbf{\Psi}^{A} = \begin{bmatrix} \mathbf{G}_{ic} \\ \mathbf{G}_{cc} \end{bmatrix} \tag{F.20}$$

The set of attachment modes spans all possible force boundary conditions that any adjacent component might impose to its interface. In CMS it is common to use the attachment modes together with free-interface normal modes.

F.3.1 Residual Attachment Modes

The *residual* attachment modes $\mathbf{\Psi}^{R}$ are attachment modes from which the elastic contribution of the kept normal modes $\mathbf{\Phi}_k$ has been removed. The flexibility matrix may be expressed in modal form by pre and post multiplying the inverse of the stiffness matrix with the identity $\mathbf{\Phi}\mathbf{\Phi}^{-1} = \mathbf{I}$.

$$\mathbf{G} = \mathbf{K}^{-1} = (\mathbf{\Phi}\mathbf{\Phi}^{-1})\mathbf{K}^{-1}(\mathbf{\Phi}\mathbf{\Phi}^{-1})^{T} = \mathbf{\Phi}\mathbf{\Lambda}^{-1}\mathbf{\Phi}^{T} \tag{F.21}$$

Taking into account that the basis of normal modes may be truncated to reduce the order of the component model, the flexibility matrix can be expressed as the sum of the contributions of the kept modes and the higher order modes.

$$\mathbf{G} = \mathbf{\Phi}_k\mathbf{\Lambda}_k^{-1}\mathbf{\Phi}_k^{T} + \mathbf{\Phi}_h\mathbf{\Lambda}_h^{-1}\mathbf{\Phi}_h^{T} \tag{F.22}$$

Then, a residual flexibility matrix $\mathbf{G}^{h}$ can be defined, in which the contribution of the kept normal modes is subtracted.

$$\mathbf{G}^{h} = \mathbf{G} - \mathbf{\Phi}_k\mathbf{\Lambda}_k^{-1}\mathbf{\Phi}_k^{T} \tag{F.23}$$

Residual attachment modes are defined as in Equation F.20 using the residual flexibility matrix $\mathbf{G}^{h}$. These modes are orthogonal to the free-interface kept normal modes $\mathbf{\Phi}_k$.

$$\mathbf{\Psi}^{R} = \begin{bmatrix} \mathbf{G}_{ic}^{h} \\ \mathbf{G}_{cc}^{h} \end{bmatrix} \tag{F.24}$$

F.3.2 Inertia-Relief Attachment Modes

The *inertia-relief* attachment modes are attachment modes from which the contribution of the rigid body modes $\mathbf{\Phi}_r$ has been removed. When a component has rigid body freedom - i.e. it is not fully constraint - Equations F.19 and F.20 cannot be used to find the attachment modes. In such cases the component stiffness matrix will be singular and therefore it can not be inverted. Instead, the flexibility matrix may be computed in an alternative way.

Assuming there are N_r rigid body modes, the component may be *temporarily restrained* at a set r of degrees of freedom to avoid rigid body motion. The stiffness matrix for the remaining *unrestrained* degrees of freedom u can be then inverted. The flexibility matrix is assembled by inserting zeros in the rows and columns for the temporary restrained degrees of freedom.

$$\mathbf{G} = \begin{bmatrix} \mathbf{K}_{uu}^{-1} & \mathbf{0}_{ur} \\ \mathbf{0}_{ru} & \mathbf{0}_{rr} \end{bmatrix} \tag{F.25}$$

The flexibility matrix $\mathbf{G}$ is singular and it has the same rank as the unconstrained stiffness matrix. This means that it describes both the elastic and rigid body behaviour of the component. In [90] the inertia-relief loading matrix $\mathbf{P}$ was introduced to filter out the rigid body characteristic of the flexibility matrix.

$$\mathbf{P} = \mathbf{I} - \mathbf{M}\mathbf{\Phi}_r\mathbf{\Phi}_r^T \tag{F.26}$$

It can be proved that an *elastic* flexibility matrix $\mathbf{G}^e$ may be obtained by pre and post multiplying the flexibility matrix $\mathbf{G}$ with the projector $\mathbf{P}$. The same $\mathbf{G}^e$ matrix is obtained regardless of which degrees of freedom r have been chosen to be temporarily restrained.

$$\mathbf{G}^e = \mathbf{P}^T\mathbf{G}\mathbf{P} \tag{F.27}$$

The inertia-relief attachment modes are defined in the same way as for constraint components with the use of the elastic flexibility matrix. These modes are orthogonal to the rigid body modes $\mathbf{\Phi}_r$.

$$\mathbf{\Psi}^{A,ir} = \begin{bmatrix} \mathbf{G}_{ic}^e \\ \mathbf{G}_{cc}^e \end{bmatrix} \tag{F.28}$$

Residual inertia-relief attachment modes may be obtained in the same way as for the residual attachment modes. These modes are orthogonal to the free-interface kept normal modes including rigid body modes $\mathbf{\Phi}_k = \begin{bmatrix} \mathbf{\Phi}_r & \mathbf{\Phi}_e \end{bmatrix}$.

Appendix G

Derivation of the Component modal-propagation method in physical coordinates

In section 5.3.1, the Component modal-propagation (CMP) perturbation method is derived based on the state-space formulation, giving rise to the following perturbation approximations for the global modes in MCB coupled-modal coordinates

$$\tilde{\Delta}\lambda_m = b^z_{mm} - \lambda_m a^z_{mm} \tag{G.1}$$

$$\tilde{\Delta}\boldsymbol{z}_m = -\frac{1}{2}a^z_{mm}\boldsymbol{z}_m - \sum_{i\neq m}\frac{b^z_{im} - \lambda_m a^z_{im}}{\lambda_i - \lambda_m}\boldsymbol{z}_i \tag{G.2}$$

where the a^z_{im} and b^z_{im} scalar weighting factors correspond to

$$a^z_{im} = \boldsymbol{z}_i^T\tilde{\Delta}\mathbf{A}^z\boldsymbol{z}_m = \boldsymbol{z}_{si}^T\tilde{\Delta}\mathbf{A}^y_{sc}\boldsymbol{x}_{cm} + \boldsymbol{x}_{ci}^T\tilde{\Delta}\mathbf{A}^{y\,T}_{sc}\boldsymbol{z}_{sm} \tag{G.3}$$

$$b^z_{im} = \boldsymbol{z}_i^T\tilde{\Delta}\mathbf{B}^z\boldsymbol{z}_m = \boldsymbol{z}_{si}^T\tilde{\Delta}\mathbf{B}^y_{sc}\boldsymbol{x}_{cm} + \boldsymbol{x}_{ci}^T\tilde{\Delta}\mathbf{B}^{y\,T}_{sc}\boldsymbol{z}_{sm} + \boldsymbol{z}_{si}^T\tilde{\Delta}\mathbf{\Lambda}^F_s\boldsymbol{z}_{sm} \tag{G.4}$$

with $\tilde{\Delta}\mathbf{A}^y_{sc} = \tilde{\Delta}\mathbf{X}^{F\,T}_s\mathbf{A}_s\mathbf{\Upsilon}^C_s$ and $\tilde{\Delta}\mathbf{B}^y_{sc} = \tilde{\Delta}\mathbf{X}^{F\,T}_s\mathbf{B}_s\mathbf{\Upsilon}^C_s$.

In this appendix these expressions are reformulated so that they are expressed in terms of the component matrices in physical coordinates $\mathbf{M}_s$, $\mathbf{C}_s$ and $\mathbf{K}_s$ rather than in terms of the component matrices in state-space coordinates $\mathbf{A}_s$ and $\mathbf{B}_s$.

G.1 Decomposition of matrices $\tilde{\Delta}\mathbf{A}^y_{sc}$ and $\tilde{\Delta}\mathbf{B}^y_{sc}$

The perturbation expression for the MCB component matrices involve the submatrices $\tilde{\Delta}\mathbf{A}^y_{sc}$ and $\tilde{\Delta}\mathbf{B}^y_{sc}$. In the CMP method, these submatrices are a product of

three state-space matrices, i.e.

$$\tilde{\Delta}\mathbf{A}_{sc}^{y} = \tilde{\Delta}\mathbf{X}_{s}^{F^T}\mathbf{A}_{s}\boldsymbol{\Upsilon}_{s}^{C} \tag{G.5}$$

$$\tilde{\Delta}\mathbf{B}_{sc}^{y} = \tilde{\Delta}\mathbf{X}_{s}^{F^T}\mathbf{B}_{s}\boldsymbol{\Upsilon}_{s}^{C} \tag{G.6}$$

which can be expressed in terms of displacement D and velocity V degrees of freedom. The state-component matrices $\mathbf{A}_s$ and $\mathbf{B}_s$ as well as the state-constraint modes matrix $\boldsymbol{\Upsilon}_s^C$ are simple assemblies of the $\mathbf{M}_s$, $\mathbf{C}_s$ and $\mathbf{K}_s$ component matrices and the $\boldsymbol{\Psi}_s^C$ constraint modes matrixrespectively

$$\mathbf{A}_s = \begin{bmatrix} \mathbf{0} & \mathbf{M} \\ \mathbf{M} & \mathbf{C} \end{bmatrix}_s \qquad \mathbf{B}_s = \begin{bmatrix} \mathbf{M} & \mathbf{0} \\ \mathbf{0} & -\mathbf{K} \end{bmatrix}_s \qquad \boldsymbol{\Upsilon}_s^C = \begin{bmatrix} \boldsymbol{\Psi}^C & \mathbf{0} \\ \mathbf{0} & \boldsymbol{\Psi}^C \end{bmatrix}_s \tag{G.7}$$

In turn, the matrix of fixed-interface state-eigenvectors may be written in terms of the fixed-interface mode shape vectors $\boldsymbol{\Phi}^F$ and their corresponding eigenvalues matrix $\boldsymbol{\Lambda}^F$

$$\mathbf{X}_s^F = \begin{bmatrix} \boldsymbol{\Phi}^F\boldsymbol{\Lambda}^F \\ \boldsymbol{\Phi}^F \end{bmatrix}_s \tag{G.8}$$

Hence, the first order perturbation approximation for the state-eigenvectors may be reformulated as

$$\tilde{\Delta}\mathbf{X}_s^F = \begin{bmatrix} \left(\tilde{\Delta}\boldsymbol{\Phi}^F\boldsymbol{\Lambda}^F + \boldsymbol{\Phi}^F\tilde{\Delta}\boldsymbol{\Lambda}^F\right) \\ \tilde{\Delta}\boldsymbol{\Phi}^F \end{bmatrix}_s \equiv \begin{bmatrix} \tilde{\Delta}\dot{\boldsymbol{\Phi}}^F \\ \tilde{\Delta}\boldsymbol{\Phi}^F \end{bmatrix}_s \tag{G.9}$$

where the notation $\tilde{\Delta}\dot{\boldsymbol{\Phi}}^F$ is introduced for the velocity DOFs.

Accordingly, equations G.5 and G.6 can be rewritten in terms of the matrices in physical coordinates, that is

$$\begin{aligned} \tilde{\Delta}\mathbf{A}_{sc}^{y} &= \begin{bmatrix} \tilde{\Delta}\dot{\boldsymbol{\Phi}}^F \\ \tilde{\Delta}\boldsymbol{\Phi}^F \end{bmatrix}_s^T \begin{bmatrix} \mathbf{0} & \mathbf{M} \\ \mathbf{M} & \mathbf{C} \end{bmatrix}_s \begin{bmatrix} \boldsymbol{\Psi}^C & \mathbf{0} \\ \mathbf{0} & \boldsymbol{\Psi}^C \end{bmatrix}_s \\ &= \begin{bmatrix} \tilde{\Delta}\boldsymbol{\Phi}^{F^T}\mathbf{M}\boldsymbol{\Psi}^C & \left(\tilde{\Delta}\dot{\boldsymbol{\Phi}}^{F^T}\mathbf{M}\boldsymbol{\Psi}^C + \tilde{\Delta}\boldsymbol{\Phi}^{F^T}\mathbf{C}\boldsymbol{\Psi}^C\right) \end{bmatrix}_s \end{aligned} \tag{G.10}$$

$$\begin{aligned} \tilde{\Delta}\mathbf{B}_{sc}^{y} &= \begin{bmatrix} \tilde{\Delta}\dot{\boldsymbol{\Phi}}^F \\ \tilde{\Delta}\boldsymbol{\Phi}^F \end{bmatrix}_s^T \begin{bmatrix} \mathbf{M} & \mathbf{0} \\ \mathbf{0} & -\mathbf{K} \end{bmatrix}_s \begin{bmatrix} \boldsymbol{\Psi}^C & \mathbf{0} \\ \mathbf{0} & \boldsymbol{\Psi}^C \end{bmatrix}_s \\ &= \begin{bmatrix} \tilde{\Delta}\dot{\boldsymbol{\Phi}}^{F^T}\mathbf{M}\boldsymbol{\Psi}^C & -\tilde{\Delta}\boldsymbol{\Phi}^{F^T}\mathbf{K}\boldsymbol{\Psi}^C \end{bmatrix}_s \end{aligned} \tag{G.11}$$

G.2 Decomposition of factors a_{im}^z and b_{im}^z

In the Morgan-Craig-Bampton CMS method the coupled-modal coordinates involve the state-space degrees of freedom of the coupling interface. Therefore, the coupling

DOFs of the MCB global eigenvectors $\boldsymbol{x}_{cm}$ – which appear in the a_{im}^z and b_{im}^z expressions – may be split into displacement D and velocity V degrees of freedom, i.e.

$$\boldsymbol{x}_{cm} = \begin{Bmatrix} \boldsymbol{x}_{cm}^V \\ \boldsymbol{x}_{cm}^D \end{Bmatrix} \tag{G.12}$$

Thence, by inserting equations G.10, G.11 and G.12 in equations G.3 and G.4 one finds an alternative expression for a_{im}^z and b_{im}^z in terms of the component matrices in physical coordinates

$$\begin{aligned} a_{im}^z = \boldsymbol{z}_{si}^T \left(\tilde{\Delta} \boldsymbol{\Phi}^{F^T} \mathbf{M} \boldsymbol{\Psi}^C \right) \boldsymbol{x}_{cm}^V + \boldsymbol{z}_{si}^T \left(\tilde{\Delta} \dot{\boldsymbol{\Phi}}^{F^T} \mathbf{M} \boldsymbol{\Psi}^C + \tilde{\Delta} \boldsymbol{\Phi}^{F^T} \mathbf{C} \boldsymbol{\Psi}^C \right) \boldsymbol{x}_{cm}^D \\ + \boldsymbol{x}_{ci}^{V^T} \left(\boldsymbol{\Psi}^{C^T} \mathbf{M} \tilde{\Delta} \boldsymbol{\Phi}^F \right) \boldsymbol{z}_{sm} + \boldsymbol{x}_{ci}^{D^T} \left(\boldsymbol{\Psi}^{C^T} \mathbf{M} \tilde{\Delta} \dot{\boldsymbol{\Phi}}^F + \boldsymbol{\Psi}^{C^T} \mathbf{C} \tilde{\Delta} \boldsymbol{\Phi}^F \right) \boldsymbol{z}_{sm} \end{aligned} \tag{G.13}$$

$$\begin{aligned} b_{im}^z = \boldsymbol{z}_{si}^T \tilde{\Delta} \boldsymbol{\Lambda}_s^F \boldsymbol{z}_{sm} + \boldsymbol{z}_{si}^T \left(\tilde{\Delta} \dot{\boldsymbol{\Phi}}^{F^T} \mathbf{M} \boldsymbol{\Psi}^C \right) \boldsymbol{x}_{cm}^V - \boldsymbol{z}_{si}^T \left(\tilde{\Delta} \boldsymbol{\Phi}^{F^T} \mathbf{K} \boldsymbol{\Psi}^C \right) \boldsymbol{x}_{cm}^D \\ + \boldsymbol{x}_{ci}^{V^T} \left(\boldsymbol{\Psi}^{C^T} \mathbf{M} \tilde{\Delta} \dot{\boldsymbol{\Phi}}^F \right) \boldsymbol{z}_{sm} - \boldsymbol{x}_{ci}^{D^T} \left(\boldsymbol{\Psi}^{C^T} \mathbf{K} \tilde{\Delta} \boldsymbol{\Phi}^F \right) \boldsymbol{z}_{sm} \end{aligned} \tag{G.14}$$

Now, analogously to the scalar products in equations G.3 and G.4, the following weighting factors are introduced

$$l_{im}^z = \boldsymbol{z}_{si}^T \tilde{\Delta} \boldsymbol{\Lambda}_s^F \boldsymbol{z}_{sm} \tag{G.15}$$

$$\hat{m}_{im}^z = \boldsymbol{z}_{si}^T \left(\tilde{\Delta} \boldsymbol{\Phi}^{F^T} \mathbf{M} \boldsymbol{\Psi}^C \right) \boldsymbol{x}_{cm}^V + \boldsymbol{x}_{ci}^{V^T} \left(\boldsymbol{\Psi}^{C^T} \mathbf{M} \tilde{\Delta} \boldsymbol{\Phi}^F \right) \boldsymbol{z}_{sm} \tag{G.16}$$

$$c_{im}^z = \boldsymbol{z}_{si}^T \left(\tilde{\Delta} \boldsymbol{\Phi}^{F^T} \mathbf{C} \boldsymbol{\Psi}^C \right) \boldsymbol{x}_{cm}^D + \boldsymbol{x}_{ci}^{D^T} \left(\boldsymbol{\Psi}^{C^T} \mathbf{C} \tilde{\Delta} \boldsymbol{\Phi}^F \right) \boldsymbol{z}_{sm} \tag{G.17}$$

$$k_{im}^z = \boldsymbol{z}_{si}^T \left(\tilde{\Delta} \boldsymbol{\Phi}^{F^T} \mathbf{K} \boldsymbol{\Psi}^C \right) \boldsymbol{x}_{cm}^D + \boldsymbol{x}_{ci}^{D^T} \left(\boldsymbol{\Psi}^{C^T} \mathbf{K} \tilde{\Delta} \boldsymbol{\Phi}^F \right) \boldsymbol{z}_{sm} \tag{G.18}$$

$$\mu_{im}^z = \boldsymbol{z}_{si}^T \left(\tilde{\Delta} \dot{\boldsymbol{\Phi}}^{F^T} \mathbf{M} \boldsymbol{\Psi}^C \right) \boldsymbol{x}_{cm}^D + \boldsymbol{x}_{ci}^{D^T} \left(\boldsymbol{\Psi}^{C^T} \mathbf{M} \tilde{\Delta} \dot{\boldsymbol{\Phi}}^F \right) \boldsymbol{z}_{sm} \tag{G.19}$$

$$\hat{\mu}_{im}^z = \boldsymbol{z}_{si}^T \left(\tilde{\Delta} \dot{\boldsymbol{\Phi}}^{F^T} \mathbf{M} \boldsymbol{\Psi}^C \right) \boldsymbol{x}_{cm}^V + \boldsymbol{x}_{ci}^{V^T} \left(\boldsymbol{\Psi}^{C^T} \mathbf{M} \tilde{\Delta} \dot{\boldsymbol{\Phi}}^F \right) \boldsymbol{z}_{sm} \tag{G.20}$$

so that the decomposed a_{im}^z and b_{im}^z read

$$a_{im}^z = \hat{m}_{im}^z + \mu_{im}^z + c_{im}^z \tag{G.21}$$

$$b_{im}^z = l_{im}^z + \hat{\mu}_{im}^z \tag{G.22}$$

G.3 Global modes perturbation approximation in physical coordinates

Finally, using these new expressions for a_{im}^z and b_{im}^z, the perturbation approximations for the global modes are reformulated as

$$\tilde{\Delta}\lambda_m = l_{mm}^z + \hat{\mu}_{mm}^z - k_{mm}^z - \lambda_m \left(\hat{m}_{mm}^z + c_{mm}^z + \mu_{mm}^z\right) \tag{G.23}$$

$$\tilde{\Delta}\boldsymbol{z}_m = -\frac{1}{2}(\hat{m}_{mm}^z + \mu_{mm}^z + c_{mm}^z)\boldsymbol{z}_m - \sum_{i \neq m} \frac{l_{im}^z + \hat{\mu}_{im}^z - k_{im}^z - \lambda_m \left(\hat{m}_{im}^z + c_{im}^z + \mu_{im}^z\right)}{\lambda_i - \lambda_m} \boldsymbol{z}_i \tag{G.24}$$

where the newly defined weighting factors are posed in terms of component parameters in physical coordinates, namely: $\mathbf{M}_s$, $\mathbf{C}_s$, $\mathbf{K}_s$, $\mathbf{\Psi}_s^C$ and $\mathbf{\Phi}_s^F / \tilde{\Delta}\mathbf{\Phi}_s^F$. These involve half the number of degrees of freedom than their analogous state-space counterparts: $\mathbf{A}_s$, $\mathbf{B}_s$, $\mathbf{\Upsilon}_s^C$ and $\tilde{\Delta}\mathbf{X}_s^F$. Consequently, the computation of the l_{im}^z, $\hat{\mu}_{im}^z$, c_{im}^z, k_{im}^z $\hat{m}_{im}^z$ and μ_{im}^z weighting factors is more efficient than the computation of a_{im}^z and b_{im}^z directly from the state-space component matrices.

G.3.1 Further simplifications

In equation G.12 the coupling DOFs of the global eigenvectors $\boldsymbol{z}_m$ have been deliberately noted as the displacement $\boldsymbol{x}_{cm}^D$ and velocity $\boldsymbol{x}_{cm}^V$ partitions of the state-space coupling DOFs for the sake of generality. This forced to introduce a hat notation on $\hat{\mu}_{im}^z$ and $\hat{m}_{im}^z$ for indicating multiplication with the velocity partition.

Yet, one might recall that state-space eigenvectors may be written in terms of the physical mode shape vectors and corresponding eigenvalues as in equation G.8. Accordingly, $\boldsymbol{x}_{cm}$ (and $\boldsymbol{x}_{ci}$) may be alternatively expressed as

$$\boldsymbol{x}_{cm} = \begin{Bmatrix} \lambda_m \boldsymbol{\phi}_{cm} \\ \boldsymbol{\phi}_{cm} \end{Bmatrix} \tag{G.25}$$

Thence, introducing $\boldsymbol{x}_{cm}^V = \lambda_m \boldsymbol{\phi}_{cm}$, $\boldsymbol{x}_{cm}^D = \boldsymbol{\phi}_{cm}$, $\boldsymbol{x}_{ci}^V = \lambda_i \boldsymbol{\phi}_{ci}$ and $\boldsymbol{x}_{ci}^D = \boldsymbol{\phi}_{ci}$ in equations G.16, G.17, G.18, G.19 and G.20 one may reformulate the weighting factors definitions in physical coordinates.

Consider the following new weighting factors definitions

$$m_{im}^z = \boldsymbol{z}_{si}^T \left(\tilde{\Delta}\mathbf{\Phi}^{F^T}\mathbf{M}\mathbf{\Psi}^C\right)\boldsymbol{\phi}_{cm} + \boldsymbol{\phi}_{ci}^T \left(\mathbf{\Psi}^{C^T}\mathbf{M}\tilde{\Delta}\mathbf{\Phi}^F\right)\boldsymbol{z}_{sm} \tag{G.26}$$

$$n_{im}^z = \boldsymbol{\phi}_{ci}^T \left(\mathbf{\Psi}^{C^T}\mathbf{M}\tilde{\Delta}\mathbf{\Phi}^F\right)\boldsymbol{z}_{sm} \tag{G.27}$$

$$\nu_{im}^z = \boldsymbol{\phi}_{ci}^T \left(\mathbf{\Psi}^{C^T}\mathbf{M}\tilde{\Delta}\dot{\mathbf{\Phi}}^F\right)\boldsymbol{z}_{sm} \tag{G.28}$$

then $\hat{\mu}^z_{im}$ and $\hat{m}^z_{im}$ can be redefined as

$$\hat{m}^z_{im} = \lambda_m m^z_{im} + (\lambda_i - \lambda_m) n^z_{im} \tag{G.29}$$

$$\hat{\mu}^z_{im} = \lambda_m \mu^z_{im} + (\lambda_i - \lambda_m) \nu^z_{im} \tag{G.30}$$

so that for $i = m$ it holds that

$$\hat{m}^z_{mm} = \lambda_m m^z_{mm} \tag{G.31}$$

$$\hat{\mu}^z_{mm} = \lambda_m \mu^z_{mm} \tag{G.32}$$

As a consequence, in the global eigenvalues perturbation approximation in equation G.23, the $\hat{\mu}^z_{mm}$ and the $\lambda_m \mu^z_{mm}$ factors cancel out and the $\lambda_m \hat{m}^z_{mm}$ factor is transformed into $\lambda^2_m m^z_{mm}$, giving rise to the following simplified expression

$$\tilde{\Delta}\lambda_m = l^z_{mm} - \left(\lambda^2_m m^z_{mm} + \lambda_m c^z_{mm} + k^z_{mm}\right) = l^z_{mm} + d^z_{mm} \tag{G.33}$$

The beauty of this expression is that the l^z_{mm} factor depends only on the perturbation in component eigenvalues $\tilde{\Delta}\Lambda^F_s$ (i.e. it corresponds to the PPF for the LMP method), and the $d^z_{mm} = -\left(\lambda^2_m m^z_{mm} + \lambda_m c^z_{mm} + k^z_{mm}\right)$ factor depends only on the perturbation in component mode shape vectors $\tilde{\Delta}\boldsymbol{\Phi}^F_s$. Moreover, d^z_{mm} completely resembles the PPF for damped eigenvalues in full coordinates[1]. This means, that this perturbation approximation for the eigenvalues is completely independent of the fact that the state-space formulation has been used for its derivation.

Similarly, for the global eigenvectors perturbation approximation, the $(b^z_{im} - \lambda_m a^z_{im})$ factors are transformed into

$$(b^z_{im} - \lambda_m a^z_{im}) = l^z_{im} - \left(\lambda^2_m m^z_{im} + \lambda_m c^z_{im} + k^z_{im}\right) + (\lambda_i - \lambda_m)(\nu^z_{im} - \lambda_m n^z_{im}) \tag{G.34}$$

which yields the following expression for the perturbed global eigenvectors in coupled-modal coordinates

$$\begin{aligned} \tilde{\Delta}\boldsymbol{z}_m = &-\frac{1}{2}\left(\lambda_m m^z_{mm} + c^z_{mm}\right)\boldsymbol{z}_m - \sum_{i \neq m} \frac{l^z_{im} - \left(\lambda^2_m m^z_{im} + \lambda_m c^z_{im} + k^z_{im}\right)}{\lambda_i - \lambda_m}\boldsymbol{z}_i \\ &- \nu^z_{mm}\boldsymbol{z}_m - \sum_{i \neq m}(\nu^z_{im} - \lambda_m n^z_{im})\boldsymbol{z}_i \end{aligned} \tag{G.35}$$

If this derivation is to be coherent with the fact that the global eigenvalues show only dependency on the component eigensolutions $\tilde{\Delta}\Lambda^F_s$ and $\tilde{\Delta}\boldsymbol{\Phi}^F_s$, the expression

[1] $\tilde{\Delta}\lambda_m = -\boldsymbol{\phi}^T_m \left[\lambda^2_m \Delta\mathbf{M} + \lambda_m \Delta\mathbf{C} + \Delta\mathbf{K}\right] \boldsymbol{\phi}_m$

for the eigenvectors perturbation shall only be dependent on $\tilde{\Delta}\Lambda_s^F$ and $\tilde{\Delta}\boldsymbol{\Phi}_s^F$ as well. This is the case if one assumes that the following equivalence holds

$$\nu_{im}^z = \lambda_m n_{im}^z = \frac{1}{2}\lambda_m m_{mm}^z \tag{G.36}$$

which implies that the $(\nu_{im}^z - \lambda_m n_{im}^z)$ factor vanishes in equation G.35. Then, the perturbation approximation for the MCB global eigenvectors would result in

$$\tilde{\Delta}\boldsymbol{z}_m = -\frac{1}{2}\left(2\lambda_m m_{mm}^z + c_{mm}^z\right)\boldsymbol{z}_m - \sum_{i\neq m}\frac{l_{im}^z - (\lambda_m^2 m_{im}^z + \lambda_m c_{im}^z + k_{im}^z)}{\lambda_i - \lambda_m}\boldsymbol{z}_i \tag{G.37}$$

where, again, the expression may be split into two parts: one only depending on $\tilde{\Delta}\Lambda_s^F$, i.e.

$$-\sum_{i\neq m}\frac{l_{im}^z}{\lambda_i - \lambda_m}\boldsymbol{z}_i$$

which corresponds to the PPF for the LMP method, and another only depending on $\tilde{\Delta}\boldsymbol{\Phi}_s^F$, i.e.

$$-\frac{1}{2}\left(2\lambda_m m_{mm}^z + c_{mm}^z\right)\boldsymbol{z}_m + \sum_{i\neq m}\frac{(\lambda_m^2 m_{im}^z + \lambda_m c_{im}^z + k_{im}^z)}{\lambda_i - \lambda_m}\boldsymbol{z}_i$$

which strongly resembles the PPF for damped eigenvectors in full coordinates[2].

[2] $\tilde{\Delta}\boldsymbol{\phi}_m = -\frac{1}{2}\left(\boldsymbol{\phi}_m^T\left[2\lambda_m\Delta\mathbf{M} + \Delta\mathbf{C}\right]\boldsymbol{\phi}_m\right)\boldsymbol{\phi}_m + \sum_{i\neq m}\frac{\boldsymbol{\phi}_i^T\left[\lambda_m^2\Delta\mathbf{M} + \lambda_m\Delta\mathbf{C} + \Delta\mathbf{K}\right]\boldsymbol{\phi}_m}{\lambda_i - \lambda_m}\boldsymbol{\phi}_i$

www.isvr.soton.ac.uk

Institute of Sound and Vibration Research (ISVR)
Faculty of Engineering and the Environment
University of Southampton
Highfield Campus building 13
SO17 1BJ Southampton
Hampshire, United Kingdom
Tel: (+44) (0)23 8059 2291
Email: sjb@isvr.soton.ac.uk